The Mössbauer Effect and Its Application in Chemistry

The Mössbauer Effect and Its Application in Chemistry

A symposium organized

by Carl W. Seidel for

Nuclear Science &

Engineering Corp.,

Pittsburgh, Pa. Held

in New York, N. Y.,

September 12, 1966.

Rolf H. Herber, *Chairman*

Library
American Chemical Society

ADVANCES IN CHEMISTRY SERIES **68**

AMERICAN CHEMICAL SOCIETY

WASHINGTON, D. C.   **1967**

Advances in Chemistry Series

Robert F. Gould, *Editor*

AMERICAN CHEMICAL SOCIETY PUBLICATIONS

FOREWORD

ADVANCES IN CHEMISTRY SERIES was founded in 1949 by the
American Chemical Society as an outlet for symposia and col-
lections of data in special areas of topical interest that could
not be accommodated in the Society's journals. It provides a
medium for symposia that would otherwise be fragmented,
their papers distributed among several journals or not pub-
lished at all. Papers are refereed critically according to ACS
editorial standards and receive the careful attention and proc-
essing characteristic of ACS publications. Papers published
in ADVANCES IN CHEMISTRY SERIES are original contributions
not published elsewhere in whole or major part and include
reports of research as well as reviews since symposia may em-
brace both types of presentation.

PREFACE

Mössbauer spectroscopy is the term now used to describe a new analytical technique which has developed using γ-ray nuclear resonance fluorescence or the Mössbauer effect. For most of the time since Rudolf Mössbauer's discovery in 1958 it was the physicist who utilized this new tool. Starting approximately in 1962 some chemists realized the potential of this new technique. Since then they have applied Mössbauer spectroscopy to the study of chemical bonding, crystal structure, electron density, ionic states, and magnetic properties as well as other properties. It is now considered a complimentary tool to other accepted spectroscopic techniques such as NMR, NQR, and ESR.

Despite all the information that might be obtained using Mössbauer spectroscopy, some of its limitations naturally discouraged many chemists from using this new technique. Unfamiliarity with the basic principles, the fact that most of the early work was done only on iron and tin, and the lack of commercially available research quality equipment until 1965 were other reasons for the lack of interest. This symposium, The Mössbauer Effect and Its Application in Chemistry, was sponsored by Nuclear Science (formerly Nuclear Science & Engineering Corp.), a division of International Chemical & Nuclear Corp., with the hope that more chemists would learn how Mössbauer spectroscopy has been and can be used.

The morning session was devoted to a general explanation of the areas of application in studying magnetic properties, oxidation states, compounds, and metal structure. In the afternoon, reviews of the Mössbauer investigations of iron, tin, iodine, tellurium, and some of the rare earth elements were presented. The meeting concluded with a discussion on the future of Mössbauer Spectroscopy in which an interested audience participated.

We would like to thank all the authors for their notable contributions, especially our able Chairman, Rolf Herber, who also delivered the introductory lecture. It is our hope that as Mössbauer spectroscopy grows, more such symposia can be held.

Pittsburgh, Pa.   CARL W. SEIDEL
August 1967

The Mössbauer Effect and
# Its Application in Chemistry

R. H. HERBER

Rutgers University, New Brunswick, N. J.

The Mössbauer effect involves the resonance fluorescence of nuclear gamma radiation and can be observed during recoilless emission and absorption of radiation in solids. It can be exploited as a spectroscopic method by observing chemically dependent hyperfine interactions. The recent determination of the nuclear radius term in the isomer shift equation for ^{119}Sn shows that the isomer shift becomes more positive with increasing s electron density at the nucleus. Detailed studies of the temperature dependence of the recoil-free fraction in ^{119}Sn and ^{129}I labeled SnI_4 show that the characteristic "Mössbauer temperatures," θ_M, are different for the two atoms. These results are typical of the kind of chemical information which can be obtained from Mössbauer spectra.

Rudolph Mössbauer in late 1957–1958 attempted to observe γ-ray resonance in such a way that the recoil energy which is lost in the usual nuclear gamma decay is compensated for by temperature broadening—the so-called Doppler broadening observed in such γ-ray spectra. He chose iridium-191, with a γ-ray energy of 129 k.e.v. and a free-atom recoil energy of 0.05 e.v. The Doppler broadening at room temperature is such that the width of the gamma line is a factor of 2 larger than this. Therefore, the line emitted by the source and the line that can populate the ground state–first excited state transition in the absorber actually overlap—*i.e.*, the total distance between $E_t - E_R$ and $E_t + E_R$ is about the same as the width of one of these lines. Figure 1 represents graphically the relationship among the line width, Γ, the transition energy, E_t, and the recoil energy, E_R.

Mössbauer attempted to observe this resonance by studying his system at elevated temperatures, at which the overlap becomes reason-
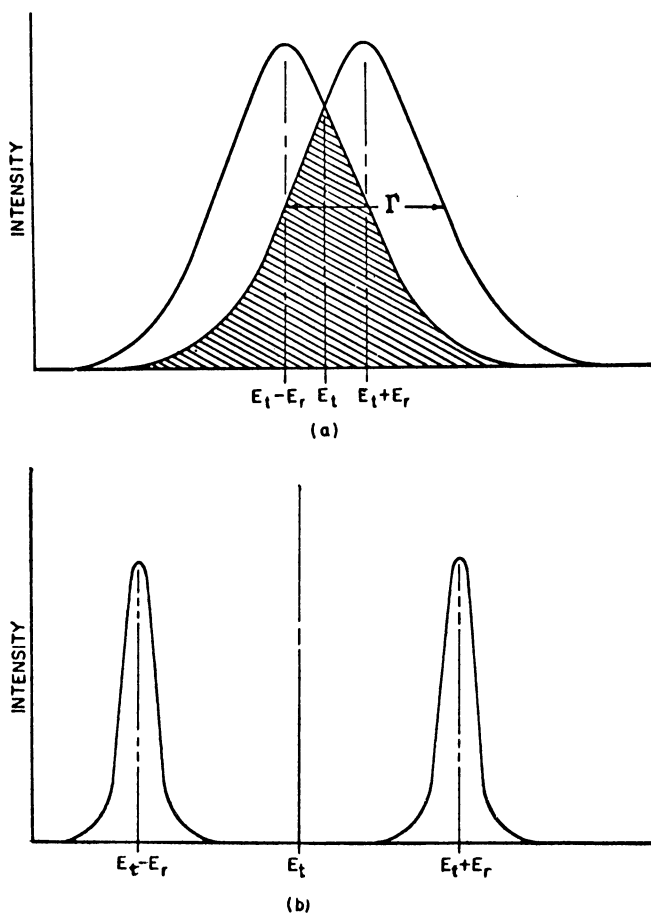
Journal of Chemical Education

Figure 1. Relation of line width, transition energy, and recoil energy. (a) Overlap (schematic) of emission and absorption lines in optical transitions. (b) Absence of overlap (schematic) of emission and absorption lines in nuclear transitions involving atoms free to recoil. Drawn to scale, separation between two lines would be about 4×10^5 the width of each line at half maximum

ably large. However, even at room temperature the two lines slightly overlap; hence, he decided to cool his samples to liquid nitrogen temperature (*ca.* 78°K.).

Instead of an increase in the transmission of the gamma radiation through his sample, he actually found a marked decrease (*ca.* 1.1%). He correctly interpreted this phenomenon in terms of so-called "zero

phonon" transitions and laid the basis for a new type of spectroscopy—Mössbauer spectroscopy.

Decay Scheme of Cobalt and Tin

The work in this field of greatest interest to chemists has involved two nuclides—iron-57, populated from the decay of cobalt-57, and tin-119. With some exceptions chemists are just now beginning to exploit other nuclides. Figure 2 shows the decay scheme of cobalt-57, which decays by electron capture through a highly excited state which decays to the first excited state with a spin of 3/2. This level decays in 91% of the cases to the ground state with a spin of 1/2, and this is the transition in question. The excited state spin of 3/2 can be split in an electrostatic field into a $\pm$ 3/2 and $\pm$ 1/2 level. We shall discuss this in terms of the quadrupole interaction, ΔE, between the electrostatic field and the first excited nuclear state. The ground state, of course, is unsplit under these circumstances. In an external magnetic field, one has in addition a nuclear Zeeman effect, with removal of the ground-state and excited-state de-
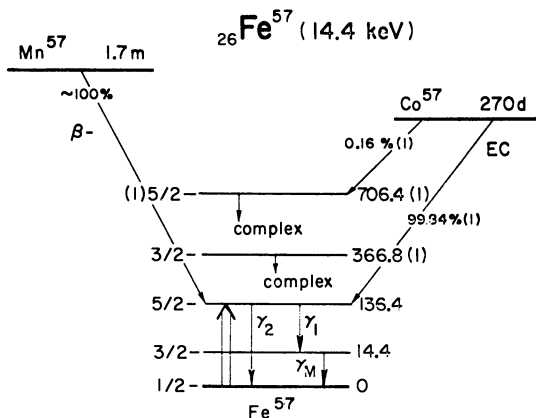
North American Aviation Science Center

Figure 2.   Decay scheme of ^{57}Co (18)

Measured Properties	E_γ, k.e.v.	I_{σ_0}
$t_{1/2}(\gamma_M) = 9.8 \times 10^{-8}$ s	γ_M: 14.39	$[I_{14}]$
$\alpha_T(\gamma_M) = 9.00$	γ_1: 122.0	$[100]$
$IA = 2.19\%$	γ_2: 136.4	$[12.5]$
$MG = +0.09024$ nm	$K_{\chi\beta}$: 6.5	$[5.61_{14}]$
(11)		
$MM = -0.154$ nm	*Derived Parameters*	
$QM = +0.285$ b	$\sigma_0 = 2.363 \times 10^{-18}$ sq.	
$\sigma_0 = 2.43 \times 10^{-18}$	cm.	
sq. cm.	$\Gamma = 4.655 \times 10^{-12}$ k.e.v.	
	$\Delta v = 0.09699$ mm./sec.	
	$E_r = 1.951 \times 10^{-3}$ e.v.	

generacy. From the four excited-state levels and the two ground-state levels, one can actually observe six of the possible eight transitions.

For tin-119, the situation is similar, except that one begins with isomeric decay. The parent is 250-day tin-119m. The precursor event is highly converted, with an internal conversion coefficient greater than 6000. This populates the first excited state, which decays to the ground state by emitting 23.8-k.e.v. γ-rays. As in the case of iron, in an electrostatic field one can split the upper level into a $\pm 3/2$ and a $\pm 1/2$ level. The ground state again remains unsplit. In an external magnetic field or internal magnetic field one can split these levels further and again see the six-line hyperfine splitting in the appropriate spectra.
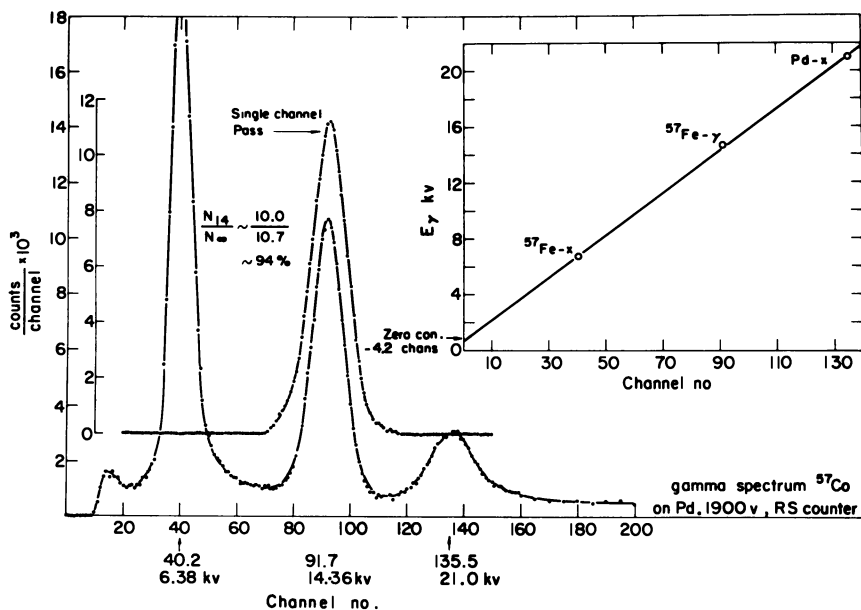

Figure 3. Pulse height spectrum of ^{57}Co gamma radiations. Window of single channel analyzer fixed to optimize intensity of 14.4-k.e.v. radiation

Once we have the appropriate nuclide, we must separate the radiation of interest from all other radiation present. A typical gamma spectrum is shown in Figure 3 for cobalt-57 in palladium. The radiations which can be identified include the 6-k.e.v. x-ray, the 14-k.e.v. γ-ray of interest, and a sum peak and palladium x-ray peak, both lying at about 21 k.e.v. If one now sets the single-channel analyzer window correctly, one observes essentially only the 14-k.e.v. peak, but all of this is not recoil-free radiation; it includes other radiation which falls into the window from various gamma quantum de-excitation processes.
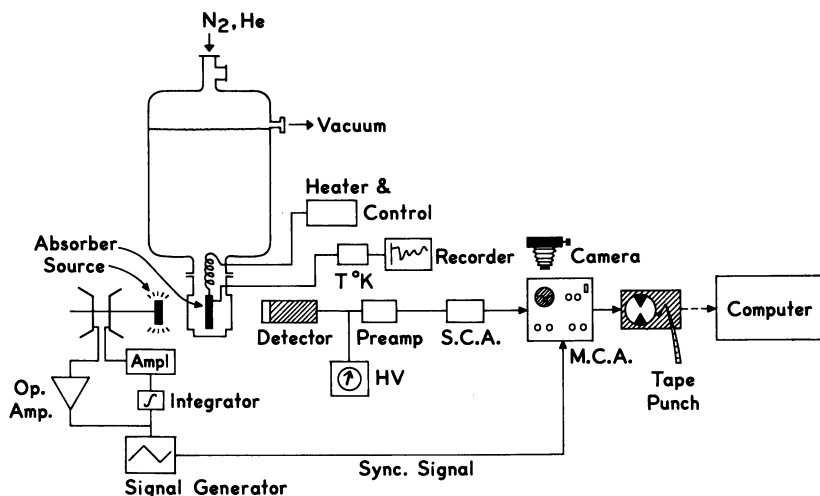
Figure 4. Block diagram of experimental arrangement for Mössbauer spectroscopy

One now passes this radiation through the window, then through an appropriate absorber, and observes the resonance by systematically destroying it. There are several techniques for doing this, but fundamentally all depend on exploiting the Doppler shift, which gives the variation in γ-ray energy with variation in the relative source-absorber velocity. Mechanical devices include cams, pendulums, hydraulic devices, rotating wheels and screws, and electromechanical transducers such as loudspeakers and LV-Syns. A simple block diagram of this latter kind of equipment with its associated electronics is shown in Figure 4. The two most important and complicated factors are choosing the right velocity, and choosing it reproducibly, and storing the information. We have begun with either a Hewlett-Packard function generator or a triangular function generator circuit, many of which are described in the literature. The signal from this is fed to an amplifier and a feedback circuit and then to a dual-voice coil loudspeaker which moves the source back and forth. One voice coil carries the drive signal; the other is used as a motion sensor. The absorber is stationary, and the radiation passes through the absorber to the detector.

The signal from the γ-ray detector goes through a preamplifier, a single-channel analyzer that delimits the pulse height window (Figure 3), and is stored as information in the multichannel analyzer in synchronization with the signal emitted from the function generator. To extract this information, one needs a serial converter and a typewriter or paper tape print-out device. A cathode ray display or some other

analog data readout method can also be used. These are the basic components of one kind of Mössbauer drive. There are, of course, other systems: cam drives, screw drives, pendulum drives, and other ways to impart that small relative velocity either to the source or to the absorber that will systematically destroy the resonance so that one can determine the extent of the resonance absorption and the various parameters which depend on it.

One of the problems associated with Mössbauer spectra is determining the position of zero relative velocity—this is not at all a trivial problem. There are several methods of doing this if one has a constant velocity drive and uses a small excursion—*i.e.*, a small travel. In this case the source is positioned at some reasonable intermediate point, and one determines a transmission rate at zero velocity. If a constant acceleration drive is used, a Mössbauer spectrum must be used to determine zero; a typical situation is shown in Figure 5, which shows the resonance of stannic oxide against stannic oxide. The bottom abscissa in this case is not in velocity units but in multichannel analyzer addresses, and these data can be analyzed in the following way. The width of the resonance line is on the order of about 50 channels, and yet the position of the resonance maximum can be determined to about ± 0.3 channel. This resonance maximum position can be determined by a simple technique (5, 25) (assuming that one has either only a single resonance line or a well-separated doublet) by making use of the information in the region of the greatest precision with respect to position of the line. The least precision is in the wings simply because the slope is so small. Similarly the precision is small at the minimum, again because the slope is small. Points lying in the sides of the Lorentzian resonance curve can be considered the most reliable. One can now take chords parallel to the base line, either manually or by computer. Although any number of such chords can in principle be taken, about 10 or so suffice in the usual case. By a least-squares fit, the position of the center of the resonance line can be determined by plotting the address against the chord width and extrapolating to zero chord width. This type of analysis applied to the SnO_2 data is shown by the scatter of points in Figure 5b (5). This useful technique allows one to determine the position of resonance lines with greater accuracy than by eye or by taking straight-line slopes and extrapolating to a point where they intercept. This method also gives information on small-line asymmetries and skewness.

The second problem in relation to Mössbauer spectroscopy, which is trivial but irksome, is agreeing on a reference point with respect to isomer shifts. Each particular nuclide has several possible chemical environments for the source and therefore several possible reference
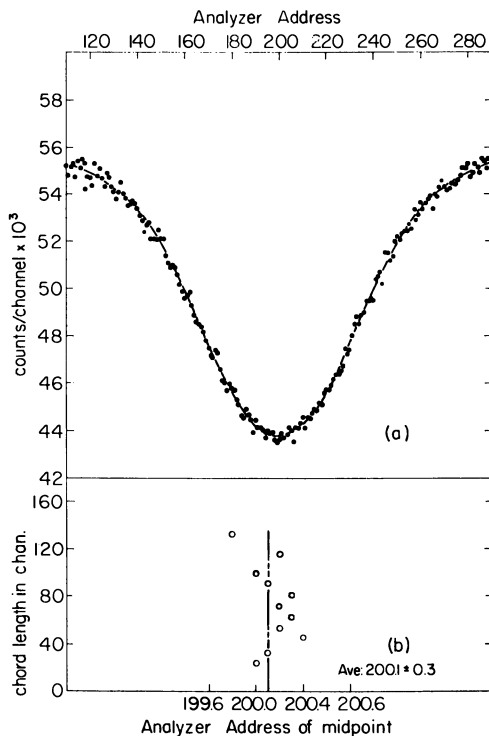
Figure 5. Sn^+O_2–SnO_2 Mössbauer spectrum showing method of locating zero relative velocity. Lower diagram shows scatter of data obtained from method-of-chords analysis. Note expanded horizontal scale

points for the isomer shift. Moreover, nominally chemically identical sources do not necessarily give the same isomer shift in high precision spectrometry. This is particularly bothersome with iron because two of the most popular reference points for iron are cobalt in copper sources and metallic iron as an absorber. Metallic iron, especially enriched iron, is usually obtained by reducing ferric oxide in graphite crucibles, and about 0.2% carbon in the iron will seriously shift the position of this resonance maximum (24). This is difficult to recognize unless one compares the spectrum of iron so reduced with the spectrum of natural iron foil which has been reduced under conditions where the possibility of carbon or silicon contamination is absent.

There has been some discussion of what to use as a reference point for the isomer shift in the case of cobalt-57. Two years ago (12) I discussed the possibility of using sodium nitroprusside, which I had origi-

nally suggested with G. K. Wertheim of the Bell Laboratories. However, there is still no general agreement about what to use for iron. A typical sodium nitroprusside spectrum is shown in Figure 6. I use this figure—not to discuss the isomer shift scales—but simply to point out that if one has two well-separated peaks, separated by 1.726 mm./sec. at 25°C. (approximately 10 times twice the natural line width), one can use the same methods of chords to locate the center of each of these lines. One can take the mid-point between those two, and again find zero—the center of the spectrum—and therefore a reference point.
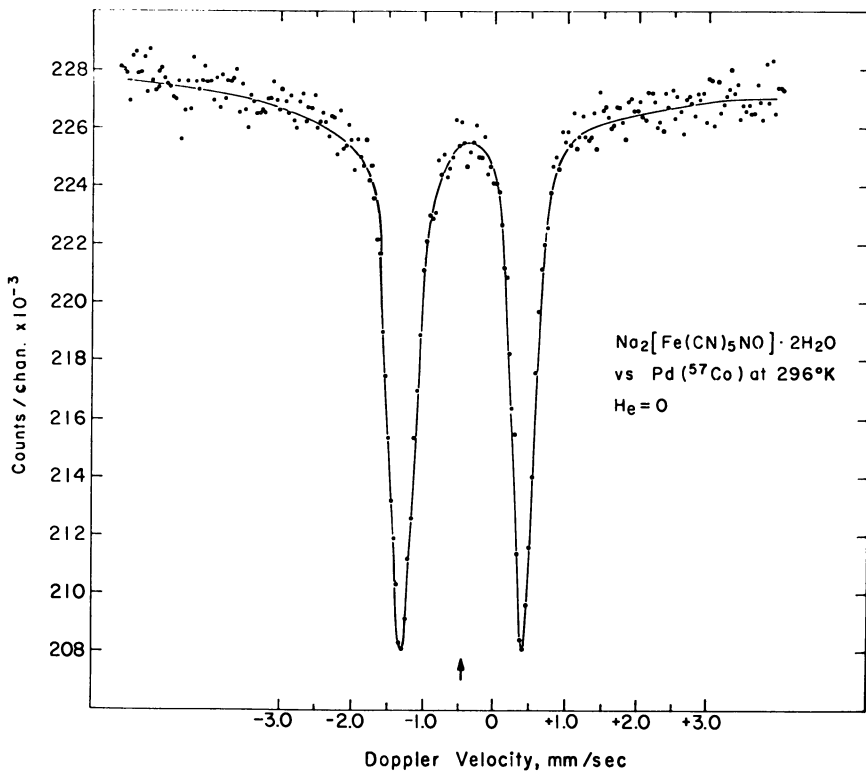

Figure 6. Mössbauer spectrum of Na₂Fe(CN)₅NO · 2H₂O at 297°K.

Let us now discuss some recent work by Sano and myself on completely characterizing barium stannate, a material first proposed by Plotnikova, Mitrofanov, and Shpinel' (21), as a source for tin Mössbauer spectroscopy. It is easily prepared, is a stoichiometric compound and has all the properties one desires in a Mössbauer matrix. The recoil-free fraction at room temperature is about 0.55 with about a 10% error. The line width extrapolated to zero absorber thickness is about 6% larger than natural—*i.e.*, the line width observed is *ca.* 0.318 mm./sec. at zero ab-
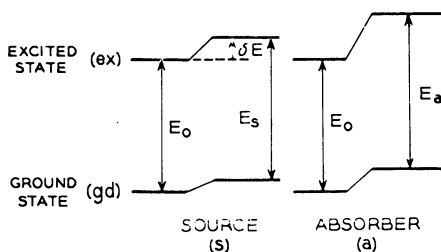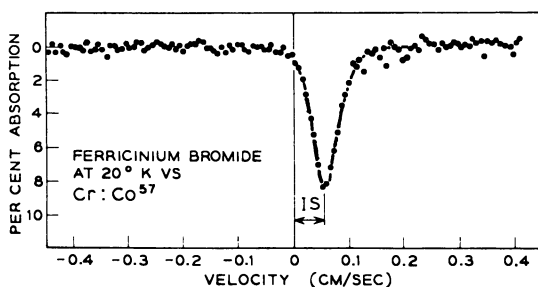
$$\delta E = \frac{2\pi}{5} Ze^2 |\Psi(0)|^2 R^2 \quad \text{(RELATIVE TO POINT NUCLEUS)}$$

$$E_s = E_0 + \frac{2\pi}{5} Ze^2 |\Psi_s(0)|^2 \left[R_{ex}^2 - R_{gd}^2 \right]$$

$$E_a = E_0 + \frac{2\pi}{5} Z_e^2 |\Psi_a(0)|^2 \left[R_{ex}^2 - R_{gd}^2 \right]$$

ISOMER SHIFT $= E_a - E_s$

$$IS = \frac{2\pi}{5} Ze^2 \left[|\Psi_a(0)|^2 - |\Psi_s(0)|^2 \right] \left[R_{ex}^2 - R_{gd}^2 \right]$$

G. K. Wertheim, "Mössbauer Effect: Prin-
ciples and Applications," Academic Press

*Figure 7.   Origin of isomer shift* (28)

sorber thickness. Its Debye temperature is 525°C., and therefore the recoil-free fraction is large at room temperature and remains essentially constant to cryogenic temperatures. It is useful as both a source and standard absorber because it can be taken from a shelf or prepared readily by mixing stoichiometric amounts of barium carbonate or barium oxide and stannic oxide and firing at 1400°C. for an hour or two; hence, it is available at low cost as a reference standard for ^{119}Sn Mössbauer spectroscopy.

Now we consider the isomer shift, which was first identified correctly by Kistner and Sunyar in 1960 in studying (15) the ferric oxide–stainless steel spectrum. A graphical summary of the origin of the isomer shift is given in Figure 7. The isomer shift arises from the fact that the nucleus is not a point source but interacts as a region of charge space

with the electrostatic environment. If the radii of the nuclear excited state and the ground state are different, this extent of interaction with the environment will be different. The characteristic parameter used to describe the origin of the isomer shift is ΔR, which is actually related to the difference in the square of the excited-state radius and the ground-state radius. Let us now refer to the bottom equation in Figure 7. If the third term, which is fixed by the nuclear configuration, is nonzero and if the absorber and source are in two chemically different environments— *i.e.*, if the electron density at the nucleus is different in the absorber and in the source—the second term is also nonzero. In addition, there is a nuclear term which will always be nonzero, so that the isomer shift will have some finite value. Depending on whether the excited state radius is larger or smaller than the ground state, the variation in the isomer shift with change in the absorber electron density will be either positive or negative. From this kind of term one can derive much useful chemical information.

A typical situation, shown at the bottom of Figure 7, is an old study by Wertheim and myself on ferricinium bromide, which shows a single resonance line (for the purposes of the present discussion). The isomer shift is the displacement from zero velocity of the resonance maximum. The isomer shift systematics for cobalt-57 have intrigued many investigators, and an explanation of these systematics was attempted fairly early by Walker, Wertheim, and Jaccarino (27). From pressure experiments (9, 17, 20, 22) $\Delta R/R$ for cobalt-57 is 1.8×10^{-3} and negative (20, 22). [The pressure experiments assume an isotropic compression. Up to 240 kbars at room temperature, the pressure dependence of the isomer shift is given adequately (20, 22) by the equation $\Delta(IS/\Delta p = (7.89 \pm 0.31) \times 10^{-4}$ mm./sec. kbar.] Hence, the isomer shift decreases as the electron density in the absorber increases—*i.e.*, if the term $\psi(0)_a^2$ is larger than $\psi(0)_s^2$, the entire chemical term is positive. Since $\Delta R/R$ is negative and the nuclear term must be positive, the isomer shift parameter under these conditions is negative as a whole. The Walker, Wertheim, and Jaccarino systematics (27) are summarized in Figure 8, which shows the $4s$ electron contribution in the configuration $3d^74s^x$. The lowest line is the situation for metallic or Fe^0 compounds. The next line is the configuration $3d^64s^x$ for Fe^{2+}, and the top line is the configuration $3d^54s^x$ for Fe^{3+} Much work has been done since on the systematics of iron isomer shifts, on which Spijkerman reports (26).

The situation for tin-119 is more confused because of the uncertainty in $\Delta R/R$. The first attempts to systematize isomer shifts for tin-119 were made by Cordey-Hayes and his co-workers (8). He assumed that ionic stannous compounds have a configuration $5s^2$, Sn^0 compounds or tetrahedral tin compounds have the configuration in which there are $4sp^3$
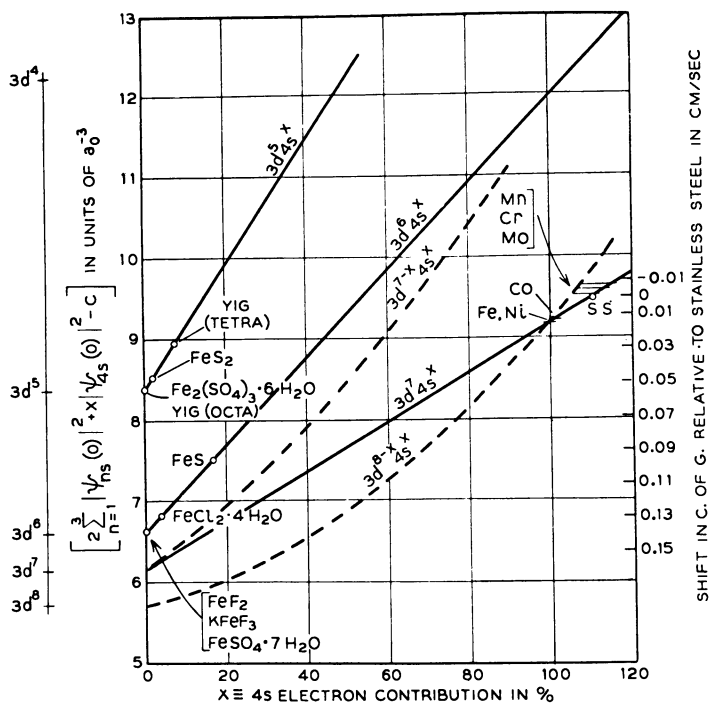
G. K. Wertheim, "Mössbauer Effect: Prin-
ciples and Applications," Academic Press

Figure 8.   Isomer shift systematics for ^{57}Fe

hybridized orbitals giving essentially a $5s^1$ configuration with some shield-
ing, and ionic stannic compounds have a configuration $5s^0$. From this,
one can obtain a correlation or presumed correlation between the isomer
shift and the electron density.

Figure 9 shows an early attempt at this correlation, based mainly on
the data of Cordey-Hayes (8). In this treatment $SnCl_2$ has approximately
the configuration $[Kr]4d^{10}5s^2$, and the tin atom in the hexafluorostan-
nate(IV) ion has the configuration $[Kr]\ 4d^{10}5s^0$. In this way the isomer
shift becomes more positive as the $5s$ electron population increases, and
from these data Cordey-Hayes concluded that ΔR was positive. Gol'dan-
skii and co-workers (1, 3, 11, 12), on the other hand, have said that this
simple treatment overlooks the influence on the overlap between the
nucleus and $1s$, $2s$, $3s$, and $4s$ electron shells as the charge state changes,
and if one takes account of this correction, a negative ΔR results. In
other words, the isomer shift decreases as the electron density increases.
Zuckerman (29) has examined all of these arguments based on electro-
negativity considerations and concludes that it is dangerous to base such
arguments on intuitive chemical considerations.

However, Belyakov (2) has recently estimated from single particle states the sign and magnitude of ΔR for several nuclides including nickel-61, zinc-67, iodine-129, xenon-129 and -131. These are all Mössbauer nuclides, of course, and he concludes from theoretical arguments that $\Delta R/R$ for tin is -2.5×10^{-4}. Again, we see a negative sign for ΔR. Ibraimov and Kuz'min (14) studied palladium tin alloys. Palladium is an electron acceptor with respect to tin. Therefore, as the alloy system becomes richer in palladium, the electron density on the tin should decrease; since the isomer shift increased as the electron density decreased, these workers again concluded that ΔR is negative. Finally, a last Russian paper that bears on this (19) concerns an experiment in which gray tin was compressed to about 120,000 atm., and the isomer shift was measured as a function of the pressure; it was again concluded that ΔR for ^{119}Sn is negative.
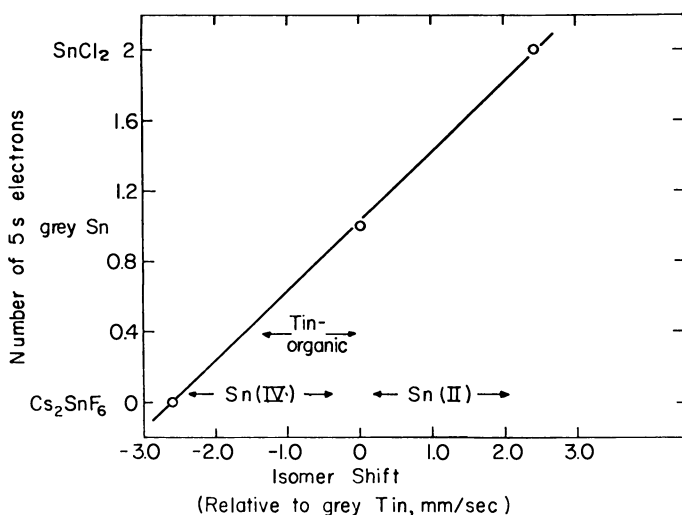

Figure 9. *Isomer shift as a function of electron configuration for* ^{119}Sn

All these conflicts can now be resolved because of what appears to be a definitive experiment by Bocquet *et al.* (4), who directly measured the internal conversion coefficients of the transition from the first nuclear level to the ground state. They directly compared the *L*, *M*, *N*, and *O* conversion electron intensities in two different states—namely, in stannic oxide and white tin. They found that the $5s$ electron density is 30% smaller in stannic oxide than in white tin, and since the isomer shift of stannic oxide is negative with respect to white tin, ΔR is clearly positive. From these data, the Brookhaven group has calculated the value for $\Delta R/R$ for tin-119 as $+3.3 \times 10^{-4}$.

Other experiments have been reported by Flinn, based on chemical arguments using self-consistent field calculations on various charge states in tin. Lees and Flinn (*16*) also conclude that $\Delta R/R$ is positive, although they do not give the magnitude for this term. Similar conclusions have been arrived at by Ruby and co-workers who also conclude from chemical evidence that ΔR is positive.

Another parameter that one can extract from a Mössbauer spectrum is the quadrupole splitting. The 3/2 state in either iron or tin is degenerate with respect to an asymmetric electrostatic field, and in such a field these levels will be split into $\pm 3/2$ and $\pm 1/2$ levels. One can observe transitions either to or from these two levels to the ground state, and this is the quadrupole splitting. It is actually $\frac{1}{2}e^2qQ$, where eq is the electrostatic field gradient—*i.e.*, the second derivative of the potential with respect to the coordinate—and eQ is the nuclear quadrupole moment. The typical quadrupole split spectrum for iron is shown in Figure 6, in which the cubic (octahedral) symmetry around the iron atom is de-
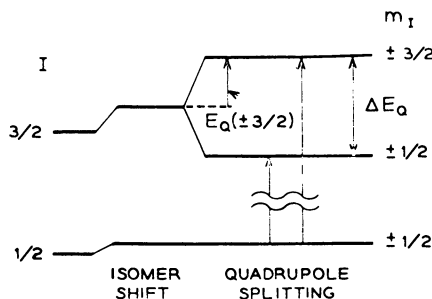
$$E_Q(m_I) = eqQ \left[\frac{3\,m_I^2 - I(I+1)}{4I(2I-1)} \right]$$

$$\Delta E_Q = E_Q(3/2) - E_Q(1/2) = \frac{eqQ}{2}$$
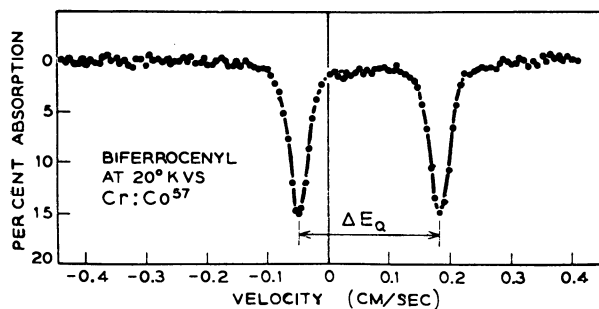
G. K. Wertheim, "Mössbauer Effect: Principles and Applications," Academic Press

Figure 10. Origin of quadrupole splitting interaction (*28*)

stroyed by replacing a CN group with an NO group. An example of quadrupole splitting observed with an organometallic compound is shown in Figure 10. This is biferrocenyl, which contains only one kind of iron atom. The resonance line is split in two, and the separation of the two lines is the quadrupole splitting, which can be on the order of up to about 10 times the experimental line width or even larger. Quadrupole splitting can be observed if the electrostatic field symmetry at the nucleus is less than cubic—*i.e.*, if two threefold or higher symmetry axes go through the Mössbauer nucleus quadrupole splitting will not be observed. It does not follow, however, that quadrupole splitting would necessarily be observed if this apparent asymmetry exists.

A typical case for tin-119 is shown in Figure 11. The upper spectrum is that of tetraphenyltin, which is, of course, a tetrahedral molecule with four threefold axes passing through the Mössbauer nucleus. Here one does not expect to observe any quadrupole splitting and, indeed, one does not. If a phenyl group is replaced with a chlorine atom as in triphenyltin chloride, the quadrupole splitting can be observed easily, as shown in the lower curve of Figure 11. Parisi has carefully examined the Mössbauer spectra of some tin hydrides (*13*), none of which shows any quadrupole splitting. In agreement with a suggestion first made by Greenwood (*10*), concerning the presence of nonbonding electron pairs at nearest neighbor atoms (Parisi's work shows this clearly), one cannot conclude from the absence of quadrupole splitting in tin-119 spectra that the chemical symmetry is cubic. The Mössbauer data clearly show that the electrical symmetry will be cubic, but the chemical symmetry may be quite different from cubic. Typical examples are molecules such as triphenyltin hydride or diphenyltin dihydride or even such absorbers as triphenyltin lithium, which one certainly expects to be noncubic—none shows any quadrupole splitting.

There is a further exploitation of the quadrupole splitting interaction which can give some chemical information. This follows from the suggestion first made by Ruby in 1963 and since developed by Collins (*7, 23*), who argue as follows: one obtains a Mössbauer spectrum of a material that shows quadrupole splitting, in the presence of an external magnetic field. The two Mössbauer levels are degenerate with respect to the spin substate (Figure 10). One can remove this degeneracy of the excited state $\pm 3/2$ and the $\pm \frac{1}{2}$ levels and the ground state $\pm \frac{1}{2}$ level by placing this material into a magnetic field. Whether the 3/2 level goes up and the 1/2 level goes down or whether inversion occurs depends on the sign of the electrostatic field gradient—*i.e.*, the shape of the electrostatic field distribution. Collins (*7*) examined the possibilities of using this information to determine the sign of the field gradient in iron and tin compounds. This is an important point because most theories of the
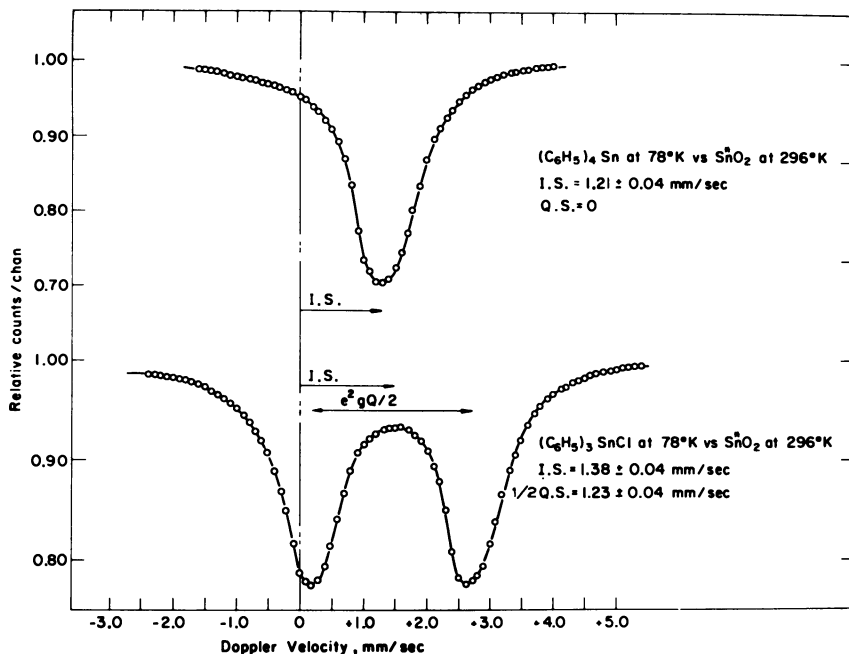
Figure 11. Mössbauer spectra of $(C_6H_5)_4Sn$ and $(C_6H_5)_3SnCl$. Substitution of halogen ligand for C_6H_5 group produces a quadrupole splitting of 2.45 ± 0.06 mm./sec. at 78°K.

chemical bond—valence bond, ligand field, and molecular orbital treatments—predict what the sign of the electrostatic field gradient should be. If the sign can be determined unambiguously, one has gone a long way toward understanding which description of the chemical bond may be applicable to a particular case.

The last major interaction to be derived from the Mössbauer spectrum is the removal of the degeneracy of the sublevels by an internal or external magnetic field and using such measurements to derive information related to the magnetic properties of the material in question. Figure 12 shows a typical spectrum of metallic iron with a six-line hyperfine structure spectrum. The two resonance lines at either end are the − 1/2 to − 3/2 and 1/2 to 3/2 transitions, respectively, and the separation between these two can be directly related to the magnitude of the internal magnetic field. Moreover, the separation between lines 2 and 4 and between lines 3 and 5 is just the ground-state splitting. This splitting, which amounts to 3.924 mm./sec. in metallic iron at room temperature, can be measured by NMR techniques and thus affords an independent (non-Mössbauer) calibration of the Doppler velocity scale in nonconstant velocity spectrometers. [Such a calibration is shown in the lower part of
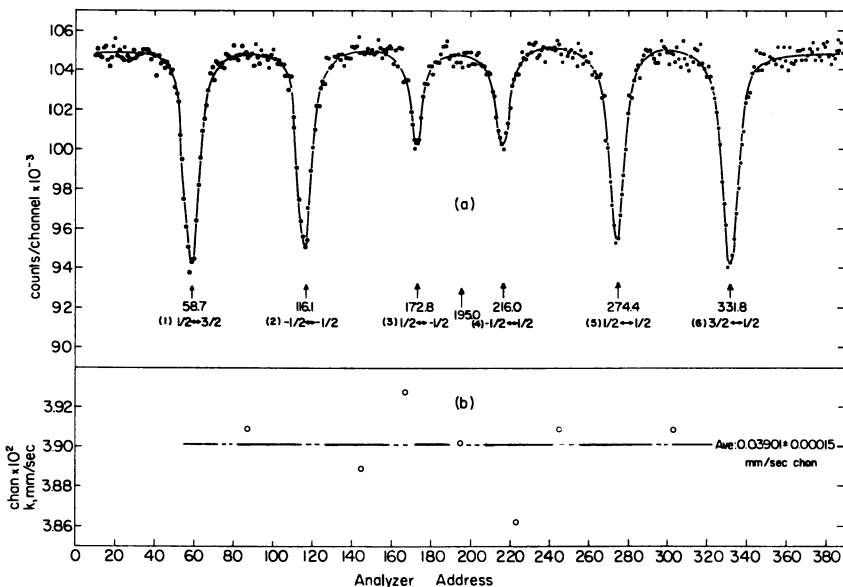
Figure 12.   Mössbauer spectrum of metallic iron at room temperature. Lower diagram shows known energy difference between various resonance peaks used to calibrate velocity scale and indicates the linearity of the velocity as a function of analyzer address

Figure 12, in which the calibration constant, k, in mm./sec. channel, is shown as a function of the analyzer address. In this manner the linearity of the velocity scale can be readily determined over the range of Doppler velocities of interest in most iron and tin Mössbauer experiments.]

Some other parameters to be derived from Mössbauer spectra concern the temperature coefficients of the various parameters—*i.e.*, isomer shift, quadrupole splitting, magnetic hyperfine interaction, line width, and effect magnitude. All have interesting temperature coefficients. Some experiments along these lines have been conducted with doubly labeled stannic iodide, in which one can view both the tin and the iodine resonance (6). A typical iodine-129 spectrum is shown in Figure 13 which represents the Mössbauer spectrum of stannic iodide labeled with iodine-129 using a zinc telluride source. Of the eight possible lines, the velocity scale used in this case spans seven. From their intensities one can calculate not only the field gradient and the isomer shift, but the anisotropy of the recoil-free fraction (the so-called Gol'danskiĭ-Karyagin effect); further, for this particular study, one can calculate the recoil-free fraction as a function of temperature and from these data the typical Mössbauer temperature that is seen by each individual atom.

Figure 14 shows the temperature dependence for the iodine resonance in SnI_4. Data are obtained at several temperatures, and the area
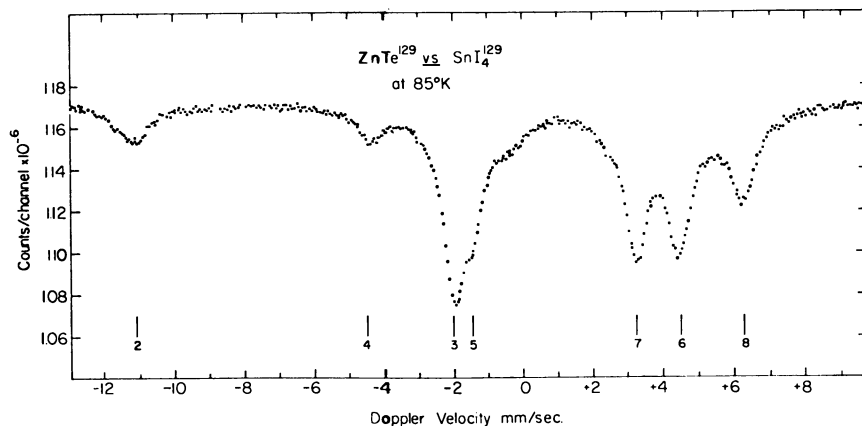
Figure 13.   Mössbauer spectrum of $SnI_4{}^{129}$
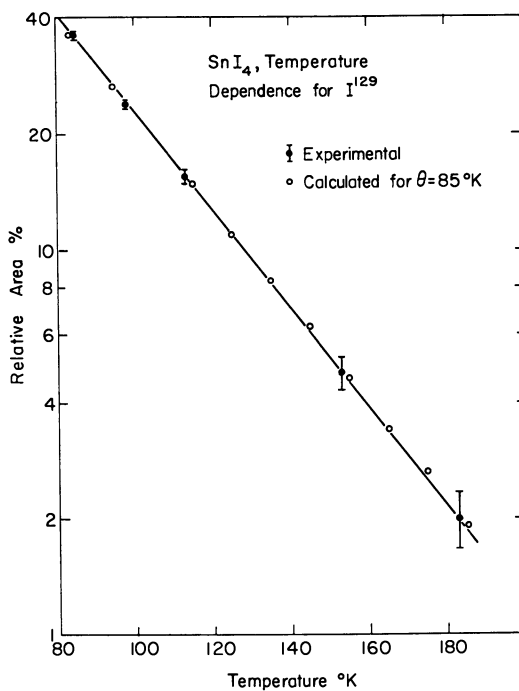
Figure 14.   Temperature dependence of recoil-free fractions for ^{129}I in SnI_4

under the resonance peaks is integrated. From the slope $d \ln A/dT$ a typical temperature of 85°K. is calculated and if the same thing is done for the tin-119 resonance, one comes to the interesting, but not unexpected, conclusion, that the Mössbauer temperature for tin is different from its value for iodine. Figure 15 shows the relevant data which lead to a Mössbauer temperature of 166°K. By comparing these two values with the known infrared and Raman frequencies of SnI_4 (a particularly simple molecule), one can draw some interesting conclusions concerning the contribution to the recoil-free fraction of so-called optical and acoustic vibrational (localized and nonlocalized) modes and their influence on the temperature dependence of the recoil-free fraction.
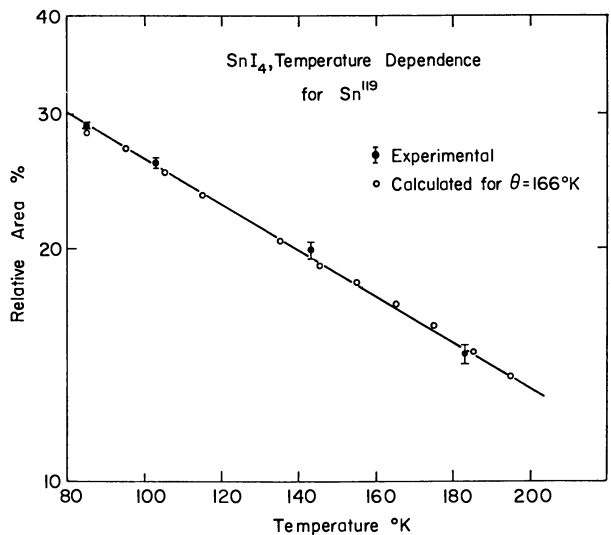
Figure 15.   Temperature dependence of recoil-free fraction for ^{119}Sn in SnI_4

Conclusions

Ten parameters or quantities can be extracted readily from Mössbauer spectra; some others are more difficult to extract. Of these, I have mentioned isomer shift, quadrupole splitting, effect magnitude, line width, magnetic splitting to measure internal and external fields, crystalline asymmetry, Gol'danskiĭ-Karyagin asymmetry (the anisotropy of the recoil-free fraction), recoil-free fraction of the source and absorber, and the calculated Mössbauer temperatures that one can extract from these temperature dependencies, the sign of the electrostatic field gradient, and finally, from the width and the variation in width of the resonance lines one can obtain information about the time scale of electrostatic relaxation

Table I.   Mössbauer Nuclides[a]

Nuclide	E_γ, k.e.v.	$t_{1/2}$, sec. $\times 10^{-8}$	Nuclide	E_γ, k.e.v.	$t_{1/2}$, sec. $\times 10^{-8}$
^{40}K	29.4	0.39	^{160}Dy	86.8	0.205
^{57}Fe	14.38	9.8	^{161}Dy	25.6	2.8
^{61}Ni	67.4	0.53		74.5	0.30
^{67}Zn	93	940	^{166}Er	80.6	0.183
^{83}Kr	9.3	14.7	^{169}Tm	8.41	0.39
^{99}Ru	90	2.0	^{170}Yb	84.2	0.161
^{107}Ag	93	4.4×10^9	^{171}Yb	66.7	[0.05]
^{119}Sn	23.8	1.85	^{177}Hf	113.0	0.052
^{121}Sb	37.2	0.35	^{181}Ta	6.25	680
^{125}Te	35.6	0.14	^{182}W	100.1	0.14
^{127}I	59	0.18	^{183}W	46.5	0.015
^{129}I	26.8	1.63		99.1	0.052
^{129}Xe	40	0.096	^{186}Os	137.2	0.084
^{131}Xe	80.2	0.050	^{187}Re	134.2	0.0010
^{133}Cs	81	0.623	^{188}Os	155.0	0.72
^{141}Pr	145	0.2	^{191}Ir	129.4	0.0131
^{149}Sm	22	0.76	^{193}Ir	73	0.60
^{151}Eu	21.6	0.88	^{195}Pt	98.9	0.017
^{153}Eu	97.5	0.014		129.7	0.055
	103.2	0.38	^{197}Au	77.3	0.18
^{155}Gd	86.5	0.586	^{237}Np	59.6	6.3
^{159}Tb	58.0	0.013			

[a] Data taken mainly from Muir *et al.* (*18*).

phenomena. This point has been discussed by Blume, Wignall, Wertheim, Ingalls, Mullen, and others. One can obtain information concerning chemical effects on a time scale that is not accessible by standard chemical experimental techniques.

Table I shows the various Mössbauer nuclides—*i.e.*, the nuclides where the Mössbauer effect has actually been seen. Not all of these are as easy to exploit as the ^{57}Fe and ^{119}Sn cases referred to above. However, with improved techniques a number of these should prove accessible to the chemist. Representative elements of almost all parts of the periodic table are tractable by these techniques. It seems clear, however, that the methods of Mössbauer spectroscopy are no longer technique-oriented but that this field is becoming a problem-oriented discipline. In other words, the Mössbauer effect is now used successfully in many cases not only to demonstrate the effect or to corroborate physical evidence obtained by other means—NMR, or infrared, or kinetic studies—but also to solve new chemical problems.

Acknowledgments

Literature Cited

(1) Belyakov, V. A., *Phys. Letters* **16**, 279 (1965).
(2) Belyakov, V. A., *Soviet Phys. JETP* **22**, 578 (1966).
(3) Bersuker, I. V., Gol'danskii, V. I., Makarov, E. F., *Soviet Phys. JETP* **22**, 486 (1966).
(4) Bocquet, J. P., Chu, Y. Y., Kistner, O. C., Perlman, H. L., Emery, G. T., *Phys. Rev. Letters* **17**, 809 (1966).
(5) Brafman, H., Greenshpan, M., Herber, R. H., *Nucl. Instr. Methods* **42**, 245 (1966).
(6) Bukshpan, S., Herber, R. H., *J. Chem. Phys.* **46**, 3375 (1967).
(7) Collins, R. L., *J. Chem. Phys.* **42**, 1072 (1965).
(8) Cordey-Hayes, H., "Applications of the Mössbauer Effect in Chemistry and Solid State Physics," I.A.E.A., Vienna, 1966, pp. 156 ff.; *J. Inorg. Nucl. Chem.* **26**, 915 (1964).
(9) DeBenedetti, S., Lang, G., Ingalls, R., *Phys. Rev. Letters* **6**, 60 (1961).
(10) Gibb, T. C., Greenwood, N. N., *J. Chem. Soc.* **1966**, 43.
(11) Gol'danskii, V. I., Makarov, E. F., *Phys. Letters* **14**, 111 (1965).
(12) Gordon Conference on Inorganic Chemistry, 1964: N. N. Greenwood, J. F. Duncan, J. Danon, V. I. Gol'danskii, J. J. Spijkerman, L. M. Epstein, *et al.*, participants.
(13) Herber, R. H., Parisi, G. I., *Inorg. Chem.* **5**, 769 (1966).
(14) Ibraimov, N. S., Kuz'min, R. N., *Soviet Phys. JETP* **48**, 103 (1965).
(15) Kistner, O. C., Sunyar, A. W., *Phys. Rev. Letters* **4**, 412 (1960).
(16) Lees, J., Flinn, P., *Phys. Letters* **19**, 186 (1965).
(17) Litster, J. D., Benedek, G. B., *J. Appl. Phys.* **34**, 688 (1963).
(18) Muir, A. H., Jr., Ando, K. J., Coogan, H. M., "Mössbauer Effect Data Index," North American Aviation Science Center, Issue 3 (1966).
(19) Panyushkin, V. N., Voronov, F. F., *Soviet Phys. JETP Letters* **2**, 97 (1965).
(20) Pipkorn, D. N., Edge, C. K., deBrunner, P., DePasquali, G., Drickamer, H. G., Frauenfelder, H., *Phys. Rev.* **135**, A1604 (1964).
(21) Plotnikova, M. V., Mitrofanov, K. P., Shpinel', V. S., *Zh. Eksperim. Teor. Fiz. Letters* **3**, 323 (1966).
(22) Pound, R. V., Benedek, G. B., Drever, R., *Phys. Rev. Letters* **7**, 405 (1961).
(23) Ruby, S. L., Flinn, P. A., *Rev. Mod. Phys.* **36**, 351 (1964).
(24) Schechter, M., Ron, M., Niedzwiedz, S., Herber, R. H., *Nucl. Inst. Methods* **44**, 268 (1966).
(25) Stöckler, H., Herber, R. H., unpublished results.
(26) Spijkerman, J. J., ADVAN. CHEM. SER. **68**, 105 (1967).
(27) Walker, L. R., Wertheim, G. K., Jaccarino, V., *Phys. Rev. Letters* **6**, 98 (1961).
(28) Wertheim, G. K., "Mössbauer Effect, Principles and Application," Academic Press, New York, 1964.
(29) Zuckerman, J. J., private communication.

Structural Studies of Compounds and Alloys Using the Mössbauer Effect

P. A. FLINN[1]

Carnegie Institute of Technology, Pittsburgh, Pa.

The Mössbauer effect, although not a substitute for other analytical methods such as x-ray diffraction, can be used to obtain several kinds of structural information about solids. In favorable cases, it is possible to obtain rather detailed information about the electronic configuration of atoms and the local symmetry of their sites by measuring the isomer shift and quadrupole splitting. If more than one valence state of a given atom is present, a semiquantitative determination of the amount of each kind is possible. In solid solutions, the amount of local or long range order can be estimated, and in certain defect structures the relation between the active atoms and the defects can be studied.

Crystal structure—*i.e.*, the relative positions of the atoms in a crystalline solid, is usually determined by methods such as x-ray diffraction, neutron diffraction, and electron diffraction. One certainly cannot determine structure directly by the Mössbauer effect; however, there are special cases where it is difficult to get complete information by diffraction methods. In some cases, two atoms may have similar scattering powers and hence they are hard to distinguish by x-ray methods. One may have a partially ordered structure where there is some distribution of different kinds of atoms among different sites. In special cases, the Mössbauer effect can be a powerful tool to understand better what is happening, but it has not become a substitute for standard diffraction methods. One aspect of structure for which the Mössbauer effect becomes quite useful is the study of defect structures—cases where there are vacancies or impurity concentrations at low levels, or the early stages of phase trans-

[1] Present address: Laboratoire de Physique du Solide, E.N.S.M.I.M., Parc de Saurupt, Nancy 54, France.

formations, when the segregation of atoms is on a scale which is difficult to detect with diffraction methods. The Mössbauer effect can also be used to study surfaces. Here again, low energy electron diffraction can be used, but it is a difficult method to apply, and in certain circumstances one gains some interesting information with the Mössbauer effect.

I regard the question of electronic structure as part of the general question of the structure of solids. We want to know not only where the nuclei are located relative to one another but what the electronic wave functions are like. This, I think, is the most important use of Mössbauer methods because it is an area in which one can learn very little by x-ray diffraction. Some years ago Weiss and DeMarco tried to determine the electron distribution in the transition metals (20). They arrived at seriously wrong answers (2) because of the inherent limitations of x-ray diffraction in looking at outer electrons, whereas the isomer shift and the quadrupole splitting of the Mössbauer spectra can give rather direct information about the electronic wave functions. I would like to begin by discussing what is known as the greatest tin controversy.

Isomer Shift

Next to ^{57}Fe, ^{119}Sn is the second "best" Mössbauer isotope, in the sense that the γ-ray energy, Mössbauer lifetime, and parent lifetime are all satisfactory. To use isomer shift measurements effectively, one must know the relative change in nuclear radius ($\delta R/R$). In the case of ^{119}Sn, the correct value for this quantity was indefinite, both as to sign and magnitude.

Herber (4) and I arrived at the same conclusion about the sign of $\delta R/R$ on quite different grounds. The nuclear theory was in controversy: Belyakov, by one method arrived at the wrong answer (3); Uher and Sorensen, using a different method of approximation (19), arrived at the right answer, but of incorrect magnitude. Calculations of this sort involve small differences between large quantities and are not very reliable. It was possible to determine the sign of $\delta R/R$ quite unambiguously, even before this new experiment, simply by considering the two allotropic forms of tin, both of which have long been well understood. Gray tin, which has the diamond structure, is a semiconductor, and the band structure has been calculated theoretically by Cohen and Bergstresser (5) and also by Bassani and Liu (1). Tin also has a metallic form—white tin—with a somewhat more complicated crystal structure. The coordination is higher, and the interatomic distance is substantially larger. This, again, has been studied extensively by non-Mössbauer experiments such as the deHaas-vanAlphen effect and the Gantmacher effect (7, 9). Weisz has performed a detailed band structure calculation (21). For

each form of tin, then, the band structure is quite well-known, both from theory and experiment. The detailed band structures are complicated, but it is possible to give a rather simple qualitative description of them.

One might expect (and it actually turns out that way) that the wave functions of the solid are primarily derived from the 5s and 5p electrons of the free atom. The bands are made up primarily of the 5s bonding and the 5s anti-bonding wave functions, and also the 5p bonding and the 5p anti-bonding. For gray tin (diamond structure) the atoms are close together with an interatomic distance of 2.8 A. This has the effect of raising the energy of the anti-bonding 5s levels somewhat above that of the 5p bonding states; therefore the occupied bands are built up from 5s bonding and the $5p_x$, $5p_y$, and $5p_z$ bonding electrons. Crudely speaking, there are three 5p electrons and one 5s electron per tin atom in gray tin.
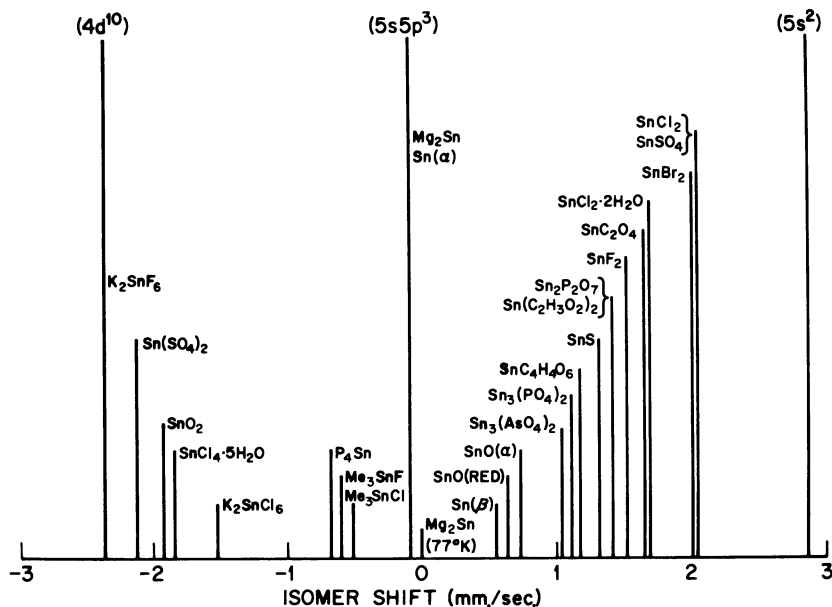
Figure 1. Isomer shifts for ^{119}Sn in various environments, relative to a Mg$_2$Sn source at 77°K. (12)

In white tin, the nearest neighbor interatomic distance is increased to about 3 A. As expected, this lowers the energy of the 5s anti-bonding functions, and in a considerable portion of the Brillouin zone the 5s anti-bonding functions lie below the 5p like functions in energy; hence, there are substantially more than one 5s electron and substantially less than three 5p electrons per atom. Judging from the Mössbauer data (one could get this presumably from the band calculations with enough effort),

the configuration is something like $5s^{1.4}5p^{2.6}$. The opposite result is essentially inconceivable; there is nothing I can think of which would bring anti-bonding $5p$ electrons below bonding $5s$ electrons in energy, which would be necessary to get less than one $5s$ electron in the metallic form. Hence, it seems quite clear that using knowledge about the allotropic forms of tin we can determine the sign of the change in electron density at the nucleus in going from gray tin to white tin. We also need a calculation of the effect on the charge density at the nucleus arising from these changes in the outer electron configuration. This was carried out by Waber, Lieberman, and Cramer (*14*) using a relativistic self-consistent field calculation for tin for several different configurations. A somewhat similar calculation using a non-relativistic method to begin with and perturbation theory, was carried out by Ruby *et al.* with essentially the same results (*16*).

These calculations show that there is no serious disturbance of the $1s$, $2s$, and $3s$ and $4s$ levels by changes in the number of $5s$ and $5p$ electrons. The leading term in the change in charge density at the nucleus is simply proportional to the number of $5s$ electrons. There are two second-order terms, one term which depends on the square of the number of $5s$ electrons, which is simply a shielding effect of one $5s$ by the other, and a term involving the product of the number of $5s$ and $5p$ electrons which is the effect of the screening of the $5p$ on the $5s$. There is essentially no effect of the $5p$ electrons on anything but the $5s$, and these two second-order terms have coefficients which are down by somewhat more than an order of magnitude from the leading term. To a good first approximation, the charge density at the nucleus depends simply on the number of $5s$ electrons, and one can make good quadratic corrections to this.

The isomer shift measurements on the two forms of tin, coupled with the knowledge of the way the wave functions behave, establish unambiguously the sign of $\delta R/R$. It is also easy to understand the pressure experiment reported by Panyushkin and Voronov (*15*). They find that the charge density at the tin nucleus decreases with increasing pressure, but there is nothing anomalous about this. As pressure reduces the interatomic distance, the energy of the anti-bonding $5s$ orbitals is raised, producing a transfer of electrons from $5s$ character into $5p$ character as the energy of s levels is raised relative to p levels. This is exactly what one would expect.

To get a fairly good number for the change in nuclear radius, we can consider a wider class of tin-containing materials. The results in Figure 1 are the work of Lees (*12*). Here we have taken arbitrarily as our origin, the source, the intermetallic compound Mg_2Sn, which provides a convenient cubic environment for tin. It gives a line which has natural

width and which, if cooled to 77°K., has a recoilless-free fraction of
about 0.7 to 0.8, so that one gets a rather good Mössbauer effect.

Compounds in which tin is covalently bonded lie near the center of
the diagram—gray tin and several organometallic compounds. Stannic
compounds lie in a comparatively narrow group near −2 mm./sec., while
stannous compounds lie in a large band to the right of zero.

One immediate question appears: why the wide range of isomer
shifts for stannous compounds? The tin ions cannot be in the ideal
$Sn^{2+}(5s^2)$ state. What is happening? All of these compounds have compli-
cated crystal structures, with tin located at a site which does not have
inversion symmetry; there is an electric field acting at the site of the tin.
This electric field produces matrix elements between the $5s$ and the $5p$
states of the tin and therefore a mixing of the two states. The ground
state under these circumstances is not a pure $5s$ state, but a mixture of
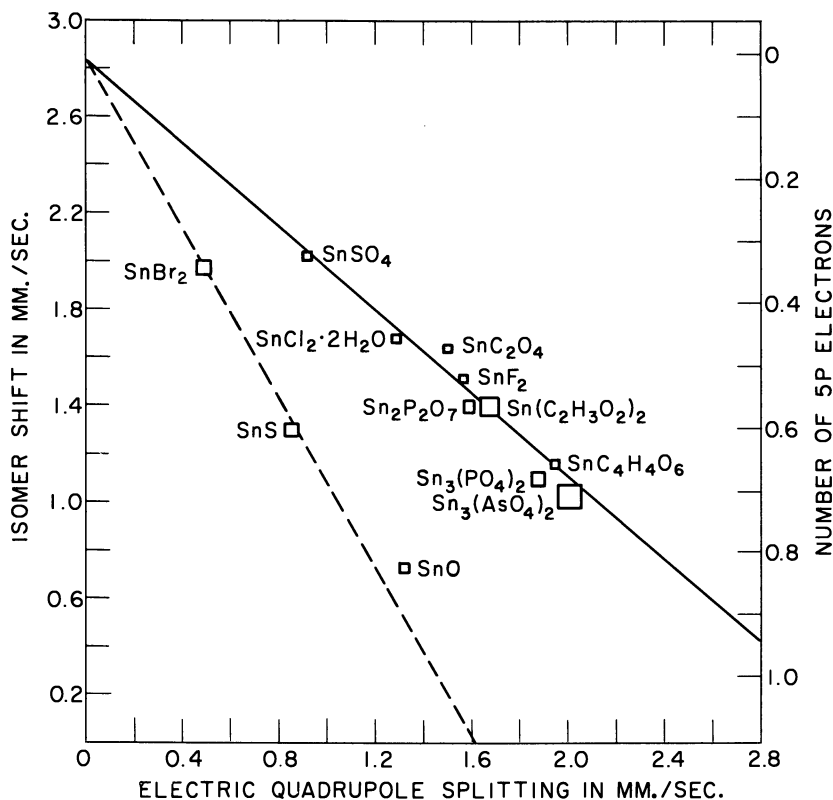$5s$ and $5p$. This is confirmed by studying the quadrupole splitting of

*Figure 2.   Relation between isomer shift and quadrupole splitting for
stannous compounds* (13)

these compounds along with the isomer shift. Since the $5s$ wave function is spherically symmetric, it produces no electric field gradient at the nucleus. The $5p$ wave function, of course, is not spherically symmetric. It does give rise to a rather large field gradient at the nucleus, and to a good first approximation the quadrupole splitting observed is simply proportional to the amount of $5p$ character in the ground state wave function. A plot of the isomer shift *vs.* the quadrupole splitting should give a straight line, and in fact, does for most stannous compounds, as shown in Figure 2 (*13*). Noting this, one can then extrapolate this curve to zero quadrupole splitting, which would correspond to an ideal stannous ion. That establishes the point on the isomer shift scale corresponding to an ideal stannous ion, which, so far as I have been able to find, does not occur in nature. There apparently is no case in which the stannous ion occurs at a point of cubic symmetry.

Having the point for a $5s5p^3$ configuration (gray tin) and the extrapolated $5s^2$ point, one has a scale for coverting isomer shift to charge density at the nucleus. We have established the value of $\delta R/R$ and we can look to see where other points would come. For example, we can look to see where an ideal stannic ion, which would have the configuration $4d^{10}$, no $n = 5$ electrons at all would be on the scale. We find that actually there seems to be one stannic compound—potassium fluorostannate—which is approximately an ideal Sn^{+4}. The tin is surrounded by six fluorines, and it is not surprising that it loses all its valence electrons to the fluorine. We find some other stannic compounds fairly close—the sulfate, the tetrafluoride, the oxide, and the chloride. The chlorostannate, for some reason, is much less ionic than the fluorostannate. One then sees that the organotin compounds, such as tetramethyl tin chloride, tetramethyl tin fluoride, tetraphenyl tin, lie slightly to the left of the ideal covalent tin configuration, which again is not surprising. We know that tin can lose outer electrons relatively easily, whereas carbon does not, so it is not surprising that tin in contact with carbon would undergo what appears to be some transfer of charge to the carbon. The phenyl group, which is unsaturated, seems to soak up somewhat more charge than the methyl group.

The relevance of the Mössbauer effect to chemistry is that now one can reinvestigate compounds such as the tin tetrahalides which were previously thought to be understood. There are molecular orbital calculations, quoted by Goldanskii, based on the assumption that the tin tetrahalides are primarily covalent in character.

The results are misleading simply because the basic set of functions used is inappropriate. The great value of the Mössbauer technique is that once $\delta R/R$ is established, one then has a rather severe test to apply to theoretical calculations concerning the structure of compounds. If

the wave functions are correct, one will obtain correct δ values for the charge density at the nucleus and from the p wave functions, correct values for the quadrupole splitting.

In interpreting the quadrupole splitting, the electric field gradients seen by the nucleus can be either primarily internal or primarily external. In cases such as the stannous ions, where one has a considerable p character to the wave function of the stannous ion, the effect is primarily internal—*i.e.*, the field gradient produced at the nucleus by its own electrons in a non-symmetric wave function is large compared with that from external sources. When one has spherically symmetric ions (—*e.g.*, the ferric ion), one can see quadrupole splittings arising from the non-cubic field of the surrounding ions in the crystal. That effect is normally much smaller than the internal effect. If an internal quadrupole splitting is present, you need consider only the effect of the wave functions of the ion itself, at least as a reasonable first approximation.

Structure of Solids

First, some questions involving the crystal structure of alloys and intermetallic compounds. Figures 3, 4, and 5 are from the work of Shirane and others on the iron-rhodium alloys (*17*). The iron-rhodium alloy system is rather interesting. If rhodium is added to pure iron, the rhodium is soluble in both the low temperature body-centered phase of iron and also the high temperature gamma phase, which is face-centered. Initially the transformation temperature is not changed drastically by adding rhodium; a body-centered solid solution exists at low temperatures, and a face centered solid solution exists at elevated temperatures., When more than about 20% rhodium is present, the transformation from the high temperature phase to the low temperature phase is sufficiently sluggish so that one can preserve the high temperature phase, at least in part, by drastic quenching. Also in the low temperature phase—somewhere about 20 or 25% rhodium—long range order appears, and continues up to approximately a 50–50 mixture. At 50–50 the ideal cesium chloride structure exists, with one kind of atom in the center of the cube, the other kind at the corners. In alloys which contain less than the ideal equiatomic amounts of rhodium, the same structure exists, but now since there is not enough rhodium to go around, some of the rhodium sites are occupied with iron. One can study this quite nicely with the Mössbauer effect.

Figure 3 shows the Mössbauer spectra for an alloy of 75% iron and 25% rhodium after two different heat treatments. Since absorption rather than transmission is plotted, these curves are right side up. The upper spectrum is taken from an alloy which was annealed in the low temperature field (cesium chloride structure), and there are two six-line patterns
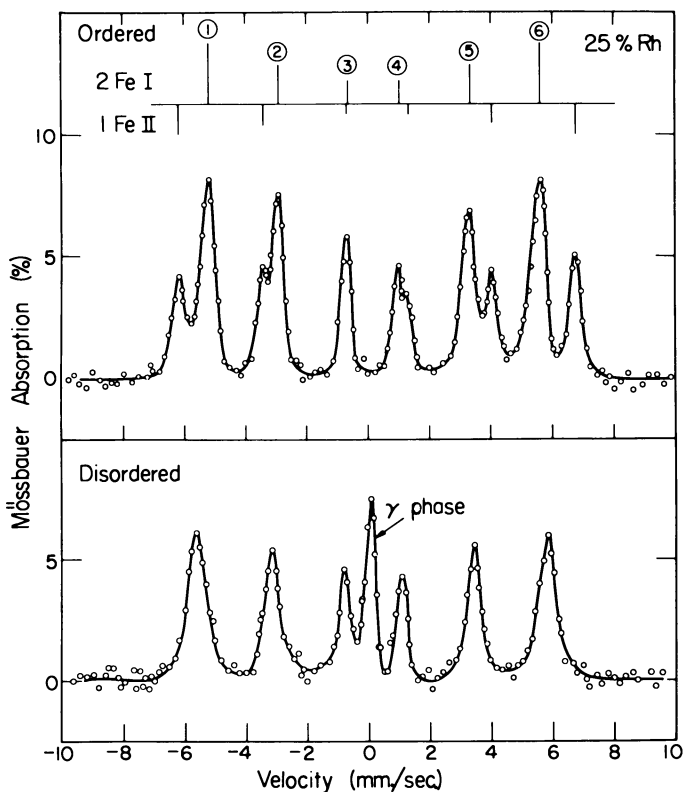
Figure 3.   Mössbauer spectra for ordered and disordered samples of an alloy of 25% rhodium and 75% iron. The disordered sample was quenched and contains retained austenite (17)

as indicated with intensities in the ratio 2:1. At the 25% composition, half of the rhodium sites will have to be occupied by irons; consequently, there will be half as many irons on rhodium sites as there are irons on proper iron sites. One can immediately identify the weaker set of lines with the irons which are on rhodium sites. The splitting of this set of lines is somewhat larger than that of the other, meaning that the magnetic field at the iron nucleus is larger if the iron is on a rhodium site and therefore has all iron neighbors. This is not surprising. There is also a slight isomer shift between the two sets of patterns, meaning there is a slightly different charge density at the nucleus for the iron in the two cases.

If the alloy is quenched so as to preserve some of the high temperature gamma phase which is not ferromagnetic, one observes a single peak at the center in addition to the six-line pattern from the disordered solid

solution. The transformation is such that no ordering in the alpha phase can occur and one obtains an almost random arrangement of the iron and rhodium atoms. The peaks are somewhat broader than in the ordered arrangement because one actually has a superposition of many six-line patterns for iron with slightly different local environments. The hyperfine field and isomer shifts are slightly different at the different iron nuclei, depending on just how many rhodium and iron neighbors each has in the random solution.

It is also interesting to look at alloys in this system at and near the equiatomic composition. Figure 4 shows just two lines of the six-line pattern—the two on the far right. At 50% rhodium every iron is completely surrounded by rhodium neighbors, and the lines are perfectly
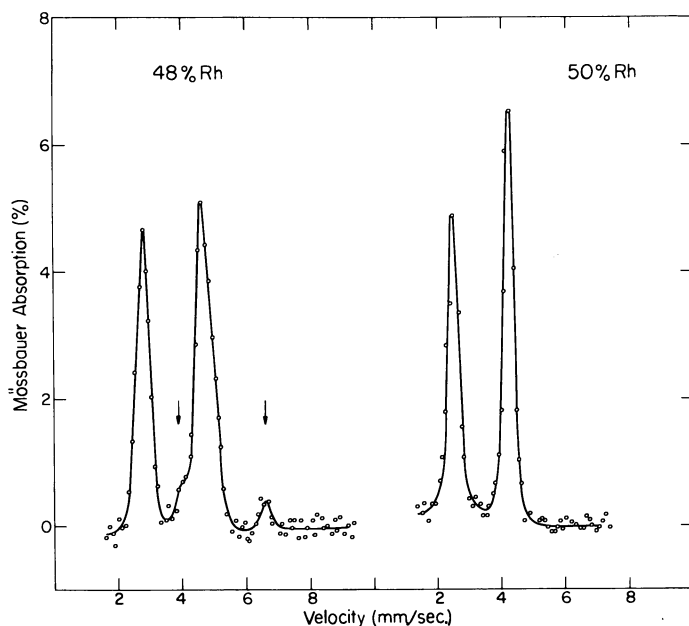
Figure 4.   Portion of the Mössbauer spectrum for iron—rhodium alloys containing 48 and 50% rhodium (17)

sharp. At 48% rhodium there are a few irons which are necessarily on rhodium sites, and their contributions to the pattern appear immediately as small peaks indicated by arrows. In this case, we see that the Mössbauer effect is very sensitive to small deviations from perfect order. Figure 5 shows the results for a moderately dilute alloy (10% rhodium). The main peak is from irons which have only iron neighbors; a smaller peak comes from those irons which, because of the statistical nature of the solid solution, have one rhodium neighbor.

Figure 6 illustrates a more complicated situation. The sample was a plain iron-carbon steel—an iron foil carburized to about 5 atomic % carbon and then quenched. One sees a rather complex pattern. There is a large central peak from some untransformed high temperature face-centered phase of iron containing carbon in solid solution, "retained austenite." There is a strong six-line pattern coming from "martensite," a distorted body-centered solid solution of carbon in iron. We also see a
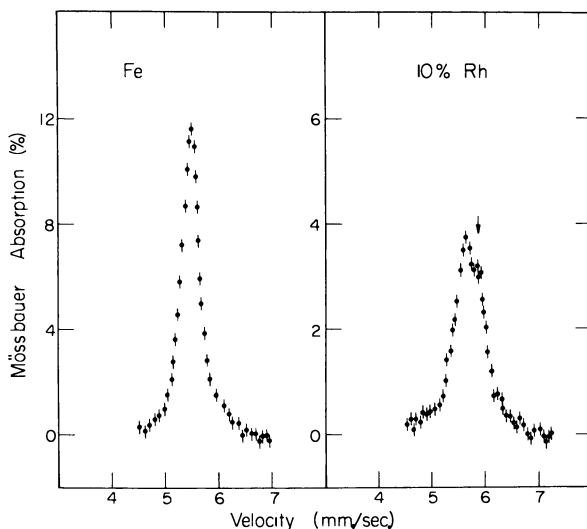

Figure 5.   Outer peak of Mössbauer spectrum showing the structure resulting from the existence of more than one local environment in an alloy of iron with 10% rhodium (17)

secondary set of peaks which are not present in really fresh martensite but occur during a few minutes of annealing at a moderate temperature, such as room temperature, and which are caused by the clustering of carbon in the martensite. This is a kind of pre-precipitation process which can be studied in some detail by studying the Mössbauer pattern of such an alloy as a function of heat treatment (8).

Surface

Finally, another type of defect one can study is a surface—*e.g.*, the surface of an aluminum oxide catalyst containing iron in the surface layers. Figure 7 shows the Mössbauer spectrum for ^{57}Fe in the surface layers of an aluminum oxide catalyst (6). One sees first of all a quadrupole splitting which is unusually large for a ferric ion. This is caused by
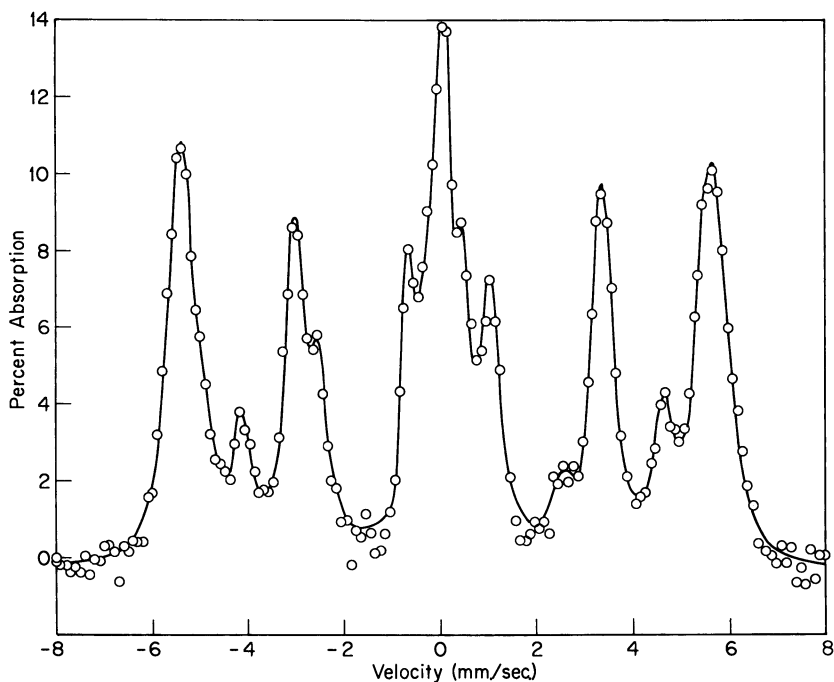
Figure 6. Mössbauer spectrum for an iron-carbon martensite containing about 5 atomic % carbon

the fact that the iron ions are in the surface and therefore in an extremely asymmetrical environment.

One also sees that at room temperature the two peaks of the quadrupole split pattern are different in intensity. This difference disappears at 77°K. It is an example of what is known as the Gol'danskiĭ effect (*10*) and is caused by the fact that the amplitude of vibration is different, parallel to the surface and normal to the surface, so that the effective resonant fraction is different for the two halves of the quadrupole splitting. This effect has been extensively studied by the Russians. In a recent paper, Suzdalev and others report a study of tin in the surface of silica gel (*18*). They put calcium ions in the surface of silica gel, then replaced them with divalent tin by ion exchange. The result was a mixture of stannous and stannic ions, and of course, the use of the Mössbauer effect made it possible to determine accurately the relative amounts of the two. They studied the amplitude of vibration of the two kinds of atoms and found, for example, for the stannous ions, the r.m.s. amplitude of vibration parallel to the surface was 0.07 A., and the r.m.s. amplitude of vibration perpendicular to the surface was about twice as great—about 0.13 A. Karasev and others have also worked on the chemistry of adsorbed
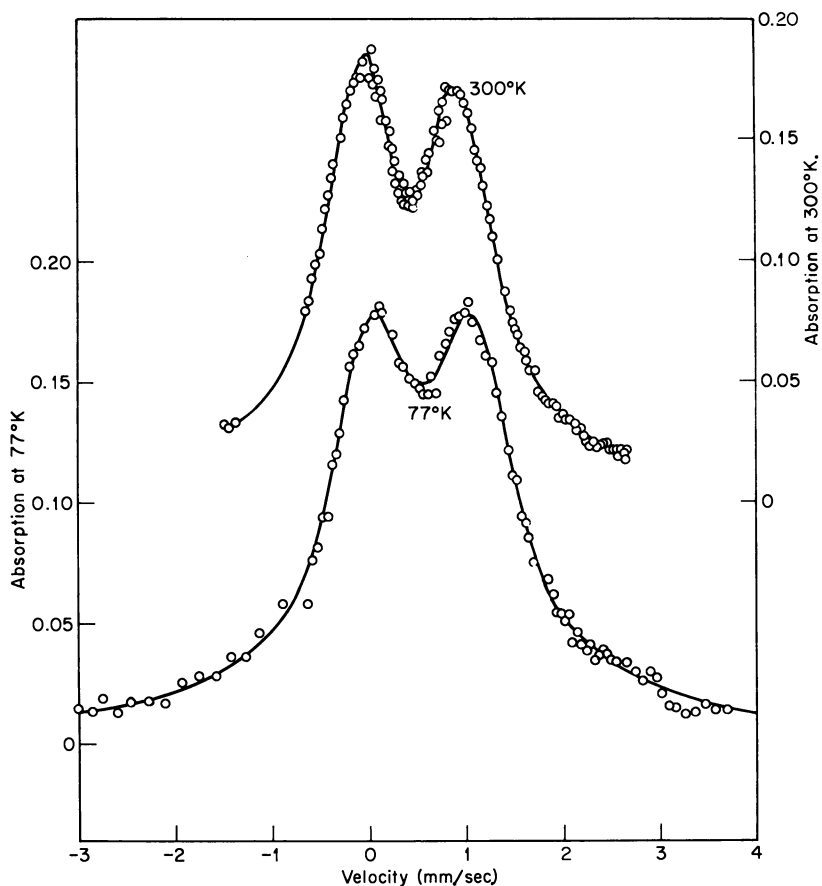
Figure 7.   Mössbauer spectra for ^{57}Fe at the surface of Al_2O_3 (6)

surface layers (*11*). They adsorbed tetraphenyl tin on silica gel and similar catalysts and, by adsorbing it under different conditions of temperature and pressure could follow in considerable detail the nature of the adsorption processes and structure of the adsorbed layer.

This is by no means a complete catalog, but, hopefully some introduction to the possibilities of studying the structure of solids with the Mössbauer effect.

Literature Cited

(1) Bassani, F., Liu, L., *Phys. Rev.* **132**, 2047 (1963).
(2) Batterman, B. W., Chipman, D. R., DeMarco, J. J., *Phys. Rev.* **135** A1612 (1964).
(3) Belyakov, V. A., *Soviet Phys. JETP (English Transl.)* **22**, 578 (1966).

(4) Bocquet, J. P., Chu, Y. Y., Kistner, O. C., Perlman, M. L., *Phys. Rev. Letters* **17**, 809 (1966).
(5) Cohen, M. L., Bergstresser, J. K., *Phys. Rev.* **141**, 789 (1966).
(6) Flinn, P. A., Ruby, S. L., Kehl, W. L., *Science* **143**, 1434 (1964).
(7) Gantmakher, V. F., *Soviet Phys. JETP (English Transl.)* **19**, 1366 (1964).
(8) Genin, J. M., Flinn, P. A., *Phys. Letters* **22**, 392 (1966).
(9) Gold, A. V., Priestley, *Phil. Mag.* **5**, 1089 (1960).
(10) Gol'danskiǐ, V. I., Makarov, E. F., Khrapov, V. V., *Phys. Letters* **3**, 344 (1963).
(11) Karasev, A. N., Polak, L. S., Shlikhter, E. B., Shpinel, V. S., *Kinetika Kataliz* **6**, 710 (1965).
(12) Lees, J. K., Ph.D. Thesis, Carnegie Institute of Technology (1966).
(13) Lees, J. K., Flinn, P. A., *Phys. Letters* **19**, 186 (1965).
(14) Liberman, D., Waber, J. T., Cromer, D. T., *Phys. Rev.* **137**, A27 (1965).
(15) Panyushkin, V. N., Voronov, F. F., *Soviet Phys. JETP Letters* **2**, 97 (1965).
(16) Ruby, S. L., Kalvius, G. M., Snyder, R. E., Beard, G. B., *Phys. Rev.* **159**, 239 (1967).
(17) Shirane, G., Chen, C. W., Flinn, P. A., Nathans, R., *Phys. Rev.* **131**, 183 (1963).
(18) Suzdalev, I. P., Gol'danskiǐ, V. I., Makarov, E. F., Plachinda, A. S., Korytko, L. A., *Soviet Phys. JETP (English Transl.)* **22**, 979 (1966).
(19) Uher, R. A., Sorenson, R. A., *Nucl. Phys.* **86**, 1 (1966).
(20) Weiss, R. J., DeMarco, J. J., *Rev. Modern Phys.* **30**, 59 (1958).
(21) Weisz, G., *Phys. Rev.* **149**, 504 (1966).

3

Study of Magnetic Properties of Materials Using the Mössbauer Effect

R. W. GRANT

North American Aviation Science Center, Thousand Oaks, Calif.

One of the most active fields of investigation using the Mössbauer effect has been studying the magnetic properties of materials via magnetic hyperfine interactions. Until the discovery of the Mössbauer effect, the possibility of observing nuclear gamma-ray transitions between individual nuclear magnetic substates seemed remote; however, the narrowness of the Mössbauer transition in some isotopes has made it possible to observe resolved transitions between these substates directly. This allows one to investigate the magnetic properties of materials. The wide range of phenomena that can be investigated by means of the magnetic hyperfine interactions make the Mössbauer effect an extremely valuable tool for studying magnetic properties.

One of the most active fields of investigation using the Mössbauer effect has been studying magnetic properties of materials *via* the magnetic hyperfine interaction. In fact, such a large fraction of the Mössbauer literature has been concerned with these studies that a concise, comprehensive review of the subject has become nearly impossible. Therefore, in this paper, an attempt is made to pick several examples from the literature which at least indicate the usefulness and scope of the Mössbauer effect for magnetic studies. A fairly exhaustive review of hyperfine interactions in magnetic materials (*11*) and a complete bibliography of Mössbauer literature (*31*) have recently been published.

Until the discovery of the Mössbauer effect, the possibility of directly observing nuclear γ-ray transitions between individual nuclear magnetic substates seemed remote because of the small energy differences involved; however, the extremely high energy resolution of Mössbauer spectroscopy has made it possible to resolve these transitions directly in some isotopes, and it is this feature that is so valuable for investigating

34

magnetic properties. To date, most magnetic studies using the Mössbauer effect have involved the isotope ^{57}Fe. Magnetic hyperfine structure (nuclear Zeeman effect) has been observed in several Mössbauer transitions, but in most cases the emphasis has been on determining nuclear moments and not using the hyperfine structure to study magnetic properties of materials [there are, of course, several exceptions (*1, 6, 39*)]. One of the main reasons that ^{57}Fe has been used so predominantly in magnetic studies is the ease with which magnetic hyperfine structure can be observed in this isotope and the fact that Fe is involved in so many interesting magnetic materials. Undoubtedly, as experimental techniques improve, several other isotopes will be useful for this purpose. The examples presented in the following discussion all involve ^{57}Fe, and therefore, by way of introduction a brief description of the magnetic hyperfine interaction is given, with particular emphasis on ^{57}Fe.

Magnetic Hyperfine Interaction

The Hamiltonian which describes the magnetic hyperfine interaction between a nucleus and its associated electrons in an atom can be written (*26*) as

$$\mathfrak{H} = -\vec{\mu} \cdot \vec{H} \tag{1}$$

where $\vec{\mu}$ is the nuclear magnetic moment, and $\vec{H}$ is the magnetic field which the electrons produce at the nucleus. The nuclear magnetic moment is related to the nuclear spin, I, by

$$\vec{\mu} = g \, \mu_N \, \vec{I} \tag{2}$$

where g is the nuclear g factor ($g = \mu/I\mu_N$) and μ_N is the nuclear magneton. One can, therefore, rewrite Equation 1 as

$$\mathfrak{H} = -g\mu_N \vec{I} \cdot \vec{H} \tag{3}$$

For a single electron or for one electron outside of a closed shell, the total angular momentum of the electronic shell, $\vec{J}$, is antiparallel to $\vec{H}$ (*26*). This is not always true for a configuration involving several electrons but is correct in most cases. Kopfermann discusses this question in considerable detail. Therefore, in the normal case where $\vec{H}$ and $\vec{J}$ are antiparallel, $\vec{\mu}$ will be parallel or antiparallel to $\vec{H}$ depending on whether g is positive or negative. If $\vec{H}$ is proportional to $\vec{J}$, Equation 3 can be written in the familiar form (*11*)

$$\mathfrak{H} = A\vec{I} \cdot \vec{J} \tag{4}$$

where A is the magnetic hyperfine structure constant. In magnetically ordered materials, $\vec{J}$ will produce an effective magnetic field at the nucleus.

We define the magnetic field observed at the nucleus as H_N. The origin of H_N is a problem of great theoretical interest and still is not quantitatively understood, mainly because several large terms of different signs can contribute to H_N, and it is difficult to calculate them with high precision [for a discussion of the origin of H_N, see e.g. (29, 38)]. For a nuclear level with $I > 0$, the magnetic hyperfine interaction splits the nuclear level into $2I + 1$ nuclear magnetic substates whose eigenvalues are

$$E_m = -g\mu_N H_N m_I \tag{5}$$

where m_I is the nuclear magnetic quantum number and has the values $m_I = I, I - 1, \ldots, -I$. From Equation 5 it is obvious that while the magnetic hyperfine interaction removes the degeneracy of a nuclear level, it does not shift the center of gravity of the multiplet.

Equation 5 also shows that the magnetic hyperfine interaction contains both a nuclear and an atomic parameter which cannot be experimentally separated. The same situation is faced in both the isomer shift and electric quadrupole interactions. However, the situation is considerably more favorable for the case of the magnetic hyperfine interaction than for the electric hyperfine interactions because one is often able to apply a large enough external magnetic field to perturb the field significantly at the nucleus. Also, many ground state magnetic moments are known from conventional measurements so that one can determine both the field at the nucleus and the excited state nuclear moment from the observed Mössbauer hyperfine structure.

The isotope ^{57}Fe has $I = 1/2$ in the ground state and $I = 3/2$ in the excited state. The presence of an internal field then produces a hyperfine splitting of the nuclear levels (Figure 1). The ground state magnetic moment is positive while the excited state moment is negative, which accounts for the reversed ordering of the m_I levels in the two states. The γ-ray which connects the excited state (14.4 k.e.v.) to the ground state in ^{57}Fe is almost exclusively magnetic dipole, $M1$, in character, which has selection rules $\Delta m_I = \pm 1, 0$; therefore, in the presence of an internal magnetic field, one can observe six transitions between these two levels (see Figure 1). The angular dependence of the individual Zeeman component transition probabilities is often of interest in magnetic studies, and this dependence is also shown in Figure 1. Lines 1, 3, 4, and 6 (which correspond to the $\Delta m_I = \pm 1$ transitions) have a $(1 + \cos^2\theta)$ angular dependence, where θ is the angle between the internal field and the γ-ray emission or absorption direction while lines 2 and 5 ($\Delta m_I = 0$) have a $\sin^2\theta$ dependence. These angular dependencies show that the total radiation pattern emitted between the two states is isotropic.

In Mössbauer studies of magnetic materials, it is often of interest to apply an external magnetic field to a sample and observe the spatial distribution of $\vec{H}_N$ as a function of external field. A parameter which characterizes this distribution and is directly measured by Mössbauer spectroscopy is $\overline{\cos^2\theta}$. For ^{57}Fe (in the thin absorber and isotropic mean square displacement approximation), this parameter is just

$$\overline{\cos^2\theta} = \frac{I_1 - I_2 + I_3 + I_4 - I_5 + I_6}{\displaystyle\sum_{i=1}^{6} I_i} = 1 - \frac{2(I_2 + I_5)}{\displaystyle\sum_{i=1}^{6} I_i} \tag{6}$$

where I_i is the intensity of the ith line following the notation used in Figure 1. Proof of this relationship is given below.

Proof of Relationship. To show that the expression in Equation 6 is valid, one sets up a probability distribution function $f(\theta,\phi)$ which describes the probability of the time average of the atomic spin, $\langle S \rangle$, intersecting a surface element on a unit sphere at θ,ϕ (θ and ϕ are the usual spherical coordinates). The observation direction is $\theta = 0$. By noting the angular intensities shown in Figure 1, one obtains the following expressions for the intensities of the various lines:

$$I_{1,6} = 3/2 \int_0^{2\pi} \int_0^{\pi} f(\theta,\phi)(1 + \cos^2\theta)\sin\theta d\theta d\phi$$

$$I_{2,5} = 2 \int_0^{2\pi} \int_0^{\pi} f(\theta,\phi)\sin^2\theta\sin\theta d\theta d\phi \tag{7}$$

$$I_{3,4} = 1/2 \int_0^{2\pi} \int_0^{\pi} f(\theta,\phi)(1 + \cos^2\theta)\sin\theta d\theta d\phi$$

Combining terms as indicated by Equation 6, we have

$$\frac{I_1 - I_2 + I_3 + I_4 - I_5 + I_6}{\displaystyle\sum_{i=1}^{6} I_i} = \frac{\displaystyle\int_0^{2\pi} \int_0^{\pi} f(\theta,\phi)\cos^2\theta\sin\theta d\theta d\phi}{\displaystyle\int_0^{2\pi} \int_0^{\pi} f(\theta,\phi)\sin\theta d\theta d\phi} \tag{8}$$

or since the denominator on the right-hand side of this equation is normalized to 1, one obtains the usual definition of an average value

$$\int_0^{2\pi} \int_0^{\pi} f(\theta,\phi)\cos^2\theta\sin\theta d\theta d\phi = \overline{\cos^2\theta} \tag{9}$$

Typical Applications

The Mössbauer effect can be used to investigate the nature of the magnetic coupling in a material—*i.e.*, whether the material is ferromag-

netic, ferrimagnetic, or antiferromagnetic, or has an even more complicated magnetic behavior. For this purpose, one usually applies an external magnetic field to a material and observes the behavior of the atomic spin distribution. The intensities of the individual Zeeman components can then be used to measure $\overline{\cos^2\theta}$ (Equation 6). If the angular relationship between the atomic spin and $\vec{H}_N$ is known, one can then determine whether the spin distribution is canting toward or away from the external field. In $3d$ transition metals, like Fe, where the atomic orbital angular momentum is quenched, one can usually assume that the time average of the atomic spin at the nucleus, $\langle S \rangle$, is colinear with $\vec{H}_N$, and this should be a fairly good approximation at least for small external magnetic fields. For this case, if the γ-ray propagation direction is along $\vec{H}_{EXT}$, θ is also the angle between $\vec{H}_{EXT}$ and $\langle S \rangle$.

In the absence of an external magnetic field, a randomly oriented sample (powder or foil with no preferential orientation) of a magnetically ordered material containing ^{57}Fe will exhibit a hyperfine spectrum with relative line intensities $I_1:I_2$: etc., of 3:2:1:1:2:3: as defined in Figure 1 (again in the thin absorber and isotropic mean square displacement approximation). The effects of finite absorber thickness· can be accurately estimated if necessary (28). The atomic spins in a ferromagnetic material such as α-iron will tend to align parallel to an external magnetic field, and this behavior results in an increase in $\overline{\cos^2\theta}$ (for a γ-ray propagation direction along $\vec{H}_{EXT}$). When the ferromagnetic material is saturated, one will observe relative line intensities of 3:0:1:1:0:3 when the γ-ray propagation direction is parallel to $\vec{H}_{EXT}$ and 3:4:1:1:4:3 when the γ-ray propagation direction is perpendicular to $\vec{H}_{EXT}$. This can be seen easily from the angular dependence of the individual Zeeman components as shown in Figure 1. The Mössbauer study of the behavior of $\vec{H}_N$ as a function of $\vec{H}_{EXT}$ in α-iron resulted in a significant contribution to the understanding of magnetism (23, 35). Hanna and co-workers observed that in magnetically saturated α-iron, $\vec{H}_N$ decreases with increasing $\vec{H}_{EXT}$, which indicates that the internal field is negative or, that is, directed in the opposite sense from the external field. This observation established the importance of the core polarization mechanism for producing internal ,fields in transition elements.

The change in the Mössbauer spectrum of an antiferromagnetic material produced by an external field is considerably less dramatic than for a ferromagnetic material. Since there is no net moment per unit cell for $\vec{H}_{EXT}$ to interact with, as a first approximation in a randomly oriented antiferromagnet, $\vec{H}_{EXT}$ will increase $\vec{H}_N$ in about half the atoms and decrease $\vec{H}_N$ in the others, depending on the orientation of an individual atomic spin. The net result is to broaden the lines of the Mössbauer

spectrum because of the distribution of internal fields, but the center of gravity of the individual lines will remain almost unchanged.

In this case, the relative line intensities will remain approximately 3:2:1:1:2:3. If the antiferromagnetic material has an extremely large magnetic anisotropy which prevents any spin rotation, one would expect that in large external magnetic fields both $\vec{H}_N$ and $\overline{\cos^2\theta}$ might increase slightly if $\vec{H}_{EXT}$ were parallel to the γ-ray propagation direction. Because the largest static magnetic fields which can be produced in a laboratory are usually still considerably smaller than $\vec{H}_N$, in most materials this effect would be small. If the magnetic anisotropy were small and the

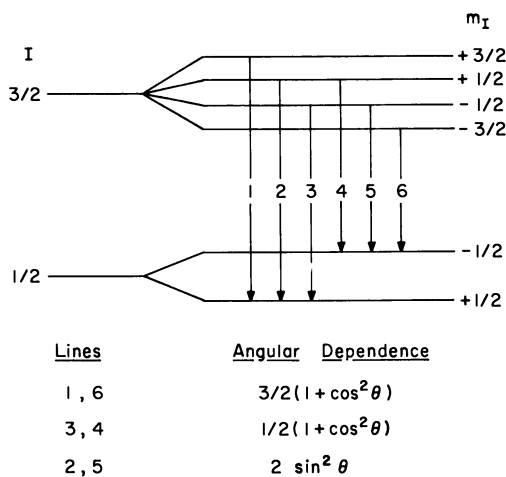| Lines	Angular Dependence
1 , 6	$3/2(1+\cos^2\theta)$
3 , 4	$1/2(1+\cos^2\theta)$
2 , 5	$2\sin^2\theta$

Figure 1. Effect of magnetic hyperfine interaction on ground state and first excited state of ^{57}Fe. The allowed transitions between the two states and the angular dependence of their intensities are indicated.

atomic spins were free to rotate, one might expect them first to align perpendicular to $\vec{H}_{EXT}$ and then cant toward $\vec{H}_{EXT}$ to lower the energy of the system. In this case, $\overline{\cos^2\theta}$ would first decrease to a minimum and then increase. The behavior of $\vec{H}_N$ would depend on how much the atomic spins canted toward $\vec{H}_{EXT}$. Unfortunately, in practice these two possibilities are usually not observed, and for most antiferromagnetic materials one merely observes the line broadening mentioned above. The Au-Fe alloy system has been studied extensively by Mössbauer spectroscopy (5, 18). The concentration dependence of the magnetic transition temperatures in gold-rich Au-Fe random solid solutions indicates the presence of different magnetic ordering processes above and below a critical concentration of ≈ 16 atom % Fe. To investigate the nature

of the magnetic ordering in the alloys dilute with respect to Fe, Mössbauer spectra in external magnetic fields up to 55 kOe. were obtained (7, 22). These studies indicated that the atomic spins were remaining spatially random and that the ordering process was antiferromagnetic in contradiction to the interpretation of conventional magnetic measurements. An example of the behavior of a typical antiferromagnet is shown in Figure 1 of Ref. 7.

The effect produced by an external magnetic field on the Mössbauer spectrum of a ferrimagnetic material is rather interesting. In this case, one usually expects the Mössbauer spectrum to consist of 12 lines which correspond to the two sets of hyperfine spectra from the two inequivalent sublattices (assuming Fe ions occupy both sublattices). In the presence of an external magnetic field, the atomic spins in the sublattice with the largest net moment tend to align parallel to $\vec{H}_{EXT}$, while those in the other sublattice align antiparallel to $\vec{H}_{EXT}$. H_N decreases for the sublattice with the larger net moment and increases for the other sublattice. For both sets of hyperfine spectra $\overline{\cos^2\theta}$ increases ($\vec{H}_{EXT} \parallel \gamma$-ray), and at saturation both spectra have relative line intensities 3:0:1:1:0:3. This behavior has been observed by Frankel *et al.* (9) in the system $Ga_{2-x}Fe_xO_3$ and is shown for $Ga_{0.8}Fe_{1.2}O_3$ in Figure 1 of Ref. 9.

The Mössbauer effect can also be used to measure the magnetic transition temperatures of magnetic materials. In fact, it has some advantages over conventional techniques since no external magnetic field is required for the measurement and one thereby avoids the usual problem of extrapolating to zero $\vec{H}_{EXT}$. Three techniques are often used to measure magnetic transition temperatures.

One can measure H_N as a function of temperature to see where H_N vanishes. If one assumes H_N is proportional to the magnetization, one can fit a Brillouin function through the data and extrapolate to zero H_N to get the magnetic transition temperature. As an example, the Néel temperature of α-Fe_2O_3 has been determined by this technique [*see* Figure 1 of Ref. *12*].

If one plots the area under the absorption curve as a function of temperature for a relatively thick absorber, a sharp discontinuity in the curve will be observed at the magnetic transition temperature—*see,* for example, Figure 11 of Ref. 35.

The previous two methods are time-consuming and involve several spectra. The third method, which is most often used and is faster, involves finding the maximum resonance in the Mössbauer spectrum of the material in the paramagnetic state just above the transition temperature. If one then plots the count rate at the Doppler velocity corresponding to this maximum resonance as a function of temperature, the first significant increase in count rate which corresponds to the onset of an internal magnetic field determines the magnetic transition temperature. This technique applied to α-Fe is shown in Figure 2, which indicates the

good sensitivity that can be obtained. In applying this method one must consider the possibilities of inhomogeneities in the sample and the occurrence of short range order—both effects cause an overestimate of the critical temperature.

A novel variation of the above technique can be used in some cases. By choosing an appropriate source so that the maximum resonance in the paramagnetic state occurs at or near zero relative velocity, one eliminates the need of a Mössbauer spectrometer completely, and the transition temperature can be determined by measuring the count rate transmitted through a stationary absorber and emitted by a stationary source as a function of temperature—*see*, for example, Refs. *18, 20*.
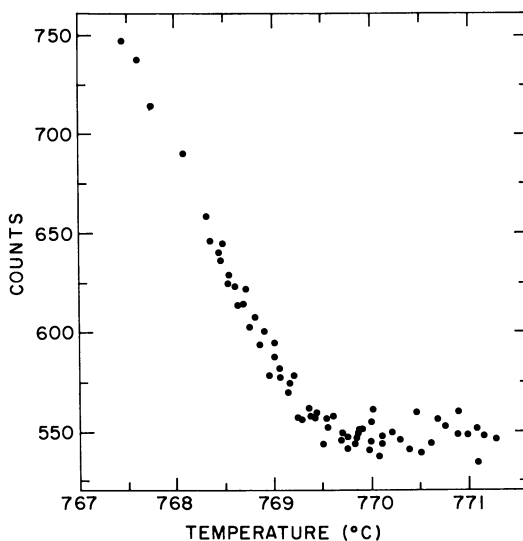

Figure 2. *Temperature dependence of the transmission in α-iron, measured at a velocity corresponding to maximum absorption just above* T_c. *Data are from Ref. 35*

Besides the more conventional studies of magnetic properties, the Mössbauer effect has also been used to investigate problems of fundamental interest. Two recent investigations involving thin films fall in this category. The first was measuring the critical thickness (occurrence of spontaneous magnetization) of ultrathin iron films. There has long been theoretical interest in two-dimensional magnetic lattices, mainly because the problem is easier to treat than the three-dimensional case. Lee, Bolduc, and Violet (*27*) have performed a Mössbauer experiment on thin films of Fe which shows an abrupt change in the saturation magnetization for films about two lattice parameters thick and implies the existence of a critical thickness. A major problem in conventional studies of this sort is achieving magnetic saturation for thin films. This

presents no problem for Mössbauer effect studies since no external magnetic field is required. The experimental technique involved preparing an absorber on a quartz substrate by evaporating alternating layers of Fe and SiO. The Fe films were separated by at least 50 A. of SiO and were assumed not to interact. In such an experiment one must, of course, consider the possibility of nonuniformities in the Fe layers. However, by looking for the existence of both a magnetic hyperfine spectrum and a paramagnetic spectrum, a good check on the uniformity of the Fe films was obtained.

Another experiment which should have considerable interest was performed by Trousdale and Lindgren (37) to measure the penetration of conduction electron spin polarization into nonmagnetic films on iron substrates. Long-range magnetic coupling in dilute alloys is usually attributed to conduction electron spin polarization. To study this phenomenon, the authors prepared sources by evaporating thin layers of Pd, Cu, and Ag on iron substrates. On top of this layer a small amount ($\sim 1/100$ atomic layer) of radioactive ^{57}Co was deposited and covered with a relatively thick layer of the nonmagnetic metal to ensure that the ^{57}Co atoms experienced bulk rather than surface conditions. Figure 3 shows the Mössbauer spectra they obtained with an intervening layer of 150 A. of Pd between the ^{57}Co and the iron substrate. These spectra show the existence of exchange fields at large distances from the Fe substrate, and by making certain assumptions concerning the relation between the hyperfine field and the exchange field, Trousdale and Lindgren have been able to calculate probability distribution functions for the exchange fields. As in the experiment previously described, one might consider the possibility of clustering of the ^{57}Co atoms which could also produce the observed hyperfine fields. However, again the Mössbauer effect provides a check on this question. A similar source was prepared on a copper substrate which showed no evidence of hyperfine structure at 4.2°K.

Mössbauer Studies of α-Fe$_2$O$_3$ and Ca$_2$Fe$_2$O$_5$

Two examples of Mössbauer studies show the detailed information that can be obtained from Mössbauer spectroscopy.

α-Fe$_2$O$_3$. One of the compounds most extensively studied by Mössbauer spectroscopy is α-Fe$_2$O$_3$. These studies are good examples of the detailed information that can be obtained concerning the magnetic properties of a material. Hematite, α-Fe$_2$O$_3$, has a rhombohedral structure with the iron sites lying on a threefold rotation axis in the (111) direction. The bulk Néel temperature is 690°C. (12). Between this temperature and the Morin transition ($T_M \simeq 260$°K.) (30), the atomic spins lie in the (111) plane, and the material exhibits weak ferromagnetism. The

moments on adjacent atoms are essentially antiferromagnetically coupled but are slightly canted toward each other to produce a small ferromagnetic moment (the Dzyaloshinsky moment) *(8)*. Below T_M the spins flip to the (111) direction, and the material behaves as a normal antiferromagnet. The Mössbauer spectrum of α-Fe_2O_3 at room temperature is shown in Figure 4a. A small quadrupole interaction is observed in
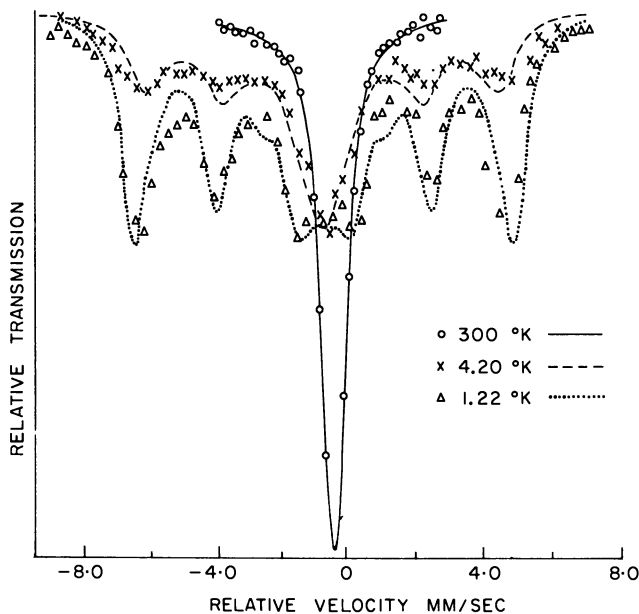

Figure 3. *Mössbauer spectra obtained using a source of isolated ^{57}Co atoms separated from an iron substrate by 150 A of Pd. Spectra at three different source temperatures are shown. Data from Ref. 37*

this spectrum, as evidenced by the difference in separation of the outer pairs of lines. The arrows indicate the line positions one would expect in the absence of a quadrupole interaction. In general, the line positions in the presence of mixed magnetic dipole and electric quadrupole interactions cannot be determined easily, but for this case, where the quadrupole interaction is much smaller than the magnetic interaction, the problem can be treated by first-order perturbation theory to obtain

$$S_1 - S_2 = -1/2\ e^2qQ(3\cos^2\phi - 1) \tag{10}$$

where S_1 and S_2 are the differences in energy between the outer lines as defined in Figure 4a, $-e$ is the charge of the electron, $eq = V_{zz}$ where V

is the electric potential and $V_{zz} = \delta^2 V / \delta z^2$, Q is the nuclear quadrupole moment, and ϕ is the angle between $\vec{H}_N$ and $\vec{V}_{zz}$. The electric field gradient in α-Fe_2O_3 is axially symmetric and directed along the threefold (111) axis.

Ono and Ito (33) have studied the quantity $S_1 - S_2$ as a function of temperature near T_M, and the results of their investigation are shown in Figure 4b. They observe that $(S_1 - S_2)_{T > T_M} \simeq -0.5(S_1 - S_2)_{T < T_M}$. This is consistent with $\phi = 90°$ ($T > T_M$) and $\phi = 0°$ ($T < T_M$) and confirms the spin-flipping process at T_M. The transition in Figure 4b takes place over a temperature range of about 50°K., which might seem to indicate that the spins turn continuously from the (111) plane to the (111) axis through the transition region. Ono and Ito have made a detailed study of one line in the spectrum as a function of temperature in the region of T_M. They observed that near T_M this line is really a doublet, which implies that the spins flip discontinuously by 90° and that the width of the transition region is associated with a distribution in the local transition temperatures.

The spin flip in α-Fe_2O_3 can also be caused by applying a large external magnetic field. Blum et al. (4) have done experiments on single crystals of α-Fe_2O_3 oriented so that the γ-ray propagation direction was along (111). At 80°K. and $\vec{H}_{EXT} = 0$, the $\Delta m = 0$ lines of the spectrum have essentially vanished, as one would expect for the atomic spins co-linear with (111). At a critical field of $H_c = 67.5 \pm 3$ kOe., the spins flip from along the trigonal axis to the (111) plane, and one observes essentially a 3:4:1:1:4:3 Mössbauer pattern characteristic of $\vec{H}_N$ perpendicular to the γ-ray propagation direction.

The Mössbauer effect in polycrystalline α-Fe_2O_3 has also been studied at room temperature ($T > T_M$) in large external magnetic fields (3). In this case the Dzyaloshinsky moment tends to align along $\vec{H}_{EXT}$, which causes the atomic spins and therefore $\vec{H}_N$ to be oriented perpendicular to $\vec{H}_{EXT}$. The Mössbauer spectrum shows a strong enhancement of the $\Delta m = 0$ lines, and $\vec{H}_N$ is observed to increase according to the relation

$$H_N = (H_{EXT}{}^2 + H_o{}^2)^{1/2} \qquad (11)$$

up to external fields of 109 kOe. H_o is the internal field observed in the absence of H_{EXT}.

The superparamagnetic properties of α-Fe_2O_3 have also been studied via the Mössbauer effect. Nakamura et al. (32) have investigated the temperature dependence of the internal field in α-Fe_2O_3 particles of approximately 50 A. diameter. At 120°K. they obtain a spectrum which is almost identical to the bulk material, except that no Morin transition has occurred and the spins still lie in the basal plane. At room temperature the magnetic hyperfine spectrum collapses (even though the bulk
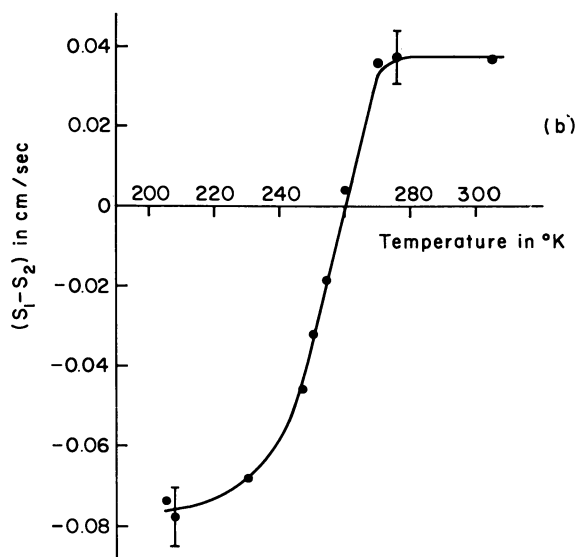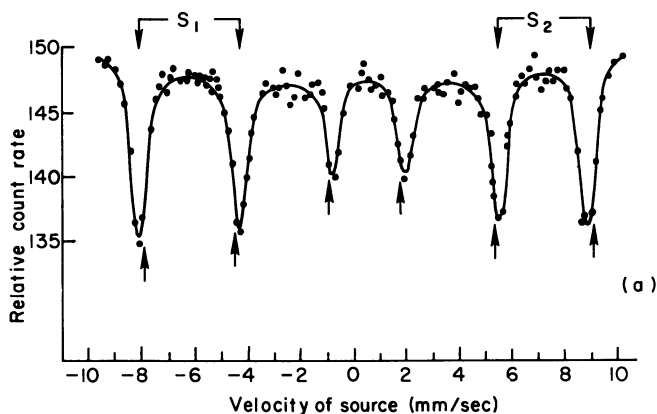
Figure 4.   (a) Mössbauer spectra of α-Fe_2O_3 (25°C.) ob-
tained with a ^{57}Co in stainless steel source (25°C.). Data
are from Ref. 25. (b) Temperature dependence of param-
eter S_1–S_2 near Morin temperature in α-Fe_2O_3. Data are
from Ref. 33

transition temperature is ~ 690°C.) because of the rapid relaxation of
the atomic spins.

$Ca_2Fe_2O_5$. Geller *et al.* (*15*) and Gonser *et al.* (*19*) have recently
used the Mössbauer effect to study $Ca_2Fe_2O_5$. This study is an example
of how the Mössbauer effect in conjunction with crystal chemical argu-
ments can be used to work out the magnetic structure of a material
without using neutron spectroscopy.

The crystal structure of this compound has been determined by Bertaut *et al.* (2). $Ca_2Fe_2O_5$ has equal numbers of Fe^{3+} ions in two crystallographically nonequivalent sites, one of octahedral and the other of tetrahedral coordination. These sites form alternating planes perpendicular to the crystallographic b axis; also perpendicular to the b axis there is a mirror plane which contains the Fe^{3+} ions in the tetrahedral sites. The Mössbauer spectrum of polycrystalline $Ca_2Fe_2O_5$, shown in Figure 5a, was obtained with a single line ^{57}Co in Pt source at room temperature. It consists of two sets of six-line spectra, one resulting from iron in the tetrahedral sites and the other from the octahedral sites. The Mössbauer spectra of $Sr_2Fe_2O_5$ and $Ba_2Fe_2O_5$, which are isostructural with $Ca_2Fe_2O_5$, have been obtained by Gallagher, MacChesney, and Buchanan (13) and are similar to this spectrum.

The spectrum resulting from the Fe^{3+} ions in the octahedral and tetrahedral sites can be identified uniquely by substituting Sc^{3+} or Ga^{3+} ions into the lattice. Typical spectra for these substituted compounds are shown in Figure 5b and c. It is well-established from work in the garnets (14, 16, 17, 36) that Sc^{3+} ions substitute almost exclusively into sites with octahedral coordination while Ga^{3+} ions prefer tetrahedral coordination with substantial amounts entering octahedral sites. The decrease in line intensity of the hyperfine spectrum having the largest internal field with Sc^{3+} substitution (and opposite behavior with Ga^{3+} substitution) establishes that the largest internal field is associated with octahedral coordination, as is observed in most ferrites. Recently, Pobell and Wittman (34) also observed the preferential substitution of Al^{3+} ions into the tetrahedral sites in brownmillerite (Ca_2AlFeO_5).

Both the unsubstituted and substituted compounds had very low magnetic susceptibilities, which because of the preferential substitution rules out the possibility that $Ca_2Fe_2O_5$ might be a compensated ferrimagnet. Therefore, the spins within each sublattice must be coupled antiferromagnetically (15). The coupling between sublattices is not uniquely determined from the experimental data; however, because of the large Fe^{3+}-O-Fe^{3+} angle which connects these sublattices (147°) and the high Néel temperature (730°K.) (21), it seems most likely that this coupling is also antiferromagnetic.

To determine the actual spin orientation, it was necessary to use a single crystal absorber. If single crystals of a material are easy to grow and cut in several directions, one can determine the spin directions by finding the γ-ray propagation direction along which the $\Delta m = 0$ lines of the spectrum vanish. However, single crystals of $Ca_2Fe_2O_5$ were difficult to grow, and the shape which was obtained required that it be cut perpendicular to the crystallographic b axis. Because of the mirror plane which intersects the b axis and the tetrahedral sites, the magnetic space

group restricts the spins of the tetrahedral sites to lie either parallel to the b axis or within the ac ane. The Mössbauer spectrum of this absorber in conjunction with a single line unpolarized source ruled out the possibility that the spins of either site were parallel to b because of the

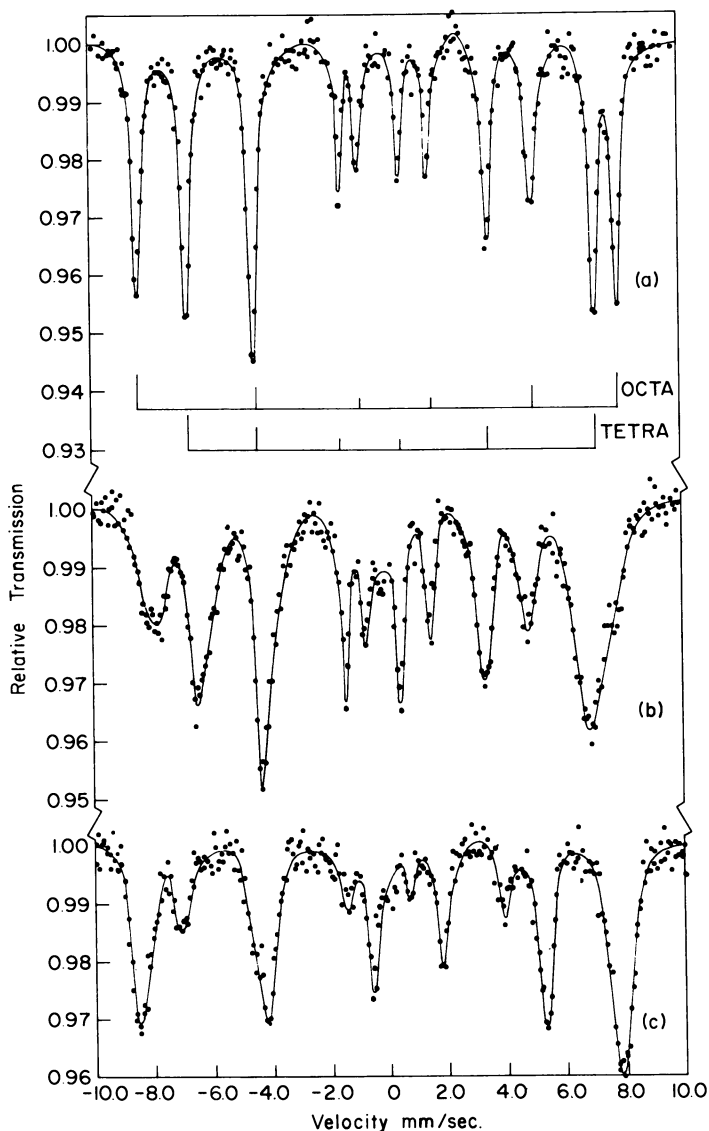Figure 5.   *Mössbauer spectra obtained with a room temperature source of* ^{57}Co *in Pt. Absorbers: (a)* $Ca_2Fe_2O_5$ *at room temperature; (b)* $Ca_2Sc_{0.5}Fe_{1.5}O_5$ *at room temperature; (c)* Ca_2FeGaO_5 *at 5°K. Data are from Ref. 15*

presence of the $\Delta m = 0$ lines. In fact, the absorption lines from both sites showed the approximate relative line intensities 3:4:1:1:4:3, which indicated that the spins in both sites were most likely in the *ac* plane.

To determine the spin orientation direction within this plane, Gonser *et al.* (*19*) extended a technique first used by Johnson, Marshall, and
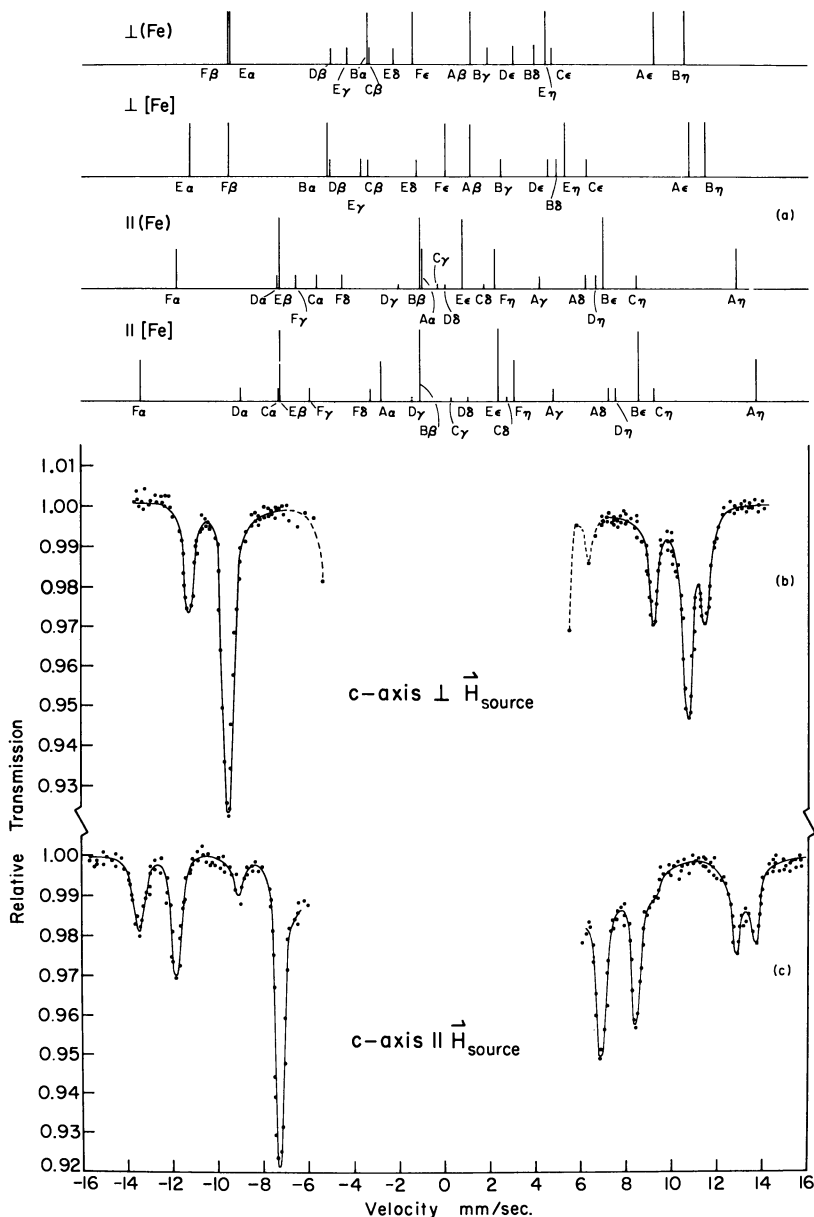
Perlow (*24*) to measure the sign of the quadrupole coupling constant in ferrous fluorosilicate. The experimental arrangement consisted of a ^{57}Co in Fe foil source at room temperature, which was magnetized to saturation in the plane of the foil in an external field of ~ 3.5 kOe. in conjunction with the single crystal absorber of $Ca_2Fe_2O_5$. γ-Rays emitted perpendicular to the source magnetization direction, $\vec{H}_{source}$, were linearly polarized, and since the emission spectrum consisted of six lines and the absorption spectrum of 12 lines when the absorber spins were oriented at an arbitrary direction, this source and absorber configuration would, in general, produce a rather complicated 72-line spectrum.

The following notation was adopted to identify the lines in the absorption pattern. The lines resulting from the octahedral sites were labeled $[\alpha]$, $[\beta]$, $[\gamma]$, $[\delta]$, $[\epsilon]$, and $[\eta]$ as a function of increasing energy while those from the tetrahedral sites were labeled (α), (β), etc. The six emission lines from the ^{57}Co in Fe source were labeled with roman letters again as a function of increasing energy. The positions of the absorption lines can be derived easily by overlapping the spectrum in Figure 5a with the spectrum obtained using the ^{57}Co in Fe source in conjunction with a single line absorber and taking into account the appropriate isomer shifts. Expressions developed by Frauenfelder and co-workers (*10*) for the angular dependence of the emission and absorption intensities of the individual Zeeman components were used to calculate the relative intensities of the absorption lines (in the thin absorber and isotropic mean square displacement approximation).

The results of this investigation are shown in Figure 6. Figure 6a shows the positions and intensities (lengths of bars) for the calculated spectra. The top two lines show the spectra expected if the spins in the tetrahedral and octahedral sites, respectively, are perpendicular to $\vec{H}_{source}$. Lines 3 and 4 are the spectra expected if the spins lie parallel to $\vec{H}_{source}$. The data obtained for $\vec{H}_{source}$ perpendicular and parallel to the crystallographic *c* axis are shown in Figures 6b and c. The absorption spectrum is so complicated near zero relative velocity that data were taken only in the high velocity region of the spectrum. The spectrum in Figure 6b can be

←————————————————————————————————

Figure 6. Predicted and experimental Mössbauer spectra for a magnetized ^{57}Co in α-iron source at room temperature and a single crystal of $Ca_2[Fe](Fe)O_5$. Crystallographic b axis of $Ca_2[Fe](Fe)O_5$ and magnetization direction of source are parallel and perpendicular to the γ-ray propagation direction, respectively.

(a) Expected absorption line locations and intensities for the octahedral [Fe] and tetrahedral (Fe) sites with the source magnetization direction perpendicular (⊥) and parallel or antiparallel (||) to the spin orientation in the absorber.

(b-c) Observed spectra with c axis perpendicular (b) and parallel (c) to source magnetization direction. Data are from Ref. 19

obtained by combining lines 1 and 2 while the spectrum in Figure 6c can be obtained by combining lines 3 and 4. These spectra establish that the spins on both the octahedral and tetrahedral sites are colinear with the crystallographic *c* axis.

Conclusions

While both the Mössbauer effect and nuclear magnetic resonance provide spectroscopic methods for studying magnetic hyperfine interactions, nuclear magnetic resonance measurements on magnetic materials are often complicated by unknown enhancement factors and line broadening owing to inhomogeneous internal fields while the Mössbauer effect does not particularly suffer from these complications. Therefore, although in principle NMR can be used to measure internal fields with considerably more accuracy, and despite the fact that only a few good Mössbauer isotopes exist, the Mössbauer effect has become a valuable and unique tool for investigating the magnetic properties of materials.

Acknowledgment

It is a pleasure to acknowledge several helpful discussions with U. Gonser, A. H. Muir, Jr., R. M. Housley, and H. Wiedersich during the preparation of this manuscript.

Literature Cited

(1) Belov, K. P., Lyubutin, I. S., *Soviet Phys. JETP (English Transl.)* **22**, 518 (1966).
(2) Bertaut, E. F., Blum, P., Sagniéres, A., *Acta Cryst.* **12**, 149 (1959).
(3) Blum, N., Freeman, A. J., Grodzins, L., *Bull. Am. Phys. Soc.* **9**, 465 (1964).
(4) Blum, N., Freeman, A. J., Shaner, J. W., Grodzins, L., *J. Appl. Phys.* **36**, 1169 (1965).
(5) Borg, R. J., Booth, R., Violet, C. E., *Phys. Rev. Letters* **11**, 464 (1963).
(6) Cohen, R. L., *Phys. Rev.* **134**, A94 (1964).
(7) Craig, P. P., Steyert, W. A., *Phys. Rev. Letters* **13**, 802 (1964).
(8) Dzyaloshinsky, I., *J. Phys. Chem. Solids* **4**, 241 (1958).
(9) Frankel, R. B., Blum, N. A., Foner, S., Freeman, A. J., Schieber, M., *Phys. Rev. Letters* **15**, 958 (1965).
(10) Frauenfelder, H., Nagle, D. E., Taylor, R. D., Cochran, D. R. F., Visscher, W. M., *Phys. Rev.* **126**, 1065 (1962).
(11) Freeman, A. J., Watson, R. E., "Magnetism," G. T. Rado and H. Suhl, eds., Vol. IIA, p. 167, Academic Press, New York, 1965.
(12) Freier, S., Greenshpan, M., Hillman, P., Shechter, H., *Phys. Letters* **2**, 191 (1962).
(13) Gallagher, P. K., MacChesney, J. B., Buchanan, D. N. E., *J. Chem Phys.* **41**, 2429 (1964); **43**, 516 (1965).
(14) Geller, S., Cape, J. A., Espinosa, G. P., Leslie, D. H., *Phys. Rev.* **148**, 522 (1966).

(15) Geller, S., Grant, R. W., Gonser, U., Wiedersich, H., Espinosa, G. P., *Phys. Letters* **20**, 115 (1966).
(16) Geller, S., Williams, H. J., Espinosa, G. P., Sherwood, R. C., *Bell System Tech. J.* **43**, 565 (1964).
(17) Gilleo, M. A., Geller, S., *Phys. Rev.* **110**, 73 (1958).
(18) Gonser, U., Grant, R. W., Meechan, C. J., Muir, A. H., Jr., Wiedersich, H., *J. Appl. Phys.* **36**, 2124 (1965).
(19) Gonser, U., Grant, R. W., Wiedersich, H., Geller, S., *Appl. Phys. Letters* **9**, 18 (1966).
(20) Gonser, U., Meechan, C. J., Muir, A. H., Wiedersich, H., *J. Appl. Phys.* **34**, 2373 (1963).
(21) Grant, R. W., Wiedersich, H., Geller, S., Gonser, U., Espinosa, G. P., *J. Appl. Phys.* **38**, 1455 (1967).
(22) Grant, R. W., Wiedersich, H., Gonser, U., *Bull. Am. Phys. Soc.* **10**, 708 (1965).
(23) Hanna, S. S., Heberle, J., Perlow, G. J., Preston, R. S., Vincent, D. H., *Phys. Rev. Letters* **4**, 513 (1960).
(24) Johnson, C. E., Marshall, W., Perlow, G. J., *Phys. Rev.* **126**, 1503 (1962).
(25) Kistner, O. C., Sunyar, A. W., *Phys. Rev. Letters* **4**, 412 (1960).
(26) Kopfermann, H., "Nuclear Moments," Academic Press, New York, 1958.
(27) Lee, E. L., Bolduc, P. E., Violet, C. E., *Phys. Rev. Letters* **13**, 800 (1964).
(28) Margulies, S., Debrunner, P., Frauenfelder, H., *Nuclear Instr.* **21**, 217 (1963).
(29) Marshall, W., Johnson, C. E., *J. Phys. Radium* **23**, 733 (1962).
(30) Morin, F. J., *Phys. Rev.* **78**, 819 (1950).
(31) Muir, A. H., Jr., Ando, K. J., Coogan, H. M., "Mössbauer Effect Data Index, 1958–1965," Interscience, New York, 1967.
(32) Nakamura, T., Shinjo, T., Endoh, Y., Yamamota, N., Shiga, M., Nakamura, Y., *Phys. Letters* **12**, 178 (1964).
(33) Ono, K., Ito, A., *J. Phys. Soc. Japan* **17**, 1012 (1962).
(34) Pobell, F., Wittmann, F., *Phys. Letters* **19**, 175 (1965).
(35) Preston, R. S., Hanna, S. S., Heberle, J., *Phys. Rev.* **128**, 2207 (1962).
(36) Streever, R. L., Uriano, G. A., *Phys. Rev.* **139**, A305 (1965).
(37) Trousdale, W. L., Lindgren, R. A., *J. Appl. Phys.* **36**, 968 (1965).
(38) Watson, R. E., Freeman, A. J., *Phys. Rev.* **123**, 2027 (1961).
(39) Wickman, H. H., Nowick, I., Wernick, J. H., Shirley, D. A., Frankel, R. B., *J. Appl. Phys.* **37**, 1246 (1966).

4

Study of Coordination Chemistry and Biochemicals Using Mössbauer Spectroscopy

LEOPOLD MAY

The Catholic University of America, Washington, D. C.

Two Mössbauer parameters—chemical shift and quadrupole splitting—can provide information about the bonding between the metal atom and its ligands, structure of the metal ligand complex, and the oxidation state of the metal. The oxidation state in iron and tin inorganic compounds can be determined from the chemical shift. The magnitude of this parameter provides an estimate of the 4s contribution to bonding in iron compounds. The second parameter, quadrupole splitting, is related to the symmetry of the ligands about the metal ion in a complex. The results obtained with hemoglobin and its complexes illustrate the role of Mössbauer spectroscopy in the study of biochemicals. A scatter plot of quadrupole splitting vs. *chemical shift shows the relationship of the biochemicals to the iron inorganic complexes. The measurements from Mössbauer spectroscopy are compared with those obtained from other structural techniques.*

Mössbauer spectroscopy can provide information directly concerning the metal ion that is coordinated to the ligands in coordination compounds. From the magnitude of the Mössbauer parameters, the oxidation state of the metal can be deduced as well as information concerning the structure of the complex and the nature of the bonding between the metal and the ligands. To illustrate some applications of Mössbauer spectroscopy, the results obtained principally with iron compounds are discussed. Included is a discussion of studies with hemoglobin, which can be considered a complex with iron coordinated to biological and organic moieties.

Two Mössbauer parameters—chemical shift and quadrupole splitting—are important in studying coordination compounds. The chemical shift, δ, is related to s electron density at the nucleus of the metal. A

52

knowledge of the s electron contribution to the bond between the metal and its ligands can give information concerning the bonds. The second parameter—the quadrupole splitting—ΔE_Q, is related to the asymmetry of the electric field at the nucleus, which is influenced by the electron configuration of the metal atom and its environment. This splitting results when the electric field gradient at the nucleus is not zero and the nucleus has a quadrupole moment.

For iron and tin the magnitude of δ has been found to be related to the oxidation state of the metal (*15, 28*) (Table I). In iron complexes, the spin of the $3d$ electrons of the iron atoms can be paired (low spin) or unpaired (high spin). In low spin ferrous and ferric complexes, δ and ΔE_Q values are similar, but the value of ΔE_Q differs greatly for the high spin complexes (Figure 1). Mössbauer spectroscopy has been used to

Table I.   Relationship between Mössbauer Chemical Shift and Oxidation State of Iron and Tin

Oxidation State	*Chemical Shift, cm./sec.*
IRON	
2+, High spin	0.145–0.165
Low spin	0.000–0.040
3+, High spin	0.060–0.115
Low spin	0.000–0.040
Standard, $Na_2[Fe(CN)_5NO]2H_2O$	0.000
TIN	
2+	0.085–0.100
4+	−0.110 to −0.280
Standard, White Tin	0.000

clarify the structure of insoluble Prussian Blue. The Mössbauer spectrum of this compound has been shown to be the combination of the spectra of the Fe^{3+} ion and $[Fe(CN)_6]^{4-}$ (*15*). Hence, the structure of the compound is $Fe_4[Fe(CN)_6]_3$ rather than a resonating mixture of $Fe^{II}(CN)_6$-Fe^{III} and $Fe^{III}(CN)_6Fe^{II}$. It has also been shown that iron in soluble Prussian Blue exists in the ratio of 1:1 for the Fe^{3+} ion and the ferrous form. The existence of the free Fe^{3+} ion is confirmed from the magnetic susceptibility measurements, from which a magnetic moment of 5.72 Bohr magnetons is derived for this compound. This corresponds to five unpaired electrons per formula weight and is characteristic of the free Fe^{3+}. Hence, the formula for soluble Prussian Blue is $K\ Fe[(CN)_6]$ (*15*).

The quantitative variation between δ and the s electron density in iron compounds was presented by Walker, Wertheim, and Jaccarino

(35). Using the free ion Hartree-Fock calculations of the s electron density at the nucleus for different $3d$ configurations of the iron atom and the Fermi-Segré-Goudsmit formula to calculate the $4s$ electron density, they plotted the total s electron density at the nucleus against the $4s$ electron contribution to a bond for different $3d$ configurations. The Mössbauer chemical shift ordinate was calibrated using the measured shifts of the most ionic divalent and trivalent salts, ferrous and ferric sulfates. The plot has been recalibrated using sodium
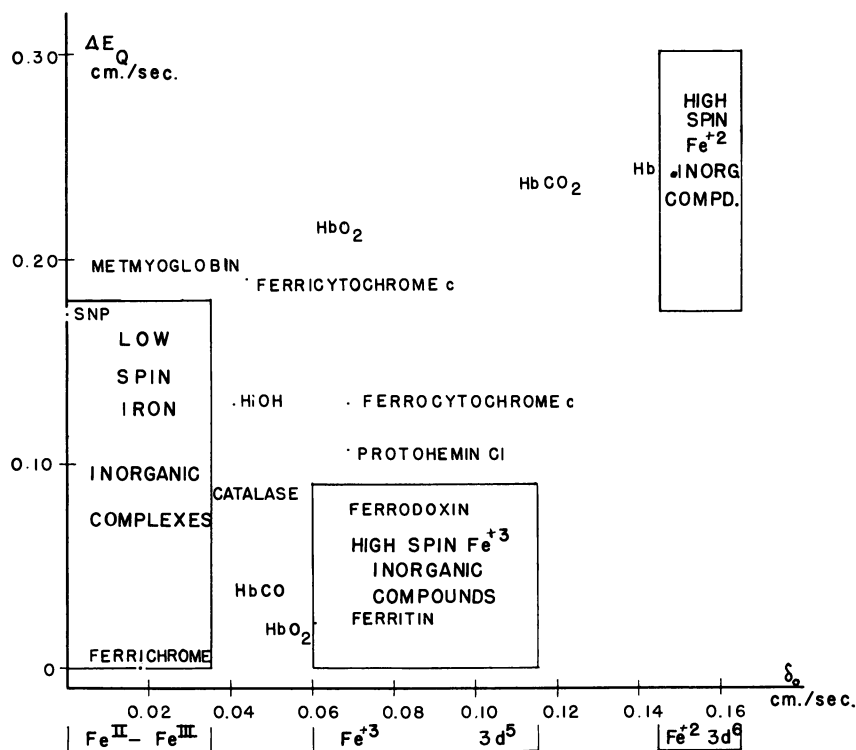

Figure 1.   Scatter plots of iron compounds. Correlation of differential chemical shift, δ_o, with quadrupole splitting, ΔE_Q, for inorganic compounds and biochemicals at room temperature. Adapted from Ref. 34.

nitroprusside as a standard and is presented in Figure 2 (34). The differential chemical shift, δ_o relates the chemical shift to the standard, assuming that δ for the standard is zero. If the δ_o is known for a complex, the $4s$ contribution to the bond between the iron and the ligands in the complex can be determined. As π-bonding of the ligands increases, δ_o decreases for both ferrous and ferric complexes. High spin complexes have values between 0.155 and 0.060 cm./sec. (Table I and Figure 2).

This permits one to determine whether the electrons in a complex are unpaired or paired. With high spin Fe^{III} complexes, δ decreases with increasing electronegativity of the ligands, but the reverse is found with

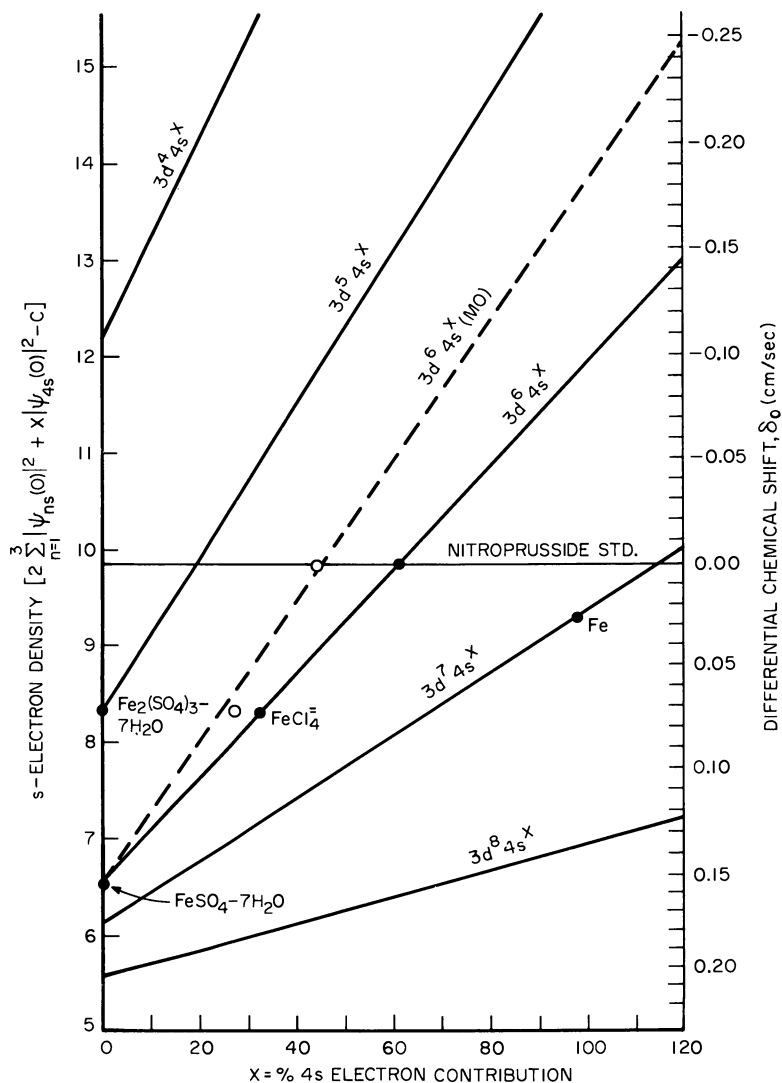*Figure 2. WWJ plot. Variation of differential chemical shift with s electron density and 4s electron contribution for iron 3d configurations. Adapted from Ref. 34.*

● δ_o vs. X_{MS}
○● δ_o vs. X_{MO} (34)
$C = 11,873 \, a_o^{-s}$

low spin Fe^{II} complexes (10). The decrease in δ_0 with low spin complexes has been explained as being caused by back donation to the vacant π^* (antibonding) orbitals of the ligand (10).

Recently, molecular orbital calculations on some iron complexes have been made by Gray and his co-workers (2, 30). These values for ferrous complexes are plotted in Figure 2 as the dashed line [$3d^6 4s^x$(MO)]. Hence, Mössbauer spectroscopy provides estimates for the $4s$ electron contribution for molecular orbital calculations. This correlation does not hold for high spin complexes such as $FeCl_4^-$ and FeF_6^{3-}. Bersuker (3, 4) has attempted to relate both δ and ΔE_Q directly to molecular orbital parameters. Using the equations developed from this approach, Bersuker, Gol'danskiï, and Makarov (5) have concluded that in tin tetrahalides the role of d_π-p_π bonding is significant.

Gol'danskiï et al. (19) found that six coordination in tin compounds is present if a large Mössbauer effect is observed at room temperature. Herber (26) has suggested that absence of the effect does not necessarily imply the absence of six coordination.

The second parameter, ΔE_Q, depends on the electric field gradient (EFG), which is influenced by the electron configuration of the metal atom. The outer electron configuration for high spin Fe^{3+} ($3d^5$) is a $^6S_{5/2}$ state and has spherical symmetry with no contribution to the EFG. Generally, no or little splitting is observed in these compounds. The configuration in high spin Fe^{2+} ($3d^6$) is in a ^5D state, and splitting is observed. The contribution to the EFG comes from a single unpaired electron (27). As the symmetry of the ligands about the metal decreases, the degeneracy of the d-orbitals decreases, and the symmetry of the EFG decreases. Hence, ΔE_Q will increase, provided this is the only effect. The nature of the change will also depend on π-bonding of the ligands. For the octahedral case with identical ligands, no splitting is observed—for example, $[Fe(CN)_6]^{4-}$. By introducing a different ligand, such as NO_2 in $[Fe(CN)_5 NO_2]$, the symmetry of the octahedral field is destroyed, and splitting is observed. Introducing SO_3^{2-} instead of NO_2 decreases the splitting.

The variation of ΔE_Q with temperature varies with the state of the iron. For example, in many spin-paired complexes and Fe^{3+} compounds the temperature coefficient is small (0 to 0.006 cm./sec.) but larger for Fe^{2+} salts (0.015 to 0.048 cm./sec.) (13). Burns (8) has suggested that the small temperature coefficient for Fe^{3+} salts arises from differential homogeneous contraction of the crystal in two axis directions.

The asymmetry of the peak intensities can provide useful information in structural analysis. The asymmetry can be ascribed to the Gol'danskiï effect (18), relaxation phenomena (6), or the crystal effect (37). The Gol'danskiï effect was observed in a number of derivatives of

the type $R_nS_nCl_{4-n}$. This effect is related to bonding between the metal and the different ligands. It should not be confused with the relaxation phenomena, in which the asymmetry arises from the lifetimes associated with each of the excited states of the metal nucleus. The asymmetry in the spectra of iron dithiocarbamates was explained in terms of electronic relaxation processes (*39*). The crystal effect is observed with single crystals.and can be eliminated by using polycrystalline samples.

Since many metallobiochemicals can be considered complexes, the Mössbauer spectra of these chemicals can be interpreted using the results previously discussed for inorganic complexes. An important class of metallobiochemicals is that in which the metal is iron. The Mössbauer spectroscopy of a number of these has been studied, and the results have been tabulated by Gonser and Grant (*20*). The hemoprotein, hemo-
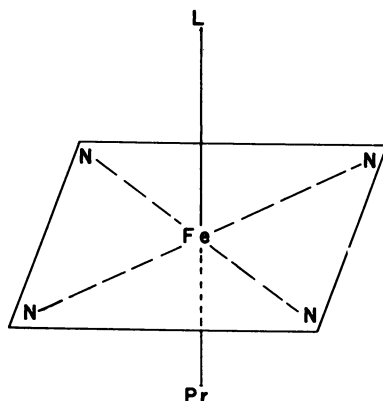

Figure 3.   Diagrammatic represen-
tation of hemoprotein structure. Pr.
= Protein, L. = Ligand

globin, has been the subject of several investigations since it is important in transporting oxygen and carbon dioxide in the blood system. The structure of hemoproteins is presented diagrammatically in Figure 3. The iron atom is located at the center of the porphyrin ring, designated by the square. Substituted pyrrole rings occupy the corners of the square, with the nitrogen of the ring coordinated to the iron. The pyrrole rings are connected through —CH═ bridges forming the porphyrin ring. The iron atom is assumed to possess axial symmetry relative to the porphyrin. In hemoglobin the ligand, Pr, is the protein globin. The sixth position, L, is occupied by various ligands such as O_2, CO, H_2O, etc. The structure of the complex may be considered to be octahedral so that results obtained with similar inorganic iron complexes may be used to interpret the results obtained with hemoglobin with different ligands, L.

Parameter	Mössbauer Spectroscopy	Magnetic Susceptibility	Electron Spin Resonance
s Electron density	δ_o		
No. of unpaired electrons	Q_t	χ_m	D
Symmetry	ΔE_Q		

Table II.   Comparison of

The Mössbauer spectra of hemoglobin (Hb) was examined in red blood cells (20) and in solution (29) at temperatures ranging from 4° to 195°K. With some samples, it was necessary to increase the ^{57}Fe content by giving the animal periodic injections of iron citrate with an enrichment to 80% ^{57}Fe. The values obtained from these studies were: δ_o, 0.115 to 0.119 cm./sec., and ΔE_Q, 0.236 to 0.240 cm./sec. These values are close to those found with ferrous compound where the *d* electrons are unpaired (Table I). This is consistent with magnetic susceptibility measurements, indicating a S = 2 state (29). When the hemoglobin is oxygenated, ΔE_Q decreases to 0.189 to 0.224 cm./sec., and δ_o is lowered to 0.045 to 0.055 cm./sec. (20, 29). The value of δ_o suggests that it is either a low spin ferrous or ferric complex. Lang and Marshall (29) suggest that it is similar to the structure that they have postulated for HbNO, whose Mössbauer spectra shows large splitting. They assume strong covalent bonding and a large spin transfer between iron and NO in this complex, suggesting that the distinction between Fe^{II} and Fe^{III} is not clear. They point out that this is consistent with the suggestion of Weiss (36) that some hemoglobin compounds do contain ferric ions. The Mössbauer data require both π_x and π_y bonding and imply a low symmetry where the NO is neither perpendicular nor parallel to the heme plane. The data for HbO$_2$ cannot be interpreted except to indicate the similarity with HbNO.

The complex, HbCO$_2$, has a spectrum similar to that of Hb and blood exposed to nitrogen atmosphere. The binding of CO$_2$ to hemoglobin does not affect the electronic configuration of the iron to any appreciable extent, suggesting that CO$_2$ is not bound as a ligand directly to the iron (21) and confirming that it is bound to some other part of the molecule (33).

Values for δ_o and ΔE_Q for some biochemicals have been plotted on the scatter plot (Figure 1). Most of these containing the porphyrin ring fall outside of the regions found for the iron inorganic complexes. The presence of this ring alters the EFG so that the ΔE_Q is increased above the values obtained for inorganic complexes. This suggests that the asymmetry of the ligands may also be greater in the biochemicals than in the inorganic complexes previously studied.

Structural Techniques

X-ray	Infrared Spectroscopy	Nuclear Magnetic Resonance	Nuclear Quadrupole Resonance
x		J	
x	x	x	ΔE_Q

As indicated in the previous discussion, Mössbauer spectroscopy provides information that when coupled with results using other structural techniques assists in determining the structure of the complex under analysis. The relationships between the various techniques are summarized in Table II. The Mössbauer chemical shift provides information about the $4s$ electron contribution to the bond between the metal and the ligands in a complex. Similar estimates can be obtained from the results of measurements on the fine structure in the x-ray absorption edge and nuclear magnetic resonance data. The number of unpaired electrons can be evaluated from magnetic susceptibility data, electron spin resonance, and the temperature coefficient of the Mössbauer quadrupole splitting (Q_T).

Information concerning the symmetry of the electric field at the metal nucleus can be found from this latter parameter, ΔE_Q, which can also be measured directly by nuclear quadrupole resonance techniques. Additional information concerning the symmetry of the ligand around the metal can be deduced from x-ray, infrared, and nuclear magnetic resonance data.

Several books (1, 16, 18, 31, 37), review articles (7, 11–15, 17, 20, 22, 24, 25, 38), and symposia (9, 23, 32) have been published that are valuable as an introduction to those interested in the application of Mössbauer spectroscopy to chemical and biochemical problems.

Literature Cited

(1) Abragam, A., "L'Effect Mössbauer et ses Applications a l'Etude des Champs Internes," Gordon and Breach, New York, 1964.
(2) Basch, H., Viste, A., Gray, H. B., *J. Chem. Phys.* **44**, 10 (1966).
(3) Bersuker, I. B., *Teor. Eksp. Khim.* **1**, 675 (1965).
(4) Bersuker, I. B., Goldanskii, V. I., Makrov, E. F., *Intern. At. Energy Agency, Tech. Rept. Ser.* **50**, 17 (1966).
(5) Bersuker, I. B., Gol'danskii, V. I., Makarov, E. F., *Teor. Eksp. Khim.* **1**, 678 (1965).
(6) Blume, M., *Phys. Rev. Letters* **14**, 96 (1965).
(7) Brady, P. R., Wigley, P. R. F., Duncan, J. F., *Rev. Pure Appl. Chem. (Australia)* **12**, 165 (1962).
(8) Burns, G., *Phys. Rev.* **123**, 1634 (1965).
(9) Compton, D. M. J., Schoen, A. H., eds., Proceedings of the 2nd International Conference on the Mössbauer Effect," Wiley, New York, 1962.

(10) Danon, J., *Intern. At. Energy Agency, Tech. Rept. Ser.* **50,** 89 (1966).
(11) Devoe, J. R., Spijkerman, J. J., *Anal. Chem.* **38,** 382R (1966).
(12) Duncan, J. F., Golding, R. M., *Quart. Rev.* **19,** 36 (1965).
(13) Fluck, E., *Advan. Inorg. Chem. Radiochem.* **6,** 433 (1964).
(14) Fluck, E., *Fortschr. Chem. Forsch.* **5,** 399 (1966).
(15) Fluck, E., Kerler, W., Neuwirth, W., *Angew. Chem., Intern. Ed.* **2,** 277 (1963).
(16) Frauenfelder, H., "The Mössbauer Effect," W. A. Benjamin, Inc., New York, 1962.
(17) Gol'danskiĭ, V. I., *Intern. Sci. Technol.*, p. 40 (December 1963).
(18) Gol'danskiĭ, V. I., "Mössbauer Effect and Its Applications in Chemistry," p. 37, Consultants Bureau, New York, 1964, Van Nostrand, New York, 1966.
(19) Gol'danskiĭ, V. I., Makarov, E. F., Stukan, R. H., Sumarova, T. N., Truktanov, V. A., Khrapov, V. V., *Dokl. Acad. Nauk SSSR* **156,** 400 (1964).
(20) Gonser, U., Grant, R. W., "Mössbauer Effect Methodology," Vol. 1, p. 20, Plenum Press, New York, 1965.
(21) Gonser, U., Grant, R. W., Kregzde, J., *Science* **143,** 680 (1964).
(22) Greenwood, N. N., *Chem. Britain* **3,** 56 (1967).
(23) Gruverman, I. J., ed., "Mössbauer Effect Methodology," Vol. 1, 1965; Vol. 2, 1966, Plenum Press, New York.
(24) Herber, R. H., *Ann. Rev. Phys. Chem.* **17,** 261 (1966).
(25) Herber, R. H., *J. Chem. Educ.* **42,** 180 (1965).
(26) Herber, R. H., "Mössbauer Effect Methodology," Vol. 1, p. 3, Plenum Press, New York, 1965.
(27) Ingalls, R. E., *Carnegie Inst. Technol., Tech. Rept.* No. 2 and 3 (1963).
(28) Kistner, O. C., Jaccarino, V., Walker, L. R., "Proceedings of 2nd International Conference on the Mössbauer Effect," D. M. J. Compton and A. E. Schoen, eds., p. 264, Wiley, New York, 1962.
(29) Lang, G., Marshall, W., *Proc. Phys. Soc. (London)* **87,** 3 (1966); *J. Mol. Biol.* **18,** 385 (1966).
(30) Manoharan, P. T., Gray, H. R., *J. Am. Chem. Soc.* **87,** 3340 (1965).
(31) Muir, A. H., Jr., Ando, K. J., Coogan, H. M., "Mössbauer Effect Data Index, 1958-1965," Interscience, New York, 1966.
(32) *Rev. Modern Phys.* **36,** 333 (1964) (Third International Conference 1963).
(33) Roughton, F. J. W., "Haemoglobin," F. J. W. Roughton and J. C. Kendrew, eds., Butterworth and Co., London, 1949.
(34) Spijkerman, J. J., Ruegg, F. C., May, L., "Mössbauer Effect Methodology," Vol. 2, p. 85, Plenum Press, New York, 1966.
(35) Walker, L. R., Wertheim, G. K., Jaccarino, V., *Phys. Rev. Letters* **6,** 98 (1961).
(36) Weiss, J. J., *Nature* **202,** 83 (1964).
(37) Wertheim, G. K., "Mössbauer Effect, Principles and Applications," p. 69, Academic Press, New York, 1964.
(38) Wertheim, G. K., *Science* **144,** 253 (1964).
(39) Wickman, H. H., Trozzolo, A. M., *Phys. Rev. Letters* **15,** 156 (1965).

RECEIVED January 10, 1967.

Mössbauer Studies of Tektites, Pyroxenes, and Olivines

J. G. MARZOLF,[1] J. T. DEHN,[2] and J. F. SALMON[3]

Woodstock College, Woodstock, Md.

Mössbauer spectra have been measured for various tektites, as well as for both natural and synthetic iron-bearing silicate minerals. These results are reported and compared with other similar studies available in the literature. The ratios of the intensities of the appropriate Mössbauer lines have been used to determine the ferric-ferrous ratios where possible. The spectra of the ferrosilite-enstatite series of pyroxenes show four lines which are interpreted as two quadrupole split doublets, and the ratio of the intensities of these lines indicates the degree of ordering in filling the available metal ion sites. Similar studies on the fayalite-forsterite series of olivines are also reported.

Tektites are natural glasses found in various strewn fields around the earth, hundreds or thousands of kilometers in diameter. Their specific gravities range from 2.3 to 2.5, and the specimens so far discovered vary from a fraction of a gram to about 3000 grams. Those found in the Far East seem to form one strewn field and are designated indochinites, javanites, philippinites, australites, etc., according to the locality in which they are found. A field in Czechoslovakia contains tektites called moldavites, while in Texas a large number of tektites called bediasites occur. Different samples have been found in Georgia and Massachusetts and on the Ivory Coast in Africa.

These objects range in age up to 30 million years. Their physical and chemical properties indicate that they were formed under violent

conditions at high temperatures ($\sim$2000°C.) in a reducing atmosphere, probably in a collision involving a comet or a meteorite (since some tektites contain iron spherules) either on earth or on the moon. More distant origins are excluded because of the amount of radioactive ^{26}Al still present in tektites.

The variety of "button," "bowl," "teardrop," "peanut," etc., forms in which tektites are found suggests a three-step process for at least some of them: (1) spin shaping after impact ejection in the molten state, (2) aerodynamic sculpturing in flight, followed by (3) long term weathering and fragmentation. Some physical factors that distinguish them from other natural glasses are the presence of flow structures and strain birefringence, the presence of siliceous glass inclusions of lower refractive index than the surrounding glass, and the absence of microlites. The index of refraction of tektites ranges from about 1.48 to 1.52 and varies inversely with their silica content and directly with their iron content (1–5%) and magnetic susceptibility (2.3 $\times$ 10^{-6} to 8.4 $\times$ 10^{-6} e.m.u./gram). The ratio of the real part of their permittivity to their permeability varies from 42 $\times$ 10^{-6} to 52 $\times$ 10^{-6} sq. mho. Their chemical composition—silica (70–80%), alumina ($\sim$10%); FeO and Fe$_2$O$_3$ (1–5% total), MgO, CaO, Na$_2$O, K$_2$O, TiO$_2$ (0.5–2.5% each), and smaller amounts of other elements—is roughly the same as that of other natural glasses yet sufficiently different to justify separate classification. For example, tektites have a higher alumina content, a higher (FeO + MgO)/(Na$_2$O + K$_2$O) ratio, an unusually low water content ($<$0.02%), and a low ferric/ferrous ratio ($\sim$0.05–0.2). O'Keefe (23) gives further information and references concerning tektites.

Mössbauer Studies of Tektites. Several groups have obtained Mössbauer spectra of tektites. A. Thorpe and F. Senftle of Howard University and the U. S. Geological Survey have cooperated with J. Spijkerman of the National Bureau of Standards. T. Kohman and his group at the Carnegie Institute of Technology in Pittsburgh have recently taken up this work also. The present study made at Woodstock College, however, appears to be the first published account.

Since tektites are glasses, x-ray diffraction analysis cannot determine the short range order which is expected to exist in the vicinity of the Fe^{2+} ions. The Mössbauer spectra discussed below confirm the existence of this short range order, verify the dominance of Fe^{2+} over Fe^{3+}, and show that the ligand coordination, which is only roughly the same for each iron ion (as indicated by the broadness of the lines), is considerably different from cubic (as evidenced by the large quadrupole splitting). In the spectra illustrated the source is Co in Pd, and Doppler velocity is given in millimeters per second, with positive values corresponding to source moving toward absorber.

Figure 1 shows a typical Mössbauer spectrum of an indochinite. The effect is on the order of a few percent. The lines are broad; the width of the line on the right is on the order of 0.8–0.9 mm. per second, which is many times the natural line width. The other line is somewhat narrower, and they are uneven in height. Spijkerman and co-workers also found a slight dip on the right-hand peak (*27*) and thought that this possibly represented a line with a large isomer shift (owing to Fe^{2+}) together with a small quadrupole splitting. This was a preliminary interpretation which was subsequently found to be incompatible with the temperature-dependent shifts of the two lines, as discussed below. Our group also looked carefully at the right-hand line, taking 5×10^6 counts per channel in velocity steps of 0.038 mm./sec. and no dip or
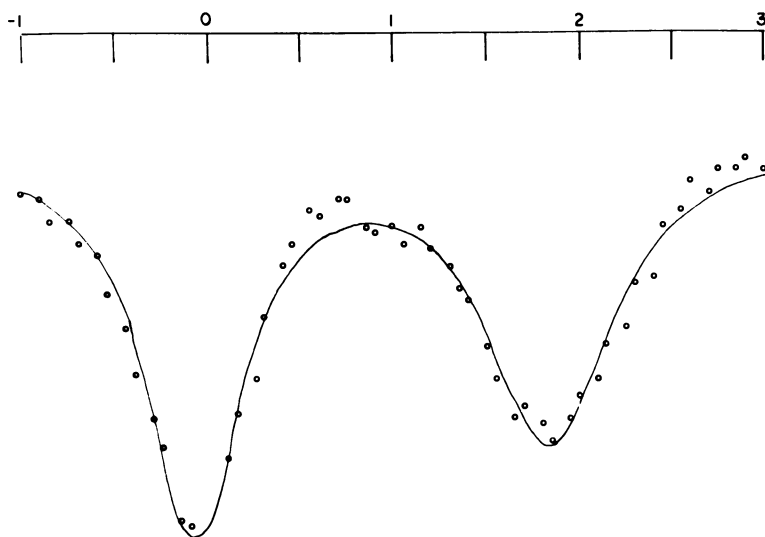

Figure 1. Mössbauer spectrum of an indochinite

indication of a doublet was observed. A number of other spectra of indochinites were taken; all have the same general appearance.

Table I lists the comparative parameters for the various indochinite spectra. Two methods were used in preparing these samples. The first two samples listed were prepared by grinding the indochinite specimen and binding the powder with water glass. The other samples were sliced with a diamond saw. The two spectral lines are given with their position, width, height, and area. The quadrupole splitting and isomer shift are listed in the columns labeled *QS* and *IS*. (The isomer shift is really a combination of isomer shift and temperature-dependent shift, and the values are relative to iron in palladium.) The raw data points were fitted with a two-peak Lorentzian using an IBM 7094 least-squares fit,

Table I. Parameters for Two Peak Lorentzians Fitted to Indochinite Spectra[a]

Sample	Pos. 1	Wid. 1	Hgt. 1	Area 1	Pos. 2	Wid. 2	Hgt. 2	Area 2	QS	IS
7–3	−0.11	0.63	3.2	6.4	1.85	0.82	2.7	6.9	1.96	0.87
7–0	−0.05	0.61	3.0	5.7	1.81	0.83	2.2	5.8	1.86	0.88
2–5	−0.08	0.63	5.1	10.0	1.83	0.80	3.9	9.8	1.91	0.88
2–1	−0.07	0.64	4.2	8.4	1.85	0.79	3.3	8.2	1.92	0.89
2–8	−0.09	0.63	4.4	8.6	1.84	0.80	3.4	8.6	1.93	0.88
2–9	−0.09	0.74	6.4	14.8	1.85	1.00	5.1	16.0	1.94	0.88
							Av.		1.92	0.88

[a] The position, width, quadrupole splitting (QS), and isomer shift (IS) are given in mm./sec. relative to Fe in Pd. The height is given as percent of the base line.

and the values listed are the parameters from this fit. The probable errors are on the order of 0.03 mm./sec., possibly a little larger. The values of the quadrupole splitting and isomer shift are all reasonably close, with a few minor variations, and yield an average value of 1.92 mm./sec. for the quadrupole splitting, and 0.88 mm./sec. for the isomer shift. Other tektites were investigated, and Figure 2 shows the spectrum of a philippinite (U.S.N.M. 1910), which has the same general shape as the in-
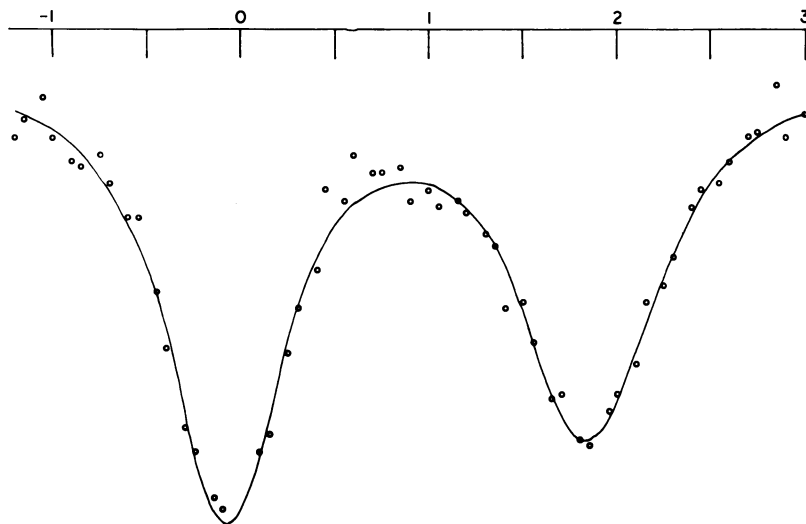

Figure 2. *Mössbauer spectrum of a philippinite*

dochinites, including the broad lines. This, of course, is not unexpected, because we are dealing with glasses. There is no crystal structure. At best, we have something akin to short range order, and so the spectra would really be the superposition of many similar but slightly shifted spectra.

Figure 3 shows the spectrum of a bediasite. All these spectra have roughly the same shape, but the tektites from different strewn fields have different isomer shifts and quadrupole splittings. For comparison, we have also investigated some iron-bearing welding glasses. The Mössbauer spectrum of one of these glasses (Pittsburgh Plate Glass 1927, shade 8) is
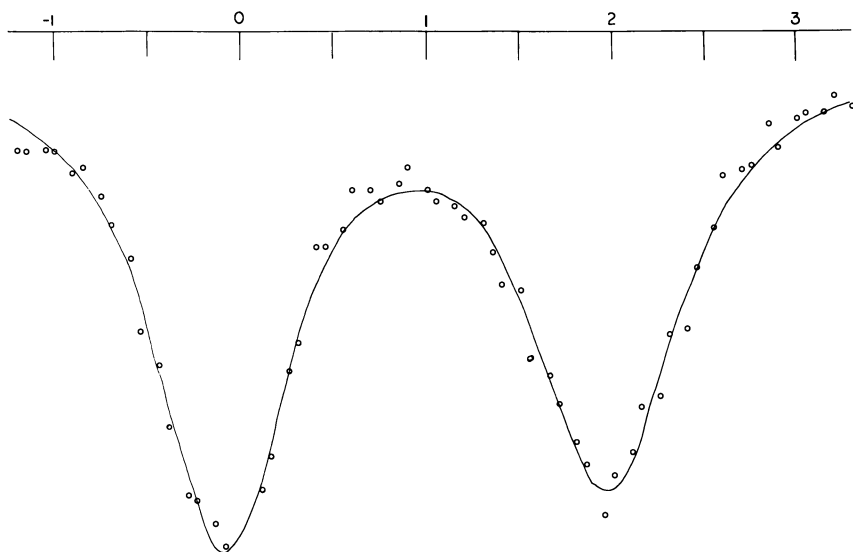

Figure 3.   *Mössbauer spectrum of a bediasite*

shown in Figure 4. This spectrum was fitted with a three-line Lorentzian because of the clear presence of the shoulder on the left-hand line. Although we have no chemical analysis of this glass, the Pittsburgh Plate Glass Co. analyses indicate the presence of both ferric and ferrous iron. The Walker-Wertheim-Jaccarino diagram (29) establishes that the smaller isomer shift is caused by Fe^{3+} while the larger is caused by Fe^{2+}.

The data from all of these spectra are compared in Table II, which lists the quadrupole splitting and the isomer shift (relative to iron in palladium) in millimeters per second and the ferric-ferrous ratio (as obtained from the Mössbauer data, by comparing the areas of the two sets of lines). The variations in the quadrupole splitting, ranging from 1.84 to 2.08 mm./sec., are certainly outside the range of experimental error and must be attributed to actual variations in the different tektites studied. The only type of tektite for which we measured many different samples was the indochinite, and the quadrupole splitting and isomer shift of these samples were the same for all samples within experimental error. Hence, these two parameters would be useful in verifying the classification of different types of tektites. The difficulties involved in
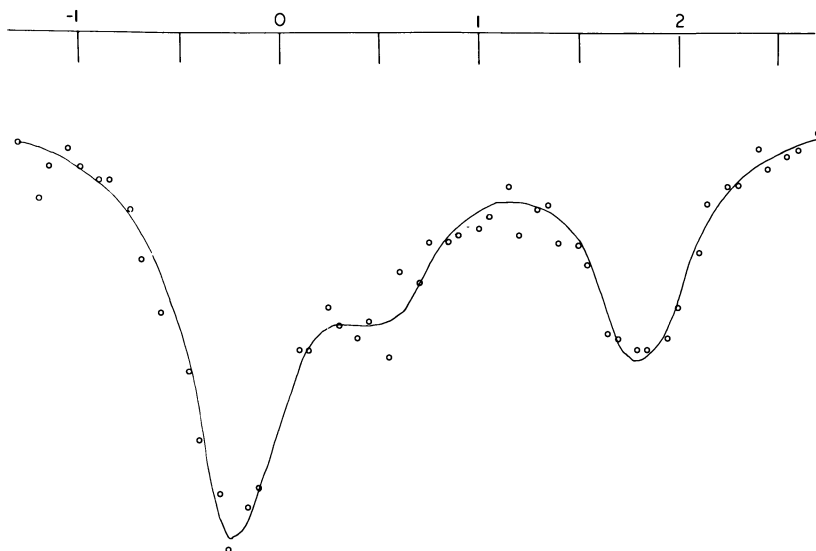
Figure 4.   Mössbauer spectrum of Pittsburgh Plate Glass, 1927 shade 8

obtaining quantitative measurements of the ferric/ferrous ratio have been discussed (28), and using the Mössbauer effect for these measurements does not appear to be more promising than the methods of wet chemistry, unless, of course, one is interested merely in an approximate figure which may be obtained quickly.

We also examined the effects of various heat treatments in both reducing and oxidizing atmospheres. An indochinite reduced for 12 hours in a hydrogen atmosphere at 950°C. yielded the Mössbauer spectrum displayed in Figure 5. The curve shown is the result of the computer fit; the data points are not given, but the closeness of fit is about the same as in the other spectra. The spectrum clearly shows that a certain amount of the original tektite remains; the two broad lines at —0.11 and 1.83 mm./sec. match the original tektite lines closely. There is also clear evidence of the presence of metallic iron since the six narrow

Table II.   Comparative Mössbauer Parameters for Various Tektites[a]

Sample	Shift	Splitting	Fe^{3+}/Fe^{2+}
Indochinites (average)	0.88	1.92	
Australite (U.S.N.M. 2302)	0.87	1.88	
Philippinite (U.S.N.M. 1910)	0.88	1.93	
Bediasite	0.92	2.08	
Moldavite	0.80	1.84	
Welding glass (P.P.G. 1927-8)	0.81	2.03	0.4–0.6

[a] Isomer shift and quadrupole splitting in mm./sec. relative to Fe in Pd.
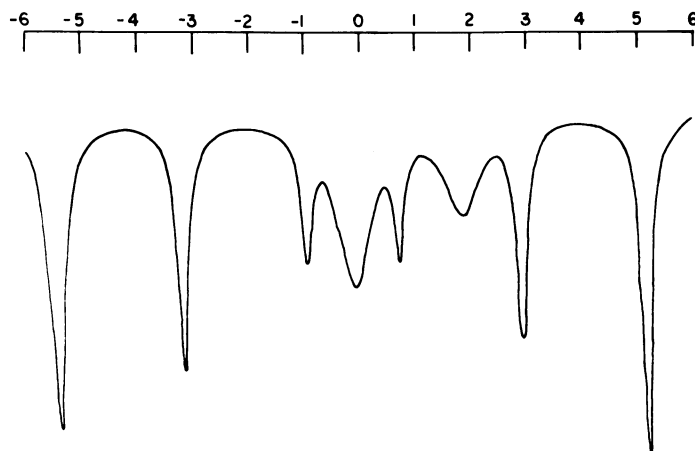
Figure 5. Room temperature Mössbauer spectrum of an indochinite after heating at 950°C. for 12 hours in a hydrogen atmosphere

lines correspond quite well with the spectrum of ordinary iron foil (internal magnetic field at the nucleus of about 330 kilogauss).

To determine whether or not the two broad and uneven lines of the ordinary (untreated) tektite spectra really belong together as a pair of quadrupole split lines, we measured the temperature dependence of the isomer shift and the quadrupole splitting. Figure 6 shows the spectrum of an indochinite measured at 450°C., which is a typical example
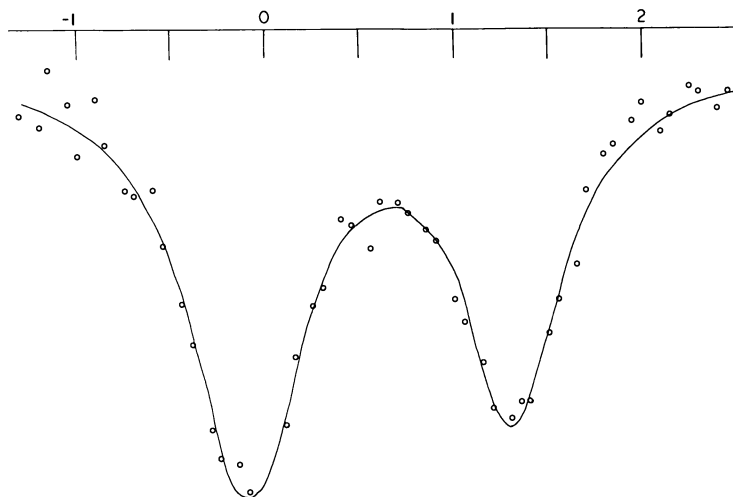

Figure 6. Mössbauer spectrum of an indochinite taken at 450°C.

of the Mössbauer spectrum of an indochinite taken at an elevated temperature. Because of the possible danger of oxidation, the samples were sliced rather than powdered to reduce surface area. In some cases an argon atmosphere (0.005% oxygen) was used. That neither oxidation nor reduction occurred was established by taking a spectrum at room temperature after the sample had been through the temperature run. An example of such a spectrum is shown in Figure 7, which corresponds well with the spectrum taken before the temperature experiments.
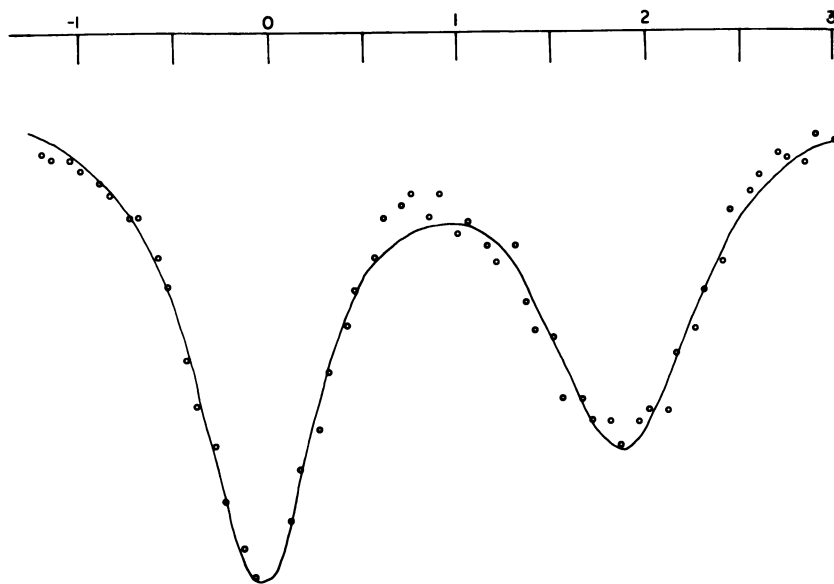

Figure 7.   Room temperature Mössbauer spectrum of an indochinite after heating at various temperatures up to 900°C.

Figure 8 gives a plot of the temperature dependence of the center shift (isomer shift plus relativistic temperature shift) on the assumption that the two lines belong together as a quadrupole split pair. The symbols represent various indochinite samples. All the measured values of the center shift fall on a straight line, whose slope yields $d(IS)/dT = -6.8 \times 10^{-4}$ mm./sec./°C., which is slightly more negative than, but within the range of most measured center shifts as a function of temperature. Thus, the two lines do belong together as a quadrupole split pair; otherwise the temperature dependence of the shift of the left line would be anomalously low, while that of the right line would be anomalously high.

The uneven heights in the two peaks of the tektite spectra (as shown in the figures and listed in Table I) cannot be explained adequately

by the Gol'danskiĭ effect (*15*) because tektites possess only short range order and, in addition, the observed asymmetry appears to be, for the most part, independent of temperature. Spin-lattice relaxation effects (*1, 5, 6*) also appear unlikely as an explanation (although possible) because of the considerable magnetic dilution (1–5% Fe) and elevated temperatures (300°–900°K.) which favor relaxation times too fast for doublet asymmetry. The simplest and most direct explanation is based on the fact that because we are dealing with a glass, there are variations in the bond distances and angles from one iron atom to the next. This will produce a change in both the isomer shift and the quadrupole splitting, and the observed spectrum is an average of many similar but slightly shifted spectra. If these variations were approximately twice as great in the quadrupole splitting as in the isomer shift, the central line —*i.e.*, the line near zero velocity—would tend to be narrower than the far line (peak 2 in Table I). In broadening the far line, the height
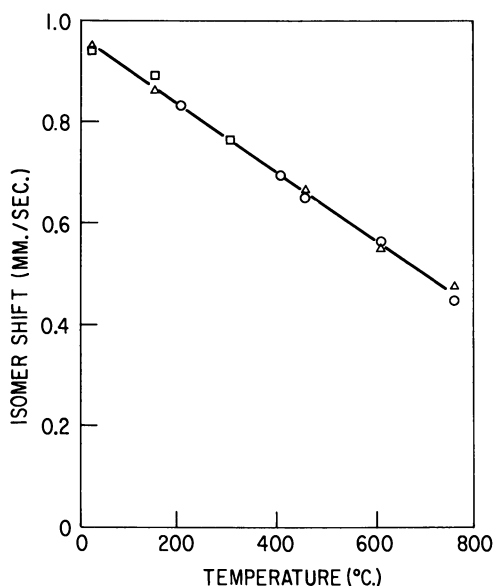

Figure 8.   *Temperature dependence of center shift of various indochinites*

would have to diminish to keep the intensities the same. In this case the areas should be the same, and in fact they are fairly close to being the same in most cases.

Mössbauer Effect in Similar Glasses and Crystals. Expression of the Mg-Fe content of tektites in terms of enstatite-ferrosilite percentages suggests a comparison with silicate minerals which contain Fe^{2+} and

show more or less the same Mössbauer parameters. Of course we do not expect quantitative conclusions concerning the Fe^{2+} coordination in tektites from such a comparison since glassy and crystalline forms of identical chemical composition can exhibit different Mössbauer parameters. For example, Kurkjian and Sigety (19) and Kurkjian and Buchanan (18) showed that crystalline ferric metaphosphate, $Fe(PO_3)_3$, exhibits a poorly resolved doublet at room temperature while the glass of the same composition shows three lines, interpreted as the superposition of an Fe^{3+} doublet and an Fe^{2+} doublet. The line widths and splittings show that the Fe^{3+} site symmetry departs more from cubic in the glass than in the crystal and that iron occupies a greater variety of sites in the glass. In spite of these differences, these authors conclude from the similarity of the Fe^{3+} isomer shifts in the glass and the crystal to each other and to yttrium iron garnet that the iron in the glass is roughly octahedrally coordinated. Their observed shifts (relative to Fe) and splittings are given in Table III.

Table III.   Room Temperature Mössbauer Parameters of Ferric Metaphosphate (19)[a]

Sample	Shift	Splitting
$[Fe^{3+}]Fe(PO_3)_3$ (crystal)	0.49	0.32
$[Fe^{3+}]Fe(PO_3)_3$ (glass)	0.46	0.88
$[Fe^{2+}]Fe(PO_3)_3$ (glass)	1.20	2.15

[a] Center shift and quadrupole splitting are in mm./sec. relative to Fe.

Mattern (21) has made Mössbauer studies of phosphate glasses of compositions $(FeO)_x (P_2O_5)_{1-x}$ and $(MgO)_a(P_2O_5)_b(FeO)_c$. His spectra may also be interpreted generally as the superposition of an Fe^{3+} doublet and an Fe^{2+} doublet. He found little change over the composition range from 0.01 to 13 atomic % iron and from room temperature to 35°K. The Fe^{3+}/Fe^{2+} ratios (from 0 to 10) determined from the relative areas of the Mössbauer peaks agreed roughly (within 10%) with those determined by chemical analysis. The discrepancy was not explained completely to the author's satisfaction, although the difficulties of determining the cause of the asymmetry of the broad-line doublets was given as a likely reason. At liquid helium temperature a six-line pattern was observed for the predominantly Fe^{3+} glasses and attributed to magnetic relaxation for samples containing less than 1% iron and to short range magnetic ordering for those with higher iron concentrations. The Fe^{2+} glasses showed only a doublet with slightly broadened lines even at liquid helium temperature.

Belyustin and co-workers (4) have observed three-line spectra in their alkali (10–20%)–iron (1–15%)–silicate glasses with the same interpre-

tation of Fe^{3+} and Fe^{2+} doublets. The glass and the minerals aegirite and fayalite are compared in Table IV. Those authors note that the short range order evident in the glass does not yield the same parameters as either mineral, nor was there any exact correspondence with any of the

Table IV.   Mössbauer Parameters of Silicate Minerals and Glasses (4)[a]

Sample	Shift	Splitting
Aegirite (Fe^{3+})	0.48	0.00
Fayalite	0.37	3.00
Fe^{3+} (glass)	0.37	0.85
Fe^{2+} (glass)	1.12	2.00

[a] Center shift and quadrupole splitting are in mm./sec. relative to Fe in Cr.

other iron silicates which they studied (but did not include in their report), such as epidote, biotite, phlogophite, and hornblende. They remark that the Fe^{3+}/Fe^{2+} ratios in their glasses derived from Mössbauer parameters again agree only qualitatively with the results of chemical analysis, but they give no satisfactory explanation for the difference. Finally (relying both on Pauling's rule that a decrease in bond ionicity means a decrease in coordination number and on the observation that a decrease in ionicity means a decrease in the Mössbauer chemical shift) they suggest that Fe^{2+} ions in glasses have a smaller coordination number (possibly as low as 4) at lower iron concentrations and hence are better vitrifiers.

The best conclusion one can draw, then, seems to be that comparisons between mineral and glass Mössbauer parameters are qualitative as far as coordination number and site symmetry in the glass are concerned. However, the crystal spectra are interesting for their own sake.

Pyroxenes and Olivines

Two groups of minerals have roughly the same Mössbauer parameters as tektites and demonstrate some of the possibilities and limitations of the Mössbauer technique. The pyroxenes have a lower silica content than tektites (45–60 mole %), less alumina (1–2%), and much higher total (Fe + Mg) (~40%) with smaller amounts of Ti, Mg, Ca, Na, K, Cr, Mn, and Ni. The olivines contain even less silica (30–40%) and have 1–2% alumina and about 60% (Fe + Mg) with smaller amounts of the same elements listed above for pyroxenes. Both types of minerals usually have low Fe^{3+}/Fe^{2+} ratios and low water content (although higher than in tektites). In the pyroxene group the solid solution series $(Mg,Fe)SiO_3$, called the enstatite-ferrosilite (En-Fs) series, shows interesting Mössbauer spectra. These minerals commonly crystallize in two

different classes: orthorhombic (space group symmetry *Pbca*) and mono-clinic (space group symmetry $P2_1/c$). They have 16 metal atoms per unit cell, eight of which belong to the site M_1 which is smaller and more nearly octahedrally coordinated with neighboring oxygen ions, while eight belong to the site M_2 which is larger and more distorted in its sixfold oxygen coordination. The $(SiO_3)_n$ chains are laterally linked by the metal atoms. In the olivine group the solid solution series $(Mg,Fe)_2SiO_4$, called the forsterite-fayalite (Fo-Fa) series, is commonly orthorhombic (space group symmetry *Pbnm*). Again we can distinguish two metal sites, each with sixfold oxygen coordination, but linking indi-vidual silicon-oxygen tetrahedra. Both sites are distorted octahedra, but they are not equivalent since a metal atom in one site is located at a center of symmetry and has two oxygens from two adjacent tetrahedra as nearest neighbors, while at the other site it lies on a reflection plane and has two oxygens from the same tetrahedron as nearest neighbors. Pyroxene specific gravities vary from 3.2 to 4.0, while their indices of refraction range from 1.65 to 1.75. Olivines are slightly denser and usually have a larger refractive index. Further details and references are given by Deer, Howie, and Zussman (*8*). The nomenclature com-monly used for the members of these series we have studied is given in Table V.

Table V.   Nomenclature for (Mg, Fe) Solid Solution Series of Olivines and Pyroxenes Treated in This Study

Mole % Iron	Pyroxene Name	Olivine Name
0–10	Enstatite	Forsterite
10–30	Bronzite	Chrysolite
30–50	Hypersthene	Hyalosiderite
50–70	Ferro-hypersthene	Hortonolite
70–90	Eulite	Ferro-hortonolite
90–100	Ferrosilite	Fayalite

Previous Mössbauer Studies of Natural Pyroxenes and Olivines. The first extensive study of iron-silicate minerals published was by deCoster and co-workers (*7, 24*). Their results are summarized in Table VI. Augite is a pyroxene containing considerable Na and Ca. No iron percentage was given for the olivine studies. The other minerals are included for comparison. The values given here for biotite are averages for their three untreated samples, which have two sites described as distorted octahedra. Heat treatment at 700°C. for one hour resulted in the emergence of a new Fe^{3+} peak in biotite.

Sprenkel-Segel and Hanna (*28*) during their Mössbauer analysis of meteorites also determined the shifts (relative to Fe) and splittings of olivine (13 to 26% Fe) and an orthopyroxene (15–26% Fe). Their values·are summarized in Table VII.

Table VI. **Mössbauer Parameters of Iron-Silicate Minerals
Studied by deCoster, Pollak, and Amelinckx (7, 24)** [a]

Mineral	Ion	Shift	Splitting
Bronzite	Fe^{2+}	1.35	2.23
Augite	Fe^{2+}	1.37	2.18
Augite	Fe^{3+}	0.54	0.84
Olivine	Fe^{2+}	1.35	3.04
Epidote	Fe^{3+}	0.53	2.07
Tourmaline	Fe^{2+}	1.15	2.10
Staurolite	Fe^{2+}	1.14	2.22
Actinolite	Fe^{2+}	1.32	2.41
Biotite, site 1	Fe^{2+}	1.21	2.40
Biotite, site 2	Fe^{2+}	1.40	2.80

[a] Doppler velocities are in mm./sec. relative to Fe in Cr.

Bancroft and co-workers (*3*) have studied various minerals of the amphibole group of composition $(Mg,Fe^{2+})_7Si_8O_{22}(OH)_2$, and by combining Mössbauer data with the results of infrared spectroscopy they were able to determine the distribution of iron ions among the M_1, M_2, M_3, and M_4 sites. They have also reported Mössbauer studies of various minerals—staurolite, gillespite, almandine, sanidine, epidote, pyroxene, and olivine (*2*)—and have proposed using quadrupole splitting to estimate compositions of orthopyroxenes, olivines, and cummingtonites. More to our purpose here, they detected no cation ordering in olivine or epidote (except for Mn in the M_2 site in tephroites), but they did observe that Fe^{2+} favored the M_2 site in orthopyroxene and the M_4 position in cummingtonite.

Recently, Evans and co-workers (*11*) studied the spectra of three orthopyroxenes with Fe/(Mg + Fe) ratios of 0.758, 0.532, and 0.280. They obtained two somewhat asymmetric lines, and their results are summarized in Table VIIIA. One of these authors had previously established by x-ray analysis (*12, 13*) that the sample with the 0.532 ratio exhibits Mg-Fe ordering, with iron preferring the larger, more distorted M_2 site. Consequently it was concluded that the "two-line" Mössbauer spectra must consist of a superposition of two quadrupole-split doublets nearly coinciding. Mössbauer parameters for iron in these

Table VII. **Mössbauer Parameters of Pyroxene and Olivine
as Determined by Sprenkel-Segel and Hanna (28)** [a]

Mineral	Shift	Splitting
Orthopyroxene	1.13	2.12
Olivine	1.13	2.98

[a] Doppler velocities are in mm./sec. relative to Fe.

Table VIII.   Mössbauer Parameters

Fe/(Mg + Fe)	Site	Shift	Splitting
A. Mössbauer parameters for "two-line" orthopyroxene spectra of varying iron content as determined by Evans, Ghose, and Hafner (11)[a]			
0.758	—	1.26	2.14
0.532	—	1.25	2.11
0.280	—	1.24	2.11
B. Approximated parameters for metal sites M_1 and M_2 extracted by computer from spectra summarized above			
0.758	1	1.27	2.57
	2	1.24	2.00
0.532	1	1.28	2.53
	2	1.26	2.11

[a] Doppler velocities are in mm./sec. relative to stainless steel.

Table IX.   Major Element Compositions

Sample	SiO_2	Al_2O_3	'FeO	Fe_2O_3
Diopside (U.S.N.M. 97545)	52.34	2.04	2.88	0.96
Hedenbergite (U.S.N.M. 61877)	48.34	0.30	22.94	1.50
Jeffersonite (U.S.N.M. R3026)	45.95	0.85	8.91	
Bronzite (U.S.N.M. 14147)	54.17	3.30	9.94	
Aegerine (U.S.N.M. 102597)	51.41	1.82	9.45	23.30
Fayalite (U.S.N.M. 85276)	29.75		66.10	0.83

Table X.   Comparative Mössbauer

Sample	Splitting	Ferrous-Ferric
Diopside (U.S.N.M. 97545)	1.97	—
Hedenbergite (U.S.N.M. 61877)	2.19	0.69
Jeffersonite (U.S.N.M. R3026)	2.11	0.60
Augite (U.S.N.M. R14923)	1.96	0.69
Bronzite (U.S.N.M. 14147)	1.81(2.75)	—
Aegerine (U.S.N.M. 102597)	1.88(2.74)	0.45
Fayalite (U.S.N.M. 85276)	2.78	—

[a] Quadrupole splitting and isomer shift are in mm./sec.

M_1 and M_2 sites were then extracted by computer from the "two-line" spectra. Their results are summarized in Table VIIIB. All of the iron presumably entered the M_2 site for the 0.280 sample, so no values are given in Table VIIIB for this case since they would be the same as the last entry in Table VIIIA. These authors estimated that 85% of the iron is in M_2 for the 0.532 sample, 63% in the M_2 site for the 0.758 sample. Assigning the M_2 site as the one preferred by Fe was based on

the x-ray results quoted above. The smaller isomer shift for M_2 was taken to mean less ionic bonding in this site.

Present Mössbauer Studies of Natural Pyroxenes and Olivines. Table IX gives the major element chemical compositions of the silicate minerals examined in this study. Table X compares the Mössbauer parameters of these minerals, while Figures 9–13 show representative Mössbauer spectra. Fayalite (Figure 9) is the only olivine in this group. The two lines are, however, somewhat broadened (0.35 and 0.39 mm./ sec.) compared with the width of natural iron foil lines observed with our source (0.24 mm./sec.) and suggest the near coincidence of two quadrupole-split doublets resulting from M_1 and M_2 sites. Analysis of this "two-line" spectrum into a four-line spectrum in the manner described by Evans *et al.* (*11*) could possibly yield parameters for the two iron sites, but this was not undertaken since both lines appear symmetric. The "two-line" quadrupole splitting of 2.78 mm./sec. is somewhat smaller

of Minerals Described in Table X

MgO	CaO	ZnO	MnO	Na₂O	Cr₂O₃	H₂O⁺
17.56	23.96		0.09		0.46	
1.06	21.30		3.70	0.14		0.46
3.61	21.55	10.15	10.20			
31.99	0.99					
0.31	2.03			11.88		
			3.20			0.19

Parameters for Various Iron Silicates[a]

Shift Ferrous-Ferric		Fe³⁺/Fe²⁺, Möss.-Chem.	
0.98	—	0	?
1.00	0.26	0.1	0.06
1.00	0.25	0.1	0
0.96	0.32	0.2	?
0.94 (0.99)	—	0	0
0.97 (0.95)	0.20	2.4	2.3
0.98	—	0	0.01

[a] relative to Fe in Pd.

for this high iron concentration sample than the values given in Tables VI and VII.

The other mineral spectra shown are pyroxenes. The bronzite sample studied (Figure 10) is almost a member of the solid-solution series listed in Table V, although small amounts of Al and Ca are present. Consequently, it should be compared with the synthetic members of this series described below. Even in this natural mineral sample there is clear

evidence of two quadrupole-split doublets belonging to two different iron sites. Using either the ratio of peak heights or the ratio of areas methods as described, 89% of the iron is in the site with the smaller quadrupole splitting (*cf.* Table XII). Figure 11 shows the spectrum of hedenbergite and Figure 12 shows that of jeffersonite. Both show the
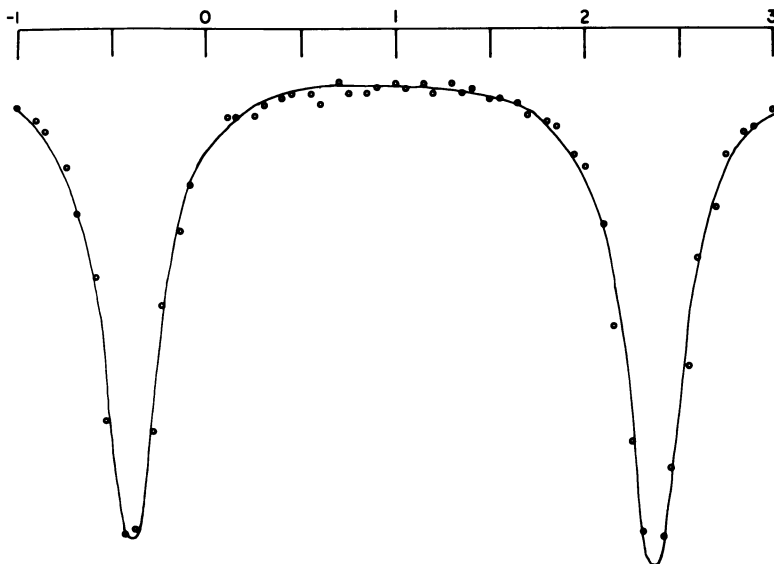
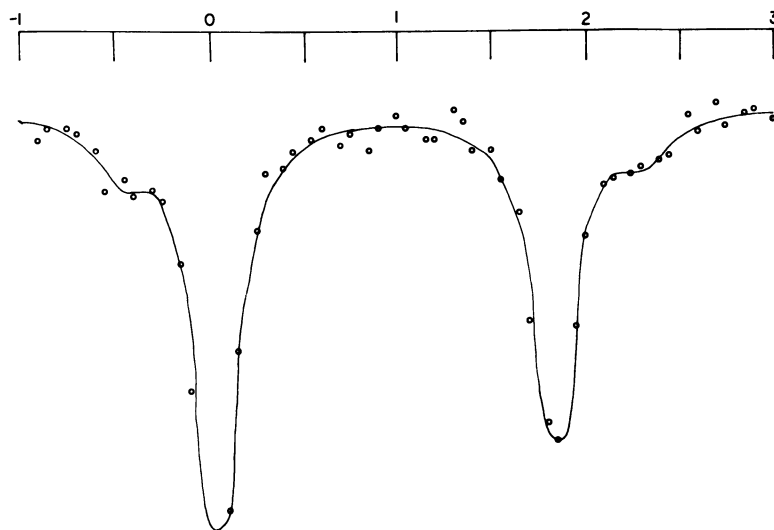

Figure 9. Mössbauer spectrum of a fayalite (Fe$_2$SiO$_4$)
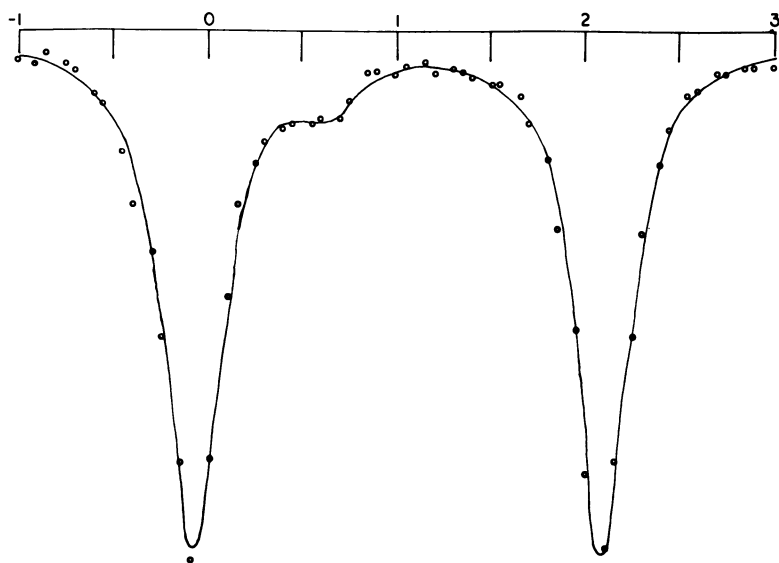

Figure 10. Mössbauer spectrum of a bronzite [(Fe,Mg)SiO$_3$]

Figure 11. Mössbauer spectrum of a hedenbergite
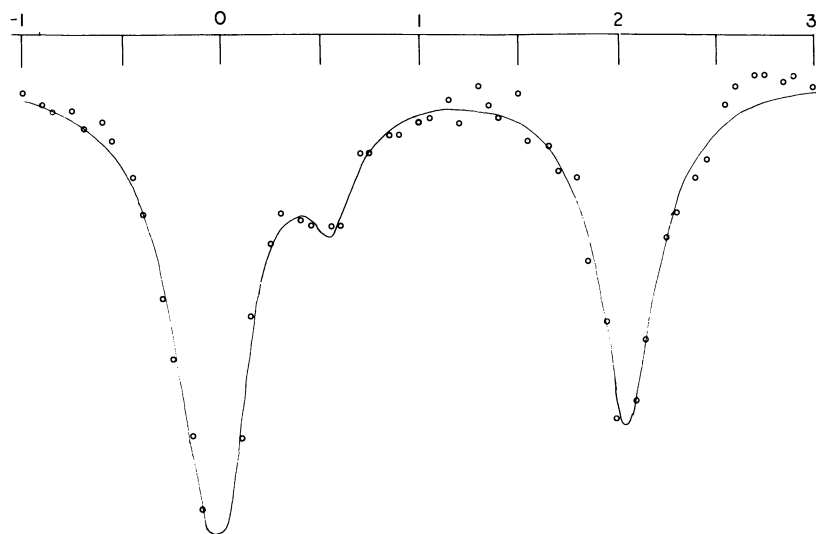
Figure 12. Mössbauer spectrum of a jeffersonite

presence of ferric iron, although only one of the Mössbauer estimates of the Fe^{3+}/Fe^{2+} ratio is in reasonable agreement with chemical analysis. The spectrum of aegerine (Figure 13) consists of a dominant Fe^{3+}

doublet plus two sets of Fe^{2+} doublets, and the Mössbauer Fe^{3+}/Fe^{2+} ratio agrees rather well with the results of chemical analysis.

As might be expected, none of these minerals has the same Mössbauer parameters as tektites since they differ both in crystal structure and chemical composition. The Fe^{2+} coordination in these samples is, of course, only nominally octahedral since they exhibit large quadrupole splittings, for the most part larger than in tektites. Their isomer shifts are also slightly larger, possibly indicating a more ionic type of bonding.
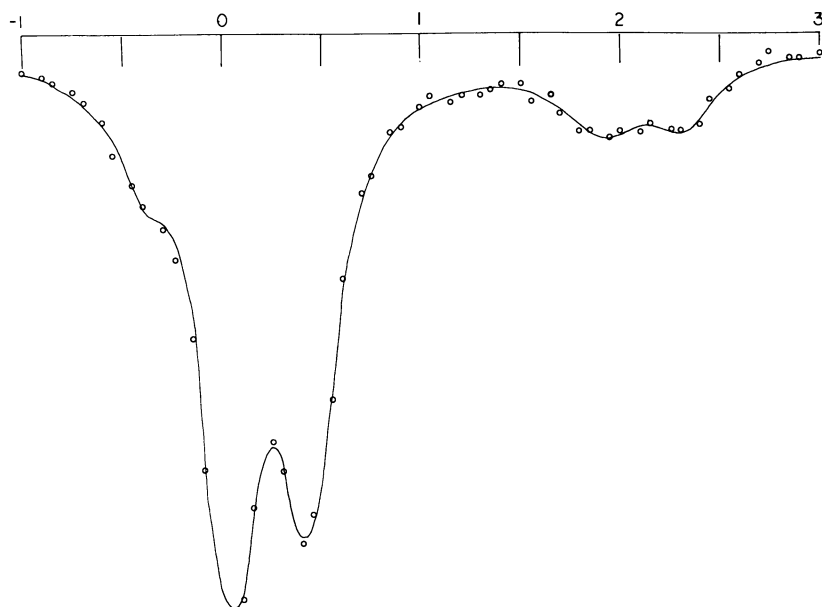
Figure 13.   Mössbauer spectrum of an aegerine

Synthetic Pyroxenes and Olivines. Figure 14 shows the Mössbauer spectra of the enstatite-ferrosilite series from $(Mg_{0.9},Fe_{0.1})SiO_3$ to $FeSiO_3$ synthesized at the Carnegie Geophysical Laboratory, Washington, D. C. The ferrosilite end member is not found in nature and was made at pressures from 18 to 45 kbars and temperatures between 1150° and 1400°C. (20). Table XI gives the shifts (relative to Pd), splittings, and line widths of members of this series. The shifts are about the same as for bronzite (Table X), although the quadrupole splittings of the synthetic samples are smaller for the M_1 site and larger for the M_2 site than those of the natural mineral. The left-hand and right-hand outermost lines in Figure 14 are labeled L_1 and R_1 since these apparently belong to site M_1, while the innermost pair is labeled L_2 and R_2 since it belongs to site M_2. No major differences were found in the Mössbauer parameters
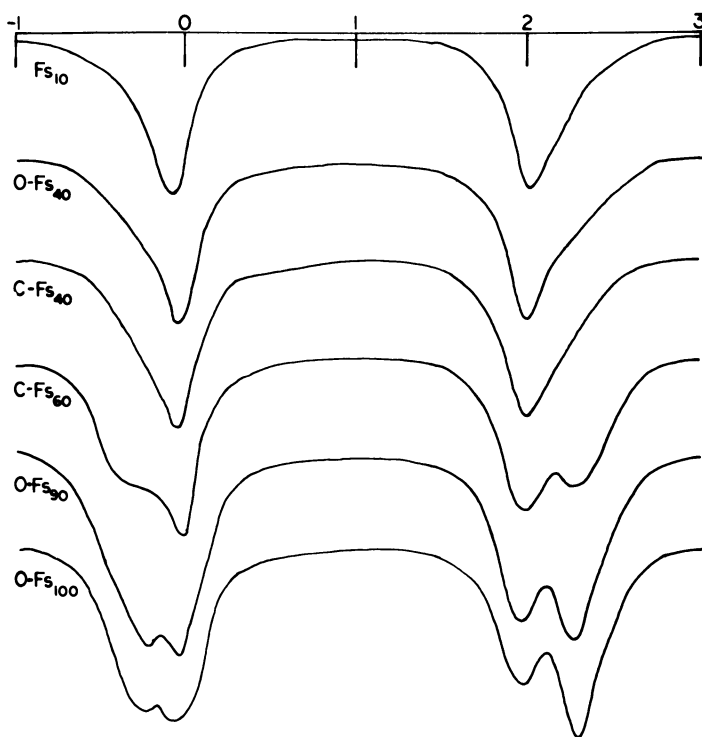
Figure 14. Mössbauer spectrum of ferrosilite-enstatite series of pyroxenes

of the monoclinic and orthorhombic varieties of these pyroxenes (designated by prefixes C- and O-), provided they had the same iron concentrations.

Table XII lists the relative peak heights (and the percentage of iron in the M_2 site obtained from these heights) together with the relative areas (and the same percentage as obtained from these areas). In either method the percentage of iron was taken to be the average of the M_2 values, $(L_2 + R_2)/2$, divided by the sum of averages of the M_1 and M_2 values—i.e., $(L_2 + R_2)/(L_1 + R_1 + L_2 + R_2)$.

The positions, widths, and heights of the lines were determined by least-squares computer fits to the sum of four Lorentzian lines with no restrictions connecting these 12 parameters. The criterion for a good fit was the sum of the squared deviations divided by the number of data points, and statistically it was reasonably satisfactory in all cases. The general trends in Tables XI and XII are clear. The discrepancies are probably caused in part by the inadequacies of the fitting procedure, especially the lack of provision for the evident peak height asymmetry

Table XI.   Mössbauer Parameters of a Synthetic Enstatite-Ferrosilite (En-Fs) Series as a Function of Iron Concentration Expressed as Percent Ferrosilite Present by Subscript on Fs

Sample	Shift		Splitting		Line Widths [a]			
	M_1	M_2	M_1	M_2	L_1	L_2	R_2	R_1
Fs_{10}	0.90	0.96	2.51	2.04	0.54	0.25	0.25	0.47
$C-Fs_{40}$	0.98	0.96	2.54	2.06	0.32	0.30	0.33	0.34
$O-Fs_{40}$ (#1)	0.94	0.95	2.60	2.04	0.32	0.31	0.27	0.42
$O-Fs_{40}$ (#2)	0.9	0.95	2.6	2.04	0.3	0.30	0.26	0.41
$C-Fs_{60}$ (#1)	0.98	0.94	2.67	2.03	0.35	0.32	0.32	0.41
$C-Fs_{60}$ (#2)	0.97	0.94	2.68	2.03	0.36	0.33	0.31	0.40
$O-Fs_{90}$ (#1)	1.00	0.95	2.52	1.90	0.43	0.25	0.27	0.38
$O-Fs_{90}$ (#2)	1.00	0.96	2.56	1.95	0.44	0.29	0.27	0.39
$O-Fs_{100}$	0.99	0.94	2.58	1.95	0.37	0.30	0.29	0.34

[a] L_i and R_i represent the left and right lines of the site M_i, $i = 1, 2$, on the usual velocity scale (mm./sec. relative to Fe in Pd.) *See* Figure 14 and text.

Table XII.   Fraction of Iron $F = (L_2 + R_2)/(L_1 + L_2 + R_2 + R_1)$ Estimated to Be in Site M_2 from the Peak Heights (F_H) and Areas (F_A)

Sample	Relative Peak Heights					Relative Areas				
	L_1	L_2	R_2	R_1	F_H	L_1	L_2	R_2	R_1	F_A
Fs_{10}	2.8	10.2	9.3	4.0	0.74	4.6	8.0	7.4	5.8	0.60
$C-Fs_{40}$	6.3	18.6	18.3	6.4	0.74	6.4	17.3	18.7	6.7	0.73
$O-Fs_{40}$ (#1)	3.9	15.7	14.3	6.6	0.74	3.9	15.4	12.2	8.7	0.69
$O-Fs_{40}$ (#2)	1.5	6.0	5.8	2.5	0.75	1.4	5.7	4.8	3.2	0.70
$C-Fs_{60}$ (#1)	11.2	14.6	14.7	12.6	0.55	12.2	14.5	14.8	16.4	0.51
$C-Fs_{60}$ (#2)	13.9	18.8	17.8	15.5	0.55	15.8	19.4	17.3	19.7	0.51
$O-Fs_{90}$ (#1)	11.2	8.5	9.7	11.9	0.44	15.2	6.6	8.2	14.2	0.33
$O-Fs_{90}$ (#2)	10.5	9.1	9.0	11.3	0.45	14.6	8.2	7.5	13.8	0.36
$O-Fs_{100}$	4.9	5.1	4.2	6.5	0.45	5.7	4.8	3.8	6.8	0.41
Bronzite (#1)	1.6	12.7	9.5	1.1	0.89	1.6	10.0	7.5	0.6	0.89
Bronzite (#2)	0.9	8.8	6.4	0.7	0.90	0.9	6.6	5.2	0.6	0.89

of the doublets, which might be caused by crystal anisotropy or magnetic relaxation effects demanding a fit to a larger number of lines. Moreover, the Lamb-Mössbauer factors were assumed to be the same for both sites, and the sites were identified as M_1 and M_2 on the basis of Ghose's x-ray results (*13*) for a natural mineral near the center of this series. Finally, small amounts of Fe^{3+} would also necessitate a more elaborate fitting procedure.

The largest percentage of iron in the M_2 site estimated for our samples (74–75%) occurs at the enstatite end of our synthetic series, as expected. However, this is rather low compared with estimates for natural minerals. For example, our bronzite specimen has a ratio Fe/ (Mg + Fe) = 0.237—*i.e.*, Fs_{24}—and was estimated to have 89% of its iron in the M_2 site. Mössbauer studies of Evans and co-workers (*11*)

indicated that their mineral sample with $Fe/(Mg + Fe) = 0.280$ had all of its iron in the M_2 site, while their sample with the ratio 0.532 had 85% of its iron in the M_2 site, in reasonable agreement with x-ray determinations (*13*). Their estimates that 71 and 73% of the iron in their 0.532 sample was in the M_2 site after heating for 7 days at 1000°C. and for 13 hours at 1100°C., respectively, makes our estimate closer to theirs for a comparable ratio, although for Fs_{53} extrapolation in Table XII would still give a somewhat smaller value of about 63%. This seems to reflect the process used to prepare our synthetic specimens. The formation of these minerals in their natural state apparently resulted in a greater ordering of iron in the M_2 site and probably involved a much slower cooling process. At the ferrosilite end of the series we have estimated that less than half of the iron is in the M_2 site, a somewhat surprising result. This appears to be true whether we use the relative peak height method or the relative area method. It may be caused by our somewhat oversimplified fitting procedure, as explained above, or it may be real. If it is the latter, we need a thorough x-ray analysis of these end members. A decrease in the M_2 site quadrupole splitting at the ferrosilite end of the series also suggests some sort of change in site geometry and bonding, as does the slight increase in the chemical shift of site M_1. More elaborate analyses are required, however, before general conclusions can be reached.

Mössbauer parameters for the "two-line" spectra of the fayalite-forsterite $(Mg,Fe)_2SiO_4$ series studied are given in Table XIII. All the samples are synthetic orthorhombic olivines made by the Carnegie Geophysical Laboratory. No attempt was made to extract two superimposed doublets from the data because neither line has any obvious asymmetry, although this might be a possible explanation of why the lines are broader than expected. The quadrupole splitting of these lines noticeably increases with decreasing iron concentration although the isomer shift remains constant. The peak heights remain fairly symmetri-

Table XIII.   Mössbauer Parameters for a Synthetic Fayalite-Fosterite (Fa-Fo) Series as a Function of Iron Concentration Expressed as % Fayalite by Subscript on Fa[a]

Sample	Shift	Splitting	Line Width		Peak Height		Height Ratio, L/R
			L	R	L	R	
Fa$_{90}$	0.98	2.80	0.27	0.34	13.3	11.9	1.12
Fa$_{50}$	0.97	2.87	0.34	0.37	24.7	24.8	1.00
Fa$_{20}$ (#1)	0.97	2.91	0.28	0.32	15.1	13.8	1.09
Fa$_{20}$ (#2)	0.97	2.91	0.30	0.34	13.2	12.7	1.04

[a] L and R represent the left and right lines on the usual velocity scale (mm./sec. relative to Fe in Pd).

cal over the entire range. There is fair agreement between the spectra of our synthetic members of the fayalite-forsterite series and of the natural mineral (almost pure fayalite) reported in Table X, and the quadrupole splitting of the natural mineral is smaller, in accord with the trend noted above.

Crystal Field Description. Since pyroxenes and olivines are usually considered ionic crystals, we expect crystal field theory to provide an approximate theoretical model. The theory for Fe^{2+} ions as applied to the Mössbauer effect has been developed by Ingalls (*17*) for the temperature-dependent occupation of the nondegenerate electronic states by the sixth d-electron responsible for most of the electric field gradient (EFG) felt by the nuclear quadrupole moment, Q. Besides splitting the electronic levels, the arrangement of charges surrounding an Fe^{2+} ion also contributes directly to the EFG at the nucleus. The quadrupole splitting may be written as

$$\tfrac{1}{2}\alpha^2 e^2 Qq[1 + (1/3)\eta^2]^{\frac{1}{2}}$$

where the EFG parameters $q = V_{zz}/e$ and $\eta = (V_{xx} - V_{yy})/V_{zz}$ consist of valence electron and lattice contributions diminished or enhanced by Sternheimer corrections for core distortion. Here e is the electronic charge, and α^2 is a covalency correction factor intended to compensate for the defects of a purely ionic model. In the perfectly ionic case, $\alpha^2 = 1$.

For the temperature range we are interested in, spin-orbit coupling effects can be neglected compared with the level splitting owing to a particular distorted arrangement of point charges around an Fe^{2+} ion. General formulas for the perturbing potential, $V = e \sum_j Z_j/r_{ij}$, a sum over any number of charges located at arbitrary positions in space, are readily available (*16*, especially Equations 2.7 and 2.8). The formulas result from the expansion of the inverse interparticle distance, $1/r_{ij}$, in tesseral or spherical harmonics and presume that the perturbing charges lie well outside the region of appreciable probability density of the perturbed charge. Corrections for this approximation were found to be negligible in our calculations. The required matrix elements may also be calculated without expanding $1/r_{ij}$. This can be done by expressing the $3d$-type wave functions used (*29*) as linear combinations of $3d$-type orbitals of the same radial part but located in a coordinate system where the Z axis points at the perturbing charge (*26*). It is then a relatively simple matter to evaluate the needed integrals in prolate spheroidal coordinates [(*25*) with the simplifications required for a point charge at one center and a charge distribution at the other center].

If we know the distorted charge arrangement around a particular iron site accurately from x-ray analysis, we should obtain a good estimate

of the electronic level splitting and both the indirect and direct contributions of the lattice to the quadrupole splitting. As a representative orthopyroxene, the x-ray analysis by Ghose (13) for $Mg_{0.93}Fe_{1.07}Si_2O_6$, the Fs_{53} case already referred to, was chosen. Morimoto's (22) x-ray coordinates for clinoenstatite were used as representative of this end of the series, while the coordinates of hortonolite ($(Mg_{0.47},Fe_{0.53})_2SiO_4$) determined from x-ray studies by Gibbs and co-workers (14) were taken as representative of the olivine series.

Preliminary calculations involving only the six nearest-neighbor oxygen ions yielded the observed temperature-dependent quadrupole splittings but were unable to distinguish the M_1 and M_2 pyroxene sites without using a covalency factor $\alpha^2 \approx 1$ for the site with the larger quadrupole splitting and $\alpha^2 \approx 0.75$ for the site with the smaller quadrupole splitting. This was true both for the orthopyroxene and the clinopyroxene calculations. (For the clinoenstatite case note that Morimoto reverses the more common designation of M_1 and M_2 sites used by Ghose.) In any case these preliminary calculations failed to yield a satisfactory independent check on the observation that the Mössbauer iron-favoring site of smaller quadrupole splitting is indeed the M_2 site of Ghose's x-ray analysis.

The necessity of assigning M_2 as the more covalent of the two sites ($\alpha^2 \approx 0.75$) is consistent with its slightly smaller quadrupole splitting (9, 10). The fact that M_2 is the more distorted octahedron and yet corresponds to the smaller quadrupole splitting is not particularly surprising since less than one-fifth of the EFG arises from the direct contribution of the lattice, the rest arising from the sixth d-electron in Fe^{2+}. A difference in the Lamb-Mössbauer fraction between the two sites is a possible complicating factor which is difficult to estimate.

The olivine calculation also was able to yield the observed doublet splitting by taking $\alpha^2 \approx 1$ for both sites. More elaborate calculations on pyroxenes and olivines are in progress.

Summary

The Mössbauer spectra have been measured for various tektites, as well as for both natural and synthetic iron-bearing silicate minerals. The tektite spectra show a pair of broad lines, unequal in both width and height, which may be interpreted as a quadrupole split doublet owing to Fe^{2+} in a glasslike environment. The mineral spectra show narrower lines, consistent with a crystal structure, and the ratios of the intensities of the appropriate Mössbauer lines have been used to determine the ferric-ferrous ratios. The values obtained this way are less precise than (but in generally good agreement with) those obtained by the methods of wet chemistry. The spectra of the ferrosilite-enstatite series of pyrox-

enes show four lines which are interpreted as two quadrupole split doublets arising from two different electric field gradients and indicating that there are two unequivalent sets of sites for the iron. The ratio of the intensities of these two doublets indicates a high degree of ordering, and the preferred site for iron has the smaller electric field gradient. Similar studies on the fayalite-forsterite series of olivines indicate that at room temperature all iron nuclei see the same electric field gradient and electron density.

Acknowledgment

Literature Cited

(1) Afanas'ev, A. M., Kagan, Yu, *Soviet Phys. JETP (English Transl.)* **18**, 1139 (1964).
(2) Bancroft, G. M., Burns, R. G., International Mineralogical Society meeting, Cambridge, England, 1966.
(3) Bancroft, G. M., Maddock, A. G., Burns, R. G., Strens, R. G. J., *Nature* **212**, 913 (1966).
(4) Belyustin, A. A., Ostanevich, Yu. M., Pisarevskiĭ, A. M., Tomilov, S. B., Bai-shi, U., Cher, L., *Soviet Phys. Solid State* **7**, 1163 (1965).
(5) Blume, M., *Phys. Rev. Letters* **14**, 96 (1965).
(6) Bradford, E., Marshall, W., *Proc. Phys. Soc. (London)* **87**, 731 (1966).
(7) de Coster, M., Pollak, H., Amelinckx, S., *Phys. Status Solidi* **3**, 283 (1963).
(8) Deer, W. A., Howie, R. A., Zussman, J., "Rock-Forming Minerals," Vols. 1 and 2, Wiley, New York, 1962.
(9) Epstein, L. M., *J. Chem. Phys.* **36**, 2731 (1962).
(10) *Ibid.*, **40**, 435 (1964).
(11) Evans, B. J., Ghose, S., Hafner, S., *J. Geol.* (to be published).
(12) Ghose, S., *Amer. Mineral.* **47**, 388 (1962).
(13) Ghose, S., *Z. Kristallogr.* **122**, 81 (1965).
(14) Gibbs, G. V., Moore, P. B., Smith, J. V., Ann. Meeting, Geol. Soc. Am., New York, N. Y., Nov. 17-20, p. 66A, 1963.
(15) Gol'danskiĭ, V. I., Makarov, E. F., Khrapov, V. V., *Phys. Letters* **3**, 344 (1963).
(16) Hutchings, M. T., *Solid State Phys.* **16**, 227 (1964).
(17) Ingalls, R., *Phys. Rev.* **133**, A787 (1964).

(18) Kurkjian, C. R., Buchanan, D. N. E., *Phys. Chem. Glasses* **5** (3), 63 (1964).
(19) Kurkjian, C. R., Sigety, E. A., VIIth International Congress on Glass, Brussels, 1965, Paper 39, 1966.
(20) Lindsley, D. H., Davis, B. T. C., MacGregor, I. D., *Science* **144**, 73 (1964).
(21) Mattern, P. L., Ph.D. thesis, Cornell University, Ithaca, N. Y., 1965.
(22) Morimoto, N., Z. *Kristallogr.* **114**, 120 (1960).
(23) O'Keefe, J. A., "Tektites," University of Chicago Press, Chicago, 1963
(24) Pollak, H., de Coster, M., Amelinckx, S., *Phys. Status Solidi* **2**, 653 (1962).
(25) Roothaan, C. C. J., *J. Chem. Phys.* **19**, 1445 (1951).
(26) Rose, M. E., "Elementary Theory of Angular Momentum," p. 60, Wiley, New York, 1957.
(27) Spijkerman, J., *et al.,* private communication.
(28) Sprenkel-Segel, E. L., Hanna, S. S., *Geochim. Cosmochim. Acta* **28**, 1913 (1964).
(29) Walker, L. R., Wertheim, G. K., Jaccarino, V., *Phys. Rev. Letters* **6**, 98 (1961).
(30) Watson, R. E., Solid State and Molecular Theory Group, M.I.T., *Tech. Rept.* **12** (1959).

6

Mössbauer Spectroscopy of Iron Compounds

N. E. ERICKSON

Brookhaven National Laboratory, Upton, N. Y.

Although several interpretations have been advanced to account for the chemical isomeric shift systematics of ^{57}Fe compounds, none of the theories reviewed is applicable to all iron compounds. This lack of generality is attributed to inherent deficiencies in the theories which largely use quantities which depend on energy differences. Since energy differences are usually poor criteria for determining electron distributions, the lack of agreement is considered not surprising. A "relative covalency" scale which is apparently valid for all octahedral ferrous or ferric compounds is presented and briefly discussed.

For chemists interested in modern theories of chemical bonding, the most useful data obtainable by the Mössbauer technique are the magnitude and sign of the electric quadrupole field gradient tensor and the magnitude of the shift, δ, (which we prefer to call the chemical isomeric, CI, shift), of the center of the Mössbauer spectrum relative to some standard absorber. Although a considerable amount of chemical and structural information is potentially available from quadrupole data on iron compounds, relatively little use has been made of such data in the literature, and we will not discuss this parameter here. We will instead restrict ourselves to two main points: review of the explanations put forth to explain CI shift data in iron compounds, and a survey of some of the correlations and generalizations which have been found.

Interpreting CI Shift Data

The CI shift of Mössbauer spectra provides a measure of the total electron density in the nucleus of an atom, $|\psi(o)|^2$, relative to some reference standard. For ^{57}Fe, δ is quite sensitive to valence, coordination number, or number and type of bonds to its ligands. Unlike chemical shifts in NMR spectra which are frequently dominated by the spin

imbalance, $|\psi(o)\uparrow|^2 - |\psi(o)\downarrow|^2$, at the nucleus, δ depends only on the total value of $|\psi(o)|^2$.

Interpretations of Shifts in High-Spin Compounds on the Basis of Partial Covalency. There have been a number of mechanisms offered to explain CI shift data in iron compounds (Table I). Walker, Wertheim, and Jaccarino (*44*) (WWJ) noted large differences between the shifts of some typical high-spin ferrous and ferric compounds. By combining the systematics of the shifts (Fe^{3+} was more negative than Fe^{2+}) with the theoretical $|\psi(o)|^2$ values of Watson (*45, 46*) for the free ion $3d^n$ configurations ($|\psi(o)|^2$ in Fe^{3+}, $3d^5$, was greater than in Fe^{2+}, $3d^6$, owing to the decrease in shielding of the $3s$ electrons primarily), WWJ concluded that the sign of $\Delta R/R$ was negative for ^{57}Fe. By assuming that in each valence state the compound with the most positive shift was completely

Table I.   Explanations of CI Shifts in ^{57}Fe

(1) Use of electronic configurations of the form:
$$3d^7 4s^x \; (3d^{n-x} 4s^x)$$
$$3d^{8-\eta-x} 4s^x$$
$$4s^{0,1,2} 3d^x$$
(2) Comparison with calculated wave functions
(3) $|\psi(o)|^2$ dependent on number of unpaired electrons in ion
(4) Electronegativity differences or nepheleuxetic effect
(5) Forward donation (s electrons)
(6) Back donation (d electrons)—spectrochemical series
(7) (π) antibonding effects

ionic, they were able to estimate $\Delta R/R$ quantitatively, and where the shifts of different compounds within a given oxidation state were less than the maximum, they attributed this to covalency effects. They represented covalency by electronic configurations of the form $3d^n 4s^x$ where x is (usually) nonintegral, and used the Fermi-Segré-Goudsmit (*19, 28*) method to calculate $|\psi(o)|^2$ for a $4s$ electron, with the assumption that the $4s$ contribution to $|\psi(o)|^2$ was proportional to x. This is not strictly true although calculations show (*45*) that $4s$ electrons affect the inner shells only slightly. This gave a satisfactory account of weakly covalent, high spin compounds, but the theory was unable to account for the shifts of the strongly covalent low spin compounds studied by WWJ—*e.g.*, the ferro- and ferricyanide ions. Hence, they speculated that since the metal atom in these compounds does not obey Hund's rules, Watson's calculations might not pertain to them. They incorrectly assigned a valance of three to iron in FeS_2, and moreover, since this compound also contains low spin iron, they should not have tried to fit this compound to their curve.

Gol'danskiĭ (*26*) criticized WWJ's choice of "calibration" points—*i.e.*, the assumption that the compound having the most positive shift was

completely ionic. He argued that critical x-ray absorption data show that even in the most ionic compounds the effective ionic charge, η, of the metal atom never equals its formal charge, and indeed the η's of tervalent transition metal ions determined by this technique are lower than the η's of the corresponding divalent ions. He proposed that shifts be interpreted in terms of covalancies represented by configurations of the form $3d^{8-\eta-x}4s^x$ where eight is the normal complement of $3d$ electrons for iron, and η is the effective charge as determined by the x-ray absorption technique, for the particular type of compound being studied ($\eta = +1.8$ and $+1.2$ respectively for high spin ferrous and ferric salts; $\eta = +1.0$ for ferro- and ferricyanide; and $\eta = +0.4$ for $Fe(CO)_5$ and ferrocene). In principle, Gol'danskiĭ's approach covers a wider range of compounds than does that of WWJ, but it requires knowledge of the effective charge (from x-ray absorption data) of the metal atom—information which is not presently known for a wide range of substances. Further, interpreting the calculated charge in terms of electronic structure is not completely unambiguous.

Brady, Duncan, and Mok (6) have proposed the use of a modified version of the WWJ plot to interpret shift data. They give curves showing the shifts to be expected for variable numbers of d electrons associated with zero, one, or two $4s$ electrons. They interpret the shifts of the ferrocyanide and ferricyanide ions in terms of $d^{10}s^2$ and d^9s^2 configurations, presumably within the framework of valence bond theory. On the other hand, they assign a d^8s^2 configuration to iron in K_2FeO_4 (Fe^{6+}). In view of the charge and tetrahedral structure of this ion, we cannot rationalize this viewpoint with even the valence bond approach to bonding.

Spijkerman, Ruegg, and May (41) have given a modified WWJ plot which uses the WWJ calibration points but uses Gray's $4s$ occupation numbers (2, 35) for some ferrous compounds to determine the slope of the line for this valence state. Apparently they did not take into account the $3d$ orbital population given by Gray's calculations and seem to have been unable to apply similar calculations to ferric compounds.
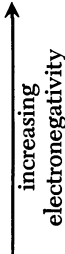
Still another modified WWJ plot has been offered by Danon (14). He, like Gol'danskiĭ, criticized the WWJ assumption that completely ionic bonding was obtained in any high spin ferric complex. He calibrated his curves by assigning to Fe in FeF_6^{-3} the configuration $3d^5 4s^{0.32}$, as computed by means of Ferreira's effective electronegativity equalization principle (20). He assumed, however, that essentially completely ionic bonding was attained in the high spin ferrous compounds with the most positive shifts. In Danon's curves, as in those of WWJ, shifts are attributed to configurations of the form $3d^n 4s^x$. For high spin Fe compounds the CI shift data can be interpreted in terms of integral or nonintegral occupation numbers of d and/or s electrons; hence, the choice of one or the other is a matter of taste.

We feel that the serious use of any presently available calculated wave functions or orbital occupation numbers to interpret CI shift data quantitatively is probably unjustified. These wave functions are usually obtained by variational calculations which fix the parameters so as to minimize the energy of the system being investigated; also, it is known that such wave functions are not very effective in calculating variables other than energy. Thus, there is no reason to believe that a calculation which has given a reasonably good energy agreement with optical absorption data, for example, can also be expected to give electron density distributions and orbital occupation numbers with equal accuracy. The accuracy of these latter quantities could be improved by more extensive calculations according to known methods—*e.g.*, by using larger basis sets. However, the metal orbitals and ligand free-ion orbitals obtained by variation to minimize the energy apparently cannot account for the considerable electron density in the bond overlap region, including the region occupied by the $3s$ electrons. In principle, of course, this distribution of density could be computed accurately if a sufficiently large basis set were used, but no one yet knows what "sufficiently large" is in this case. A promising practical approach to this problem appears to be to search for a radially dependent scaling factor, in place of the one that consists simply in the choice of an effective charge of the metal ion.

Interpreting Shifts in High Spin Compounds Based on Anion Electronegativity and Nepheleuxetic Ability. Ono, Ito, and Hirahara (*36*) suggested that the CI shift was determined by the electronegativity of the anion. In a study of some FeX compounds where X is a group VIb dianion, they found a correlation between the shift and the electronegativity of the anion—*i.e.*, the greater the electronegativity, the more positive the shift. Using later data which include the halides, we see (Table II) that there is a fairly good correlation provided we deal exclusively with high spin compounds.

Closely related to this is the suggestion that the value of δ is determined by the position of the anion in the nepheleuxetic series (*10, 12, 18*). Jørgensen (*33*) has summarized arguments which indicate that the electronegativity value of a ligand and its nepheleuxetic ability are related to similar effects. The (limited) interdependence of the nepheleuxetic effect and the value of δ can be ascribed to two mechanisms (recall that the nepheleuxetic effect is the fractional reduction, β, of the interelectronic repulsion parameters relative to those found in the free ion). The decrease in β is frequently taken to imply that the radial portions of the d wave functions have increased on forming a complex (more exactly, that $<1/r>$ has decreased). One possible mechanism by which this could happen is to introduce some $4s$ electron character in the metal wave function. This would provide a small amount of shielding for the

Table II.   Correlation of CI Shifts with Electronegativity

	δ^{a}	
FeF$_2$	1.32[b]	
FeO	1.22[c]	
FeCl$_2$	1.13[b]	increasing electronegativity ↑
FeS	0.88[c]	
FeSe	0.64[c]	
FeTe	0.66[c]	

[a] All shifts are at room temperature in mm./sec. Zero velocity is defined with respect to the center of a natural iron foil absorber. Sodium nitroprusside has a shift of −0.26 mm./sec. on this scale. In Ref. 18 a typographical error inadvertently gave this shift as −0.361 mm./sec.
[b] Data from N. E. Erickson (18).
[c] Data from K. Ono, A. Ito, and E. Hirahara (36).

3d electrons, causing them to expand slightly. Both of these effects would cause δ to become less positive (as is observed) although as noted earlier, the change in the 3d wave functions owing solely to this mechanism would be small. This is borne out by the observation that the decreases in β are frequently larger than can be reasonably accounted for simply by 4s covalency (33).

Another mechanism involves 3d expansion without the necessity of invoking 4s augmentation on the metal. On a simple electrostatic model, the negative array of ligands surrounding the metal atom increases the electrostatic energy of the 3d shell. If some of the metal electron cloud overlaps the negative ligand charge, the outer portions of the d wave functions feel a smaller attractive nuclear force and thus expand. This, in turn, makes δ less positive.

The two effects above constitute what is called central field covalency since they affect both the σ and the π orbitals on the metal to the same extent. There is also, of course, symmetry restricted covalency which acts differently on metal orbitals of different symmetries. This type of covalency shows up in optical absorption spectra as differences in the values of β_{33} and β_{55} as compared with β_{35}. The first two β's refer to transitions within a given symmetry subshell while β_{35} refers to transitions between the two subshells. This evidence of covalency almost of necessity forces one to admit the existence of chemical bonds since it is difficult to explain on a solely electrostatic model. The expansion of the metal orbitals can be caused either by backbonding to vacant ligand orbitals, or it may be a result of more or less extensive overlap of ligand electron density in the bond region. Whether or not this overlap density can properly be assigned metal 3d character is what we questioned above. At any

rate, provided this overlap extends inside part of the $3s$ orbital, it will tend to make δ more positive. This is counteracted by the partial loss of "true" metal d electrons which tends to drive δ negative. Provided we restrict our attention to high spin ferrous compounds, the loss of "true" metal d electrons seems to dominate the shift since the shift becomes progressively more negative as the nepheleuxetic ability of the ligand increases.

Shifts in Low Spin Compounds. The parallelism between the nepheleuxetic effect and δ in the case of high spin compounds does not hold for low spin compounds. Thus, iron cyanide compounds have more negative shifts than iron bromide compounds of the same geometry and metal valence even though the bromide ion produces a larger decrease in β than does the cyanide ion (*33*). This can perhaps be taken to imply that for the cyanide ion where there is thought to be back donation to vacant ligand orbitals, the lack of extensive ligand electron density in the metal π-orbital region permits the shift to decrease towards its "true" value for a given fractional loss of d electrons while for bromine the overlap density tends to hold δ more positive. What we suggest, in effect, is that the overlap density is more important in decreasing the value of β than it is in decreasing δ.

This leads us naturally to the observation that in low spin compounds the CI shift correlates with the position of the ligand in the spectrochemical series (*13, 18, 21*). The idea behind this observation is that the value of the crystal field splitting parameter, Δ, in low spin compounds increases because the ligand withdraws metal $d\pi$ electrons into its vacant orbitals. The greater the π acceptor ability of the ligand, the larger the value of Δ. Since the loss of metal d electrons decreases the shielding of the inner s shells, δ is expected to decrease, and this is observed. The correlation between Δ and δ in low spin compounds is striking. Figure 1 shows a schematic illustration of this correlation for some low spin Fe^{2+} complexes. The slope of the line has no significance except to illustrate that the shift becomes more negative as the π-acceptor ability (as judged from its position in the spectrochemical series) of the ligand increases. The data points with flags pointing down and to the right of the line are for fully substituted octahedral complexes. The data points with flags pointing up and to the left of the line are for mixed ligand complexes also of (at least pseudo) octahedral geometry. We have done this to show that there is, at least to some extent, a partial additivity of shifts depending on the number and kind of ligands attached to the metal atom (*18, 30*). This apparent additivity must be validated before one can meaningfully use measurements on the various $[Fe^{2+}(CN)_5X]$ complexes to assign or discuss the relative π-acceptor ability of the ligand X. For this correlation to be meaningful, the valence state

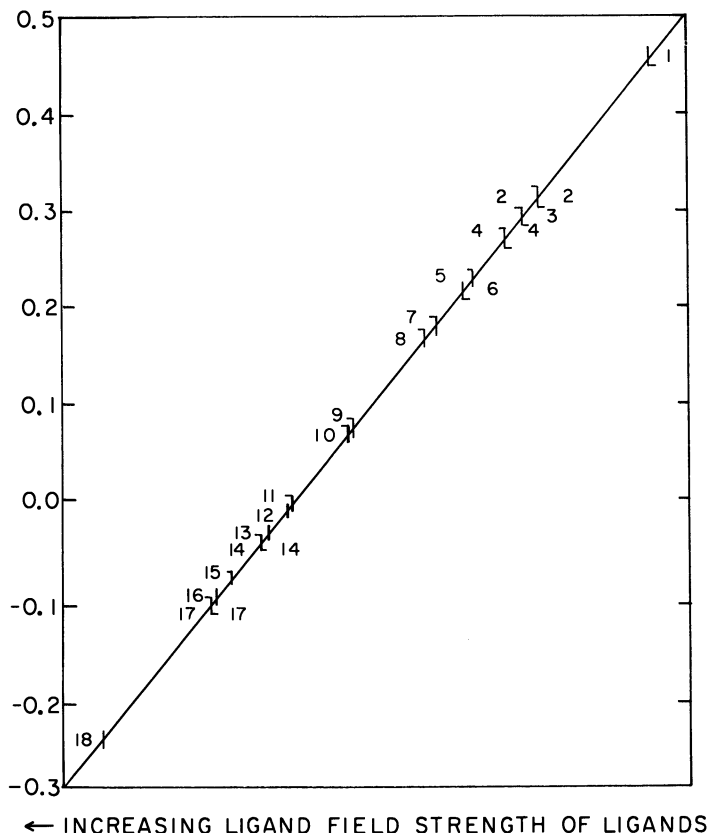← INCREASING LIGAND FIELD STRENGTH OF LIGANDS

Figure 1. Dependence of CI shift on spectrochemical series positioning of ligands bonded to low spin ferrous iron. In general, the total ligand field strength increases from right to left. Bars with flags pointing to the right represent fully substituted pseudo-octahedral complexes. Bars with flags pointing to the left represent mixed ligand complexes where both fully substituted end members have been studied. Bars without flags represent mixed ligand complexes where only one fully substituted end member has been studied. The numbers correspond to the following compounds or ions:

(1) ferrocene	(10) $[Fe(bipy)(CN)_4]^{2-}$
(2) $[Fe(phen)_3]^{2+}$	(11) $[Fe(CN)_5NH_3]^{3-}$
(3) $[Fe(CN)_5NO_2]^{4-}$	(12) $[Fe(CN)_5NO_2]^{4-}$
(4) $[Fe(bipy)_3]^{2+}$	(13) $[Fe(CN)_5SO_3]^{5-}$
(5) cis-$[Fe(phen)_2(CN)_2]$	(14) $[Fe(CN)_6]^{4-}$
(6) $[Fe(terpy)_2]^{2+}$	(15) $[Fe(CN)_2(CH_3NC)_4]$
(7) trans-$[Fe(phen)_2(CN)_2]$	(16) $[Fe(CN)_5CO]^{3-}$
(8) $[Fe(bipy)_2(CN)_2]$	(17) $[Fe(CH_3NC)_6]^{2+}$
(9) $[Fe(phen)(CN)_4]^{2-}$	(18) $[Fe(CN)_5NO]^{2-}$

and coordination number of the metal must be the same in all the compounds. Danon (*13*) derived the ordering $NO^+ > CO > CN^-$ by comparing the shifts of $[Fe(CN)_5NO]^{2-}$, $Fe(CO)_5$, and $[Fe(CN)_6]^{4-}$. The middle compound not only does not have the same metal valence as the other two, it does not even have the same geometry; hence, the fact that this ordering is correct must be considered to be fortuitous. In Figure 1 the data points without flags are for mixed ligand compounds where both end members are not obtainable. Since the concept of the partial additivity of shifts is not completely independent of geometry, the cis and trans isomers of $Fe(CH_3NC)_4(CN)_2$ and $Fe(phen)_2(CN)_2$ do not show identical shifts (*18*). (Berrett and Fitzsimmons (*3*) reported, however, that they found the same shift for both isomers of each pair. Our data (*18*) show definitely that the shifts within the members of a pair are not identical.) As more data become available on cis-trans isomers, we may be able to shed some light on the problem of explaining the trans or cis effect found in substitution reactions. The main difficulty with iron in a study of this kind seems to be preparing such compounds.

A similar correlation of δ and Δ can be found in low spin ferric compounds, but it is studied with better advantage in the ferrous series, where the range of shifts is greater. The most positive shift in ferrous compounds consistent with fully low spin bonding appears to be in the range $+0.4 \rightarrow +0.5$ mm./sec. with respect to an iron foil absorber defined to have zero shift, while the corresponding value for low spin ferric compounds seems to be in the range $+0.1 \rightarrow +0.15$ mm./sec. The shifts of compounds with iron in intermediate spin states ($S = 1$ for Fe^{2+}, $S = 3/2$ for Fe^{3+}) are usually more positive than the fully low spin complexes, while compounds that are completely high spin have shifts that are even more positive as a rule. This is shown schematically in Figure 2. In some cases not enough data are available to define the extreme shift positions of some of the lines.

Duncan and Golding (*16*) observed a trend similar to this although they included only fully high spin or fully low spin compounds. They argued that this could be explained by considering either configurational mixing and/or the exchange interaction of the unpaired d electrons with the inner s shells. Some unexplained mechanism is supposed to increase $|\psi(o)|^2$ when the number of unpaired electrons increases. This is an interesting conclusion but at variance with Watson's results (*45*) which show that $|\psi(o)|^2$ total appears to be the same in both spin-restricted and spin-unrestricted calculations. They also state that in a magnetically ordered substance, both δ and the internal magnetic field at a nucleus depend on the total electron density at the nucleus. This is incorrect since the internal magnetic field depends on the spin imbalance, $|\psi(o)\uparrow|^2 - |\psi(o)\downarrow|^2$, at the nucleus if we neglect (as Duncan and Golding did)
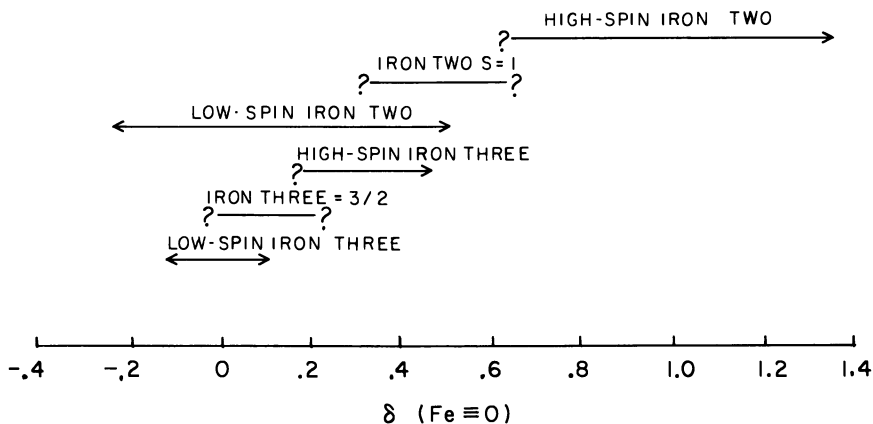
Figure 2.   Range of CI shifts in iron compounds characteristic of various va-
lencies and spin states. Question marks at the ends of the lines indicate the
extreme limits have not been well defined

spin-orbit, dipolar, and unquenched angular momentum terms. We attribute this correlation of δ and spin state to secondary features of the same cause—namely, that strong delocalization *via* π-bonding allows some of the electrons to become spin-paired and at the same time, the delocalization allows δ to decrease. Duncan and Golding's prediction (*16*) that low spin Fe^{2+} should be more negative than low spin Fe^{3+} is not borne out by experiment when we compare (as we should) compounds having the same ligands in both valence states.

Several authors (*8, 9, 30*) have analyzed their shift data for zero valent iron compounds, especially, as offering evidence for the importance of forward donation of $4s$ electron density. In one case, Collins and Pettit (*8*) found a correlation between the shifts of a series of closely related iron carbonyl compounds and their quadrupole splitting. They argued that increased $4s$ donation made the shifts negative although we might note that the quadrupole splittings also increased as the shifts became negative. This sort of correlation is not expected if we assume that the approach used by Townes and Dailey (*15, 43*) to interpret quadrupole coupling constants can be applied to iron. In this approach, an increase in *s* character in the bonds will cause the quadrupole splitting to decrease since *s*-type orbitals produce no field gradients. We have interpreted these results elsewhere (*18*) and attributed the shift and splitting behavior to an increase in π-bond donation to the carbonyls as the shifts became more negative.

Fractional 4s Character. The invocation of varying amounts of $4s$ character to interpret CI shift data has a certain simplicity that is lacking in the other explanations that have been presented, but it also has several

serious difficulties. First is the rather small range over which the fractional $4s$ character needs to be varied to account for a given shift. In the WWJ plot (*44*) a range of 0 to 60% $4s$ character will account for essentially all the shifts that have been measured in ferrous compounds, while in ferric compounds, the range is 0 to *ca.* 20%. Danon's (*14*) revision of this plot changes these values to the range 0 to *ca.* 140% for ferrous, and 30 to *ca.* 80% for ferric compounds, thus giving a somewhat greater flexibility in fitting the shifts to other parameters, such as the effective charge.

If one takes the fractional $4s$ contribution approach too seriously, one runs into difficulty in trying to account simultaneously both for shift values and other experimental data such as the nepheleuxetic parameters. It has been shown that $4s$ character does not need to be invoked to explain the observed β values, and in many cases $4s$ character is not able to account for the small values of β. By totally ignoring any possible changes in the d wave functions and their influence on the shift, this mechanism divorces itself from any correspondence with modern inorganic chemistry and such now common measures of covalency as the spectrochemical or nepheleuxetic series.

One of the most serious difficulties with this approach appears when one looks at the shifts of the higher valence iron compounds. The shift found for Fe^{4+} is somewhat less negative than predicted by the WWJ curves, but more dramatic is the large discrepancy between the (extrapolated) predicted and experimental shifts found for Fe^{6+}. The experimental value is considerably less negative than predicted (*47*). Danon's curves (*14*) do not predict quite as negative a value for given pure d^n configuration, and from that viewpoint they appear to be somewhat better. However, since Danon uses 32% $4s$ character for the most ionic ferric compounds, he would probably have to use as much, or more, $4s$ character for Fe^{6+}, and this would make his predicted value at least as far off as that of WWJ.

Hybridization. Wertheim and Herber (*47*), who first reported data for Fe^{6+}, realized that one could not interpret the shift in terms of $4s$ covalency and had to somehow get some electron density back on the metal in order to shield the $3s$ electrons. Accordingly, they proposed that since the ion has tetrahedral symmetry, the metal used sd^3 hybridized bonds and also that there was considerable d electron augmentation *via* double bond character from the oxygens back to the metal. Gallagher, MacChesney, and Buchanan (*23*) have proposed essentially the same mechanism of ligand to metal d electron donation to account for the shifts of some Fe^{4+} compounds they studied. These results then seem to confirm that strong antibonding exists in compounds where the metal has a high formal positive valency (*33*).

Still another example of what we interpret as evidence of donation of electrons from ligand to metal which results in metal s shielding are some recent data on a series of FeX_2 compounds where X is a group Vb or VIb element (25, 42). [We would like to thank Dr. Temperley for pointing out to us that A. Gerard has also studied some of these compounds.] All of these compounds have a marcasite structure containing iron coordinated octahedrally (distorted) to six X atoms and X atoms coordinated tetrahedrally to three metal and one X atom. They all contain discrete X_2 units as in FeS_2. The interesting feature of the CI shifts of these compounds is that the shift becomes more positive as the atomic number of the X group increases (Table III). This behavior is opposite that found by Ono *et al.* (36) for the FeX series with X a group VIb dianion. We suspect the interpretation of these results can be found in the following type of reasoning. If we assume for the time being that the X atoms undergo a valence bond type of sp^3 hybridization, then for the VIb X_2^{2-} ions the resultant filled orbitals are in the proper orientation to form σ bonds with the vacant metal $d\sigma$ orbitals (iron in these compounds is low spin). As the size of these ions increases, or as the atomic number increases, there will be more electron density in the region of the metal; also the energy of these orbitals will be higher, and the electrons will be more apt to be transferred towards the metal. This increased electron density apparently shields the $3s$ or $4s$ electron cloud sufficiently to cause δ to become more positive as the anion size (or atomic number) increases. A similar conclusion can be reached using molecular orbital theory since now the filled π-antibonding orbitals of the X_2 groups (assuming the bonding of the X atom is dominated by the X—X bond) takes the place of the sp^3 hybrid orbitals.

Table III. CI Shifts of Some Marcasite Structure Compounds

$Fe(VIb)_2$	$\delta^{a,\,b}$	$Fe(Vb)_2$	δ^{a}
FeS_2	0.27[c]	FeP_2	~0.09[d]
$FeSe_2$	0.39[c]	$FeAs_2$	0.31[c]
$FeTe_2$	0.47[c]	$FeSb_2$	0.45[c]

[a] All shifts are room temperature values in mm./sec. Zero is defined with respect to the center of a natural iron foil absorber.
[b] For comparison, the shifts of the Fe(VIb) compounds are FeO, 1.13; FeS, 0.88; FeSe, 0.64; FeTe, 0.66 *See* Table II.
[c] Data from A. A. Temperley and H. W. Lefevre (42).
[d] Data from A. Gerard (25).

We do not believe that an $Fe^{4+}X_2^{4-}$ valence formulation (32, 42) is supported by the shift data for the group Vb dianion compounds. The shifts are so similar for the Vb and VIb compounds that it is highly unlikely we are dealing with Fe^{4+}. It is also rather implausible that a

group, X_2, such as As_2^{4-} would remain reduced with as strongly an oxidizing agent as Fe^{4+}. We feel that the slightly more negative shifts found for the $Fe(Vb)_2$ compounds, as opposed to the corresponding $Fe(VIb)_2$ compounds with adjacent elements, reflects a somewhat smaller amount of donation towards the iron. The implication that the $(Vb)_2^{2-}$ ions should now be paramagnetic is not contradicted by the magnetic data on these compounds (*32*). They have low but not insignificant magnetic moments, and it is not unreasonable to assume the existence of some long range spin interaction between X_2^{2-} groups which would decrease the moment below that expected for two unpaired electrons, per X_2^{2-} group.

The same sort of reverse shift behavior is found in $KFeS_2$ and $KFeO_2$ (*21*). In these high-spin tetrahedral ferric complexes, sulfur produces a more positive shift than does oxygen—the reverse behavior of that obtained with high spin ferrous compounds. Since sulfur is certainly less stable as a divalent anion than oxygen, we suspect that the antibonding properties of sulfur have transferred enough electron density back to the metal to reverse the relative shift behavior found in ferrous compounds.

The possibility of strong antibonding on the part of the ligand makes the results of pressure studies of the CI shift of iron compounds interesting. For iron in various metal hosts the shifts become more negative with increasing pressure, indicating an increase in $|\psi(o)|^2$ as the volume decreases (*17, 39*) (presumably owing to a compression of the $4s$ wave functions). However, if ligand-to-metal antibonding effects are important, such pressure *vs.* shift behavior will hold in general only at sufficiently great pressures, where the inner s shells are certainly contracted, with a consequent increase in $|\psi(o)|^2$. At more modest pressures the opposite behavior may be expected. This should be remembered in any pressure study designed to investigate the sign of $\Delta R/R$ in a nuclear transition. Care must be taken to choose substances that are not expected to exhibit this type of antibonding behavior. One must also take account of possible phase changes or change in bond structure with pressure. One or more of these mechanisms presumably accounts for the conflicting data obtained in pressure studies of tin [*31, 37;* although in both references the shift with increasing pressure was positive, in one case the absorber (SnO_2) was under pressure while in the other, the source (Sn) was pressurized. This would normally cause the shifts to be in opposite directions.].

A possible example of the type of effect discussed above may be provided by the shift data for Fe^{4+} in $BaFeO_3$ ($\delta = -0.29$ with respect to copper source) and $SrFeO_3$ ($\delta = -0.17$ with respect to copper source). Gallagher *et al.* (*23, 24*) proposed that the larger size of the barium ion causes the lattice to expand, which in turn allows the Fe–O bond length to increase. They felt that this increased bond distance would decrease

the amount of contribution of ligand electron density to the metal d orbitals, and this was why the barium compound showed the more negative shift. The change in bond length is essentially equivalent to what would be accomplished by varying the pressure (neglecting a possible contribution to the shift owing to a change in the vibrational spectrum of the solid) and may perhaps be an indirect proof of the above mechanism. However, the structures of the two compounds are not identical, so the difference in shifts may be caused by this fact.

Table IV. Dependence of CI Shifts on Geometry

		Octahedral				Tetrahedral			
Isotope	Compound	δ^a	Ref.		Compound	δ^a	Ref.	$\Delta R/R$
$^{57}Fe^{2+}$	$FeCl_2$	+1.14	18		$[Et_4N]_2[FeCl_4]$	$+0.88^b$	1	—
$^{57}Fe^{3+}$	$FeCl_3$	$+0.40^b$	1		$[Me_4N][FeCl_4]$	$+0.20^b$	1	—
	$[Co(en)_3][FeCl_6]$	$+0.40^b$	1		$BaFeO_{2.5}$	-0.06^c	24	—
	$BaFeO_{2.5}$	$+0.10^c$	24					—
	Li_3FeF_6	+0.45	18					—
	NH_4FeF_4	+0.45	18					—
$^{129}I^{1-}$	KI	-0.45^d	40					+
$^{129}I^{7+}$	$Na_3H_2IO_6$	-3.35^d	40		KIO_4	-2.05^d	40	+
$^{127}I^{7+}$	$Na_3H_2IO_6$	1.19^d	40		KIO_4	0.68^d	40	—
$^{119}Sn^{4+}$	$(NH_4)_2SnCl_6$	-1.9^e	11		$SnCl_4$	-1.3^e	11	+
	Cs_2SnF_6	-2.6^e	11					+
	SnF_4	-2.5^e	11					+

^{a} All shifts are room temperature values in mm./sec. with zero velocity defined with respect to the center of a natural iron foil absorber unless otherwise noted. Sodium nitroprusside has a shift of -0.26 mm./sec. on this scale.
^{b} Extrapolated to room temperature.
^{c} Shift given relative to copper source.
^{d} Shift given relative to ZnTe source. Both source and absorber are at liquid hydrogen temperatures.
^{e} Shift given relative to grey tin absorber. Absorber at 80°K.

General Features of CI Shift Data

Limitations of space forbid further detailed examination or criticism of the relative merits of these proposed interpretations of CI shift data. We will restrict ourselves to some qualitative observations.

To illustrate the effect of geometry on the CI shift, Table IV shows some data for several pairs of high spin tetrahedral and octahedral iron complex ions. In each case the shift of tetrahedral ion is more negative than that of the octahedral ion, and the difference in shift is rather substantial. We feel that in these cases the differences in shifts can be ascribed to differences in $4s$ covalency; six electronegative ligands are more able to draw off s electron density than are four. Apparently it makes little difference whether the six ligands belong exclusively to a

single metal atom, $[FeCl_6]^{3-}$, or are part of an extended lattice, $FeCl_3$. Hence, the compound with the empirical formula NH_4FeF_4 does not contain a tetrahedral $[FeF_4]^-$ ion but must instead possess (distorted) octahedrally coordinated iron.

This same relationship between shift and coordination number is found with iodine compounds (*38, 40*). Tetrahedrally coordinated I^{7+} in KIO_4 has a higher value of $|\psi(o)|^2$ than does the octahedrally coordinated I^{7+} ion in IO_6^{5-}. If we extend this concept to ^{119}Sn, the Mössbauer data (*7, 11*) indicate that $\Delta R/R$ for ^{119}Sn is positive and not negative as Gol'danskiǐ has recently proposed (*4, 27*). This conclusion agrees with that of Bocquet *et al.* (*5*), who showed by means of electron conversion in the radioactive decay of ^{119m}Sn that $|\psi(o)|^2$ was larger in white tin than in SnO_2. The small difference in shift between SnF_4 and $[SnF_6]^{2-}$ reflects the fact that solid SnF_4 contains octahedrally coordinated tin.

It has long been known that whereas there are large differences in shift between high spin ferrous and ferric complexes with the same anion, the difference in shift between similar low spin ferrous and ferric compounds is much smaller. One possible explanation is that the "covalency" of a ligand (we do not attempt to define this hazy term) may depend on the oxidation state of the metal to which it is bonded—*e.g.*, a highly charged ion might tend to induce strong covalent character in any and all ligands bonded to it. Another possible interpretation is that one might assign a constant "covalency" to a ligand and attribute the smaller difference in shifts in low spin compounds to a reluctance of the ferric ion to allow much variation in electron density in its environs, in keeping with the fact that the variation in shifts found in ferric compounds is much less than that found for ferrous complexes. Still another possibility is that the mode of bonding is altered between high and low spin bonding, and in low spin ferric complexes there are some compensating effects that tend to keep the range of shifts quite small.

Figure 3 shows a relationship we have discovered (*18*) between $\Delta\delta$ and $\bar{\delta}$, where $\Delta\delta = \delta(2+) - \delta(3+)$ is the difference in shift of similar

pairs of octahedral ferrous-ferric complexes, and $\bar{\delta} = \dfrac{\delta(2+) + \delta(3+)}{2}$

is the average shift of that pair (taken in part from Ref. *18*). The plot includes data for 10 pairs of compounds and includes both high and low spin complexes. The fact that this relationship holds for both spin states suggests that despite the considerable differences in the magnetic properties, the changes in electron density distribution on going from one spin state to the other are changes in degree, not kind. This is not in agreement with simple valence bond theory which more or less demands a qualitative change in bonding.
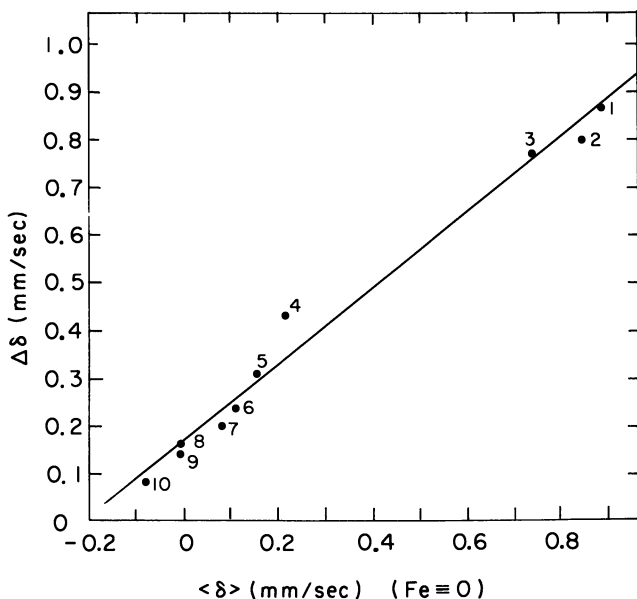
Figure 3. Plot of the difference in shift of similar pairs of ferrous and ferric compounds $(\delta_{Fe^{2+}} - \delta_{Fe^{3+}})$ vs. the average shift $(\delta_{Fe^{2+}} + \delta_{Fe^{3+}}/2)$ of that pair. The numbers refer to the pairs of compounds: (1) FeF_2–FeF_3; (2) $Fe(NH_4)_2(SO_4)_2 \cdot 6H_2O$–$Fe(NH_4)(SO_4)_2 \cdot 12H_2O$; (3) $FeCl_2$–$FeCl_3$; (4) $[Fe(phen)_3]Cl_2$–$[Fe(phen)_3](ClO_4)_3$; (5) $[Fe(bipy)_3]Cl_2$–$[Fe(bipy)_3](ClO_4)_3$; (6) $[Fe(phen)_2(CN)_2]$–$[Fe(phen)_2(CN)_2]ClO_4$; (7) $[Fe(bipy)_2(CN)_2]$–$[Fe(bipy)_2(CN)_2]ClO_4$; (8) $K_2[Fe(phen)(CN)_4]$–$K[Fe(phen)(CN)_4]$; (9) $K_2[Fe(bipy)(CN)_4]$–$K[Fe(bipy)(CN)_4]$; (10) $K_4[Fe(CN)_6]$–$K_3[Fe(CN)_6]$

Another form of the plot of these data which has certain advantages, in view of the fact that it is not always possible to prepare both valence states with a given ligand, is shown in Figure 4. Here the shifts, δ, of individual members of the 10 pairs are plotted against the average shift, $\bar{\delta}$, of the relevant pair. Here there are two well-separated straight lines, each characteristic of a single valence state. If we assume that this plot has some general validity—i.e., that it holds for all octahedral iron compounds regardless of whether or not they can be prepared in both valence states, we can use the data on single compounds as a measure of the "relative covalency" of a ligand. On the right hand side of Figure 4, we have defined an arbitrary "relative covalency" scale, ranging from 0 to 12 in units of 1 mm./sec. and covering the entire range of shifts found in Fe^{2+} or Fe^{3+} compounds. From this plot it is seen that a given ligand has a unique "relative covalency" value independent of the valence of the metal. This ordering can hardly be independent of the metal atom, but it would be interesting to see how closely Mössbauer data for other

metal systems agree with this ordering found in iron. Whether this uniqueness of "relative covalency" values is real or simply an artifact of the manner in which the graph is drawn, is not entirely clear. Some other kinds of experimental information are needed to clarify this point.

It is a common misconception that there exists a large gap in the shifts characteristic of high and low spin compounds (*6, 16, 41*). This conclusion was apparently reached by considering only a narrow range of high spin compounds where the nearest ligand neighbors were. essentially identical—*e.g.*, it apparently makes little difference in the shift whether a nearest ligand, oxygen for example, is an O^{2-} ion or part of a carboxyl group as in the acetate ion. In this respect CI shifts are similar to nepheleuxetic β parameters. Figure 4 shows Ono, Ito and Hirahara's (*36*) shift values for the Fe^{2+} (VIb) compounds; they nearly bridge this supposed shift gap. Undoubtedly other examples of compounds showing such intermediate shifts will be found although they will probably involve the use of somewhat exotic ligands.
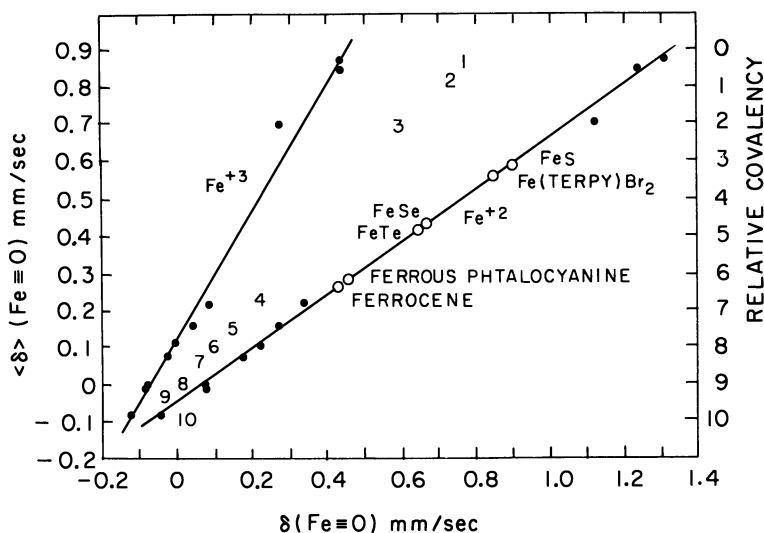
Figure 4.   Plot of the shift of various pairs of ferrous and ferric compounds vs. the average shift $(\delta_{Fe^{2+}} + \delta_{Fe^{3+}}/2)$ of that pair. The numbers refer to the pairs of compounds plotted in Figure 3. Also included are some points for some individual ferrous compounds

All the data in Figures 3 and 4 are room temperature shift values. The question as to the temperature at which shift values best represent true measures of relative values of $|\psi(o)|^2$ is somewhat difficult to decide since most substances do not have the same shift-temperature coefficient.

Fluck *et al.* (*21*) have argued that low temperature shift values are the ones that should be used to compare $|\psi(o)|^2$ values. A powerful counter-argument to this is that it is at low temperatures that differences in shifts owing to different absorber Debye temperatures are largest. At sufficiently high temperatures, on the other hand, the temperature-dependent velocity shift contribution becomes identical for all substances. However, direct, high temperature shift measurement comparisons may suffer from another effect—namely, $|\psi(o)|^2$ may itself depend on temperature because of changes in bond length or other factors. Maradudin *et al.* (*34*) have accordingly proposed that shift data taken at high temperatures be extrapolated linearly to absolute zero. This procedure would presumably correct for both temperature-dependent velocity and $|\psi(o)|^2$ effects. We question whether this extrapolation is necessary or desirable, however. Most other measurements of bond covalency are made at or near room temperature, and since these other measurements also seem to show temperature effects (*22*), it would seem that intercomparison can be made most meaningfully at the same temperature, provided, always, that it is the same bond covalency that is measured by the different methods. As far as Mössbauer shift measurements are concerned, this temperature should be greater than ~0.6 times the Debye temperature, θ_D, of the substance with the highest characteristic temperature since the slopes of the temperature-dependent velocity shifts approach the free atom value at $T/\theta_D \simeq 0.6$. In practice then, room temperature shift measurements, which are the most convenient to obtain, possibly provide the most meaningful data for comparison since most iron-containing substances have characteristic temperatures near or below room temperature (*see*, however, Ref. *29*).

Conclusion

As this abbreviated review has indicated there is no universally accepted interpretation of CI shifts in iron compounds, and most of the empirical correlations that have been found are limited to either one spin state, or to one or two valence states. In most cases it is clear that the failure to find extended agreement between data and theory is because the theory has been forced to a limit where its approximations are no longer valid. Probably the main reason for the limited success of empirical correlations—*e.g.*, the CI shift with the nepheleuxetic and spectrochemical series or with electronegativity differences—is that the CI shift depends on electron density distributions while the other quantities by-and-large depend on, or are measures of, electronic energy level differences. Since there is usually no simple relationship between the two quantities, the limited agreement is not surprising. It is clear that the

theoretician now has a more demanding measure of the correctness of his wave functions, and it is hoped that he will make use of it.

Despite the shortcomings noted above, CI shifts can and do provide useful information. When used in conjunction with other data such as magnetic susceptibility or quadrupole splitting, one can often make an unambiguous assignment of coordination number, spin state, or a ligand's "relative covalency." By studying the systematics of shift behavior in closely related compounds, one can interpret the bonding at least qualitatively in terms of effective *s*-electron loss or gain. As in the marcasite structure compounds discussed above, the shift data may alter some of our ideas concerning covalency or oxidation state.

We close with a plea to investigators to report shift data with respect to a standard absorber, either clean iron foil or sodium nitroprusside or both. The logic behind this request is obvious since anyone who has tried to intercompare results between different papers, knows how frustrating it can be when no common substances were studied. We also suggest that inherently narrow line sources be used—*i.e.*, Cu, Pt, Pd, or Cr. Stainless steel sources are usually so broad that they can often mask important features of the spectrum. Of the host matrices mentioned we prefer Cu since it doesn't give rise to any interfering x-rays and when prepared properly doesn't show any broadening at low temperatures.

Acknowledgment

Literature Cited

(1) Bancroft, G. M., Maddock, A. G., Ong, W. K., Prince, R. H., *J. Chem. Soc.* **1966**, 723A.
(2) Basch, H., Viste, A., Gray, H. B., *J. Chem. Phys.* **44**, 10 (1966).
(3) Berrett, R. R., Fitzsimmons, B. W., *Chem. Commun.* **1966**, 91.
(4) Bersuker, I. B., Gol'danskiĭ, V. I., Makarov, E. F., *Soviet Phys. JETP (English Transl.)* **22**, 485 (1966).
(5) Bocquet, J.-P., Chu, Y. Y., Kistner, O. C., Perlman, M. L., Emery, G. T., *Phys. Rev. Letters* **17**, 809 (1966).
(6) Brady, P. R., Duncan, J. F., Mok, K. F., *Proc. Roy. Soc.* **287A**, 343 (1965).
(7) Bryukhanov, V. A., DeHagin, N. N., Opalako, A. A., Shpinel, V. S., *Soviet Phys. JETP (English Transl.)* **11**, 310 (1963).
(8) Collins, R. L., Pettit, R., *J. Chem. Phys.* **39**, 3433 (1963).
(9) Collins, R. L., Pettit, R., *J. Am. Chem. Soc.* **85**, 2332 (1963).
(10) Collins, R. L., Pettit, R., Baker, W. A., *J. Inorg. Nucl. Chem.* **28**, 1001 (1966).
(11) Cordey-Hayes, M., *J. Inorg. Nucl. Chem.* **26**, 915 (1964).
(12) Danon, J., *Rev. Mod. Phys.* **36**, 459 (1964).

(13) Danon, J., *J. Chem. Phys.* **39,** 236 (1962).
(14) Danon, J., "IAEA Panel on Applications of the Mössbauer Effect in Chemistry and Solid State Physics," p. 89, International Atomic Energy Agency, Vienna, 1965.
(15) Dass, T. P., Hahn, E. L., "Nuclear Quadrupole Resonance Spectroscopy," Solid State Physics, Suppl. 1, Academic Press, New York, 1958.
(16) Duncan, J. F., Golding, R. M., *Quart Rev. (London)* **19,** 36 (1965).
(17) Edge, C. K., Ingalls, R., Debrunner, P., Drickamer, H. G., Frauenfelder, H., *Phys. Rev.* **138,** A729 (1965).
(18) Erickson, N. E., Ph.D. Thesis, University of Washington, 1964 (unpublished).
(19) Fermi, E., Segré, E., *Z. Physik* **82,** 729 (1933).
(20) Ferreira, R., *Trans. Faraday Soc.* **59,** 1064 (1963).
(21) Fluck, E., Kerler, W., Neuwirth, W., *Angew. Chem. Intern. Ed.* **2,** 277 (1963).
(22) Freeman, R., Murray, G. R., Richards, R. E., *Proc. Roy. Soc.* **A242,** 455 (1957).
(23) Gallagher, P. K., MacChesney, J. B., Buchanon, D. N. E., *J. Chem. Phys.* **41,** 2429 (1964).
(24) *Ibid.,* **43,** 516 (1965).
(25) Gerard, A., "Colloque International sur les derives Semi-Metalliques," Paris, 1965.
(26) Gol'danskiĭ, V. I., *Proc. Dubna Conf. Mössbauer Effect,* Consultants Bureau, New York, 1963.
(27) Gol'danskiĭ, V. I., Makarev, E. F., *Phys. Letters* **14,** 111' (1965).
(28) Goudsmit, S. A., *Phys. Rev.* **43,** 636 (1933).
(29) Hazony, Y., *J. Chem. Phys.* **45,** 2664 (1966).
(30) Herber, R. H., King, R. B., Wertheim, G. K., *Inorg. Chem.* **3,** 101 (1964).
(31) Herber, R. H., Spijkerman, J., *J. Chem. Phys.* **42,** 4312 (1965).
(32) Hulliger, F., Mooser, E., *J. Phys. Chem. Solids* **26,** 429 (1965).
(33) Jørgensen, C. K., *Progr. Inorg. Chem.* **4,** 73 (1962).
(34) Maradudin, A. A., Flinn, P. A., Ruby, S., *Phys. Rev.* **126,** 9 (1962).
(35) Manoharan, P. T., Gray, H. B., *J. Am. Chem. Soc.* **87,** 3340 (1965).
(36) Ono, K., Ito, A., Hirahara, E., *J. Phys. Soc. Japan* **17,** 1615 (1962).
(37) Panyushkin, V. N., Voronov, F. F., *Soviet Phys. JETP (English Transl.)* **2,** 97 (1965).
(38) Perlow, G. J., Perlow, M. R., *J. Chem. Phys.* **45,** 2193 (1966).
(39) Pipkorn, D. N., Edge, C. K., Debranner, P., DePasquali, G., Drickamer, A. K., Frauenfelder, H., *Phys. Rev.* **135,** A1604 (1964).
(40) Rama Reddy, K., DeSousa Barros, F., DeBenedetti, S., *Phys. Letters* **20,** 297 (1966).
(41) Spijkerman, J. J., Ruegg, F. C., May, L., "Mössbauer Effect Methodology," Vol. II (to be published).
(42) Temperley, A. A., Lefevre, H. W., *J. Phys. Chem. Solids* **27,** 85 (1966).
(43) Townes, C., Dailey, B., *J. Chem. Phys.* **17,** 782 (1949).
(44) Walker, L. R., Wertheim, G. K., Jaccarino, V., *Phys. Rev. Letters* **6,** 98 (1961).
(45) Watson, R. E., *Phys. Rev.* **119,** 1934 (1960).
(46) Watson, R. E., *MIT Tech. Rept. No.* **12,** (1959).
(47) Wertheim, G. K., Herber, R. H., *J. Chem. Phys.* **36,** 2497 (1962).

The Mössbauer Chemical Shift in Tin Chemistry

JON J. SPIJKERMAN

National Bureau of Standards, Washington, D.C.

The Mössbauer spectra of many organic and inorganic tin compounds have been published. From these data, the oxidation state of tin in most compounds can be determined. To interpret the Mössbauer spectra properly, the relationship between the chemical shift and the electron density at the tin nucleus must be established, which requires that the magnitude and sign of $\Delta R/R$ must be firmly established. This factor relates the change in the effective charge radius of the tin nucleus from the excited to the ground state. In most instances, this factor is known from the nuclear shell model calculation. However, for tin $\Delta R/R$ must be evaluated experimentally. Our various experiments were designed to obtain this factor in order to interpret correctly the chemical shift observed for tin compounds.

The applications of Mössbauer spectroscopy to chemistry were clearly demonstrated by the many experiments with ^{57}Fe. The large resonance effects at room temperature and the narrow linewidth made this isotope ideal for investigating the structure of iron compounds and lead to the rapid development of this new spectroscopy. The conditions for a second suitable isotope, ^{119}Sn, were not as favorable. At first the higher gamma ray energy of 23.8 k.e.v. required the measurements to be made at low temperatures, and the spectral resolution is not as good as for ^{57}Fe. Furthermore, the theoretical interpretation of the chemical shift caused considerable difficulty. However, the development of ^{119}Sn Mössbauer spectroscopy is unique and will serve as a guide for the many isotopes available.

The most suitable radioisotope for tin Mössbauer work is the 250-day half-life, ^{119}Sn^m, although ^{119}Sb could be used. The ^{119}Sn^m source emits a 25.8-k.e.v. K x-ray, which cannot be distinguished from the Mössbauer

gamma radiation with a NaI(Tl) crystal scintillation detector, but it can be easily filtered out by a 0.004-inch palladium foil. Initially, grey (alpha) tin was used for a source (1, 4, 21) with a resonance effect at room temperature of about 4%. Mg_2Sn has also been used extensively, but it has a low resonance effect at room temperature. A much higher effect at the cost of poor resolution was obtained with SnO_2, the line broadening caused by unresolved quadrupole splitting (10). As more data became available, new sources were developed. At present, the effect can be observed readily at room temperature with a Pd_3Sn source, with a linewidth of 0.072 cm./sec. (22), or with a $BaSnO_3$ source (8). The effect has not been observed using [119]Sb, mainly because of the difficulty in obtaining the isotope. It would provide additional measurements on the chemical effects produced by a nuclear transition on a time scale five times faster than the [57]Co–[57]Fe transition provides, owing to the difference in lifetimes of the Mössbauer levels.

s Electron Density and the Sign of ΔR/R

The unique contribution of Mössbauer spectroscopy to chemistry is the direct determination of changes in the s electron density at the Mössbauer nucleus for various compounds by measuring their chemical shift. Interpreting the chemical shift for [119]Sn compounds, in contrast to [57]Fe, has resulted in a great controversy.

The electron-nucleus interaction, or Fermi contact term, arises from:

(1) The mixing of the excited electronic states containing unpaired s electrons with the ground state.

(2) Spin polarization caused by spin exchange.

(3) Ligand-orbital mixing.

The relationship between the chemical shift, δ, and the s electron density (20) can be expressed as:

$$\delta = \frac{4\pi}{5E} Z e^2 R^2 c \frac{\Delta R}{R} S(z) \left[\sum_{n=1}^{5} |\psi_{na}(0)|^2 - \sum_{n=1}^{5} |\psi_{ns}(0)|^2 \right]$$

or

$$\delta = B \frac{\Delta R}{R} \left[|\psi_a|^2 - |\psi_s|^2 \right]$$

where B is a constant determined by the energy E_γ of the Mössbauer radiation, the atomic number Z, the average nuclear charge radius R, and the relativistic correction factor $S(z)$. $\Delta R/R$ is the change of the nuclear charge radius from the excited to the ground state. Since B and $\Delta R/R$ are constant for a particular isotope, the chemical shift δ is thus a function of the difference in the s electron density at the nucleus of the
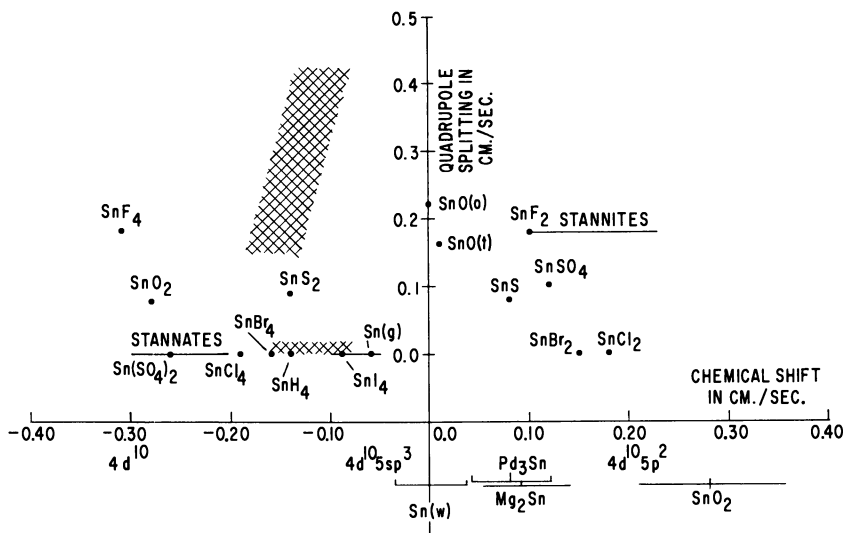
Figure 1.   Correlation diagram of the quadrupole splitting and chemical shift for tin compounds at 78°K. Data from Herber (9), Lees and Flinn (16), and Cordey-Hayes (5)

source and absorber, and hence it is determined by the chemical or metallurgical properties. $\Delta R/R$ can be obtained from a nuclear shell model calculations, and Uher and Sorenson (23) obtained a positive value for ^{119}Sn. However, these calculations are not too reliable for $\Delta R/R$, and an experimental approach must be used, either by a direct measurement or by comparison with other spectroscopic techniques.

The scatter plot in Figure 1 gives correlation of the quadrupole splitting and the chemical shift (at 78°K.) for several tin compounds (5, 9, 16) using white tin (beta) for a chemical shift reference. The various sources and their linewidths are also shown.

Sn^{2+}, Sn^{4+}, Sn^0 and the organotin compounds fall in characteristic regions, which can be used to determine formal valence states of new compounds. Kistner *et al.* (14) first determined the sign of $\Delta R/R$ from the chemical shift and *s* configuration of several tin compounds. This was further confirmed by the work of Shpinel *et al.* (21) and Boyle *et al.* (4) from the observed chemical shift and ligand electronegativity of the tin tetrahalides (Figure 1). Since the electronegativity for the tin tetra- halides decreases from fluorine to iodine (and hence the electron density at the Sn nucleus increases with increasing chemical shift), $\Delta R/R$ is posi- tive. Quadrupole splitting for these compounds has been observed only for SnF_4 owing to the distorted octahedral structure of this compound (12). Further information as to the sign of $\Delta R/R$ can be obtained from

the shift of x-ray emission lines and critical absorption edges with chemical composition. Nordling (17) measured the shift of the L absorption edges for Sn, SnO, and SnO$_2$, which indicated that the electron binding energies are larger in the oxide than in the metal. Similar results were obtained by Sumbauv and Mezentsev (19) for the K_α emission lines of these compounds. Their interpretation would indicate a positive value of $\Delta R/R$. However, from the x-ray energy diagram in Figure 2 it is clear that the result of this interpretation depends on the band structure of the solid. In this particular case, the measurements were made for a conductor (Sn), semiconductor (SnO), and nonconducting (SnO$_2$). This difficulty is clearly demonstrated by the absence of the shift between the L$_{III}$ edge of SnO and SnO$_2$, while the Mössbauer chemical shift for these compounds is large.
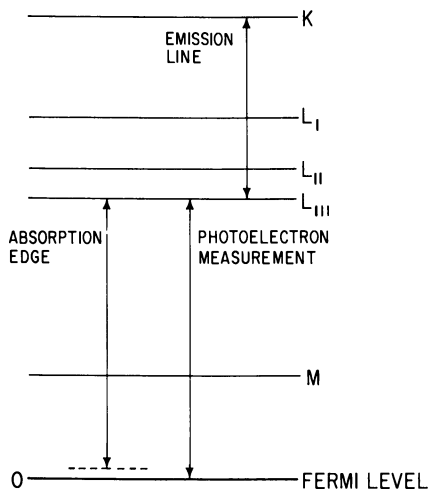
Figure 2.   Energy level diagram for x-ray transitions

Divalent Tin Compounds

The problem of the sign of $\Delta R/R$ for the divalent tin compounds was investigated by Lees and Flinn (16). In the relationship between the quadrupole splitting and chemical shift for the stannous compounds, two distinct correlations became apparent—compounds with a linear covalent bond, and compounds with a predominantly planar bond. Furthermore, there exists a linear relationship between the number of 5 p electrons and the chemical shift and hence the total s electron density. Using free tin ion wave functions in a self-consistent field calculation, they showed that the direct effect of adding 5s electrons is considerably

larger than the effect of screening by the p electrons on the s electron density at the tin nucleus, and $\Delta R/R$ is positive (Table I).

Table I.   Sign of $\Delta R/R$ of the ^{119}Sn Nucleus

Year	Method	Investigators	Sign of $\Delta R/R$	Reference
1961	Correlation of chemical shift and *s* configuration	Kistner, Jaccarino, Walker	+	*14*
1962	Tetrahalides of tin	Shpinel, Bryukahanov, Delyagin; Boyle, Dunburry, Edwards	+	*21*
1965	X-ray absorption edges	Nordling, Sumbuav, Mezentsev	+	*17* *19*
1965	Chemical shift in stannous compounds	Lees, Flinn	+	*16*
1965	Theoretical, change in tin atom radius with ionization	Gol'danskiĭ, Makarov	−	*7*
1965	High pressure experiment	Panyuskin, Voronov	−	*18*
1966	Correlation with N.Q.R.	Bersuker, Gol'danskiĭ, Makarov	−	*2*
1966	Sn-Pd system	Snediker	−	*22*
1966	Ba(Ti,Sn)O$_3$ solid solutions	Krizhanskiĭ, Rogozev, Popov	−	*15*
1966	Outer-shell internal conversion	Bocquet, Chu, Kistner, Perlman	+	*3*

By late 1965 the sign of $\Delta R/R$ was considered negative owing to the interpretation of Gol'danskiĭ and subsequent experiments. Gol'danskiĭ (*7*) investigated the effect of ionization on the tin atom radius and the effect of this change on the *s* electron density at the nucleus, resulting in the sign change of $\Delta R/R$. The negative sign of $\Delta R/R$ was also demonstrated (*18*) by the decrease in chemical shift with high pressure applied to a tin crystal and the increase in chemical shift as a function of lattice spacing for the Pd–Sn solid solution (*22*). A similar pressure experiment was made for SnO$_2$ (*10*), which showed an increase in the chemical shift for higher pressure, but the associated distortion of the oxygen bonds made this experiment inconclusive. Krizhanskiĭ, Rogozev, and Popov (*15*) found a similar result for the Ba(Ti,Sn)O$_3$ solid solutions.

The correlation of Mössbauer spectroscopy with N.Q.R. (2) for the tin tetrahalides, led to a re-evaluation of the original interpretation (21), using $d\pi$-$p\pi$ bonding, and it also gave a negative $\Delta R/R$.

All the above-mentioned methods give an indirect measurement of $\Delta R/R$. The controversy was settled by a direct measurement by the chemical effect on outer shell internal conversion in ^{119}Sn by Bocquet et al. (3).

The relative intensity of the 23.875-k.e.v. O line of the x-ray spectra emitted by the ^{119}Sn^m source depended on the chemical form of the source. The measurement of the internal conversion-intensity of the O lines and the chemical shift for white tin and SnO$_2$ directly confirmed that $\Delta R/R$ is positive for ^{119}Sn. This result agrees with the earlier chemical interpretations. The negative values obtained in Refs. 2, 15, 18, and 22 are caused by the lack of correction for sp^3 hybridization.
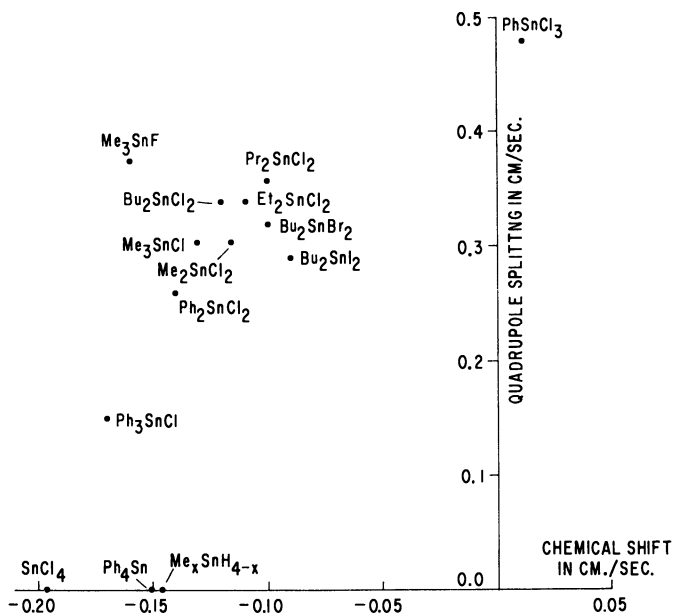
Figure 3.   Correlation diagram for organotin compounds

Bonding in Tin Compounds

With the sign of $\Delta R/R$ established, the structure and bonding of tin compounds can be investigated. From the scatter plot in Figure 1, the Sn^{4+} compounds fall to the left of white tin, while the Sn^{2+} compounds fall to the right. The organotin compounds are clustered in the cross-

hatched area, and specific compounds are represented in Figure 3. Quadrupole splitting of less than 0.1 cm./sec. is difficult to resolve, and the spectra are generally published as singlets. The organotin halides show large quadrupole splittings caused by the deviations from tetrahedral symmetry. However, the expected splitting in the methylstannates was not observed.

From the relationship of the chemical shift with the 5s electron density, Lees and Flinn (*16*) found a shift of 0.277 cm./sec. for the ideal ($5s^2$) stannous ion. The 5s electron density can also be calibrated from the correlation of the NMR coupling constant with the Mössbauer chemical shift. This is shown in Figure 4 for the methylstannanes, using the
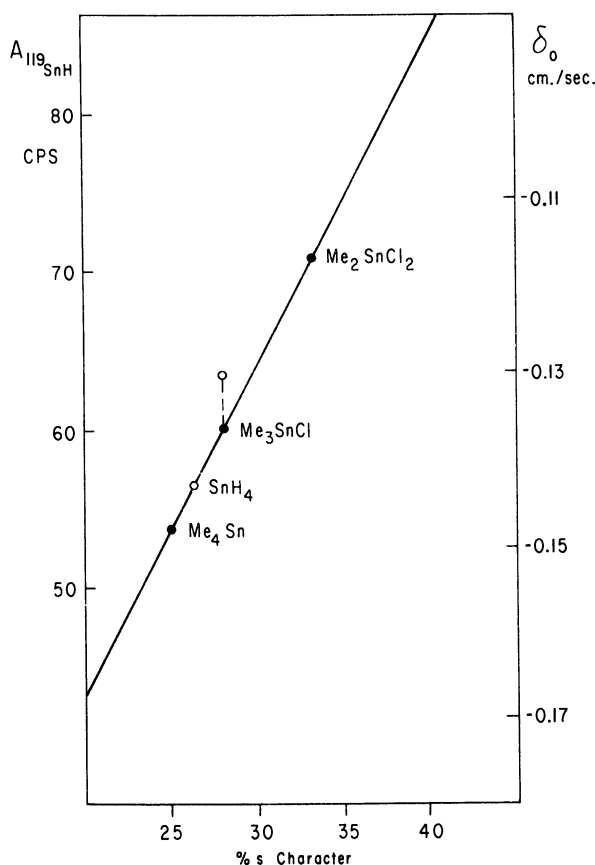
Figure 4.   Correlation of the NMR coupling coefficient $A_{119}{}_{SnH}$ *with % 5s character and the Mössbauer chemical shift for methylstannanes. Data from Holmes and Kaesz (11)*

data of Holmes and Kaesz (*11*). Likewise the NMR Knight shift gives a measure of the 5s electron density for the unpaired electrons. Kanekar *et al.* (*13*) measured the chemical shifts for a series of Sn-Pt alloys and derived 5s electron densities using the NMR data of Dharmatti *et al* (*6*). The agreement between these methods is far from satisfactory, and until more complete self-consistent field and molecular orbital calculations are available, the chemical shift for tin compounds will give only a qualitative measure of the *s* electron density at the tin nucleus.

Literature Cited

(1) Barloutand, R., Picou, J. L., Trara, C., *Compt. Rend.* **250,** 319, 2705 (1960).
(2) Bersuker, N. B., Gol'danskiĭ, V. I., Makarov, E. F., *Soviet Phys. JETP (English Transl.)* **49,** 699 (1965); **22,** 485 (1966).
(3) Bocquet, J. P., Chu, Y. Y., Kistner, O. C., Perlman, M. L., *Phys. Rev. Letters* **17,** 809 (1966).
(4) Boyle, A. J. F., Banbury, D. S., Edwards, C., *Proc. Phys. Soc.* **79,** 416 (1962).
(5) Cordey-Hayes, M., *J. Inorg. Nucl. Chem.* **26,** 915, 2306 (1964).
(6) Dharmatti, S. S., Udaya Shankar Rao, V., Vijayaraghavan, R., *Proc. Intern. Conf. Magnetism Nottingham, 1964,* 393.
(7) Gol'danskiĭ, V. I., Makarov, E. F., *Phys. Letters* **14,** 111 (1965).
(8) Herber, R., private communication.
(9) Herber, R. H., "Applications of the Mössbauer Effect in Chemistry and Solid-state Physics," p. 121, IAEA, Vienna, Austria, 1966.
(10) Herber, R. H., Spijkerman, J. J., *J. Chem. Phys.* **42,** 4312 (1965).
(11) Holmes, R., Kaesz, H. D., *J. Am. Chem. Soc.* **83,** 3903 (1961).
(12) Hoppe, R., Daehue, W., *Naturwiss.* **49,** 254 (1962).
(13) Kanekar, C. R., Mallikarjuna Rao, K. R. P., Udaya Shankar Rao, V., *Phys. Letters* **19,** 95 (1965).
(14) Kistner, O. C., Jaccarino, V., Walker, L. R., *Proc. Intern. Conf. Mössbauer Effect, 2nd,* Wiley, New York, 1961.
(15) Krizhanskiĭ, L. M., Rogozev, B. I., Popov, G. V., *ZhETF Pis'ma* **3,** 382 (1966).
(16) Lees, J., Flinn, P. A., *Phys. Letters* **19,** 186 (1965).
(17) Nordling, C., *Ark. F. fysik* **15,** 241 (1958).
(18) Panyuskin, V. N., Voronov, E. F., *JETP Letters* **2,** 97 (1965).
(19) Sumbuav, O. I., Mezentsev, A. F., *Soviet Phys. JETP (English Transl.)* **21,** 295 (1965).
(20) Shirley, D. A., *Rev. Mod. Phys.* **36,** 339 (1964).
(21) Shpinel, V. S., Bryukhanov, V. A., Delyagin, N. N., *Soviet Phys. JETP (English Transl.)* **14,** 1256 (1962).
(22) Snediker, D. K., "Mössbauer Effect Methodology," Vol. 2, p. 161, Plenum Press, New York, 1966.
(23) Uher, R. A., Sorensen, R. A., *Nucl. Phys.* **86,** 1 (1966).

Received April 3, 1967.

Mössbauer Spectroscopy of the Rare Earths

A. F. CLIFFORD

Virginia Polytechnic Institute, Blacksburg, Va.

Applications of Mössbauer spectroscopy to strictly chemical problems of the lanthanides have been few. Nevertheless, some interesting chemical relationships can be derived from physical work—e.g., that of Hüfner on ^{151}Eu. The relative degrees of ionicity of various europium compounds implied agrees with Pearson's designation of lanthanide ions as "hard acids." Likewise, data from the recent work of Nowik on dysprosium intermetallics suggests "valences" of the metals in the alloys—a topic of considerable interest to chemists. Almost no chemical information on the lanthanides has been derived from quadrupole splittings. However, we have recently investigated compounds of europium in which the bonding or crystal environment apparently causes quadrupole splitting. Asymmetric broadening attributable to quadrupole splitting has been observed in Eu_2O_3, and evidence for quadrupole splitting has been found in other compounds.

A s of September 1966, nuclear gamma ray resonance (the Mössbauer effect) has been observed in at least nine of the rare earth elements: ^{160}Dy, ^{161}Dy, ^{166}Er, ^{151}Eu, ^{153}Eu, ^{155}Gd, ^{156}Gd, ^{237}Np, ^{141}Pr, ^{159}Tb, ^{169}Tm, ^{170}Yb, and ^{171}Yb. In some of these cases the energy of the Mössbauer transition is so high (*e.g.*, ^{141}Pr, 145 k.e.v.) or the line width so broad (*e.g.*, ^{159}Tb, $t_{\frac{1}{2}} = 0.13$ nsec.) that it severely limits any usefulness for studying chemical problems. In the case of alpha-emitting elements, radiation damage to the crystal matrix may becloud the chemistry being investigated. In several more cases, as the nuclear properties of the isotopes become better known, more usable nuclides may become evident. In most of the cases cited above the aim of the study has been to investigate nuclear or physical effects. In particular, considerable attention has been paid to the magnetic hyperfine splitting. Although there are no Mössbauer studies on the rare earths of avowedly chemical nature in the

113

literature, there are nevertheless several from which information of interest to chemists can be drawn. The following discussion is not intended to be a complete account of the Mössbauer studies of the rare earths but rather a presentation of examples of some work which has been done and some of the chemical implications which can be drawn from it.

Degree of Ionic Nature in Solid Rare Earth Compounds

Brix, Hüfner, Kienle, and Quitmann (4) carried out an interesting study on a series of compounds of divalent and trivalent europium using the 21.6-k.e.v., 8.8 nsec. level of europium-151 activated by a $^{151}SmF_3$

Table I. Differences in Energy in Terms of Isomer Shift of the 21.7-k.e.v. Line of ^{151}Eu in Different Europium Compounds Compared with SmF₃ Source

Substance	E(cm./sec.)	T, °K.	Ref.
Eu_2S_3	+(0.14 ± 0.05)	room	4, 11
Eu_2Te_3	+(0.10 ± 0.05)	room	4, 11
EuIG	+(0.050 + 0.005)	room	4, 11
$Eu(C_2H_5SO_4)_3$	+(0.025 + 0.005)	room	4, 11
Eu_2O_3	< 0.005	room	4, 11
Eu metal	−(0.78 ± 0.02)	room	4, 11
Eu metal	−(0.81 ± 0.03)	4	2[a]
Eu metal	−(0.82 ± 0.03)	100	2[a]
EuO	−(1.09 ± 0.05)	5	18[a]
EuO	−(1.18 ± 0.06)	room	4, 11
EuS	−(1.12 ± 0.05)	5	18[a]
EuS	−(1.18 ± 0.05)	room	4, 11
EuSe	−(1.22 ± 0.05)	room	4, 11
EuTe	−(1.23 ± 0.05)	room	4, 11
$Eu(C_5H_5)_2$	−(1.32 ± 0.05)	room	4, 11
$EuCl_2$	−(1.34 ± 0.05)	room	4, 11
$EuCO_3$	−(1.37 ± 0.06)	room	4, 11
$Eu(OH)_2$	−(1.49 ± 0.05)	room	4, 11
$EuSO_4$	−(1.43 ± 0.08)	room	4, 11
$EuSO_4$	−(1.5 ± 0.1)	var.	14[a]

[a] Eu_2O_3 source.

source. The results of this study are given in Table I. Except as noted, both source and absorber were at room temperature. Fine structure was not observed except for the magnetic splitting in the europium iron garnet (EuIG) and in the metal.

These results may at first seem somewhat surprising, for since it can be deduced that a more negative isomer shift corresponds to decreasing s electron density at the nucleus, within each valence group this implies an increasing degree of ionic nature. Indeed, the more positive shift for

all Eu(II) compounds relative to Eu(III) is in complete accord with the shielding expected of the extra $4f$ electron for the $5s$ electrons, reducing the s electron density at the nucleus. Chemical intuition suggests that the more polarizable the anion associated with a given cation, the less ionic the compound should be. Yet, at least according to Shirley's data (*18*) for the europium(II) chalcogenides, the reverse is true. Even the data of Brix *et al.* (*4*) imply the same thing, although the numbers given are the same within the assigned limits of error. On the other hand, for the trivalent chalcogenides the trend is the reverse (or possibly shows a minimum in ionic nature at the sulfide).

However, examination of the crystal structures of the monochalcogenides of the divalent rare earths, which have rock salt structure (*12*), reveals a systematic trend which is consistent with the interpretation of the Mössbauer spectra. The data are shown in Table II. Here, for Eu(II), Sm(II), and Yb(II) the interatomic distances are uniformly less than the sum of the ionic radii in the sulfides and more than the sum of the ionic radii in the tellurides. Although this implies some uncertainty in the "absolute" values of the ionic radii (attributable mostly to the divalent rare earth ion), nevertheless, since the error owing to the radius of the rare earth ion is constant, the trend is quite evident and indicates a decreasing degree of covalency or polarization and an increasing degree of ionic nature in going from the sulfides to the tellurides.

Table II.   Interatomic Distances (A.) in Chalcogenides of the Divalent Rare Earths (*12*)

Compound			*EuO*	*EuS*	*EuSe*	*EuTe*
Interatomic Distance (d)				2.985	3.093	3.293
Sum of Ionic Radii (Σ)			2.54	2.992	3.097	3.26
d–Σ				−0.007	−0.004	+0.03
	SmS	*SmSe*	*SmTe*	*YbS*	*YbSe*	*YbTe*
d	2.985	3.100	3.297	2.839	2.966	3.181
Σ	2.998	3.103	3.27	2.88	2.98	3.14
d–Σ	−0.013	−0.003	+0.03	−0.04	−0.01	+0.04

This trend toward greater ionic nature with increasing polarizability of the anion agrees with the concepts recently promulgated by Pearson (*17*), outlining the difference between "soft" acids and "soft" bases on the one hand and "hard" acids and "hard" bases on the other. Because of their electronic structure and relatively small ability to provide covalent bonding orbitals and backbonding, the rare earth ions are typical hard acids. As such, their strongest bonding occurs with the ligands having the highest charge density. Consequently, as seen in both the Mössbauer and the crystal data the electronic involvement of the anion

with the cation becomes less on going from the oxides to the tellurides of the divalent elements, the effect tapering off in the selenide and telluride where almost complete ionicity is attained.

In the case of the trivalent chalcogenides the trend apparently becomes mixed because of the much greater polarizing power of the trivalent cation with its higher charge and poorer shielding, and the most covalent bonding occurs at the sulfide in the chalcogenide series. This is similar to the case of the copper(II) and other divalent transition metal ions in similar series of complexes.

From the divalent chalcogenides the trend continues as expected, through the cyclopentadienide, which has been shown to be ionic in the case of other rare earths, alkaline earths and even manganese(II), through the chloride, the hydroxide (which is a strong base comparable to calcium hydroxide), and finally to the highly ionic sulfate.

Table III.   Isomer Shifts (mm./sec.) for ^{161}Dy vs. Dy_2O_3

Absorber	T, °K.	E (mm./sec.)	Ref.
Dy metal	300	1.9 ± 0.2	16
DyNi$_2$	300	1.7 ± 0.2	16
DyCo$_2$	300	1.7 ± 0.2	16
DyMn$_2$	var.	1.65 ± 0.2	15
DyFe$_2$	var.	1.6 ± 0.2	16
DyNi	var.	1.45 ± 0.2	15
DyRh$_2$	var.	1.2 ± 0.2	15
DyRu$_2$	var.	1.0 ± 0.2	15
DyFe$_5$	var.	0.8 ± 0.2	15
DyNi$_5$	var.	0.65 ± 0.2	15
DyAl$_2$	300	0.6 ± 0.2	16
DyCo$_5$	var.	0.5 ± 0.2	15
DyPt$_2$	var.	0.45 ± 0.2	15
DyIr$_2$	var.	0.3 ± 0.2	15
Dy$_2$O$_3$	var.	0	16
DyCu$_2$	var.	−0.2 ± 0.2	15
DyGa$_2$	var.	−0.4 ± 0.2	15

"Valence" in the Metallic State

Europium has been characterized by several workers (3, 13) as divalent in the metallic state. This is again borne out by the isomer shift of the metal, which is clearly much closer to that of the covalent divalent compounds than that of the covalent trivalent compounds. (The comparison should be made with covalent compounds because in the metallic state the atoms are bonded together by sharing the valence electrons.)

Again, although the purpose of a recent study by Nowik et al. (15) was to study the free ion hyperfine fields in intermetallic compounds of

dysprosium, the isomer shifts for dysprosium–161 obtained show a high degree of order and contribute to the chemist's question, "what is the valence of the metal atoms in a metal or an alloy?" Without going into the various theories and methods, more or less sophisticated, of estimating such valences, suffice it to say that the "valence" of an atom in a binary alloy must be a function of such factors at least as the degree of overlap of orbitals, the number of available electrons on the variable element X (in AX_n), and the difference in size and the difference in electronegativity between A and X. The data shown in Table III summarize the work of Nowik *et al.*

The chemical implications of these data are as follows. Since dysprosium metal has been described, along with most of the other rare earths, as trivalent and since dysprosium in Dy_2O_3 is close to being truly trivalent as judged from the evidence cited above for Eu_2O_3, it would appear that here we are actually dealing with variations in the degree of trivalency of dysprosium in the alloys. Since comparisons for alloys of different crystal structure would be difficult, attention will be confined to the alloys DyX_2 which all have the same structure.

Although dysprosium metal itself has been considered to be in the trivalent state, by comparison with Dy_2O_3 the isomer shift of 1.9 mm./sec. indicates that it is in fact somewhat less than trivalent. The second metals in the alloys listed are all more electronegative than dysprosium itself and would be expected to remove electrons from dysprosium in proportion to their electronegativities provided other influencing factors are kept constant. Among the examples given this can be seen to be true in the case of $DyRh_2$ (*I.S.* = 1.2 mm./sec.) and $DyIr_2$ (*I.S.* = 0.3 mm./sec.) where the radii of Rh and Ir are very similar but where iridium is more electronegative than rhodium. The case of $DyNi_2$ (1.9 mm./sec.) and $DyCu_2$ (−0.2 mm./sec.) is more marked, where the nickel and copper atoms have about the same size, but copper is much more electronegative than nickel.

The size of the atoms of the second element may also be important. Other studies have shown that atoms of dissimilar size tend to prevent release of electrons into the conduction bands, thus localizing the electrons on the atoms. This should be expected to increase the *s* electron density in the atoms affected. This appears to be the case in the series $DyNi_2$ (1.9), $DyCo_2$ (1.7), $DyFe_2$ (1.6), $DyMn_2$ (1.65), where the "valence" of the dysprosium appears to increase with increasing size of the atoms of the second element. In this series the electronegativities remain roughly constant, while the atomic radii increase from Ni ($r = 1.25A.$) to Mn ($r = 1.37A.$). For $DyRh_2$ (1.2) and $DyRu_2$ (1.0) and again for $DyPt_2$ (0.45) and $DyIr_2$ (0.3) the same is true. In the case of $DyAl_2$ (0.55) and $DyGa_2$ (−0.4) with a larger difference in radius, a

larger effect is seen and in the same direction. At first sight it is surprising that aluminum and gallium should produce such a marked negative shift in dysprosium since their electronegativities are about the same as that of iron. It must be remembered, however, that because of the electronic structure, these elements have high electron affinities and like silicon are effective electron sinks.

Iron-57 Doping of Rare Earth Oxides

Since in appropriate cases of the rare earths it is possible to observe quadrupole splittings of considerable magnitude (1) as well as significant isomer shifts, there are many possibilities for applying the Mössbauer effect to rare earth chemistry. Our first attempt to do this (and our first venture into the Mössbauer field) was actually an attempt to examine the chemistry of a rare earth system by an iron-57 probe.

We had observed earlier (9, 10) an interesting hysteresis phenomenon in praseodymium oxide, such that when the partial pressure of oxygen over the nonstoichiometric oxide was changed, the composition of the oxide, PrO_x ($1.5 < x < 2.0$), changed in a manner typical of hysteresis phenomena. Examinations of the system revealed that this was not a kinetic phenomenon and furthermore that the system obeyed closely the corollaries proposed by Everett (5, 6, 7, 8) in his domain theory of hysteresis. This being so, the various praseodymium atoms in the nonstoichiometric oxide undergoing hysteresis must be characterized by subtle differences in electronic environment. Given sufficiently large and sharp isomer shifts and quadrupole splittings Mössbauer spectroscopy should be ideal for investigating this system. Unfortunately there is no praseodymium isotope which is useful for Mössbauer work since the first excited state of the only stable isotope, ^{141}Pr, lies at 145 k.e.v. and has a lifetime of 2 nsec. Consequently, we turned to iron-doping of praseodymium oxide in an attempt to use iron as a stand-in for praseodymium and used the Nuclear Science & Engineering Corp. (NSEC) Model B spectrometer. The doping was generally at the 3 atom % level and resulted in solid solution of the Fe_2O_3 in the PrO_x as judged by the absence of the typical Fe_2O_3 spectrum. Iron-doping was also done on La_2O_3, Eu_2O_3, and Er_2O_3 to obtain standards for Pr_2O_3. Doping of Pr_2O_3 was attempted but failed because of the ease of oxidizing Pr_2O_3. PrO_2 (prepared under high pressure oxygen) and CeO_2 were also iron-doped with the expectation that under the influence of either the great stability of CeO_2 or the high pressure of oxygen the iron would follow the rare earth into quadrivalency. The spectra showed conclusively, however, that the iron remained obdurately trivalent. This study consequently seems not to have been so much a study of the changing environment of rare earth atoms as a study of what happens to an iron impurity
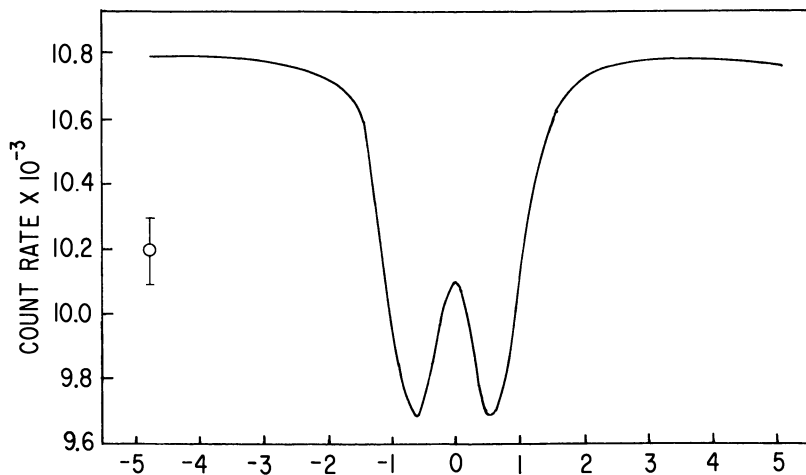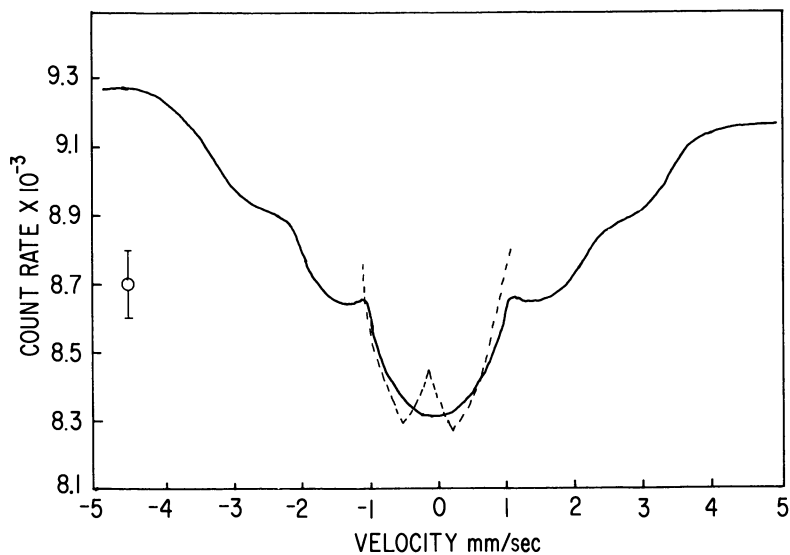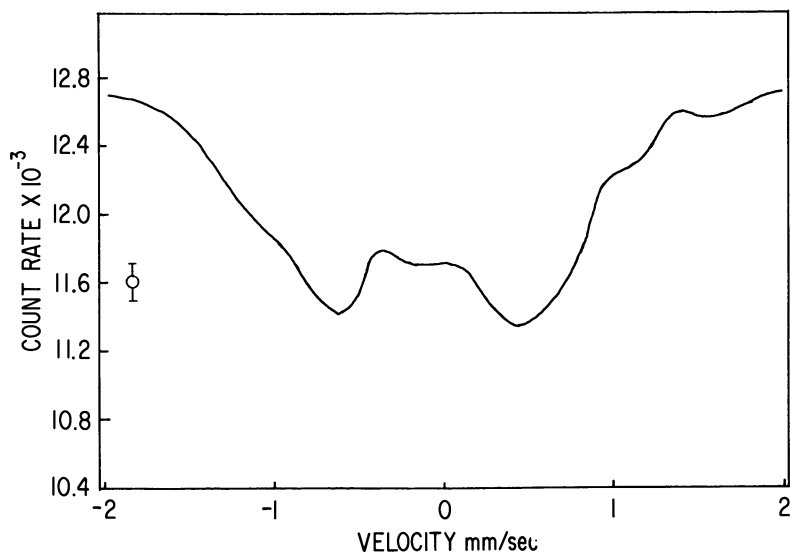
Figure 1.   Mössbauer spectrum of $^{57}Fe(III)$ (3 mole %) in Er_2O_3 taken with NSEC Model B spectrometer (> 200 points; average of three spectra)

in a rare earth oxide undergoing oxidation. It appears from the spectra (Figures 1–3) that as PrO_x is oxidized from $PrO_{1.5}$, the 3% iron impurity remains in the trivalent condition in metal lattice sites in the crystal even up to a composition of $PrO_{1.83}$. At compositions approaching PrO_2 (or CeO_2) some iron atoms appear to be forced into interstitial sites to
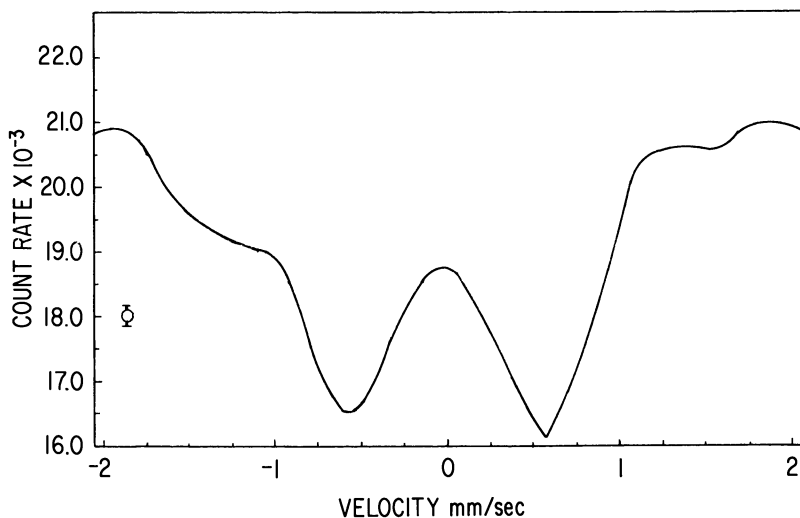
Figure 2.   Mössbauer spectrum of $^{57}Fe(III)$ (3 mole %) in $PrO_{1.83}$ taken with NSEC Model B spectrometer (> 100 points; average of three spectra)
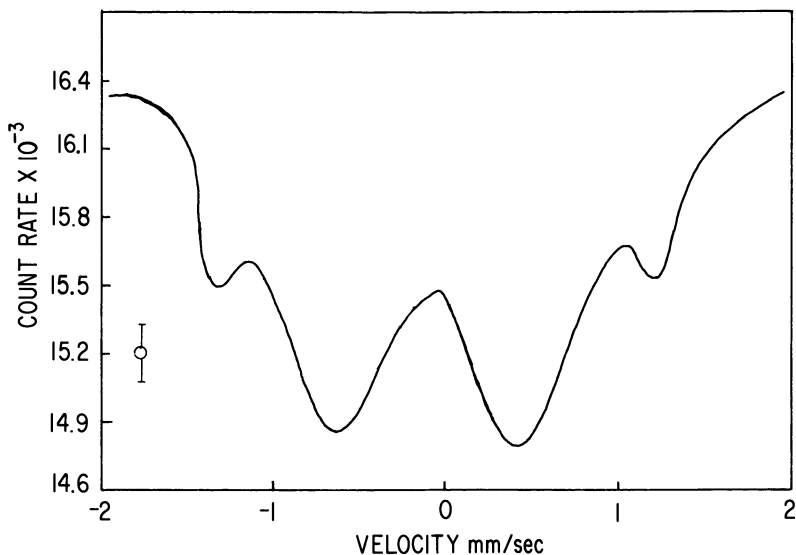
Figure 3.   Mössbauer spectrum of $^{57}Fe(III)$ (3 mole %) in PrO_2 taken with NSEC Model B spectrometer (> 200 points; average of three spectra)
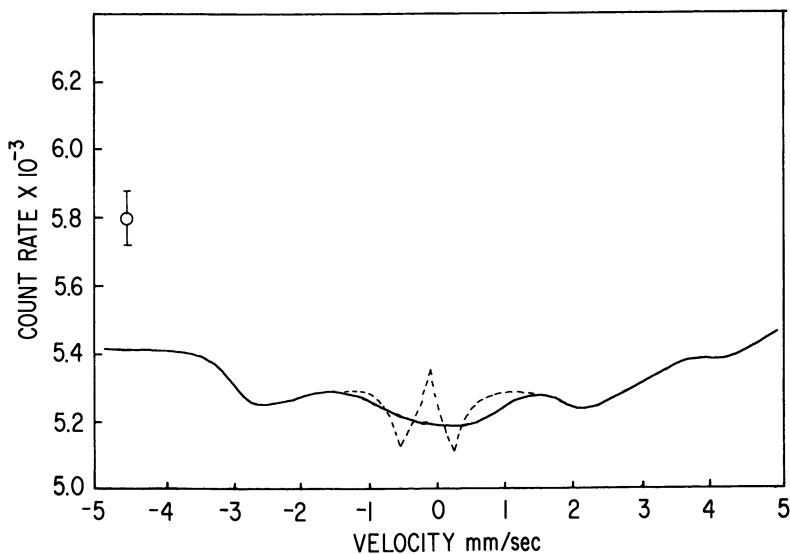
Figure 4.   Mössbauer spectrum of $^{57}Fe(III)$ (1 mole %) in CeO_2 taken with NSEC Model B spectrometer (> 200 points; average of three spectra).   The dashed line suggests that unresolved splitting may be responsible for the great breadth of the central peak

Figure 5.   Mössbauer spectrum of $^{57}Fe(III)$ (3 mole %) in CeO_2 taken with NSEC Model B spectrometer (> 200 points; average of three spectra). The dashed line suggests that unresolved quadrupole splitting may be responsible for the great breadth of the central peak

Figure 6.   Mössbauer spectrum of $^{57}Fe(III)$ (3 mole %) in La_2O_3 taken with NSEC Model B spectrometer (> 100 points; average of three spectra)
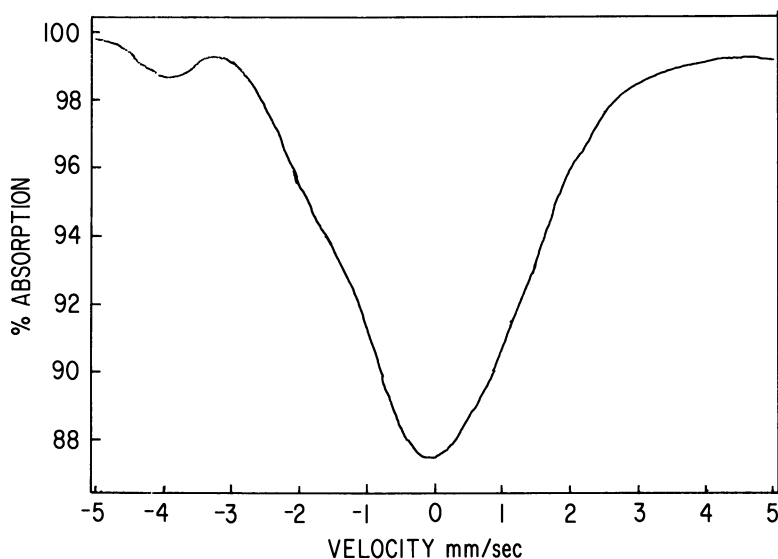
Figure 7. ^{151}Eu *Mössbauer spectrum of EuF$_3$ in liquid nitrogen taken with NSEC Model B spectrometer ($\sim$ 100 points; baseline $\sim$ 13,000 $\pm$ 114 counts per point)*

compensate for the iron atoms' remaining in lattice sites; furthermore, the interstitial sites in some cases apparently are of at least two different degrees of asymmetry. The six-line spectra (Figures 4–6) would seem not to be caused by magnetic splitting as judged by consideration of the diamagnetism of Ce(IV) and the magnetic diluteness of the iron(III) dissolved in it. The experimental data are collected in Table IV.

The idea of doping praseodymium oxide with another rare earth with an appropriate Mössbauer nuclide is an obvious one. For reasons of availability of the parent and ability to be handled by the NSEC Model B spectrometer the nuclide chosen was europium-151. Considerable effort has now been put into investigating the characteristics of this nuclide. Although the results are still preliminary in nature, suffice it to say that because of the almost invariable asymmetry of the spectra we believe (1) that attaining a truly monochromatic source is practically impossible at room temperature even using SmF$_3$, as we did, and (2) that we are observing incipient quadrupole splitting in Eu$_2$O$_3$ and possibly in EuF$_3$. Experimental curves for EuF$_3$ and Eu$_2$O$_3$ are shown in Figures 7 and 8. The Eu$_2$O$_3$ curve (SmF$_3$ source) shown in Figure 8 has a standard deviation $\pm 0.2\%$ of y values from Lorentzian distribution, but the negative deviation in every independent run is consistently greater in the range -2 to -4 mm. per second than the deviation on the positive side of the curve, implying some unresolved quadrupole splitting.
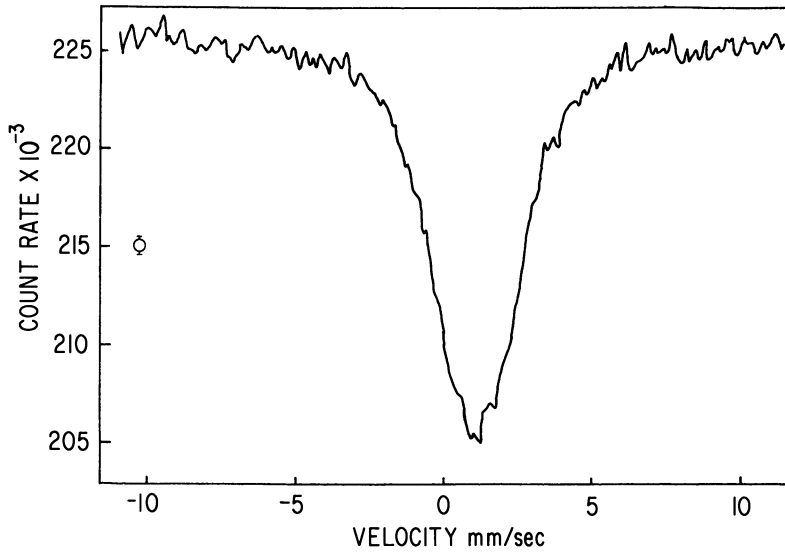
Figure 8.   ¹⁵¹Eu Mössbauer spectrum of Eu₂O₃ taken with electromechanical spectrometer. $\delta = +1.037 \pm 0.014$ *mm./sec.; FWHM = 3.40 ± 0.08 mm./sec.*
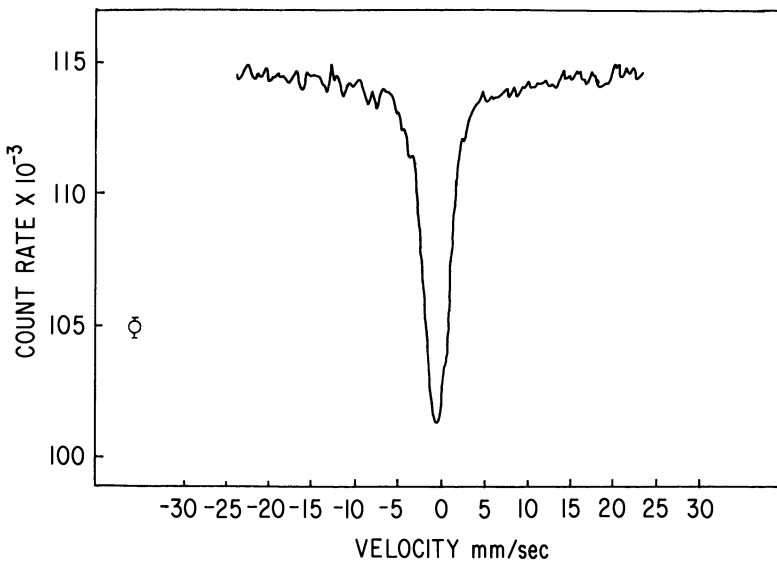
Figure 9.   ¹⁵¹Eu Mössbauer spectrum of commercial "EuF₂" taken with electro-mechanical spectrometer

A bit of a chemical application arose in our attempts to find a monochromatic source or absorber. Since EuF_2 has fluorite structure, there should be no quadrupole splitting. When a spectrum was taken of a commercial sample of "EuF_2" it was found that the europium present was essentially completely trivalent. The experimental spectrum is shown in Figure 9.

The search for monochromatic sources and absorbers will be continued. Likely compounds are MS, MSe, MTe, MN, MP, MAs, MSb, MBi,

Table IV. ^{57}Fe Mössbauer Spectrum Data for Doped Rare Earth Compounds

Sample	Lattice Type	Isomer Shift (mm./sec.)	Quadrupole Splitting (mm./sec.)
La_2O_3	Hex.(A)	-0.090 ± 0.005	1.059 ± 0.08
Er_2O_3	b.c.c.(C)	-0.044 ± 0.03	1.187 ± 0.06
Eu_2O_3	Monoclinic(B)	-0.045 ± 0.05	$0.610 \pm .10$
	b.c.c.(C)	-0.035 ± 0.06	1.370 ± 0.20
$Pr(OH)_3$	Hex.	$+0.005 \pm .02$	$0.770 \pm .05$
CeO_2 (1%)	f.c.c.(F)	unresolved	spectrum
CeO_2 (3%)	f.c.c.(F)	$-0.125 \pm .10$	$0.750 \pm .15$
		$+0.013 \pm .05$	$2.775 \pm .25$
		$+0.025 \pm .05$	$5.050 \pm .30$
PrO_2	f.c.c.(F)	$-0.080 \pm .04$	$1.105 \pm .08$
		$-0.030 \pm .10$	2.590 ± 0.20
$PrO_{1.83}$	f.c.c.	$-0.083 \pm .04$	$1.125 \pm .08$
$BaFeO_3$		$-0.340 \pm .04$	
$Na_2Fe(CN)_5(NO) \cdot 2H_2O$		$-0.600 \pm .02$	1.700 ± 0.03

and the like, where M is the pertinent rare earth element. It is unfortunate in this regard that there are no common rare earth salts with polyatomic anions which have high structural symmetry.

Speculations on Future Work

In conclusion I should like to consider a few of the chemical investigations which might be accomplished in the rare earth field by Mössbauer spectroscopy. The study of nonstoichiometric oxides has been discussed earlier, but there is the problem of finding an appropriate doping nuclide for the praseodymium oxide system. The element most capable of following the changes in oxidation state of the praseodymium is terbium-159, which does have a Mössbauer state, however, with a rather broad resonance (58.0 k.e.v., $t_{\frac{1}{2}} = 0.13$ nsec.). Nevertheless, with a sufficiently monochromatic source, sufficient resolution may be possible which would give information on the changing density and symmetry of the electronic environment of the terbium atoms as $PrO_{1.5}$ is oxidized continuously to PrO_2, or better as $TbO_{1.5}$ itself is oxidized to TbO_2.

A similar system easier to implement (and which is high on our list of prospects) is the nonstoichiometric hydride system, for which almost any appropriate rare earth could be used. Here the high crystal symmetry of the dihydride, MH_2, would gradually be lowered as the stoichiometry changes from MH_2 toward MH_3. It will be most interesting to see in what manner the "valence" of the metal atom (as indicated by the isomer shift) changes as this happens. Appropriate nuclides for such a study would be ^{161}Dy (25.6 k.e.v., 28 nsec.), which has a sharp resonance but for which the quadrupole splitting pattern is complicated ($I = 5/2^- - 5/2^+$), ^{169}Tm (8.41 k.e.v., 3.9 nsec.) whose resonance is broader but which has a simple quadrupole splitting ($I = 3/2^+ - 1/2^+$), and ^{237}Np, which has a sharp resonance (33.2 k.e.v., 68 nsec.) but which has a complicated quadrupole splitting ($I = 7/2^+ - 5/2^+$) and also suffers from the effects of α-radiation damage. Neptunium could also be used in the nonstoichiometric oxide studies.

Examination of the electronic states of catalysts and of rare earth dopants in phosphors are other applications which come to mind. When more is known about some of the yet unexplored properties of other possible Mössbauer nuclides, Mössbauer spectroscopy bids fair to being a powerful tool in rare earth chemistry.

Literature Cited

(1) Barnes, R. C., Mössbauer, R. L., Kankeleit, E., Poindexter, J. M., *Phys. Rev.* **136**, A175 (1964).
(2) Barrett, P. H., Shirley, D. A., *Phys. Rev.* **131**, 123 (1963).
(3) Bommer, H., *Z. Anorg. Allgem. Chem.* **242**, 277 (1939).
(4) Brix, P., Hüfner, S., Kienle, P., Quitmann, D., *Phys. Letters* **13**, 140 (1964).
(5) Everett, D. H., Whitton, W. I., *Trans. Faraday Soc.* **48**, 749 (1952).
(6) Everett, D. H., Smith, F. W., *Trans. Faraday Soc.* **50**, 187 (1954).
(7) Everett, D. H., *Trans. Faraday Soc.* **50**, 1077 (1955).
(8) Everett, D. H., *Trans. Faraday Soc.* **51**, 1551 (1955).
(9) Faeth, P. A., Clifford, A. F., *J. Phys. Chem.* **67**, 1453 (1963).
(10) Honig, J. M., Clifford, A. F., Faeth, P. A., *Inorg. Chem.* **2**, 791 (1963).
(11) Hüfner, S., Kienle, P., Quitmann, D., Brix, P., *Z. Phys.* **187**, 67 (1965).
(12) Iandelli, A., "Rare Earth Research," E. V. Kleber, ed., Macmillan, New York, 1961.
(13) Klemm, W., Bommer, H., *Z. Anorg. Allgem. Chem.* **231**, 138 (1937).
(14) Nowik, I., Ofer, S., *Rev. Mod. Phys.* **36**, 392 (1964).
(15) Nowik, I., Ofer, S., Wernick, J. H., *Phys. Letters* **20**, 232 (1966).
(16) Ofer, S., Segal, E., *Phys. Rev.* **141**, 448 (1966).
(17) Pearson, R. G., *J. Am. Chem. Soc.* **85**, 3533 (1963).
(18) Shirley, D. A., Frankel, R. B., Wickman, H. H., *Rev. Mod. Phys.* **36**, 392 (1964).

9

Mössbauer Spectroscopy of Iodine

D. W. HAFEMEISTER

Carnegie Institute of Technology, Pittsburgh, Pa.

Results obtained from the alkali iodides on the isomer shift, the NMR chemical shift and its pressure dependence, and dynamic quadrupole coupling are compared. These results are discussed in terms of shielding by the 5p electrons and of Löwdin's technique of symmetrical orthogonalization which takes into account the distortion of the free ion functions by overlap. The recoilless fractions for all the alkali iodides are approximately constant at 80°K. Recent results include hybridization effects inferred from the isomer shifts of the iodates and the periodates, magnetic and electric quadrupole hyperfine splittings, and results obtained from molecular iodine and other iodine compounds. The properties of the 57.6-k.e.v. transition of ^{127}I and the 27.7-k.e.v. transition of ^{129}I are compared.

In a few short years the isotopes of iodine, ^{127}I and ^{129}I, have been used to study a variety of scientific problems. This paper reviews some of the findings of several investigators.

Since the iodine ion, I⁻, is a halide ion, it allows one to investigate the electronic structure and lattice dynamics of the alkali halides. Thus far, ^{127}I and ^{129}I are the only halogen atoms and ^{133}Cs and ^{40}K are the only alkali atoms that have been successfully utilized in Mössbauer experiments. Historically the alkali halides have been of theoretical interest because of the extreme simplicity of their crystal structure, their closed-shell electronic configurations, and the availability of a wide range of the cation-anion mass ratio. In addition, the ease of obtaining single crystals has allowed experimenters to study many of their properties by such diverse experimental methods as nuclear magnetic resonance (NMR), dynamic quadrupole coupling, specific heats, and inelastic neutron scattering. Measurements and calculations in the alkali halides of the isomer shifts and the recoilless fractions, *f*, allow further tests of the theoretical models which have developed in this mature field.

126

Iodine can form many different formal valence states. By combining the isomer shift data for the iodate ion, IO_3^-, the periodate ion, IO_4^-, and the paraperiodate ion, IO_6^{5-}, with the corresponding values of the quadrupole coupling constant, eqQ, it is possible to discuss the nature of the iodine-oxygen bond. In addition, diverse compounds such as molecular iodine, $KICl_2$, $KICl_4$, ICl, IBr, and HI have been investigated. The signs of the electric field gradient have been deduced for these compounds from the asymmetry of the electric quadrupole hyperfine structure.

Because the interactions measured in Mössbauer experiments are products of atomic and nuclear factors, experiments on iodine isotopes have yielded values of the change of nuclear radius between the ground state and the excited state, $\Delta R/R$, quadrupole moment values Q, and magnetic moment values, μ, as well as electric field gradients and internal magnetic fields.

The decay of ^{125}I can be used to study the Mössbauer effect of ^{125}Te, and the decay of ^{129}I can be used to study the Mössbauer effect of ^{129}Xe in an iodine site.

Experimental Considerations

The 27.7-k.e.v. level in ^{129}I and the 57.6-k.e.v. level in ^{127}I are populated by the beta decay of ^{129}Te and ^{127}Te, respectively. Figure 1 shows the relevant portions of the decay schemes for the two isotopes. The Mössbauer gamma-rays are indicated by the three-dimensional arrows. For completeness we have included the 39.6-k.e.v. ^{129}Xe Mössbauer gamma-ray which has been studied by Perlow and Perlow (28, 30). Because the half-life (33) of the 27.7-k.e.v. state (16.8 $\pm$ 0.2 nsec.) is considerably longer than the half-life (12) of the 57.6-k.e.v. state (1.86 $\pm$ 0.11 nsec.), the minimum observable line width of ^{129}I ($2\Gamma_m = 0.59$ mm./sec.) is much sharper than the minimum observable line width of ^{127}I ($2\Gamma_m = 2.54$ mm./sec.). Because the energy (3, 33) of the ^{129}I transition (27.78 $\pm$ 0.05, 27.72 $\pm$ 0.06 k.e.v.) is about one-half the energy (12) of the ^{127}I transition (57.6 $\pm$ 0.02 k.e.v.), the depth of the ^{129}I dip is almost an order of magnitude greater than the ^{127}I dip. Thus the signal-noise ratio and the resolution of the spectra obtained from ^{129}I are considerably better than those obtained from the spectra of ^{127}I. However, because ^{127}I is the 100% naturally abundant stable isotope of iodine and ^{129}I is a long-lived radioactive fission product ($T_{1/2} = 1.6 \times 10^9 y$), the sample preparation for the absorbers of ^{127}I will be much less complicated since many of the absorbers can be obtained commercially with ease. In synthesizing an iodine compound, ^{129}I is more difficult because of radioactivity hazards and the high efficiency chemical process that must be used. The cost of the ^{129}I for an alkali iodide ^{129}I absorber is about $50.
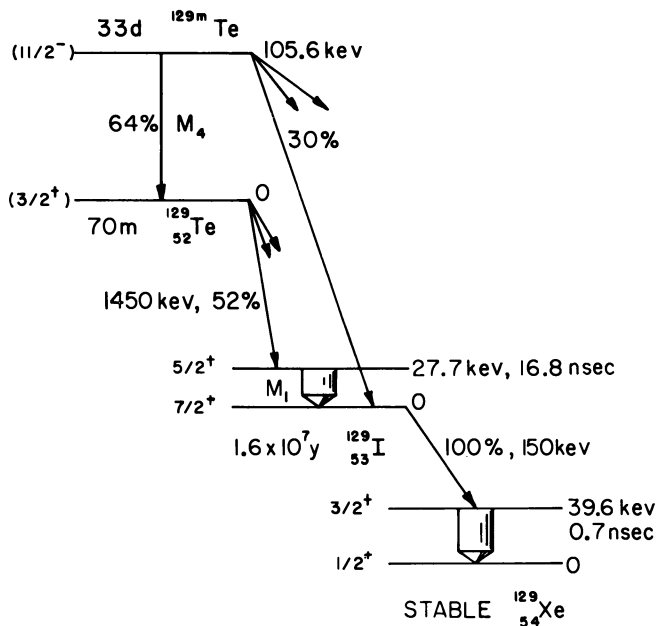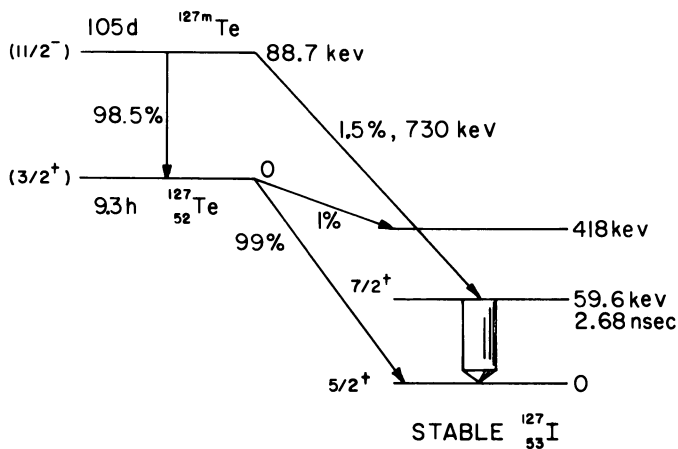
Figure 1. Relevant part of ^{127}Te-^{127}I and ^{129}Te-^{129}I-^{129}Xe
decay schemes. Mössbauer transitions indicated by three-
dimensional arrows

Other factors to be considered by the experimentalist are that the
high spins ($5/2^+$ and $7/2^+$) of the nuclear states involved cause the
hyperfine spectra to consist of many components (eight for quadrupole
splitting and 18 for magnetic splitting). Therefore, large electric field

gradients and large magnetic fields are needed to resolve the hyperfine structure of the spectra. Since most iodine compounds are not tightly bound ($\theta \approx 120°$K.), the absorbers must be cooled to at least liquid nitrogen temperature.

^{129}I in the absorber decays by β emission ($E_o = 150$ k.e.v., $T_{1/2} = 1.6 \times 10^7$ y) to the 39.6-k.e.v. excited state of ^{129}Xe. This state in Xe is strongly converted, giving an x-ray of 29.4 k.e.v. Since this x-ray and the 27.7-k.e.v. γ-ray cannot be resolved by a scintillation counter, some investigators have inserted a 70 mg./sq. cm. selectively absorbing indium foil between the ^{129}I absorber and the scintillation detector. This foil reduces the number of xenon x-rays by a factor of about 11 and the 27.7-k.e.v. γ-rays by a factor of about 2. The position and thickness of the foil are critical since the 24.0-k.e.v. x-rays of the indium also contribute to the background. The position and thickness can be optimized to maximize the signal to background ratio.

^{129}Te, $^{129}Te^m$, $^{127}Te^m$ Sources

Both the 33-day 105.6-k.e.v. isomeric state of ^{129}Te and the 70-minute ground state of ^{129}Te can be used to populate the 27.7-k.e.v. Mössbauer state of ^{129}I. To avoid the 27.2-k.e.v. x-rays resulting from the internal conversion of the 105.6-k.e.v. state, it is preferable to use the short-lived 70-minute ground state activity. Since the cross-section for ^{129}Te production in the ground state is much larger than that of the 105.6-k.e.v. isomeric state and the ground state is much shorter lived, almost all activity comes from the ground state. If a reactor is not conveniently located, the isomeric state can be used but with a resultant reduction in the amplitude of the Mössbauer dip by about a factor of 3. However, if about an order of magnitude more counts are obtained from a ^{129}Te^m source than from a ^{129}Te source, the statistical reliability of the ^{129}Te^m data will be equally good.

Contrary to the case of ^{129}I, using the decay of the isomeric state of ^{129}Te is preferable to using the decay of the ground state for Mössbauer studies of ^{127}I. This preference results from the more favorable γ-ray branching to the 57.6-k.e.v. state from the metastable state.

In most of the experiments on ^{127}I and ^{129}I, ZnTe has been used for the source compound. Because of its cubic, nonmagnetic environment, it emits a single, unsplit γ-ray line. Figure 2 shows data taken with a ^{66}Zn^{129}Te source and a K^{129}I absorber (*13*). Recently Perlow and Perlow (*29*) obtained enhanced results using Te(OH)$_6$ as a source material. This material increased the area of the Mössbauer pattern by a factor of about 2, but its single line pattern is slightly broadened and it has a large positive isomer shift.
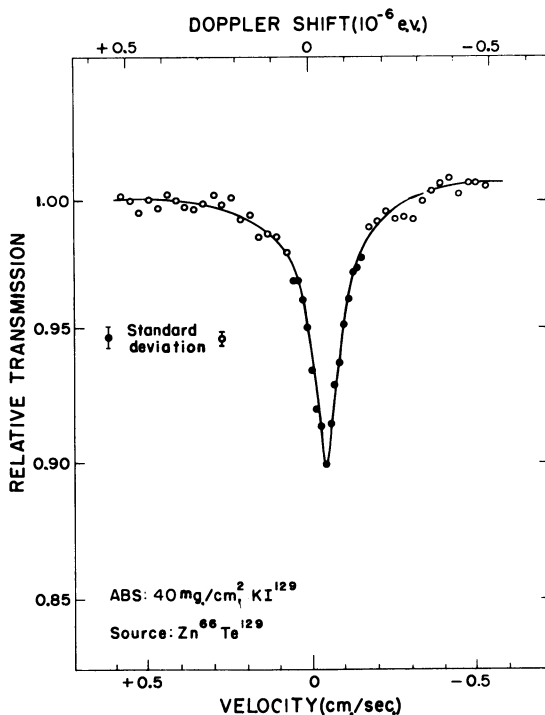
Figure 2. Relative transmission of 27.7-k.e.v. gamma-rays from a $^{66}Zn^{129}Te$ source through a K^{129} I absorber as a function of source velocity

Enriched ^{126}Te or ^{128}Te should be used for the reactor irradiation to eliminate unwanted background radiations from the other tellurium isotopes. Radiation damage to the source is unimportant since annealing (*13*) the ZnTe after irradiation did not change line intensity or width.

Isomer Shifts in Alkali Halides

Theoretical Considerations. We define the isomer shift as δ positive when source and absorber move toward each other, and thus a positive δ corresponds to an absorber transition energy higher than that of the source.

An expression for δ in terms of the source and absorber nonrelativistic s electron densities at the origin, $|\psi_s(0)|^2$ and $|\psi_a(0)|^2$, respectively, can be obtained by considering the electrostatic interaction between the s electrons and a nucleus with a uniform charge density. A relativistic calculation yields (*7*):

$$\delta = \frac{c}{E_\gamma} \frac{2\pi \, a_o^{2-2\rho} 2^{2\rho} e^2 (1+\rho)}{z^{1-2\rho}[\Gamma(2\rho+1)]^2 \, 2\rho(2\rho+3)(2\rho+1)} \qquad (1)$$
$$[R_{ex}^{2\rho} - R_{gnd}^{2\rho}][|\psi_a(0)|^2 - |\psi_s(0)|^2]$$

where E_γ is the γ-ray energy, a_o is the Bohr radius, $\rho = (1 - \alpha^2 Z^2)^{1/2}$, and R_{ex} and R_{gnd} are the nuclear radii for the excited state and the ground state, respectively. For the case of ^{129}I ($Z = 53$, $A = 129$, $R = 1.2 \times 10^{-13} A^{1/3}$ cm. $= 6.06 \times 10^{-13}$ cm.) Equation 1 becomes

$$\delta = 2.23 \times 10^{-23} \frac{\Delta R}{R} \left[|\psi_a(0)|^2 - |\psi_s(0)|^2 \right] \text{cm./sec.} \qquad (2)$$

where $\Delta R/R = (R_{ex} - R_{gnd})/R_{gnd}$. We show below that a positive δ corresponds to an s electron density greater than the ZnTe source.

To use Equation 2 to determine s electron density differences, it must be "calibrated"—*i.e.*, source-absorber or absorber-absorber combinations must be found for which the s electron density difference is known. The most common method for calibrating the isomeric shift formula is to measure isomeric shifts for absorbers with different numbers of outer shell s electrons—*e.g.*, by using compounds with the absorbing atoms in different valence states. The accuracy of this method depends on how much is known about the chemical bonds in suitably chosen absorber compounds, in particular about their ionicity and their hybridization. $|\psi(0)|^2$ can be obtained for an outer s electron from the Fermi-Segré formula or preferably from Hartree-Fock calculations.

Perlow and Ruby (*31*) and Ramma Reddy, Barros, and De Benedetti (*2, 32*) have compared the isomer shifts of a set of ^{127}I compounds with the isomer shifts from an identical set of ^{129}I compounds. This procedure allowed removal of the calculated values of the electronic densities of the compounds. The two isomer shift scales were linearly related by a constant factor, and thus they did not observe any noticeable effect of the valence state of the electronic cloud on the nuclear matter. Ramma Reddy, Barros, and De Benedetti (*32*) obtained:

$$\frac{(\Delta R)_{127}}{(\Delta R)_{129}} = -0.78 \pm 0.04 \qquad (3)$$

Calibration of the ^{129}I Isomeric Shift Scale with Isomeric and NMR Chemical Shift Data. The alkali iodide isomeric shifts (*5*) relative to ZnTe are displayed in Table I and in Figure 3.

Data on the number of iodine $5p$ electrons for the alkali iodides are available from the NMR chemical shift measurements of Bloembergen and Sorokin (*4*) and from the dynamic quadrupole coupling measurements of Menes and Bolef (*25*). From the NMR method, the change of the magnetic field at the nucleus caused by the paramagnetism of the $5p$ electrons is measured. From the dynamic quadrupole-coupling method, the attenuation of a sound wave caused by the nuclear spin-phonon interaction is measured. Both of these effects are proportional to the number of $5p$ holes, $h_p = 6 - y$, where the I^- configuration may be written as $5s^2 5p^y$. The xenon configuration corresponds to $h_p = 0$ and

<div align="right">Table I.   Alkali</div>

The alkali iodide isomeric shifts (13); number of iodine ion p holes calculated rupole resonance data (25); the sum of overlap integrals (11); the fractional iodine ion density computed from the isomeric shift data, Equation 7, and δ.

Compound	Isomeric shift, cm./sec. wrt ZnTe $+ = toward^a$	Number of p Holes, h_p	
		From chem. shift^b	From dynamic quad.^{c}
LiI	-0.038 ± 0.0025	0.112	
NaI	-0.046 ± 0.0025	0.040	0.085
KI	-0.051 ± 0.0025	0.033	0.035
RbI	-0.043 ± 0.0025	0.055	0.070
CsI	-0.037 ± 0.0025	0.165	0.165

^{a} See (13).
^{b} See (4).

$y = 6$. The values of h_p determined by these workers are compared with the isomeric shifts of the alkali iodides in Figure 3 and Table I. The behavior of h_p is similar to that of the isomer shift, and as a first approximation, we can assume from this that the I⁻ $5s$ electron density as measured by the Mössbauer effect depends linearly on the number of $5p$ holes, h_p. This linearity is not surprising since the changes of electron populations, $\Delta h_p \sim 0.1$ in the alkali iodides, are small. Recently Boyle and Perlow (5) observed a similar linearity between the NMR chemical shift and the isomer shift in the cesium halides.

The linear dependence between δ and h_p can be used to calibrate the ^{129}I isomeric shift scale in the following way. An increase in the number of $5p$ electrons will decrease $|\psi(0)|^2$ by increasing the shielding of the $5s$ electrons (the effective nuclear charge will be decreased for the $5s$). This effect may be expressed quantitatively (13) by using Slater's shielding coefficients and the Fermi-Segré formula or by using the non-relativistic Hartree-Fock SCF results for the $5s^25p^5$ and the $5s^25p^6$ electronic configurations. The relative change in the $5s$ electron density obtained by these methods is:

$$\frac{\Delta|\psi_{5s}(0)|^2}{|\psi_o(0)|^2} = 0.097[h_p{}^{(1)} - h_p{}^{(2)}] \tag{4}$$

Iodide Data

by Menes and Bolef (*25*) from chemical shift data (*4*) and dynamic quad-
deviation of the iodine ion 5*s* electron density from the $5s^2 5p^6$ closed-shell
$= -0.055$ cm./sec.; the alkali ion polarizability; and the type of lattice.

Sum of Overlaps,[a] $\Sigma(S_{5s\nu})^2$ ν	$\dfrac{\Delta\|\psi_{5s}(0)\|^2}{\|\psi_0(0)\|^2}$	Alkali Ion Polarizability	Lattice
0.05923	−0.014	0.029	NaCl
0.03141	−0.0075	0.408	NaCl
0.01784	−0.0034	1.334	NaCl
0.01447	−0.010	1.979	NaCl
0.02434	−0.015	3.335	CsCl

[c] See (*25*).
[d] See (*11*).
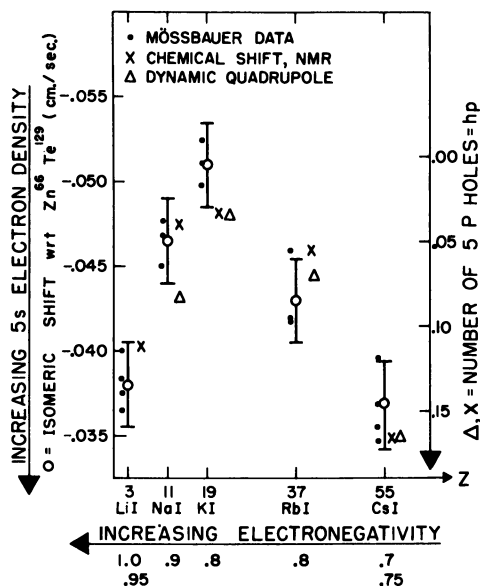
*Figure 3.   Isomer shifts, O (13), and num-
ber of iodine p holes, h_p, obtained from
NMR chemical shift (4), ×, and from dy-
namic quadrupole coupling (25), Δ, vs.
alkali atomic number for alkali iodides.
Data points for each alkali spread horizon-
tally for clarity*

by applying (13) the Fermi-Segré equation with Slater shielding coefficients, and

$$\frac{\Delta|\psi_{5s}(0)|^2}{|\psi_o(0)|^2} = 0.058 \, [h_p^{(1)} - h_p^{(2)}] \tag{5}$$

from the nonrelativistic Hartree-Fock results. The numbers of $5p$ holes for alkali iodides 1 and 2 are denoted by $h_p(1)$ and $h_p(2)$, and $|\psi_o(0)|^2$ is the nonrelativistic $5s$ electron density at the nucleus for the completely filled s and p shells. Equations 4 and 5 demonstrate the linear increase of $5s$ density as the number of p holes is increased. Equations 4 and 5 consider only the dependence of $|\psi(0)|^2$ on the $5p$ population and not the direct changes in $|\psi(0)|^2$ caused by overlap. The latter phenomenon is discussed below. One $5p$ hole ($h_p = 1$) increases the $5s$ density by about 6–10%, which is in accordance with the results of the isotope shift (23). We use the value of 9.7%. On the other hand, the change in isomeric shift for two different alkali iodides can be written according to Equation 2 as:

$$\Delta\delta = \delta^{(1)} - \delta^{(2)} = \text{constant} \, \frac{\Delta|\psi_{5s}(0)|^2}{|\psi_o(0)|^2} \tag{6}$$

The best value of the calibration constant in this equation has been found by a least-squares fit between the δ and h_p data (Table I and Figure 3). Combining Equations 4, 5, and 6, we obtain

$$\frac{\Delta|\psi_{5s}(0)|^2}{|\psi_o(0)|^2} = 0.84 \, \Delta\delta \quad (\delta \text{ in cm./sec.}) \tag{7}$$

This value of the calibration constant is not accurate (about 25%) because of certain approximations made by Memes and Bolef and by Blembergen and Serokin and the approximate nature of Equation 4. The chemical shift corresponding to the closed electron shell is not accurately known. This uncertainty, however, does not affect the calibration constant in Equations 4 and 5. The least-squares fit also gives the shift for the closed shell ($h_p = 0$) relative to ZnTe, $\delta_o = -0.055$ cm./sec. The values of $\Delta|\psi_{5s}(0)|^2/|\psi_o(0)|^2$ in Table I are calculated from Equation 7 relative to δ_o. Combining Equations 2 and 7 shows that the sign of $\Delta R/R$ is positive.

Interpretating Alkali Iodide Data. The alkali iodide data given above show that the idealized model of ionic crystals is inadequate since $\delta \neq$ constant and $h_p \neq 0$. To interpret the data one must consider the effects on the iodine $5p$ population by covalency, deformation of the charge cloud by electrostatic interaction, and deformation by overlap.

From the simple theory of electronegativity an approximately linear relation between the isomeric shift and the alkali electronegativity is expected. This trend is seen when going from LiI to KI (Figure 3) but

is not observed for RbI and CsI. It is not surprising that effects other than electronegativity appear in the alkali iodide δ data since the alkali electronegativity changes by only 20% while the alkali ionic radius changes by a factor of 2 and the dipole polarizability changes by a factor of 110.

For a completely ionic bond the ionicity, I, must be 1; for a completely covalent bond, $I = 0$. For the alkali iodides the ionicity and hence the number of iodine $5p$ electrons ($y = 5 + 1$) should increase from LiI to CsI since the electronegativity difference between iodine and the alkali increases. This implies that the iodine ion configuration, $5s^2 5p^y$, should most closely approach the $5s^2 5p^6$ xenon configuration for CsI. Since $|\psi(0)|^2$ is decreased by increases in the $5p$ population, we would expect on the basis of electronegativity alone that $|\psi(0)|^2$ would decrease monotonically from LiI to CsI since their bonds have become more ionic. However, since RbI and CsI deviate completely, we must investigate the effects of the electrostatic interaction and overlap.

Such serious deviations from the predictions of electronegativity are not often found in Mössbauer experiments. In particular, Alexsandrov *et al.* (*1*) and others have found a linear relation between δ and electronegativity for the tin tetrahalides. Since the differences in electronegativity are much larger for the halogens than the alkalies, the difference in ionicity is much more important for the tin tetrahalides than for the alkali iodides.

The simple theory of electronegativity fails in this discussion because it is based merely on electron transfer energies and determines only the approximate number of electrons transferred, and it does not consider the interactions which take place after transfer. Several calculations in the alkali halides of the cohesive energy (*24*), the elastic constants (*24*), the equilibrium spacing (*24*), and the NMR chemical shift (*17, 18, 22*) and its pressure dependence (*15*) have assumed complete ionicity. Because these calculations based on complete ionicity agree remarkably well with the experimental data, we are not surprised that the electronegativity concept of covalency fails completely for the alkali iodide isomer shifts.

Overlapping Ion Model. The ground-state wave function for an individual electron in an ionic crystal has been discussed by Löwdin (*24*). To explain the macroscopic properties of the alkali halides, Löwdin has introduced the symmetrical orthogonalization technique. He has shown that an atomic orbital, ψ_μ, in an alkali halide can be given by

$$\psi_\mu = \sum_\alpha \phi_\alpha \, (1 + S)^{-\frac{1}{2}}_{\alpha\mu}$$

$$= \phi_\mu - 1/2 \sum_\alpha \phi_\alpha \, S_{\alpha\mu} + 3/8 \sum_{\alpha,\beta} \phi_\alpha S_{\alpha\beta} S_{\beta\mu} \, \cdots \qquad (8)$$

with the summation extending over all neighbors in the crystal; ϕ_μ satisfy the free-ion Hartree-Fock equations, and $S_{\alpha\mu}$ is the overlap matrix expressed in the free-ion Hartree-Fock basis and is given by

$$S_{\alpha\mu} = <\phi_\alpha|\phi_\mu> - \delta_{\alpha\mu} \qquad (9)$$

where $\delta_{\alpha\mu}$ is the Kronecker delta. Thus, the ψ_μ in Equation 8 are an orthonormal set of atomic orbitals which use the Hartree-Fock free-ion basis set and acknowledge the nonzero overlap between the neighbors in the crystal. Within the framework of the symmetric orthogonalization technique, Löwdin has calculated (24) for the alkali halides values of the cohesive energy, the elastic constants, C_{ij}, the compressibility, β, the equilibrium lattice spacing, and the pressure for the transition from the NaCl to the CsCl crystal structure.

In addition Kondo and Yamashita (22), and others (15, 17, 18) have used Löwdin's work by applying the symmetrical orthogonalization technique to the chemical shifts in the alkali halides. All of these results agree remarkably well with the experimental data.

To calculate the isomer shift (11) the electron density is obtained easily using the symmetric orthogonalization technique:

$$\rho(r) = 2 \sum_\mu \psi_\mu{}^*(r)\psi_\mu(r) = 2 \sum_{\alpha,\beta} (1 + S)^{-1}_{\alpha\beta} \phi_\alpha{}^*(r)\phi_\beta(r)$$

$$= 2 \sum_\alpha |\phi_\alpha(r)|^2 - 2 \sum_{\alpha,\beta} S_{\alpha\beta}\phi_\alpha{}^*(r)\phi_\beta(r)$$

$$+ 2 \sum_{\alpha,\nu} |\phi_\alpha(r)|^2 (S_{\alpha\nu})^2 + \ldots$$

$$= 2 \sum_\alpha |\phi_\alpha(r)|^2 \left[1.0 + \sum_\nu (S_{\alpha\nu})^2 \right]$$

$$- 2 \sum_{\alpha,\nu} S_{\alpha\nu}\phi_\alpha{}^*(r)\phi_\nu(r) + \ldots \qquad (10)$$

where

$$(1 + S)^{-1}_{\alpha\beta} = \sum_\mu (1 + S)^{-\frac{1}{2}}_{\alpha\mu} (1 + S)^{-\frac{1}{2}*}_{\mu\beta}$$

The sums are over all $n/2$ free-ion atomic orbitals in the crystal. As all $S_{\alpha\nu}$ are zero if α and ν are on the same center, it is clear that $\rho(r)$ increases in the regions near the nucleus. The terms involving $S_{\alpha\nu}$ for near neighbors in the last term of Equation 10 are multiplied by the free-ion product, $\phi_\alpha{}^*(r) \phi_\nu(r)$ (α and ν are on different centers), which is extremely small when $r \gg 0$ from one of the centers. Thus, the negative term in Equation 10 is important only when r is large. Thus, the

symmetric orthogonalization method leads to increased electron density at the nucleus and decreased electron density in the regions between the ions in the lattice.
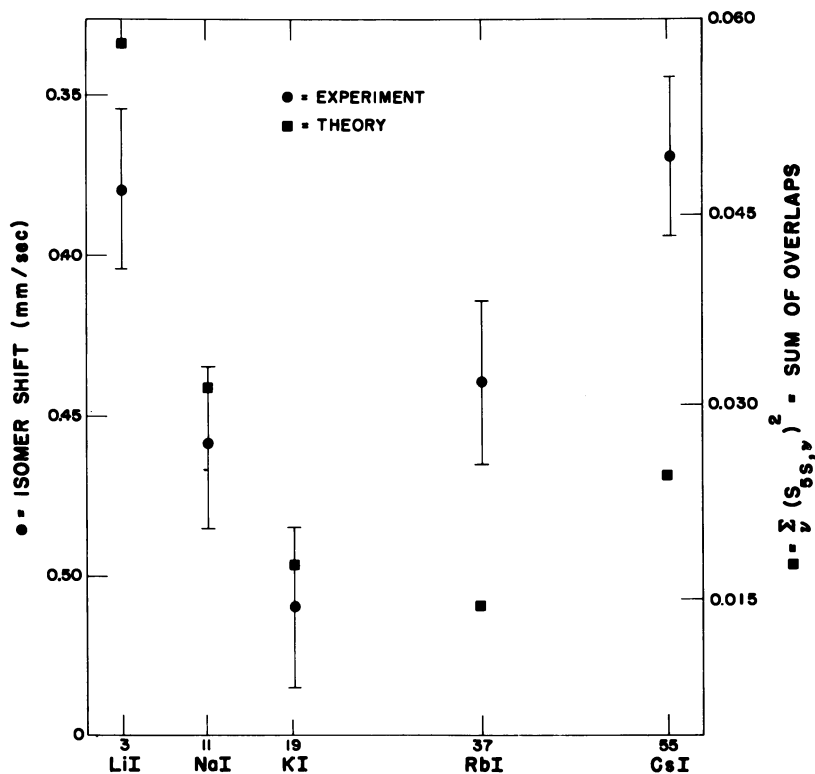
Figure 4. Experimental (13) and calculated (11) isomer shifts for alkali iodides. Overlapping ion model predicts that shifts will be proportional to the sum of the overlaps, Equation 13

Since only *s* electrons have a nonzero density at the nucleus, a good approximation to the *s* electron density at the iodine nucleus in the alkali iodide lattices is

$$|\psi_{I^-}(0)|^2 = 2 \sum_{\mu} \psi_{\mu}(0)\psi_{\mu}(0)$$

$$= 2 \sum_{\mu}^{ns} |\phi_{\mu}(0)|^2 \left[1.0 + \sum_{\nu} (S_{\mu\nu})^2 \right] \qquad (11)$$

where the sum over μ is over the *s* orbitals in I⁻, and the sum over ν is over all neighboring ions.

Since the overlap of an inner shell on one ion with the outer shell on another ion is at least on order of magnitude less than the outer-shell–outer-shell overlaps, only the 5s orbital in Equation 11 for I$^-$ will participate appreciably in the overlap deformation. Using this approximation, Equation 11 becomes

$$|\psi_{I^-}(0)|^2 = 2|\phi_{1s}(0)|^2 + 2|\phi_{2s}(0)|^2 + 2|\phi_{3s}(0)|^2$$

$$+ 2|\phi_{4s}(0)|^2 + 2|\phi_{5s}(0)|^2 \left[1.0 + \sum_{\nu} (S_{5s\nu})^2 \right] \qquad (12)$$

with only the last term varying from lattice to lattice. The inner-shell s electron densities, which are approximately constant from lattice to lattice, cancel in the difference equation for the relative isomer shifts of the alkali halides:

$$\Delta\delta_{ab} = \delta_a - \delta_b = \text{const.} \left[\sum_{\nu} (S_{5s\nu})^2 - \sum_{\mu} (5_{5s\mu})^2 \right] \qquad (13)$$

where the first term is for the a lattice, and the second term for the b lattice. The values for the sums of overlaps over the neighboring atoms are:

NaCl-Type Lattice

Nearest neighbors $$\sum_{\nu} (S_{s\nu})^2 = 6[(S_{ss'})^2 + (S_{sp\sigma})^2]$$

Next-nearest neighbors $$\sum_{\nu} (S_{s\nu})^2 = 12[(S_{ss'})^2 + (S_{sp\sigma})^2]$$

CsCl-Type Lattice

Nearest neighbors $$\sum_{\nu} (S_{s\nu})^2 = 8[(S_{ss'})^2 + (S_{sp\sigma})^2]$$

Next-nearest neighbors $$\sum_{\nu} (S_{s\nu})^2 = 6[(S_{ss'})^2 + (S_{sp\sigma})^2]$$

The appropriate sums have been calculated (11), and the results are given in Figure 4 and Table I.

The trend of the calculated values of $\sum_{\nu}(S_{5s\nu})^2$ agrees fairly well with the experimental values. These trends are a result of the competing NN alkali-iodide and NNN iodide-iodide overlaps. When the alkali Z is increased, the alkali-iodide overlaps increase because of the increased alkali size while the iodide-iodide overlaps decrease because their separation with distance increases.

The alkali iodide shifts are greatest at the extreme Z iodides, LiI and CsI, and are smallest at the middle alkali iodide, KI. The NaI and RbI shifts are between these extremes. This same variation has been observed (15) in the NMR chemical shifts. Figure 5 shows the values of the chemical shifts which were calculated (15) with the wave function given by Equation 8.
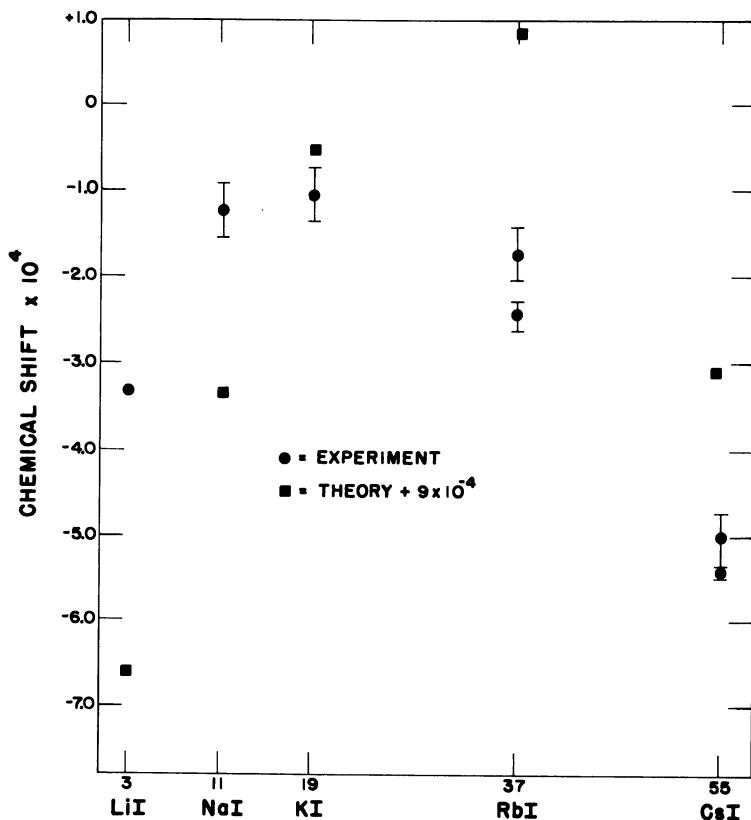
Figure 5. Experimental and calculated (15) NMR chemical shifts in alkali iodides. NMR chemical shifts calculated from wave function given by Equation 8 and corrected for shift of reference sample with respect to free I⁻ ion, −9 × 10⁻⁴

The result of the electrostatic multipole interaction is to deplete primarily the 5p-shell electrons in the I⁻ ion. The number of electrons originally in the 5p closed shell are lost to excited states. Since the 5p excitation is primarily to the 6s shell, the direct effect on the s electron density at the nucleus will be much smaller than the 5s density. As a result of the depletion of 5p electrons, however, the nucleus will be less shielded, and the 5s electrons will have a greater probability of being at
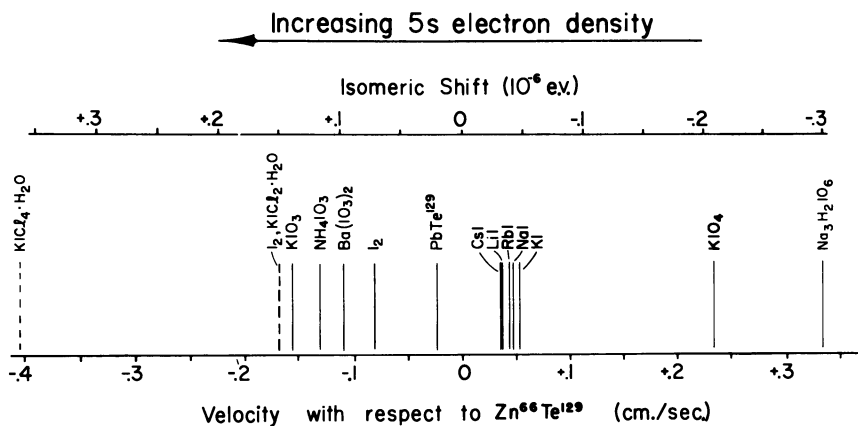
Figure 6. Compilation of isomeric shifts in
^{129}I compounds. The ^{127}I data converted to
^{129}I scale and is indicated by dashed lines. A
positive velocity corresponds to the ZnTe
source moving towards the absorber. Note
lack of agreement between shifts for molec-
ular iodine

the nucleus. Thus, the electrostatic as well as the overlap effects both
increase the s electron density at the nucleus in the same relative order.
Numerical estimates of this effect have been attempted (11). They (11)
have shown that the effect of the attractive electrostatic interaction
on the isomer shift is considerably less than the repulsive overlap effect.
Certainly the true isomer shifts are caused by all of these effects—i.e.,
overlap, electrostatic, covalency, and shielding. At present it appears
that shielding and overlap are the most important.

Relationship between Isomer Shift and Quadrupole Splitting in Some Iodine Compounds

Iodates and Periodates. Figure 6 shows some of the ^{129}I isomeric
shift data that have been calculated for a few iodine compounds. The
^{127}I data were converted to this scale from the measured linearity (32)
of the two scales and are denoted by the dashed lines. The I^-, $(IO_3)^-$,
and $(IO_4)^-$ shifts fall into three distinct groups. The $(IO_3)^-$ and $(IO_4)^-$
shifts relative to I^- may be qualitatively explained as follows. In the
alkali iodides, the I^- ion has almost the xenon configuration, $5s^25p^6$. X-ray
diffraction data show that for the $(IO_3)^-$ compounds the I-O bond angles
are very close to 90°, and thus they consist chiefly of $5p$ electrons (small
sp hybridization) (8). Removing $5p$ electrons from atomic orbits increases
$|\psi(0)|^2$ and raises the energy of the γ transition. In the $(IO_4)^-$ ion, each
iodine atom is surrounded by a tetrahedron of oxygen atoms with 109°

angles between the I—O bonds. There should now be a considerable *sp* hybridization, leading to a removal of $5s$ electrons from the atomic orbits of iodine. The decrease of $|\psi(0)|^2$ shifts the γ line to a lower energy, below that of I⁻. Thus, there are two counteracting effects on $|\psi(0)|^2$: an increase caused by the removal of $5p$ electrons and a decrease caused by the removal of s electrons in hybridized *sp* bonds. Hafemeister, De Pasquali, and deWaard (*13*) discuss these two effects in a semiquantitative manner.

Other Iodine Compounds. By studying the isomer shift and the quadrupole *hfs* for a series of ¹²⁷I compounds, Perlow and Perlow (*29*) have calibrated the isomer shift scale which is independent of Equation 7. The number of p holes, h_p, for the compounds of I_2, $KICl_4 \cdot H_2O$, $KICl_2 \cdot H_2O$, and ICl has been inferred from the measured value of the quadrupole coupling constant, eqQ, and from the symmetry of the iodine lattice site. Since they found that the isomer shifts and h_p are linearly related for these compounds, it appears that s electrons do not participate directly in the bonding, and the *sp* hybridization is negligible. Because of this linearity, they have been able to determine $\partial\delta/\partial h_p$, which leads to a calibration of the isomer shift scale.

Molecular Iodine. Figure 7 shows the data taken by Pasternak, Simopoulos, and Hazony (*26*) on molecular iodine. Because of the large field gradient in molecular iodine, they were able to obtain an accurate value for the ratio of the quadrupole moment of the excited state of ¹²⁹I to the quadrupole moment of the ground state, $Q^*/Q = +1.237 \pm 0.002$. In a similar way Perlow and Ruby (*31*) obtained the ratio $Q^*/Q = 0.896 \pm 0.002$ for ¹²⁷I by studying $KICl_2 \cdot H_2O$ and $KICl_4 \cdot H_2O$. The asymmetry of the spectra of Figure 7 can be used to show that the field gradient in molecular iodine is positive. This is expected, since the field gradient at the iodine nucleus arises from a p electron vacancy in the Xe closed shell, and this vacancy behaves like a positive charge.

There is strong evidence that the interhalogen bonds are essentially pure p bonds. By assuming for I_2 that $h_p = 1$, the isomer shift and this value for h_p continue the trends of Figure 3 and thus support the picture of pure p bonding for molecular iodine. In addition, Pasternak and Sonnino (*27*) have also studied IBr, ICl, I_2Cl_6, and ICN.

Magnetic Hyperfine Structure. The magnetic fields in most magnetic iodine and tellurium compounds are not sufficient to separate the 18 magnetic hyperfine lines of the two iodine isotopes. Several measurements (*13, 21, 34, 36*) have indicated that fields of only about 100 kilogauss can be expected from such compounds. Therefore, other methods must be utilized.

One of these is an external magnet. By using a superconducting magnet of 50-kG. on a $K^{129}I$ absorber, deWaard and Heberle (*38*)
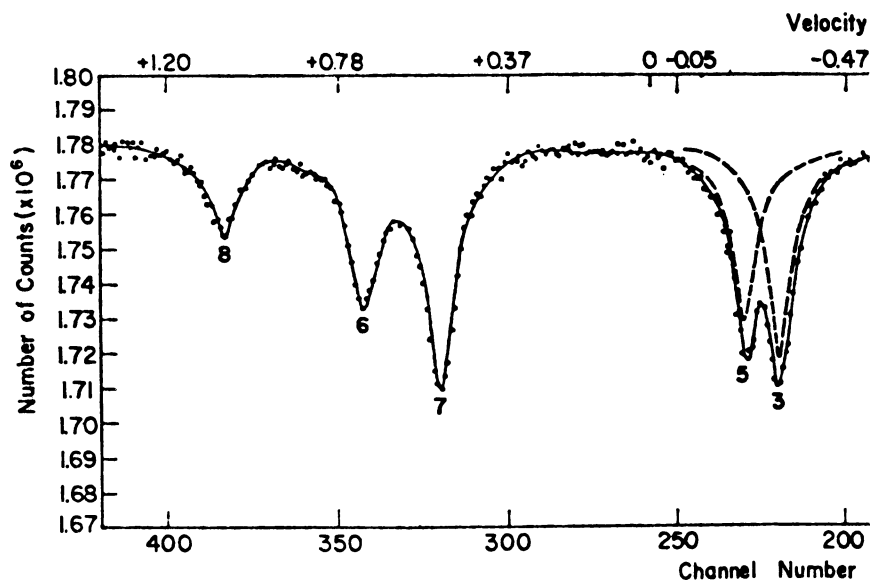
Figure 7.   Relative transmission through molecular iodine I_2 obtained by and their relative intensities resulting

partially separated the magnetic hyperfine lines and obtained the ratio of the magnetic moment of the excited state to the magnetic moment of the ground state.

Another method is the conduction-electron polarization effect (CEP) discussed by Shirley and Westenbarger (35). deWaard and Drentje (37) have utilized this effect by driving [129]Te[m] atoms into a thin iron foil with an isotope separator. They obtained an immense magnetic hyperfine splitting and cleanly separated the *hfs* lines. From these measurements they determined that the magnetic field at the iodine nucleus was 1130 ± 40 kilogauss.

Recoilless Fractions

Alkali Iodides. Figure 8 shows the experimental data obtained for the recoilless fraction, *f*, at 80°K. The area (13), line width (13), and the temperature (26) methods have all been used to analyze these data. Uncertainties in the background corrections (13) are caused by rather large errors. However, the striking feature is that the recoilless fraction changes only little from LiI to CsI.

The recoilless fraction, *f*, has been calculated (13) for monotomic lattices using the Debye approximation. When the specific heat Debye temperatures of the alkali iodides are inserted in the Debye-Waller factor, a large variation of *f* follows (from 0.79 in LiI to 0.15μCsI). It is not
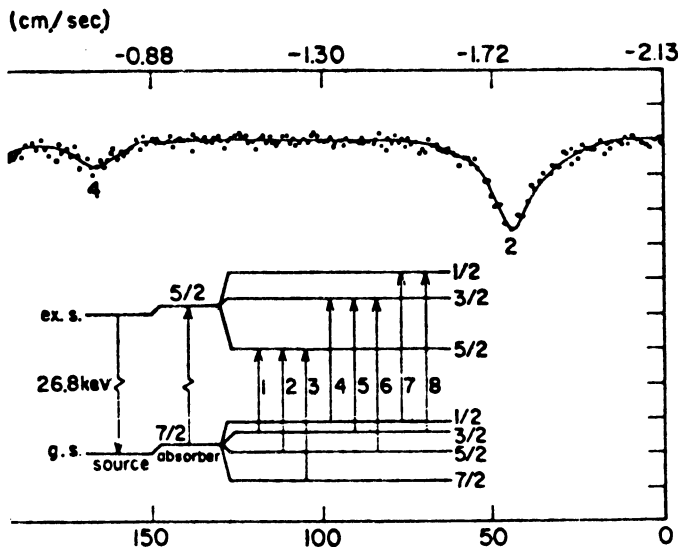
Pasternak, Simopoulos, and Hazony (25). Vertical lines represent transitions from the quadrupole interaction

surprising that these calculations intended for monatomic lattices do not agree with our diatomic data. However, there is fair agreement between the experimental value of f for CsI and the value computed from the Debye temperatures (Figure 8). One would expect the Debye approximation to be most successful when the mass differences between alkali and halogen atoms are small.

Kagan and Maslov (20) have calculated f for the diatomic NaCl lattice. Their results are given in terms of the C_{11} and C_{44} elastic constants and the atomic masses and they agree moderately well (6, 13) with the data.

By using the Mössbauer effect of [133]Cs, Boyle and Perlow (6) have recently measured the recoilless fraction in the cesium halides. Their results indicate that the effective Mössbauer Debye temperature slowly decreases monotonically (from 109° to 96°K.) as the mass of the cation is increased (from CsF to CsI). They have explained (6) their results by showing that a decrease in the energy gap between the acoustical and optical branches of the phonon spectrum will decrease the slope of the acoustical branch and thus lower the effective Mössbauer Debye temperature.

Figure 8 also shows values of f that have been calculated by two other methods. In the first, Jaswal (19) has used lattice-vibration eigenfrequencies and eigenvectors which have been calculated in the first Brillouin zone using the deformation-dipole model for the lattice. This

model takes into account the short-range forces, long-range Coulomb forces, polarization, and deformation of the ions. In addition, Jaswal has calculated the second-order Doppler shift by using these techniques. In the second, Disatnik, Fainstein, and Lipkin (9) have related specific heat data to the recoilless fraction data for the alkali iodides by considering a fictitious iodine crystal where all the atoms have the iodine mass, but the forces between atoms are those of the alkali iodide crystal. From Figure 8 it is clear that more accurate data must be taken to clarify the merits of these theoretical models.
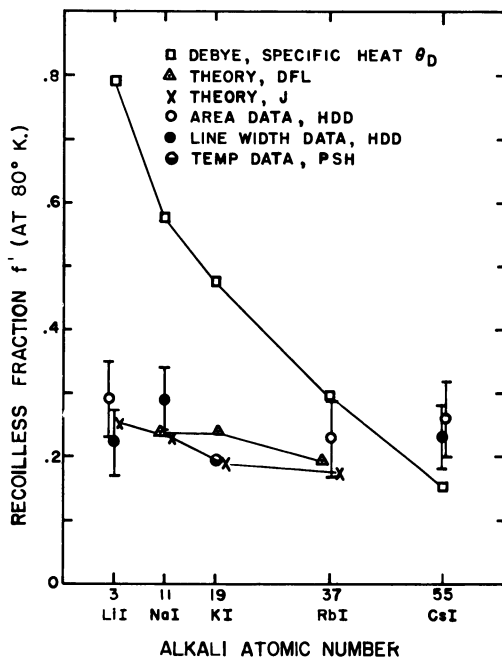
Figure 8. Theoretical and experimental values of recoilless fraction, f for alkali iodides at 80°K. DFL symbolizes Ref. (9), J—(19), HDD—(13), PSH—(26)

Recoilless Optical Absorption in Alkali Halides. Recently Fitchen *et al.* (10) have observed zero phonon transitions of color centers in the alkali halides using optical absorption techniques. They have measured the temperature dependence of the intensity of the zero phonon line, and from this have determined the characteristic temperatures for the process. In contrast to the Mössbauer results, they have found characteristic temperatures not too different from the alkali halide Debye temperatures.

Other Compounds. The molecular crystal I_2 has been studied by Pasternak, Simopoulos, and Hazony (*26*). By measuring the temperature dependence of the recoilless fraction they obtained an effective Mössbauer temperature, $\theta_M = 60°K.$, which is considerably less than the range found for the alkali iodides, $\theta_M = 100°$ to $120°K.$ Because the covalent intramolecular bonding in I_2 is much stronger than the intermolecular bonding, it is reasonable to assume for data interpretation that the recoil energy is taken up by the entire I_2 molecule.

By studying $Na_3H_2IO_6$, Perlow and Perlow (*29*) have shown that the paraperiodate ion, IO_6^{-5}, displays an extremely large recoilless fraction which gives $\theta_M = 280°K.$ They also obtained large recoilless fraction f from similar compounds with high formal ionic charge, $Te(OH)_6$ ($\theta_M = 175°K.$) and the perxenate ion (*30*), XeO_6^{-4} ($\theta_M = 280°K.$). These authors have explained the enhanced values of θ_M by separating the internal motion of the central atom with respect to its ligands from the motion of the ion as a whole with respect to the crystal—*i.e.*, $<x^2>$ $= <x^2_{int}> + <x^2_{ion}>$ and by considering the effect of the ionic charge on the phonon frequency spectrum. It follows that compounds such as these with large formal ionic charges will display considerably larger values of θ_M. In addition to being an interesting scientific phenomenon, this result can serve as a partial guideline for future experimenters who need compounds with large values of θ_M. Such large values of θ_M have also recently been observed by Heberle *et al.* (*16*) in a study of dilute iodine impurities in iron. These authors have indicated that θ_M lies between 270° and 370°K. for such a system.

Acknowledgment

Literature Cited

(1) Aleksandrov, A., Delyagin, N., Mitrofanov, K., Polak, L., Shpinel, V., *JETP* **43**, 1242 (1963).
(2) Barros, F. deS., Ivantchev, N., Jha, S., Rama Reddy, K., *Phys. Letters* **13**, 142 (1964).
(3) Bemis, C. E., Fransson, K., *Phys. Letters* **19**, 567 (1965).
(4) Bloembergen, N., Sorokin, P., *Phys. Rev.* **110**, 865 (1958).
(5) Boyle, A. J. F., Perlow, G. J., *Phys. Rev.* **149**, 165 (1966).
(6) *Ibid.*, **151**, 211 (1966).
(7) Breit, G., *Rev. Mod. Phys.* **30**, 507 (1958).
(8) Das, T. P., Hahn, E. L., "Nuclear Quadrupole Resonance Spectroscopy," p. 141, Academic Press, New York, 1958.
(9) Disatnik, Y., Fainstein, D., Lipkin, H. J., *Phys. Rev.* **139**, A292 (1965).

(10) Fitchen, D. B., Silsbee, R. H., Fulton, T. A., Wolf, E. L., *Phys. Rev. Letters* **11**, 275 (1963).
(11) Flygare, W. H., Hafemeister, D. W., *J. Chem. Phys.* **43**, 789 (1965).
(12) Geiger, J. S., Graham, R. L., Bergstron, I., Brown, F., *Nucl. Phys.* **68**, 358 (1965).
(13) Hafemeister, D. W., DePasquali, G., Waard, H. de, *Phys. Rev.* **135**, B1089 (1964).
(14) Hafemeister, D. W., Flygare, W. H., *J. Chem. Phys.* **43**, 795 (1965).
(15) *Ibid.*, **44**, 3584 (1966).
(16) Heberle, J. W., Waard, H. de, Drentje, S. A., Schurer, P., *Bull. Am. Phys. Soc.* **12**, 25 (1967).
(17) Ikenberry, D., Das, T. P., *J. Chem. Phys.* **43**, 2199 (1965).
(18) Ikenberry, D., Das, T. P., *Phys. Rev.* **138**, A822 (1965).
(19) Jaswal, S. S., *Phys. Rev.* **144**, 353 (1966).
(20) Kagan, Yu, Moslov, V. A., *Zh. Eksperim. i Teor. Fiz.* **41**, 1296 (1961); English translation: *Soviet Phys. JETP* **14**, 922 (1962).
(21) Kalvius, G. M., Oppliger, L. D., Ruby, S. L., *Phys. Letters* **18**, 241 (1965).
(22) Kondo, J., Yamashita, J., *J. Phys. Chem. Solids* **10**, 245 (1959).
(23) Kopfermann, H., "Nuclear Moments," Academic Press, New York, 1958.
(24) Löwdin, P. O., Ph.D. Thesis, Uppsala University, Sweden, 1948; *Advan. Phys.* **5**, 1 (1956).
(25) Menes, M., Bolef, D., *J. Phys. Chem. Solids* **19**, 79 (1961).
(26) Pasternak, M., Simopoulos, A., Hazony, Y., *Phys. Rev.* **140**, A1892 (1965).
(27) Pasternak, M., Sonnino, T., to be published.
(28) Perlow, G. J., *Phys. Rev.* **135**, B1102 (1964).
(29) Perlow, G. J., Perlow, M. R., *J. Chem. Phys.* **45**, 2193 (1966).
(30) Perlow, G. J., Perlow, M. R., *Rev. Mod. Phys.* **36**, 353 (1964).
(31) Perlow, G. J., Ruby, S. L., *Phys. Letters* **13**, 198 (1964).
(32) Rama Reddy, K., Barros, F. deS., DeBenedetti, S., *Phys. Letters* **20**, 297 (1966).
(33) Sanders, R., Waard, H. de, *Phys. Rev.* **146**, 907 (1966).
(34) Shikazono, N., *J. Phys. Soc. Japan* **18**, 925 (1963).
(35) Shirley, D. A., Westenbarger, G. A., *Phys. Rev.* **138**, A170 (1965).
(36) Waard, H. de, private communication.
(37) Waard, H. de, Drentje, S. A., *Phys. Letters* **20**, 38 (1966).
(38) Waard, H. de, Heberle, J., *Phys. Rev.* **136**, B1615 (1964).

RECEIVED January 1, 1967.

Mössbauer Spectroscopy of Tellurium

C. E. VIOLET

Lawrence Radiation Laboratory, University of California, Livermore, Calif.

The Mössbauer effect in ^{125}Te can provide information on both the nuclear properties of the 35.6-k.e.v. first excited state of ^{125}Te and the chemical properties of pure Te and Te compounds. Nuclear properties which have already been determined include the quadrupole moment, $|Q_1| = 0.20 \pm 0.03$ barn, and the magnetic moment, $\mu_1 = +0.60 \pm 0.02$ nm. Information on chemical bonding of Te can be obtained from the ^{125}Te Mössbauer spectra of various Te compounds. The isomer shift which is related to the valence s electrons gives a measure of the ionic character while the quadrupole splitting can provide information on ionic character and hybridized covalent bonds.

Studies of the Mössbauer effect associated with the 35.6-k.e.v. transition from the first excited state $\left(\frac{3}{2}+\right)$ to the ground state $\left(\frac{1}{2}+\right)$ of ^{125}Te have provided information on the ^{125}Te nucleus and the properties of pure Te and Te compounds between liquid helium and liquid nitrogen temperatures (*3, 5, 7, 8, 12, 13, 15, 16, 17*). The Mössbauer effect might also be observable in another isotope of tellurium, ^{123}Te. However, the high transition energy, 159 k.e.v., makes the effect difficult to observe, and the associated line width is about an order of magnitude greater than that of the ^{125}Te transition, resulting in a corresponding decrease in energy resolution. Since the solid-state aspects of the Mössbauer effect are independent of the nuclear transition, it is sufficient to use the more readily observable ^{125}Te transition to study the properties of Te and its compounds. In this presentation we discuss experimental aspects associated with measuring the resonance spectra of ^{125}Te, review important experimental results, and suggest further ^{125}Te Mössbauer experimentations which might yield useful results.

Sources

^{125}Te Mössbauer sources with convenient lifetimes can be made from ^{125}Sb, ^{125}I, or the 58d isomer of ^{125}Te. This is evident from the level diagram shown in Figure 1. Single line sources can be made with ^{125}Sb and ^{125}I if these isotopes are incorporated into materials of cubic symmetry, thereby avoiding quadrupole effects. This has been done by electroplating ^{125}Sb or ^{125}I on a copper foil and annealing (13, 16). Sources have also been made by neutron irradiation of pure Te enriched with ^{124}Te (5). The 58-day ^{125}Te isomer is then produced by neutron capture of ^{124}Te. However, pure Te is noncubic, and a two-line source results from the associated quadrupole effect. For a source of ^{125}I in Cu, the recoilless fraction at 82°K. is about 20% (16).

These ^{125}Te sources emit 27.4-k.e.v. K_α and 31.1-k.e.v. K_β x-rays of Te, as well as the 35.6-k.e.v. γ-rays, in the ratios:

$$K_\alpha : K_\beta : \gamma = 1 : 0.22 : 0.073$$

The low γ-ray intensity relative to the K x-ray background therefore presents a problem of obtaining a reasonably good signal-to-background ratio.

Detectors

Three types of detectors have been used in observing the ^{125}Te Mössbauer effect: proportional counters, NaI crystals, and Li-drifted Ge crystals. Figure 2a shows the source spectrum obtained with a Xe-filled proportional counter. The Te K_α and K_β rays and the γ-rays which constitute the high-energy group are barely resolvable. The escape peak for this counter is visible at lower energy. Setting the single-channel analyzer window to detect the 35.6-k.e.v. gammas results in a signal-to-background ratio of about 6 to 1. Figure 2b shows the source spectrum as detected by a thin NaI (Tl) crystal with a Cu absorber (336 mg. per sq. cm.) and an Al absorber (137 mg. per sq. cm.) placed in front of the source. In this case the components of the high-energy group are unresolved. This problem can be circumvented by setting the single-channel analyzer to detect the escape peak (2). Since the K edge of iodine is 33.16 k.e.v., the Te x-rays make no contribution to the escape peak. The signal-to-background ratio associated with this technique is about 10:1. The Cu absorber enhances the intensity of the gammas relative to the K x-rays, and the Al absorber "stops" the 7-k.e.v. Cu x-rays generated in the Cu absorber. This same technique could also be used with the Xe proportional counter. Using Li-drifted Ge detectors, the 35.6 k.e.v. gammas can be virtually separated from the x-ray background,

$$_{52}Te^{125} \ (35.6 \ \text{kev})$$
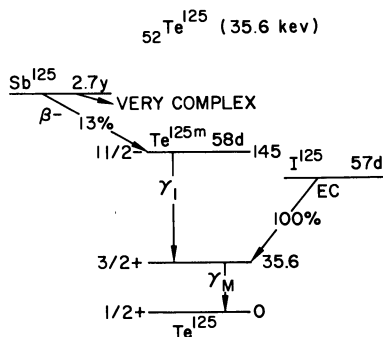
Figure 1.   Level diagram for ^{125}Te. Half life of $\left(\frac{3}{2} + \right)$ level is $\tau_{1/2}$ $(\gamma_M) = 1.4 \times 10^{-9}$ s. Corresponding full width at half maximum of Mössbauer line is $\Delta v = 0.27$ cm./ sec., assuming no experimental broadening
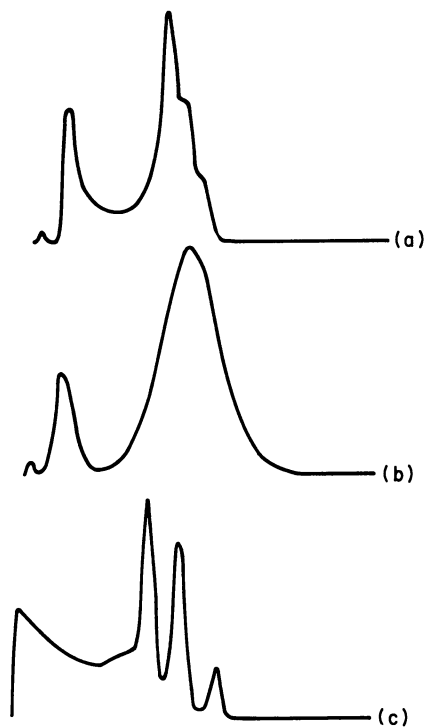
Figure 2. ^{125}I source spectra for (a) xenon proportional counter, (b) NaI (Tl) crystal, (c) Li-drifted Ge crystal

as shown in Figure 2c. The preamplifier has a cooled field-effect transistor to reduce noise in the input stage. The signal-to-noise ratio which we observe with this detector is about 20:1.

Nuclear Properties

Excited State Magnetic Moment. The magnetic moment of the ^{125}Te 35.6-k.e.v. level has been measured by Shikazono (*13*) and Huntzicker *et al.* (*8*). Sources were prepared by diffusing ^{125}Sb into metallic Fe foils. The ^{125}Te impurities produced by the decay of ^{125}Sb experience a hyperfine field at the ^{125}Te nucleus transferred from the ferromagnetic Fe host. The spins (Figure 3) of the 35.6-k.e.v. level $\left(\frac{2}{3}\right)$ and the ground state $\left(\frac{1}{2}\right)$ are the same as for the well-known ^{57}Fe transition, and the splitting of the two levels by the magnetic hyperfine interaction is similar (*10*). A Mössbauer spectrum for a ^{125}Sb-in-Fe source and a single-line ZnTe absorber is shown in Figure 3 (*6*). The line intensities are in the ratios 3:2:1:1:2:3, which demonstrates that the ratio of the first excited-state to ground-state magnetic moments must be negative. [The same intensity ratios exist in the magnetic hyperfine spectrum of ^{57}Fe, where the ratio of the first excited-state moment to the ground-state moment is $(\mu_1/\mu_0) = -1.715$ (*10*).] Using an independent determination of the ^{125}Te ground-state magnetic moment, $\mu_0 = -0.88715$ nm. (*9*), and the measured line separations in Figure 3, Huntzicker *et al.* (*8*) determined the ^{125}Te first excited-state magnetic moment: $\mu_1 = +0.60 \pm 0.02$ nm.

Electric Quadrupole Moment. A Mössbauer resonance spectrum typical of a ^{125}Te-in-Te absorber, and a single line ^{125}I-in-Cu source is shown in Figure 4. The quadrupole splitting at 4.8°K. is 0.76 ± 0.02 cm. per second or $(0.90 \pm 0.03) \times 10^{-6}$ e.v. (*16, 17*).

The quadrupole splitting for a nonaxially symmetric field gradient with spin $I = \frac{3}{2}$ is given by (*4*)

$$\Delta E = \frac{1}{2} eq Q \left(1 + \frac{1}{3}\eta^2\right)^{\frac{1}{2}} \tag{1}$$

To calculate the nuclear quadrupole moment from the measured quadrupole splitting, it is necessary to know the electric field gradient, q, at the Te nucleus as well as the asymmetry parameter, η. These can be calculated in the Townes and Dailey approximation (*4*) by knowing the chemical bonding in Te.

The arrangement of the atoms in a Te crystal is shown in Figure 5a. The atoms are arranged in spiral chains. The bonds between adjacent atoms on the same chain are covalent whereas between chains they are
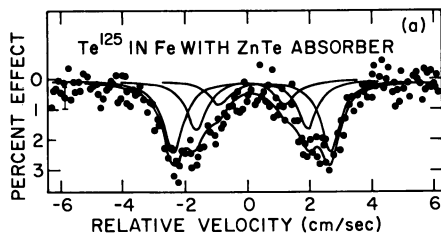
Figure 3.   *Magnetic hyperfine spectrum
of ^{125}Te as impurity in metallic Fe*
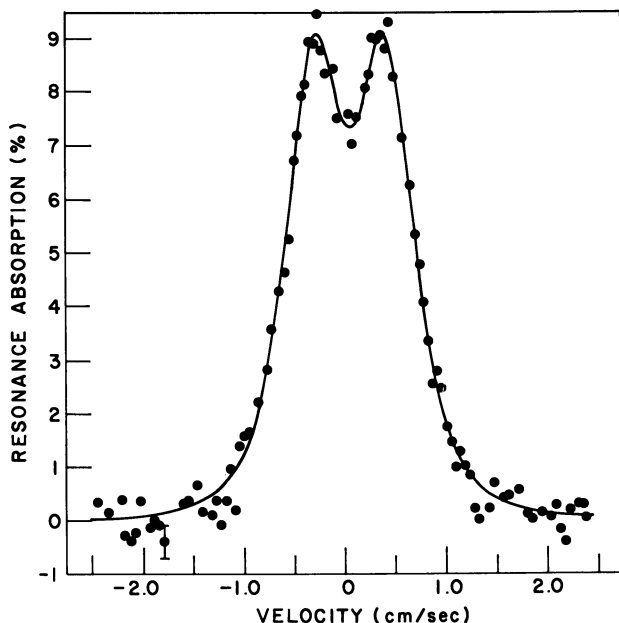
Figure 4.   *Electric quadrupole spectrum of ^{125}Te in
pure Te at 4.8°K. Source, ^{125}I in Cu at 82°K. Total
absorber thickness, 30.0 mg./sq. cm. of tellurium en-
riched in ^{125}Te—i.e., $^{125}Te/Te = 40.4\%$. Individual
lines of this doublet have a full width at half maximum
of 0.73 cm./sec. Our experimental line widths for
absorbers vary from 0.67–1.01 cm./sec.*

a weak mixture of electronic and van der Waals binding. Because of
the strong binding between atoms on the same chain, the chain can be
treated as a single molecule.

Considering only bonding between adjacent atoms on the same chain,
the principal axes of the field gradient tensor are shown in Figure 5b.
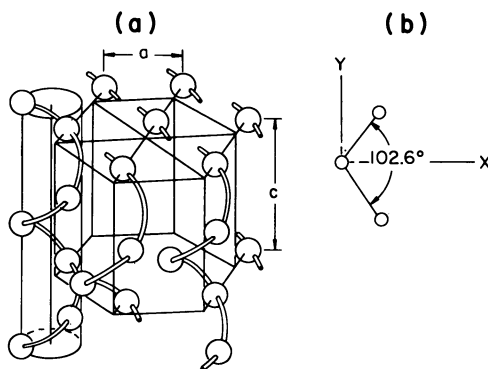
Figure 5.   Arrangement of atoms in (a) crystal structure of pure Te and (b) principal axes of electric field gradient

From the atomic orbitals s, p_x, p_y, and p_z, the following set of molecular orbitals can be constructed:

$$\psi_1 = (1 - 2\alpha)^{1/2}\, s - (2\alpha)^{1/2}\, p_x$$

$$\psi_2 = \alpha^{1/2}\, s + \left[\frac{1}{2}(1 - 2\alpha)\right]^{1/2} p_x + \sqrt{\frac{1}{2}}\,(p_y)$$

$$\psi_3 = \alpha^{1/2}\, s + \left[\frac{1}{2}(1 - 2\alpha)\right]^{1/2} p_x - \sqrt{\frac{1}{2}}\,(p_y)$$

$$\psi_4 = p_z$$

(2)

The amount of s character in the bonding orbitals, ψ_2 and ψ_3 is determined from $\alpha = \cos\theta/(\cos\theta - 1)$, where θ is the bonding angle. For the bonding angle of Te ($\theta = 102.6°$) we have $\alpha = 0.179$. One can now determine the number of unbalanced p electrons (U_p) and the asymmetry parameter

$$U_p = \frac{1}{2} N_x + \frac{1}{2} N_y - N_z = \alpha - 1 = -0.821$$

$$\eta = \frac{3(N_y - N_x)}{N_x + N_y - 2N_z} = \frac{3\alpha}{1 - \alpha} = 0.654$$

(3)

where N_x, N_y, and N_z are the electron populations in the p_x, p_y, and p_z states.

For atomic Te the contribution to q from one unbalanced p electron is $q_{atTe} = 3.9 \times 10^6$ e.s.u. (1). Thus the contribution to the field gradient at the Te nucleus owing to bonding along the molecular chain is -3.2×10^{16} e.s.u., weighted by the fractional importance of such bonding.

The fractional importance of bonding along the chains can be obtained by comparing with the situation in crystalline iodine (11). Iodine

exists as a molecular crystal (bond length 2.70 A.) but has next nearest neighbors at 3.54 A. compared with 4.30 A. for the sum of the van der Waals radii. In tellurium (bond length 2.86 A.) the next nearest neighbors on adjacent chains are at 3.45 A. compared with 4.40 A. for the sum of the van der Waals radii. Thus the importance of bonding along the chains in tellurium should be comparable with that for nearest-neighbor bonding in crystalline iodine—namely, about 89% (*11*). Accordingly, we take the fractional importance of this bonding to be

$$f = 0.89 \, {}^{+0.04}_{-0.08}$$

The choice of wave functions to describe bonding between chains is considerably more difficult than for bonding along the chains. Most of the bond angles for next-nearest-neighbor bonding are considerably less than 90° (60° and 80°) so that "bent" bonds are required. This in itself is evidence of the relative unimportance of such bonding. Nonetheless, if various bonding schemes are tried, one finds a distribution of positive and negative q's with a mean value which is nearly zero. From this analysis we take the field gradient owing to bonding between chains to be $q' = (0.0 \pm 0.8) \times 10^{16}$ e.s.u. From these considerations the field gradient can be determined from $q = fU_p q_{atTe} + (1 - f)q' = \left(-2.8 \, {}^{+0.3}_{-0.4} \right) \times 10^{16}$ e.s.u. Some d-hybridization may also be involved, but d orbitals make a negligible contribution to the field gradient (*4*). The correction for the Sternheimer effect is also negligible in the Townes and Dailey approximation (*4*). For spin $\frac{3}{2}$, the magnitude but not the sign of the quadrupole coupling can be determined from the quadrupole data alone (*4*). From these considerations and Equation 1, the magnitude of the electric quadrupole moment of the ^{125}Te first excited state becomes: $|Q_1| = 0.20 \pm 0.03$ barn.

Chemical Properties

Chemical Bonding. From the above calculations, it is clear that information on chemical bonding of Te compounds can be inferred from the associated quadrupole splitting data. We have neglected the ionic character of the Te bonds in tellurium. However, this parameter may need to be included in bonding calculations of Te compounds as is done, for example, in the Townes and Dailey approximation.

The isomer shift associated with Mössbauer resonance spectra also provides information on chemical bonding. The isomer shift is given by

$$\delta = \text{const} \left[|\psi_a (0) |^2 - |\psi_s (0) |^2 \right] \left[<R_{ex}{}^2> - <R_{gr}{}^2> \right] \qquad (4)$$

where

$|\psi_{a,s}(0)|^2 =$ electron densities at the nucleus for absorber and source

$<R_{ex}^2>$ and $<R_{gr}^2>$ = mean square charge radius of the excited state and ground state

The only appreciable contributions to the electron densities at the nucleus are from s electrons. Usually only valence s electrons are considered because the inner s electrons are much less affected by chemical bonding. Therefore, the isomer shift "gives a unique measure of the role of s electrons in chemical bonds and thus provides a physical foundation for the chemical concept of ionic character" (14).

The compound Na_2TeO_4 is an exceptional case in which the chemical bonding can be understood in terms of simple concepts. Accordingly, Buym and Grodzins (3) have stated that the electron density at the Te nucleus in Na_2TeO_4 is less than in Te. This, combined with their measured isomer shift in Na_2TeO_4, led to the conclusion that the charge radius

Table I. Isomer Shifts and Quadrupole Splittings at Liquid Nitrogen Temperature

	Symmetry	Isomer Shift,[a] Cm./Sec.	Quadrupole Splitting, Cm./Sec.	Magnetic Order	Magnetic Ordering Temp., °K.
ZnTe	fcc	−0.04 (1)	<0.07		
MnTe	Hex	−0.03 (2)	0.3 (1)	Antiferro-magnetic	323
FeTe	Tetr	0.00 (2)	0.3 (1)	Antiferro-magnetic	63
Fe_2Te_3	Hex	+0.05 (5)	0.37 (5)	Antiferro-magnetic	?
NiTe	Hex	+0.08 (5)	0.25 (5)	?	?
CoTe	Hex	+0.04 (5)	0.32 (5)	Ferro-magnetic	~1273
PbTe	fcc	0.00 (5)	<0.07		
Bi_2Te_3	Rhomb	−0.015 (5)	0.13 (5)		
Te		0	0.74 (2)		
TeO_2	Tetr.	+0.03 (1)	0.73 (1)		
Na_2TeO_3	?	−0.01 (1)	0.66 (2)		
Na_2TeO_4	Cubic	−0.15 (1)[b]	<0.07		
Te F_4	?	−0.01 (5)	0.7 (1)		
Te I_4	?	+0.05 (5)	0.6 (1)		
Te in Cu	Cubic	−0.05 (1)	<0.07		

[a] Relative to Te source at LN temperature or below.
[b] Ref. 3.

is larger in the excited state than in the ground state. The assertion of Buyrn and Grodzins pertaining to electron densities can be substantiated by applying hybridized bonding concepts to the chemical bonding of Te in Na_2TeO_4.

In Na_2TeO_4 the Te atom is most likely in the center of a regular tetrahedron formed by the four oxygen atoms, and the bonding is described by sp^3 hybridization. One Te electron is considered to be in each of the four bonding orbitals, and α' (the *s* character of each orbital) is 25%. In pure Te there are six electrons in the outer shell. One electron is considered to be in each of the bonding orbitals, ψ_2 and ψ_3, and two electrons in each of the nonbonding orbitals, ψ_1 and ψ_4 (*see* Equation 2). Thus the contribution to the electron density at the Te nucleus owing to the outer shell electrons is proportional to

$$\sum_{i=1}^{4} n_i |\psi_i(0)|^2 = 2(1-\alpha) \tag{5}$$

where n_i is the number of electrons in ψ_i.

We recall that the amount of *s* character in the bonding orbitals of Te is $\alpha = 0.18$. Assuming that only the outer shell electrons effect a change in electron density at the Te nucleus and that the electron density at the Te nucleus is proportional to the summation over all outer shell orbitals of the number of electrons in an orbital, weighted by the *s* character of the orbital, we have for the ratio of electron densities at the Te nucleus in Na_2TeO_4 and Te:

$$\frac{|\psi(0)|^2 (Na_2TeO_4)}{|\psi(0)|^2 (Te)} = \frac{4\alpha'}{2(1-\alpha)} = \frac{1}{1.6}$$

in agreement with Buyrn and Grodzins. Since the isomer shift in Na_2TeO_4 is negative relative to a Te source, $<R_{ex}^2>$ must be greater than $<R_{gr}^2>$ by Equation 4. Using this information and the measured quadrupole moment of the ^{125}Te first excited state, the following estimate of the charge radius difference has been given by Shirley (*14*): $(<R_{ex}^2> - <R_{gr}^2>)^{1/2}/R \approx +9 \times 10^{-4}$.

Quadrupole Splitting and Isomer Shift. The quadrupole splitting and isomer shift for several Te compounds are given in Table I and plotted in Figure 6. From these results we make the following observations:

A correlation between the isomer shift and quadrupole splitting is adumbrated. However, more data would be needed to confirm this. Such a correlation might be consistent with the molecular orbital approach and the linear relationships in Equations 3 and 5. The decreased quadru-
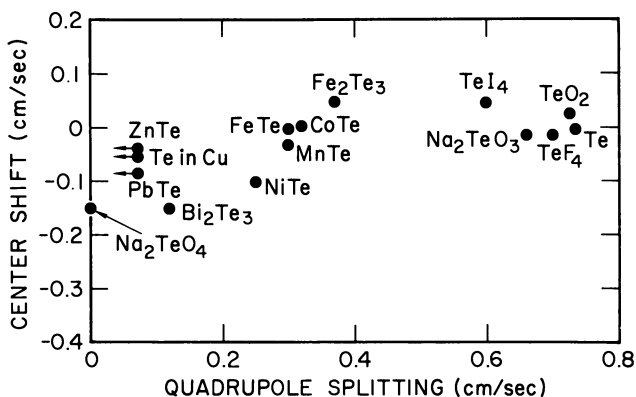
Figure 6.   Isomer shift and quadrupole splitting in Te compounds

pole splitting in the Te intermetallics relative to the Te compounds suggests possibly a greater ionic character in the intermetallic bonding than in the bonding of the compounds.

At liquid nitrogen temperature, FeTe is above its Néel temperature, but MnTe, CoTe, and NiTe are far below their Néel or Curie temperatures. The fact that no magnetic hyperfine splitting is observed in ferromagnetic CoTe suggests that the transferred hyperfine field is small. Magnetic hyperfine splitting appears to be absent for MnTe and NiTe also. However, the presence of a transferred hyperfine field in these antiferromagnetic materials may not be detectable in our Mössbauer experiments. Therefore, we can draw no conclusions about the transferred hyperfine field in MnTe and NiTe from our data.

Te intermetallics and compounds of noncubic symmetry exhibit quadrupole splitting, as expected; ^{125}Te in lattices of cubic symmetry exhibits no detectable quadrupole effect.

While the variation in quadrupole splitting is appreciable, the range of isomer shifts is relatively small. Therefore, it may prove difficult to obtain significant information from the isomer shift of Te compounds.

Conclusions and Future Experiments

The Mössbauer effect in ^{125}Te is readily observable at liquid nitrogen temperatures or lower, and considerable solid-state physics information on Te compounds and intermetallics is now available. However, there has been almost no attempt to understand this information in detail. An interpretation of the quadrupole splitting and isomer shifts in Te compounds in terms of bonding calculations would have intrinsic value and might also elucidate aspects of sulfur bonding. Alternatively, sulfur bonding might be studied by substituting Te for some of the S in the material of interest. If the Te took up normal S sites, some information might be obtained on sulfur bonding in these materials. Such materials

as sulfur-containing amino acids and vulcanized rubber might be investigated by this technique. With [125]Sb of ^{125}I sources, properties of antimony and iodine compounds might also be studied.

Single crystals of Te are highly anisotropic and occur as either right-hand or left-hand crystals. It would be interesting to use the [125]Te Mössbauer effect to measure the anisotropic Debye-Waller factor in such crystals.

From the decrease in quadrupole splitting in Te with increasing temperature, Violet and Booth (*16*) inferred a molecular torsional frequency corresponding to 33 cm.[-1]. This suggests that the [125]Te Mössbauer effect may be a method of examining molecular motions in Te compounds at frequencies corresponding to the far-infrared.

In a forthcoming paper entitled "Structural Studies of some Tellurium Compounds Using the Mössbauer Effect in [125]Te and [129]I Nuclei" by M. Pasternak and S. Bukshpan, structural information on tellurium, TeO_2 + $Te(NO_3)_4$ was obtained. The quadrupole moment of the [125]Te first excited state was also determined as -0.19 ± 0.02 barns.

Literature Cited

(1) Barnes, R. G., Smith, W. V., *Phys. Rev.* **93**, 95 (1954).
(2) Booth, R., Violet, C. E., *Nucl. Instr. Methods* **25**, 1 (1963).
(3) Buyrn, A. B., Grodzins, L., *Bull. Am. Phys. Soc.* **8**, 43 (1963).
(4) Das, T. P., Hahn, E. L., "Nuclear Quadrupole Resonance Spectroscopy," "Solid State Physics," Suppl. 1, Academic Press, New York, 1958.
(5) Frankel, R. B., Barrett, P. H., Shirley, D. A., *Bull. Am. Phys. Soc.* **7**, 600 (1962).
(6) Frankel, R. B., Huntzicker, J., Matthias, E., Rosenblum, S. S., Shirley, D. A., Stone, N. J., *Phys. Letters* **15**, 163 (1965).
(7) Hein, P. Z., Shapiro, V. G., Spinel, V. S., *Soviet Phys. JETP (English Transl.)* **15**, 489 (1962).
(8) Huntzicker, J. J., Frankel, R. B., Stone, N. J., Shirley, D. A., *Bull. Am. Phys. Soc.* **9**, 741 (1964).
(9) Lindgren, I., "Perturbed Angular Correlations," E. Karlsson, E. Matthias, K. Siegbahn, eds., p. 379, North Holland Publishing Co., Amsterdam, 1964.
(10) Preston, R. S., Hanna, S. S., Heberle, J., *Phys. Rev.* **128**, 2207 (1962).
(11) Robinson, H., Dehmelt, H. G., Gordy, W., *J. Chem. Phys.* **22**, 511 (1954).
(12) Shikazono, Naomoto, *J. Phys. Soc. Japan* **18**, 925 (1963).

(13) Shikazono, Naomoto, Shoji, T., Takekoshi, H., Tseng, P. K., *J. Phys. Soc. Japan* **17,** 1205 (1962).
(14) Shirley, D. A., *Rev. Mod. Phys.* **36,** 339 (1964).
(15) Stepanov, E. P., Aleshin, K. P., Manapov, R. A., Samoilov, B. N., Sklyarevsky, V. V., Stankevich, V. G., *Phys. Letters* **6,** 155 (1963).
(16) Violet, C. E., Booth, Rex, *Phys. Rev.* **144,** 225 (1966).
(17) Violet, C. E., Booth, Rex, Wooten, F., *Phys. Letters* **5,** 23 (1963).

Discussion[1]

Carl W. Seidel: During this discussion I hope that the panel and the audience will comment on the future of Mössbauer spectroscopy in chemistry, both as an investigative tool for different elements and as to the type of information that is or may be available from Mössbauer spectroscopy. We will begin with questions on Dr. Herber's paper.

J. J. Zuckerman (Cornell University): Would Dr. Herber and Dr. Sano like to propose the barium tin compound as a standard in Mössbauer spectroscopy—a standard we desperately need at this point.

R. H. Herber: Dr. Sano really has done most of the work on barium stannate in our laboratory. This material has one weakness when compared with the standard in cobalt-57 spectroscopy—*i.e.*, it has no quadrupole splitting. Otherwise, it is a stoichiometric compound which one can presumably prepare easily and reproducibly. I am not the person to propose it as a standard. Moreover, there are some other suitable candidates we haven't as yet studied, which should be considered.

J. J. Spijkerman: We have been looking for a good tin standard for almost a year now. Tin oxide is too wide, although this was accepted at the Gordon Conference. We thought of making a sandwich of two metals and obtaining two singlets, but that didn't work out very well. Dr. Snedeker has looked into the metal organotin compounds, some of which seem promising. However, if they have a large quadrupole splitting, they are very asymmetric and hence unstable. Perhaps the best solution is to combine white tin, which is quite reproducible, and barium stannate to give an artificial doublet. At least it allows one to calibrate the velocity spectrum and chemical shift simultaneously. We are going to perform all the measurements and standardization required on these compounds. It would help if the Mössbauer workers cooperated in choosing a standard. However, at the moment it doesn't look very good.

Dr. Herber: One of the organic compounds we synthesized some years ago was a toluene dithiol complex that apparently forms a polymer, is quite stable, and produces a suitable Mössbauer spectrum at room temperature.

Dr. Spijkerman: About a month ago we thought of sending out a letter to anyone who had ever published anything on tin to ask their opinion. However, we haven't done it so far. I would like to see a tin

---

[1] All speakers present except C. E. Violet

standard, and I think we should obtain one soon because the situation becomes more confusing with time.

A. F. Peterson (M & T Chemicals, Inc., Rahway, N. J.): Barium stannate is a commercial product M & T Chemicals manufactures.

Dr. Spijkerman: What is its purity?

Dr. Peterson: Off-hand I cannot answer, but the company probably manufactured it from a stannic hydrate, and I am sure that if there is sufficient interest, they would certainly produce a pure barium stannate as a standard.

Dr. Spijkerman: I still feel we should have a doublet because it is so time consuming to set up a spectrometer for iron, determine the velocity calibration, and then have to take off the source, change the detector and everything around to do a tin measurement. If we can get a standard for tin I think we should have a doublet that makes a velocity calibration possible. I would like to see a doublet that has approximately 3 or 4 mm./sec. (quadrupole) splittings—artificial if need be.

P. A. Flinn: Regarding a calibration standard, there are some ferro and antiferromagnetic compounds of tin. One in particular, $FeSn_2$, which is antiferromagnetic, has a good magnetic splitting of the tin pattern and provides a possible alternative to a quadrupole splitting.

Dr. Spijkerman: $FeSn_2$ is quite difficult to make.

Dr. Flinn: On the contrary there is an easy way to make it and although it hasn't been published, it's no secret. Co-precipitate iron and tin from aqueous solution, fire the precipitate in air to make the mixed oxides, and then reduce it in pure hydrogen.

Dr. Spijkerman: What is the splitting?

Dr. Flinn: I've forgotten the exact value, but it is quite large—a bit larger than with quadrupole splittings (about 3.3 mm./sec.) [V. I. Nikolaev, Shcherbina, Y. I., Yakinov, S. S., *JETP* **18**, 878 (1964)].

Dr. Spijkerman: Six lines or two?

Dr. Flinn: The six lines aren't fully resolved unfortunately (but probably would be with a natural width source).

Dr. Spijkerman: No, that will not do. The spectral lines should be resolved; otherwise manual and computer curve fitting could give different results.

T. D. Thomas (Princeton University): The sodium nitroprusside proposed has a splitting of about 2 mm./sec., whereas one has experiments that seem to go to 50 mm./sec.

Dr. Spijkerman: In iron?

Dr. Thomas: No, in general. I was thinking of it as a velocity calibration, not as a zero point calibration. What is the situation on obtaining standards which give a velocity calibration over a wider range so that very accurate estimates of this splitting are not necessary?

Dr. Spijkerman: For iron it would be quite difficult. Furthermore, the largest magnetic splitting that I have seen is in iron oxide, which is about 8–10 mm./sec., but that is not very reproducible.

N. E. Erickson: Regarding iron for calibration, some workers run in a time mode but use a sinusoidal drive. This results in an extremely nonlinear velocity scale, and a two-line pattern, such as in sodium nitroprusside, is just not reasonable for a standard. One needs more lines, with a wider separation. I would like a standard which gives six lines, and hence I favor iron. Perhaps the Bureau of Standards, and I know I have spoken with you (Spijkerman) about this and you argue against it, could calibrate iron foils, which would provide a known six line spectrum.

Dr. Spijkerman: One possibility is to precipitate iron and copper to give clean six-line spectra. We don't know how reproducible it is, but we are more than willing to use a six-line spectra as a secondary standard. However, iron foils (particularly commercial foils) data were not reproducible enough for use as a primary standard. We have observed a small quadrupole effect in some iron foils. The internal magnetic field seems to change with carbon concentration. I think that Dr. Flinn has obtained some data on this, and Dr. Bruce Christ at the Bureau of Standards measured the internal magnetic field as a function of carbon concentration. Iron does oxidize relatively easily, and we have never been able to obtain reproduction from one foil to the next. Sodium nitroprusside is reproducible as far as quadrupole splitting, and chemical shift goes to within 2×10^{-4} cm./sec. per second, which is more than adequate for any desired Mössbauer work. The position of the six iron lines can vary by five times this limit.

P. R. Girodot (The University of Texas at Arlington): A recent report stated that hemoglobin contained three globins and not two attached to the central iron atom, as shown by the Sorel effect. If so, it would not be octahedral but 7-coordinated. In this case, is there any evidence to support this idea or disprove it from the Mössbauer data presently available?

L. May: From the current data this could not be proved or disproved. I think that is the data Corwin published in *Chemical and Engineering News* [43 (22), 36 (1965)], and I believe that is as far as it has gone.

Dr. Spijkerman: I would be willing to have hemoglobin 7-coordinated because we worked on the iron EDTA salts, which show a very asymmetric quadrupole splitting, and they are 7-coordinated. The spectra of hemoglobin and the iron EDTA salts are quite similar. I think that spin-spin relaxation occurs, which is more pronounced with 7-coordination than one would expect for 6 or 4. If this is the case, there might be some indication of it, but the Mössbauer spectrum certainly doesn't indicate it from the chemical shift or quadrupole splitting.

H. Stöckler (Rutgers University): Can you explain the splitting of tin oxide (SnO_2) as being caused by the difference in the several kinds of tin-oxygen bonds present?

Dr. Spijkerman: You mean in SnO_2? Originally when Dr. Herber and I worked on SnO_2 we attributed this to twining of the crystal. Dr. Coffeeberg *et al.* (Corning Glass Works) revealed to us some unpublished x-ray data, which indicated that two of the Sn-O bonds were different. Hence, the situation is similar to that in SnF_4. Of the six oxygen-tin bonds, two are different from the other four, and this gives rise to an electric field gradient at the nucleus.

Dr. Stöckler: I can't agree with that because Baur said that the bond lengths are the same within ±0.001 A.; however, the tin-oxygen bond angles are 102°, 78°, and 90°, and I think one attributes splitting to the difference in bond angles. It has a normal rutile structure. I don't think the bond lengths are so important because they are equal to within ±0.001 A.

Dr. Spijkerman: How much of an electric field gradient would there be?

Dr. Stöckler: Well, approximately 0.5 mm./sec. quadrupole splitting.

Dr. Herber: At the time of this work it was clear that the tin-oxygen distances are all essentially the same, as Dr. Stöckler says. The bond angles are not all 90°, as we pointed out. A subsequent calculation was done by Dr. Coffeeberg and co-workers. Assuming point charges and an ionicity of the tin-oxygen based on bond lengths, one obtains approximately the appropriate magnitude of the field gradient. Hence, I think there is little doubt that the major contribution to the field gradient in stannic oxide is this departure from octahedral symmetry. There is one other point that bears on this. Laboratory-prepared samples of stannic oxide do twin over the short distances, and this twining smears out the resultant data. This is why even at high resolution one has difficulty in deciding just what the quadrupole splitting is, although remeasuring such samples in our laboratory with somewhat higher precision had given a value of the quadrupole splitting about twice as large as we thought originally. However, the major origin of the quadrupole splitting is clearly in this non-90° bond angle.

Dr. Zuckerman: There is a rule which Dr. Flinn has worked on— *i.e.*, the rule which separates the isomer shift of Sn(II) from Sn(IV). As far as I know, there are no violations to this rule although we are searching very hard to find one. Is it clear that the white tin line separates Sn(II) from Sn(IV)?

Dr. Spijkerman: I think so. Yes.

Dr. Zuckerman: We would also need an equal or more powerful test to tell us the valence state independent of Mössbauer experiments in

order to produce a contradiction. I suppose that would be found in the internuclear distances.

Dr. Spijkerman: Yes, x-ray or NMR data would be quite valuable, particularly if NMR data on tin were more available. Even in my last slide which showed the correlation of the s character with NMR coupling coefficients and Mössbauer spectroscopy chemical shifts, I am not sure this is correct. At least it is a beginning of assigning 5 s character with chemical shift.

Dr. Zuckerman: Would you comment on Dr. Gol'danskiĭ's suggestion concerning the explanation of the isomer shift in tin compounds which concerns the ratio of the atomic sizes?

Dr. Spijkerman: This was the basis on which Gol'danskiĭ changed the $\Delta R/R$ from a positive to a negative value. Recent calculations by Bersuker have shown the effect of $d_\pi\text{-}p_\pi$ interactions, which are considerable in the tin tetrahalogens and change the effective 5s electron density owing to shielding. Gol'danskiĭ proposed that despite the decrease in the number of 5s electrons of tin in going from SnI_4 to $SnCl_4$, the quantity of $|\psi_s(o)|^2$ increases, owing to a decrease in the effective s electron localization. Essentially, one might think of the classical radius of the s orbital expanding as a function of ionization, but that is not true, as Lees and Flinn have shown in their calculations of the Fermi-Segré equation.

Dr. Zuckerman: Perhaps the other feature of that suggestion is its removal of the argument from experimental test. Apart from the difference between Sn(II) and Sn(IV), (which according to Rundle does give a difference in internuclear distance) when comparing molecular compounds within one valence state in a heteronuclear system, one cannot assign an exact radius to each of the atoms. There are no experimental verifications possible.

Dr. Spijkerman: I actually tried to use the Gol'danskiĭ change in ionization for Sn(II) states and still obtained a positive value for $\Delta R/R$. If Gol'danskiĭ had made his calculations for divalent tin at the time, it could have shown a discrepancy.

L. Keys (General Electric Co., Cincinnati, Ohio): With what degree of certainty can we assume that the sign of $\Delta R/R$ is known, especially in view of the fact that while you point out the importance of knowing the sign, there is no mention of what it is. Recent developments at Brookhaven prompted me to question this. What has led you to a definite conclusion?

Dr. Spijkerman: $\Delta R/R$ is a wonderful example of "follow the leader." I think up to the time of Gol'danskiĭ's work it was believed that $\Delta R/R$ was positive, but the Brookhaven experiment is so direct that there is no argument.

A. F. Clifford: Do you feel we have one nuclide established now?

Dr. Spijkerman: Iron is no problem either. Iodine isn't. Tin is established now.

Dr. Flinn: The tin case is peculiarly difficult from the point of view of nuclear theory. There are some cases where the nuclear theory is clear cut, and one not only obtains a good value but a definite sign and a fairly good estimate of the magnitude. This just happened to be a bad one.

Dr. Spijkerman: As you approach the magic numbers, it becomes quite difficult to do.

Dr. Zuckerman: Could Dr. Spijkerman reassure us by telling us that the value of $\Delta R/R$ is invariant with chemical state?

Dr. Spijkerman: I think Dr. Herber could comment on this.

Dr. Herber: There was an interesting controversy between a German group which I think involves Kienle and others and an Israeli group composed of Cohen, Atzmony, Ofer and others. They took one of the rare earths, which is particularly suitable for answering this question. Europium has two Mössbauer isotopes (^{151}Eu and ^{153}Eu), and one can synthesize the analogous chemical compounds, of course, with both isotopes and expect that the ratio of two isomer shifts for the two sets of compounds will be the same. The Israeli group claims they are different. The German group claims they are the same. Now, this, of course, would be an interesting situation if it were true. This problem has been studied diligently by both groups—both trying to prove that they are right. At the moment it is unresolved, but there must be a small effect. That is, one can't say that the effect is non-zero because the nucleus is going to interact with the electrostatic environment, and different nuclei will interact differently; therefore one expects that there is an effect. Whether this effect is large or small compared with the measurable parameters is something I can't really decide at the moment. One has the same situation with iodine populated from tellurium decay and iodine populated from xenon decay or xenon populated from iodone decay. But there the ratios of the isomer shift for analogous compounds, whether used as source or absorbers, were quite identical except for a calibration constant. As a matter of fact, the early Perlow paper shows a good correlation between these.

D. W. Hafemeister: In addition there is a recent paper by Rama Reddy, Barros, and deBenedetti in which they cancelled out the iodine chemistry and obtained the ratio of $(\Delta R)_{127}$ divided by $(\Delta R)_{129}$. They quoted a value of about -0.78 ± 0.04, so they were claiming linearity for the two different isotopes to *ca.* 5%. Wilets has calculated the polarizability of the nucleus, but I think that this effect is really quite small.

Dr. Spijkerman: These experiments (referred to in Dr. Herber's comment) were on europium-151 and europium-153.

Brother Columba (University of Notre Dame): With regard to earlier discussion on whether the data all support that divalent tin is positive, we have run about 30 coordination compounds of divalent tin, and all the isomer shifts are strongly positive.

Dr. Spijkerman: We obtained from Du Pont an 8-coordinated tin compound which was Sn(II) and it also fell into the positive range.

Dr. Stöckler: Is the structure known for such a compound?

Dr. Spijkerman: Muetterties and Wright (Du Pont) investigated this 8-coordinate chelate.

Dr. Clifford: What compound was it?

Dr. Spijkerman: Dr. Snediker obtained a tin tropolone chelate from Du Pont, which is asymmetric. We wanted to investigate it for use as a standard, but Du Pont did not want to release it. Its preparation has been published [*J. Am. Chem. Soc.* **87**, 4706 (1965)].

Dr. Erickson: Dr. Clifford, did I interpret your talk and slides correctly to mean that you found large quadrupole splittings for iron in some of the rare earth oxides?

Dr. Clifford: Yes, the quadrupole splitting for iron in rare earth oxides was perhaps 1½ times the value reported in any of the iron oxides themselves. This is probably caused by the fact that in the iron oxides the asymmetry in the crystal is in the second coordination sphere. In other words, it is caused by the presence or absence of the nearest iron atoms in the lattice, whereas in the rare earth oxides, it's an oxygen deficiency in the first coordination sphere of the iron, assuming that the iron took a normal lattice position in the rare earth oxide.

Dr. Erickson: Have you studied the splittings as a function of temperature? Just glancing at the spectra they look suspiciously like examples of relaxation effects where one obtains unresolved hyperfine spectra of all sorts. I believe that these samples were quite dilute and would be analogous to the iron-doped aluminum oxide systems, where one does find hyperfine lines even though the compound is, from magnetic susceptibility data, paramagnetic and not ferromagnetically aligned.

Dr. Clifford: At the time this work was done we weren't set up for cryostating, so this was done only at one temperature. It is a point that should be investigated, and we are set up for it now.

Dr. Thomas (to Dr. Hafemeister): You mentioned the possibility of studying iodine in three different ways—either by decay to iodine or decay from iodine to either tellurium or xenon. Hence, you will end up either with tellurium as iodine or with xenon as an iodine complex. Since the electron's immediate environment of the nucleus will depend on its Z, aren't you likely to obtain different results depending on which way you do it?

Dr. Hafemeister: Yes, and that's why we used the iodine absorbers —to be sure of always being in a satisfactory position. I mentioned the other approaches because sometimes workers wish to study ^{129}Xe or ^{125}Te in an iodine site, and they should be aware that there are other ways to attack the iodine problem. However, for straightforward chemistry one should use ^{127}I and ^{129}I in the absorbers.

Dr. Spijkerman: Has anyone run these iodine clathrates?

Dr. Hafemeister: Not that I am aware of.

Dr. Clifford: It is my impression that Na_2TeO_4 (mentioned in Dr. Violet's paper) is a polymer with 6-coordination about the tellurium, not a monomer with 4-coordination. Has any recent x-ray work been done on this compound?

R. W. Grant: Dr. Violet's text simply says that it is tetrahedrally coordinated with four oxygens around it.

Dr. Clifford: The alkali tellurates are, of course, quite different chemically from the selenates and the sulfates, which are definitely monomeric. I think even the alkali tellurates are highly insoluble, for example, which would seem quite unlikely if this were a monomeric anion. On the other hand, if this is polymeric, then the oxygens should be nonequivalent, and depending on how much quadrupole splitting can be expected, one might see some which isn't reported.

Mr. Seidel: We have discussed four elements and one class of elements. What is the future for the other elements that exhibit the Mössbauer effect, and will any particular one be important in the next year or so?

Dr. Hafemeister: Perlow and Boyle at Argonne have studied ^{133}Cs and the cesium halides.

Dr. Flinn: Antimony would be exciting to many chemists. Antimony-121 is the Mössbauer isotope of antimony. The first work was done at Wayne State University, and recently there has been a good deal of work by Ruby and others at Argonne which should be appearing shortly. It seems that antimony is similar to tin in its relationship between isomer shift and the various compounds. It is better than tin in that the isomer shift is about five times larger so that precise measurements are possible. Thanks to Ruby's work, the changes with chemical environment are well understood. The $\Delta R/R$ situation is clear cut, but there are some difficulties in preparing a satisfactory source. The parent is tin-121 which is made by neutron capture by tin-120. The reaction has one of the smallest cross-sections in existence—one can place the tin in a reactor for a year and not produce much even then. However, when a source is obtained, you are in business for a while. Its half-life is 25 years.

Dr. Spijkerman: Maybe a linear accelerator can make a ^{121}Sn source.

Dr. Flinn: I wondered if that would work. Have you made any?

Dr. Spijkerman: No, but we plan to try.

Dr. Flinn: It seems that one should be able to make it that way. If it could be produced by any other reaction, it would help. However, because its energy is 37 kv., one must work at nitrogen not helium temperatures. I think it will be almost as pleasant to work with as tin.

Dr. Spijkerman: Actually, Pd_3Sn or Pd_3Sb both have cubic symmetry and are fairly closely packed; hence, Pd_3Sn might be a good source for antimony since both intermetallics are cubic and there will be no change in environment.

Dr. Erickson: For those interested in coordination chemistry, certain other transition metal atoms are suitable for Mössbauer spectroscopy. One in particular is ruthenium which is just below iron in the Periodic Table. It is a difficult isotope to work with since it requires helium temperatures almost exclusively. I don't know whether it is possible to work at nitrogen temperatures or not, but Kistner at Brookhaven has examined various ruthenium compounds from the 2+ to the 8+ oxidation states with interesting results. These are not published yet, but at least his work offers the possibility of going down one element below the other in the Periodic Table to study chemical effects. Osmium, which is below ruthenium, can also be Mössbauered. Some sort of systematic study like this involving elements in the various transition series would be extremely interesting.

R. H. Goodman (Dept. of Mines, Canada): Has anyone observed the Mössbauer effect with the 13.5 k.e.v. gamma of germanium-73?

Dr. Spijkerman: No.

Dr. Flinn: Have you?

Dr. Goodman: I haven't.

J. L. Thompson (Idaho State University): Is anyone interested in excitation of the Mössbauer states directly? Is the necessity of having an accelerator prohibitive in this type of Mössbauer work?

Dr. Hafemeister: Most isotopes really can be studied just as well or better by beta decay. I can think of only one that can't—*i.e.*, potassium-40. This is a strange case because it is an odd-odd nucleus, and there are only about four odd-odd nuclei that are stable. An odd-odd nucleus means that it decays to the neighboring even-even nuclei, and in this case one cannot populate it by beta decay. However, in most cases one does just as well with beta decay, particularly since using a nuclear reaction for direct population is so expensive. It can be done, so there should be a good reason to spend the money. Radiation damage studies by these techniques are feasible and may well be useful.

Dr. Herber: We were interested in seeing whether we could get the 23.8-kv. level in tin-119 by Coulomb excitation. The $B(E2)$ for this is quite small, but it can be done. However, the experiment is not

feasible because to separate the Mössbauer line from all the other extraneous material, one must do coincidence measurements. For iron-57, this has been done by workers at Johns Hopkins among others, but one must select the correct nuclear system so that one can use, let's say coincidence techniques, or some other method of separating out the gamma line of interest from everything else. If this is not done in any kind of in-beam experiment, there will be trouble with intensity.

Dr. Hafemeister: If you pulse the accelerator and remove all the short-lived activity and if the Mössbauer isotope remains awhile, then you can throw away the coincidence requirement.

Dr. Herber: This is certainly one technique.

Brother Columba: Dr. Flinn, is the antimony transition from the 3/2 to the 1/2 state, and is the spectrum a simple one?

L. Bowan (North Carolina State University): It is a 7/2 to 5/2 transition.

Dr. Flinn: However, it is not prohibitively troublesome if one obtains a single-line source, which is possible. There are various possible cubic environments for antimony, and you don't encounter the problem with magnetic effects that you do with the rare earths. It is a little more trouble, but it is quite manageable, and it doesn't interfere seriously with the experiments.

Dr. Hafemeister: One exciting Mössbauer experiment was done at MIT by Grodzens and Cohen and co-workers. They tried to obtain the value of $\Delta R/R$ between members of a rotational band. It was extremely exciting because supposedly the wave functions in these rotation nuclei are well understood, and nuclear calculations are feasible. There are few such parameters one can measure in nuclear physics quite as nicely.

Dr. Stöckler: Dr. Herber mentioned change in the $5s$ electron density in tin as measured by internal conversion methods. What was the percent change observed?

Dr. Herber: Going from SnO_2 to white tin it was about a 30% effect (an increase) in the $5s$ density. Since the isomer shifts of the two chemical forms are well-known, one can readily calculate the sign of $\Delta R/R$ from these data.

Dr. Stöckler: In such experiments one looks at a small difference in the internal conversion coefficient owing to the difference in electron population of one electron shell. Doesn't this introduce a large error?

Dr. Herber: Yes, but in the Brookhaven experiments the internal conversion data were normalized to the N-line intensity. There was no requirement to determine the *total* internal conversion coefficient. Hence, the error could be kept to about 10 to 15%.

Dr. Erickson: The total change in alpha is insignificant. The change in the conversion coefficient of the 5s level accounts for a small portion of the total internal conversion coefficient.

Dr. Stöckler: What, if any, is the effect of the difference in the recoil-free fraction of the two compounds of tin?

Dr. Erickson: There would be no (negligible) effect on say the f value.

Dr. Keys: In view of recent studies by Mullen at Argonne and Amelinckx at Euratom in Belgium on the effects of radiation damage to Fe in NaCl and KCl using the Mössbauer technique, do there seem to be any future applications of this technique to studying radiation damage in metals? For example, could one study the difference between Fe interstitials and Fe vacancies (or any other Mössbauer metal isotope with a nuclear spin in the ground and/or excited state equal to or greater than 3/2) by their differences in quadrupole splitting? The concentration of defects here can be controlled easily by varying the radiation fluence so that the only limitation would appear to be the magnitude of the quadrupole splitting. One could choose also an enriched system such as Fe-57 or Au-197 which has almost a 100% abundance to assure having Mössbauer isotopes near the studied defect.

Dr. Flinn: The difficulty in using the Mössbauer effect to study radiation damage is that only a small fraction of the atoms in the material studied are in or near damaged regions and will make a proportionately small contribution to the observed spectrum. Using a material containing many atoms of the proper isotope does not help much; one needs to have the resonant atoms concentrated in the damaged regions. This might be accomplished by producing the source nuclei *in situ—e.g.,* cobalt-57 by a *d-p* reaction on iron-56, or possibly by producing absorber nuclei by the damaging reaction—*e.g.,* start with iron-56 *free* of iron-57 and produce iron-57 in it by neutron capture.

Mr. Seidel: Our appreciation is extended to all the speakers for their interesting papers and to the audience for their questions. We look forward to other such symposia on the development of Mössbauer Spectroscopy.

Appendix

Below is a list of selected references on Mössbauer spectroscopy for additional reading.

BOOKS

Abragam, A., "L'Effect Mössbauer et Ses Applications a L'etude des Champs Internes," Gordon & Breach, New York, 1964.

Frauenfelder, H., "The Mössbauer Effect," W. A. Benjamin, Inc., New York, 1962.

Gol'danskiǐ, V. I., "The Mössbauer Effect and Its Applications in Chemistry," Consultants Bureau Enterprises, Inc., New York, 1964. (D. Van Nostrand Co., New York, 1966.)

Muir, A. H. Jr., Ando, K. J., Covyan, H. M., "Mössbauer Effect Data Index," North American Aviation Science Center, Issue 3, 1965.

Wertheim, G. K., "Mössbauer Effect," Academic Press, New York, 1964.

REVIEW ARTICLES

Brady, P. R., Wigley, P. R. F., Duncan, J. F., *Rev. Pure Appl. Chem.* **12,** 165 (1962).

Devoe, J. R., Spijkerman, J. J., *Anal. Chem.* **38,** 382R (1966).

Duncan, J. F., Golding, R. M., *Quart. Rev.* **19,** 36 (1965).

Fluck, E., Kerler, W., Neuwirth, W., *Angew. Chem. Intern. Ed. Engl.* **2,** 277 (1963).

Fluck, E., *Advan. Inorg. Chem. Radiochem.* **6,** 433 (1964).

Fluck, E., *Fortschr. Chem. Forsch.* **5,** 399 (1966).

Gol'danskiǐ, V. I., *Intern. Sci. Technol.* **1963,** 40.

Greenwood, N. N., *Chem. Britain* **3** (2), 56 (1967).

Herber, R. H., *J. Chem. Ed.* **42,** 180 (1965).

Herber, R. H., *Ann. Rev. Phys. Chem.* **17,** 261 (1966).

Wertheim, G. K., *Science* **144,** 253 (1964).

SYMPOSIA

Compton, D. M. J., Schwen, A. H., "Transactions of the Second Conference on the Mössbauer Effect," John Wiley & Sons, New York, 1962.

Gruverman, I. J., ed., "Mössbauer Effect Methodology," Plenum Press, New York, 1966.

"Third International Conference on the Mössbauer Effect," *Rev. Mod. Phys.* **36,** 333 (1964).

"Applications of the Mössbauer Effect in Chemistry and Solid-State Physics," *Intern. At. Energy Agency, Tech. Dept. Ser. No.* **50,** Vienna, 1966.

INDEX

175

L

La$_2$O$_3$	118
Lattice size effects	97
Ligand antibonding	97
Linear polarized γ-rays	49
Long-range magnetic coupling	42
Low spin compounds	91

M

Magnetic	
anisotropy	39
field at the nucleus	35
hyperfine interaction	35
in ^{57}Fe	15
hyperfine structure	141
properties of materials	34
transition temperatures	40
Marcasite structure compounds	96
Martensite	31
Matrix, tin-barium stannate	8
Metallic state	
of dysprosium	116
valence in the	116
Methylstannanes	111
Methylstannates	111
Mg$_2$Sn	106
Mineral and glass Mössbauer	
parameters, comparison of	71
Moldavites	61
Molecular orbital parameters,	
chemical shift and	56
Monochromatic sources for rare	
earths	122
Morin transition in α-Fe$_2$O$_3$	42
Mössbauer	
detectors	148
drives	5
nuclides	19
parameters	18
temperature coefficients of	16
spectra of hemoglobin and its	
complexes	58

N

Na. *See also* Sodium	
Na$_2$TeO$_4$	166
Nepheleuxitic effect	89
Neptunium-237	125
NMR chemical shift	131, 139
NMR coupling coefficient	111
Nuclear	
charge radius	106
magnetic quantum number	36
magnetic substates	36
radius, change in	22
Zeeman effect	35
Nucleus, magnetic field at the	35

O

Olivines	61, 71
crystal field calculations for	82
synthetic	77

Optical absorption in alkali halides,	
recoilless	144
Ordering of Fe^{2+}	
in the enstatite-ferrosilite series	80
in silicate minerals	73
Organotin compounds	26, 107
Organotin halides	110
Overlapping ion model	135
Oxidation state of tin, chemical	
shift and	53

P

Pd-Sn solid solution	109
Pd$_3$Sn	106, 167
Philippinites	61
Phosphate glasses, ferric meta-	70
Phosphors	125
Pi-bonding on chemical shift in iron	
complexes, effect of	54
Polarized sources	47
Praesodymium oxide, hysteresis in	118
PrO$_{1.83}$	119
PrO$_2$	120
Preferential substitution	46
Pressure *vs.* chemical shift	109
Pressure shifts	97
Pyroxenes	61, 71
crystal field calculations for	82
synthetic	77
sites, covalency factor for	
inequivalent	83

Q

Quadrupole moment, electric	150
Quadrupole splitting	107, 110
asymmetry	56
in europium oxide	122
in ^{57}Fe compounds	14
vs. isomer shift	154
in iodine compounds	140
in stannous compounds	25
in ^{119}Sn (IV) compounds	14
and symmetry in iron	
complexes	56
temperature variation of	56

R

Radiation damage to iron in halides	169
Rare earth	
chalcogenides, interatomic	
distances in	115
compounds	
doped	124
ionic nature in solid	114
hydrides	125
oxides	
iron in	165
iron-57 doping of	118
Rare earths	113
monochromatic sources for	122
Recoil-free fraction in stannic	
iodide	18
Recoilless fractions	142